



HAL
open science

Modeling of the deformation of resin bonded foundry sand core during casting

Hiba Bargaoui

► **To cite this version:**

Hiba Bargaoui. Modeling of the deformation of resin bonded foundry sand core during casting. Mechanics [physics.med-ph]. Université Paris sciences et lettres, 2019. English. NNT : 2019PSLEM004 . tel-02439083

HAL Id: tel-02439083

<https://pastel.hal.science/tel-02439083>

Submitted on 14 Jan 2020

HAL is a multi-disciplinary open access archive for the deposit and dissemination of scientific research documents, whether they are published or not. The documents may come from teaching and research institutions in France or abroad, or from public or private research centers.

L'archive ouverte pluridisciplinaire **HAL**, est destinée au dépôt et à la diffusion de documents scientifiques de niveau recherche, publiés ou non, émanant des établissements d'enseignement et de recherche français ou étrangers, des laboratoires publics ou privés.

THÈSE DE DOCTORAT
DE L'UNIVERSITÉ PSL

Préparée à MINES ParisTech

**Simulation de la déformation des noyaux de fonderie
durant la coulée**
**Modeling of the deformation of resin bonded foundry sand
core during casting**

Soutenue par

Hiba BARGAOU

Le 31 01 2019

École doctorale n°621

**Ingénierie des Systèmes,
Matériaux, Mécanique, Én-
ergétique**

Spécialité

Mécanique

Composition du jury :

Florence DINZART
Maître de conférences HDR, LEM3, UL *Rapporteur*

Jianfu SHAO
Professeur, Université de Lille *Rapporteur*

Bruno FAYOLLE
Professeur, ENSAM Paris *Président*

Rolf MAHNKEN
Professeur, Université de Paderborn *Examineur*

Denis MASSINON
Dr, directeur innovation, Montupet *Examineur*

Farida AZZOUZ
Dr, Mines Paristech *Maître de thèse*

Georges CAILLETAUD
Professeur, Mines Paristech *Directeur de thèse*

Contents

Contents	1
1 Introduction	5
1.1 Industrial context	6
1.2 Objectives and approaches	9
1.3 Outline of the dissertation	10
2 Literature review	11
2.1 Cast manufacture process	12
2.1.1 Tools fabrication	13
2.1.2 Coring	14
2.1.3 Melting	14
2.1.4 Casting and solidification	15
2.1.5 Decoring, heat treatment, machining and controls	15
2.2 Sand casting	15
2.2.1 Green sand (clay sand) for sand moulds	15
2.2.2 Chemically bonded sand, for sand cores	17
2.2.3 Sand cores manufacturing processes	17
2.3 PUCB process	18
2.3.1 The binder	18
2.3.2 The sand	19
2.3.3 Structure of the PUCB sand	21
2.4 Characterization of the molding material	23
2.4.1 Green sand characterization	23
2.4.2 Characterization of the resin bonded sand cores	25
2.5 Generalities about polymers	27
2.5.1 Thermoplastic polymers	29
2.5.2 Thermosetting polymers	29
2.5.3 Polyurethanes	30
2.5.4 High temperature properties of polymers	31
2.6 Summary	34
2.7 Résumé en français	35
3 Experimental characterization	37
3.1 Sand core thermal history	38
3.2 Study of the industrial sand cores at Montupet	39
3.2.1 Manufacturing of PUCB sand cores	39
3.2.2 Experimental characterization: bending creep tests	41
3.3 Creep bending tests at CDM introducing laser measurements	46

3.4	Synthesis of the pre-existing tests	48
3.5	Development of a new testing protocol: Experimental methods for resin characterization	50
3.5.1	Differential Scanning calorimetry (DSC)	50
3.5.2	Thermogravimetric analysis (TGA)	50
3.5.3	Dilatometry	50
3.5.4	Dynamic Mechanical Analysis (DMA)	51
3.5.5	Tensile tests	52
3.5.6	Creep tests	52
3.6	Development of a new testing protocol: Experimental methods for sand core characterization	53
3.6.1	Dilatometry	53
3.6.2	DMA tests	53
3.6.3	Compression tests	54
3.6.4	Four-point bending tests	54
3.6.5	Four-point bending tests for temperatures above 300 °C	58
3.7	Results and discussions	61
3.7.1	Resin and core thermophysical characterization	61
3.7.2	Resin thermomechanical characterization	71
3.7.3	Sand core thermomechanical characterization	78
3.8	Summary	89
3.9	Résumé en français	90
4	A thermomechanical model of resin bonded sand core behavior	101
4.1	Generalities about material modeling	102
4.2	Plasticity criteria for geomaterials: monophasic materials	103
4.2.1	Mohr-Coulomb criterion	103
4.2.2	Drucker-Prager criterion	103
4.2.3	Cam-Clay and Modified Cam-Clay criteria	104
4.2.4	Discussion	106
4.3	Models for granular materials: multiphase materials	106
4.3.1	Models for cemented geomaterials	106
4.3.2	Models for foundry green sand	107
4.3.3	Micropolar elasto-plasticity model for Cold-Box sand	111
4.3.4	Discrete elements method	111
4.3.5	Summary	112
4.4	A new model for resin bonded sand core	112
4.4.1	General framework	112
4.4.2	Modeling of the binder behavior	112
4.4.3	Modeling of the core behavior	114
4.4.4	Summary	116
4.5	Model calibration	117
4.5.1	Introduction	117
4.5.2	Model calibration strategy	117
4.5.3	Simulation of the resin behavior	117
4.5.4	Simulation of the behavior of the sand core	118
4.6	Summary	123
4.7	Résumé en français	124

5	Model validation on a technological specimen	135
5.1	Design and instrumentation of the technological specimen	136
5.1.1	The metallic mold and aluminum cast	136
5.1.2	Aluminum alloy	137
5.1.3	Technological specimen designs	137
5.1.4	Measurement techniques	139
5.2	Instrumentation protocol	140
5.2.1	Specimen preparation	141
5.2.2	Instrumentation stages	142
5.3	Instrumentation results	144
5.3.1	”Dog bone” design	144
5.3.2	”CDG” design	154
5.4	Numerical validation of the model on ”CDG” design	161
5.4.1	Mesh of the specimen	161
5.4.2	Numerical simulation	161
5.4.3	Results and discussion	163
5.5	Summary	164
5.6	Résumé en français	165
6	Conclusion and perspectives	171
6.1	Conclusion	172
6.2	Perspectives	173
	References	174
	Appendix	183
	Appendix of chapter 1	185
	Appendix of chapter 4	187

Chapter 1

Introduction

Contents

1.1	Industrial context	6
1.2	Objectives and approaches	9
1.3	Outline of the dissertation	10

1.1 Industrial context

The automotive industry's requirements for a high level of quality and dimensional accuracy of metal components are constantly increasing. As cylinder head is a critical part, its design is critical for an optimum behaviour of the engine. This is why metallurgical and mechanical properties and fatigue resistance in operation have been intensively studied by the scientific and engineering community in the past century. Numerical simulations with fluid-mechanics codes allow the investigation of the metal filling and of the solidification stage, but the control of the whole casting process remains an unsolved problem in view of obtaining defects-free products. Specifically, the behaviour of the sand core (chemically bonded sand with a resin binder) used to obtain the internal cavities in the cylinder head is still neglected (it is generally considered as non-deformable). This is no longer an acceptable assumption, since engineers wish to introduce more complex cooling systems involving thinner and thinner walls. When exposed to high temperatures and the metallo-static pressure, they tend to deform, causing defects in the cast, that could ultimately generate leaks or premature cracking in the component. Some heuristic modifications have been introduced in the core box by industrial partners, but they remain very expensive.

As a typical example, Figure 1.1a shows a water jacket sand core and Figure 1.1b the corresponding cast with an amazing deformation of 10 mm of the water jacket cavity with respect to the reference horizontal position. As mentioned by the company Montupet, this defect is caused by the sand core deformation during casting. Even if the reason for this deviation is not clarified, several modifications of the core box were tested. One of the attempts consists in adding plugs in order to prevent deformation. They come in contact with the prop of the inferior sand core as shown in Figure 1.2. This solution involves a modification of the cast design to which the customer may be reluctant, and additional machining steps, that makes it expensive. Generally, each time a deformation area is identified with an initial sand core shape, this is compensated in the updated version of the sand core by introducing a weak zone in the opposite side.

For the numerical modeling of the casting process, the Magma software ¹, is used to predict the casting quality by simulating the filling, solidification and cooling operations, stress and strain development in cast, and microstructure formation. The simulation of the casting process is based on a modular structure which includes a standard database for bonded sand. The core thermomechanical behavior cannot be simulated using Magma. However the heat exchange with the cast, thermoelastic and conductivity properties are taken into account. Unfortunately, the properties are given for an unknown percentage of binder, and an unknown type, so that it is impossible for the user to be sure that these data are compatible with his specific case. More importantly, the knowledge related to core properties at high temperatures remains very poor. The data summarized in Table 1.1 are available only at room temperature. The evolution with temperature is known only for a few parameters (Figure 1.3). In brief, there is a lack of knowledge of the used binder type, properties and behavior as well.

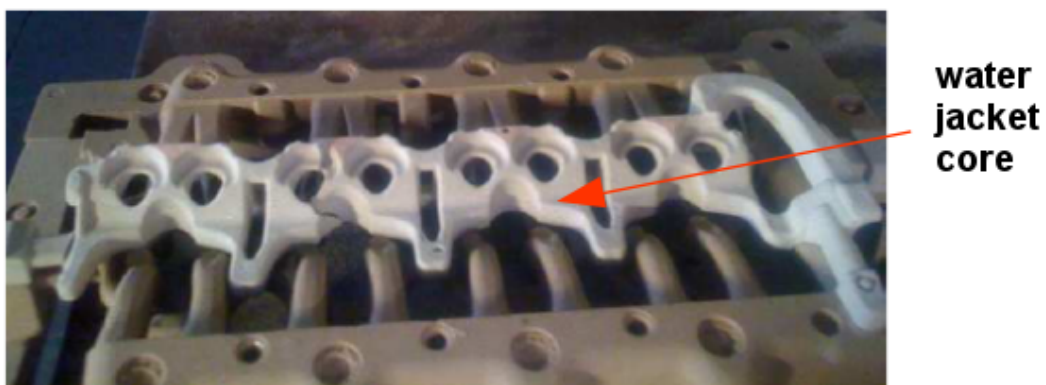
For these reasons, it is of a paramount importance to:

- Understand the mechanisms of the core deformation;

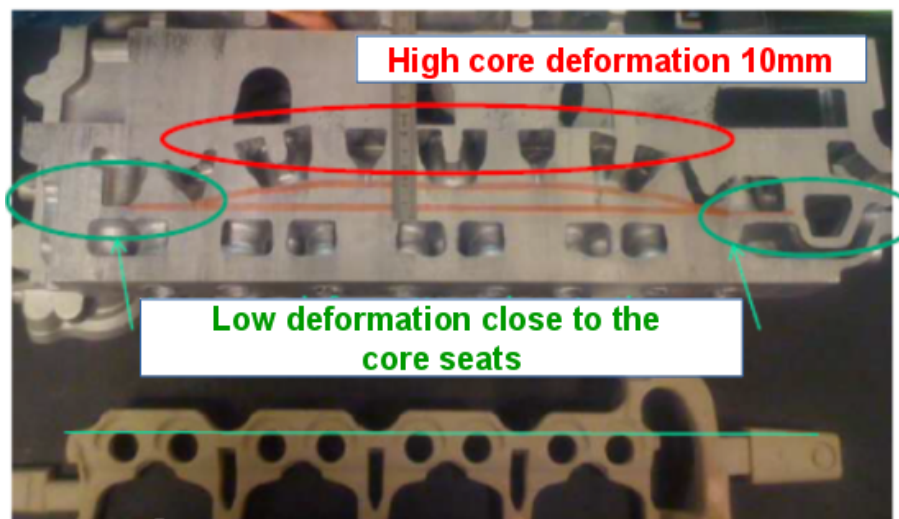
¹<https://www.magma-soft.de/en/>

- Determine its properties at high temperatures;
- Model the core behavior during casting in order to control the whole process.

Throughout the above summary, apart from the fact that we are interested in a complex heterogeneous material which will be studied in detail in section 2.2, the issue is to understand and model the core behavior under complex loadings. Moreover, the model must be able to capture the core deformation mechanisms. There is thus a real need to define a “robust” behavior model for industrial applications. “Robustness” is guaranteed by achieving a threefold challenge: (1) the physical mechanisms of the deformation must be captured; (2) the model has to be suitable for numerical implementation and applicable for real size structure simulations; (3) model parameters should allow a clear identification process. Solving these problems is the strongest driving force of the present study.



(a)



(b)

Figure 1.1: Defect in a cylinder head where in (a) the used water jacket core (b) the deformation in the cast of the cavity obtained with the water jacket core [Mon13].

There is a lack of information in the literature regarding the behavior of the resin bonded sand cores at high temperatures. Many studies were made on cylinder head

¹<https://www.magmaflow.de/en/>

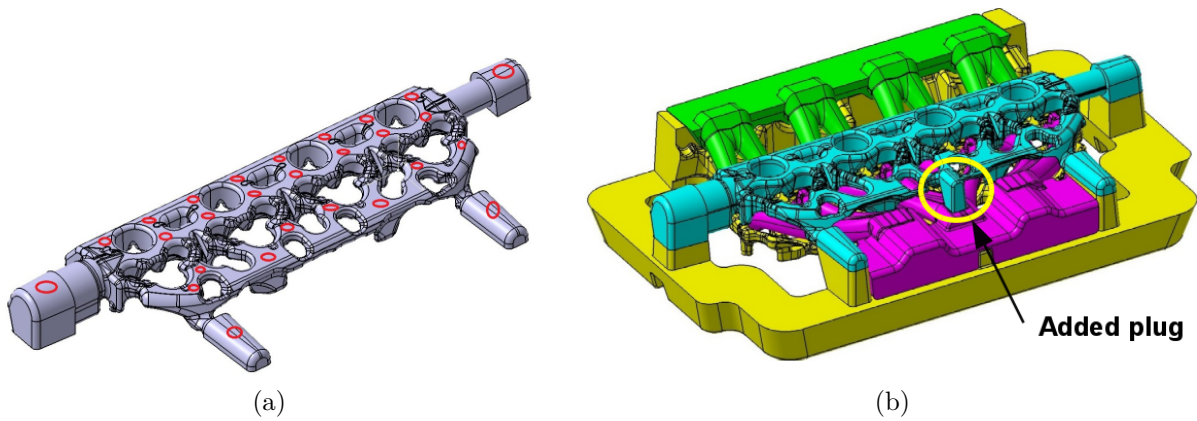


Figure 1.2: Modifications of a core to prevent deformation where in (a) the initial design of the core (b) the core design with addition of a plug [Mon13].

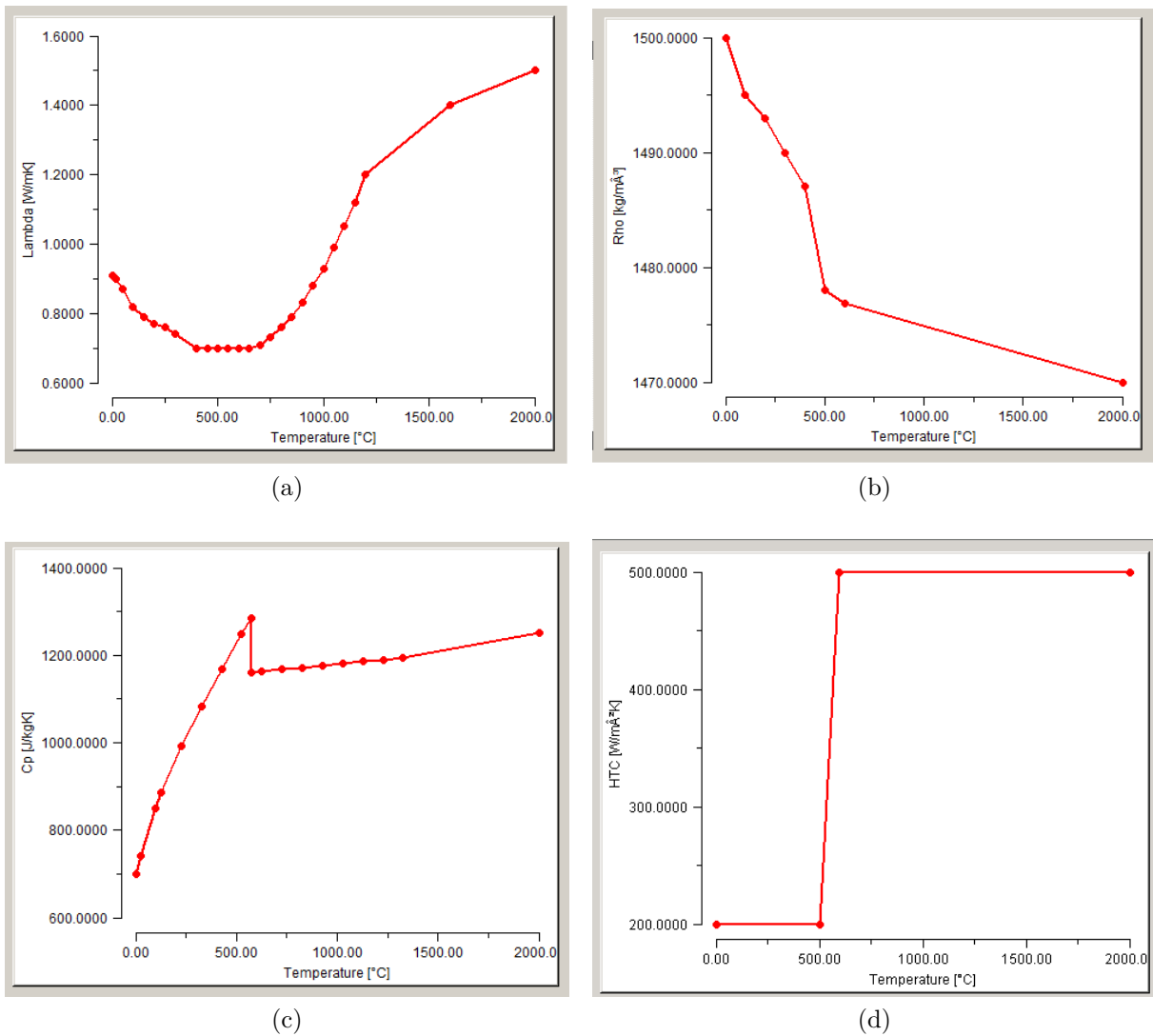


Figure 1.3: Evolution with temperature of (a) thermal conductivity (b) density (c) specific heat and (d) heat exchange coefficient with aluminum ¹.

Table 1.1: Standard core database in MAGMA software for cold box sand core process

Parameter	Value
Young modulus	1500 MPa
Yield stress	15 MPa
Poisson ratio	0.3
Thermal expansion coefficient	$1 e^{-6} \text{ } ^\circ\text{C}^{-1}$
Tensile strength	3 MPa
Hardening coefficient (non linear)	10
Permeability	50 cm ³ /min

casting to characterize the aluminum cast properties, microstructure, damage and fatigue [Gui01,Bar04,Nic99,Sal06,Mar12]. Works were performed in [Sam85] to incorporate the exchanges at the sand-metal interface [Met01], while recent works aim to validate the numerical models by using experimental test bench for thermal measurements as in [Sul12,Mot12,Mot13a]. Now it becomes important to fully incorporate mould and core characterization and modeling in the prediction of the foundry casting process. It is surprising that this was addressed many years ago through works on the thermomechanical behavior of green sand moulds (silica particles, clay, water content, mineral carbon) as in [Azz95,AS96] but not followed by studies on the chemically bonded sand cores (resin, silica particles). The models for green sand moulds can then not be used to predict the sand cores behavior because of the difference in the deformation mechanisms. In addition, among the few existing works on the sand core [Cay10,Thi08,Mot13b,Ino13,Sta16], no one has fully investigated the material deformation mechanisms or attempted to model the thermomechanical behavior during casting with a subsequent validation on industrial parts. Performing different thermomechanical and thermophysical tests under complex loadings and developing a thermomechanical behavior model for such a material is of great interest in order to optimize the casting process.

1.2 Objectives and approaches

The present work focuses only on the casting stage in the manufacture process. It aims at a better understanding and modeling of the thermomechanical behavior of resin bonded foundry sand cores. The principal objectives are to understand the involved mechanisms in the deformation and enrich the finite element code Zset database with information related to material properties, embedded in easy-to-manage constitutive equations. All the deformation mechanisms need to be investigated in the present study: thermophysical and thermomechanical tests conducted on both the bonding resin and the sand core. Observations at the microscopic scale were exploited for investigating binder damage due to thermal decomposition. In parallel with the experimental work, a major part of the study needs to be dedicated to the development of a phenomenological model to describe the sand core behavior. The implementation and calibration of the model will be done using the Zset software ¹. The validation of the model is made on a technological specimen. This last comparison is designed to reveal the applicability of the core model

¹<https://www.zset-software.com/>

to complex loadings during casting.

1.3 Outline of the dissertation

The present dissertation consists of five chapters after the present introduction. In the second chapter, a literature review is presented, which constitutes a background for the whole dissertation. First, a study of the casting process is given, followed by a summary on sand core casting. Details on the core making process at Montupet are then given. Then, a review of sand cores characterization as well as polymer properties are presented.

Chapter 3 constitutes the first part of the present work, which deals with the experimental characterization. First, the mechanical tests used for the study of the thermomechanical behaviour of the cores developed at Montupet are revised, followed by a comparison of these results with tests conducted at “Centre des Matériaux”. Second, the tests performed on the sand cores in the present study are presented. These experiments include thermophysical analyses (DSC, DMA, dilatometry and thermomechanical analyses) and mechanical tests (tensile tests, creep and four-point bending). Methods for exploiting experimental results are also discussed in detail. These experimental results are then used to identify the physical mechanisms responsible for the core behavior.

Chapter 4 presents the development, implementation and identification of the constitutive equations describing the sand core behaviour. The proposed model is implemented in the code Zset and identified.

Chapter 5 and Chapter 6 constitute the third part, which presents the industrial applications and the final discussion. Chapter 5 provides details on the technological specimen design and the related instrumentation. The specimen is intended for validation of the models in terms of deformation prediction. Finally Chapter 6 is the place for the discussions, conclusions and perspectives of the present study.

Chapter 2

Literature review

Contents

2.1	Cast manufacture process	12
2.1.1	Tools fabrication	13
2.1.2	Coring	14
2.1.3	Melting	14
2.1.4	Casting and solidification	15
2.1.5	Decorating, heat treatment, machining and controls	15
2.2	Sand casting	15
2.2.1	Green sand (clay sand) for sand moulds	15
2.2.2	Chemically bonded sand, for sand cores	17
2.2.3	Sand cores manufacturing processes	17
2.3	PUCB process	18
2.3.1	The binder	18
2.3.2	The sand	19
2.3.3	Structure of the PUCB sand	21
2.4	Characterization of the molding material	23
2.4.1	Green sand characterization	23
2.4.2	Characterization of the resin bonded sand cores	25
2.5	Generalities about polymers	27
2.5.1	Thermoplastic polymers	29
2.5.2	Thermosetting polymers	29
2.5.3	Polyurethanes	30
2.5.4	High temperature properties of polymers	31
2.6	Summary	34
2.7	Résumé en français	35

Introduction

This first chapter is dedicated to the literature review. It is divided in five sections:

The first section deals with the industrial manufacture process. This review helps understand the different technological aspects of the cast manufacture process and the use of resin bonded foundry sand cores.

The second section presents the studied material. Details about its composition and the different existing core making processes are then shown.

The third section describes the core making process used at Montupet, the sand core components and structure.

The fourth section presents the main studies that are available to characterize sand core behaviour. The experimental characterization of the sand core components at high temperatures are discussed as well.

The fifth section deals with polymers, focusing on their properties and the specific polyurethane binder used in foundry.

2.1 Cast manufacture process

Figure 2.1 presents examples of cylinder heads manufactured by Montupet for Ford and BMW car engines respectively on the right and the left. The cylinder head serves as a housing for parts as the intake and exhaust valves, springs and lifters and the combustion chamber. The cavities in the cylinder head allow the air and fuel to flow inside the cylinder while permitting the exhaust gases to flow out of it. The cooling channels allow for the extraction of the heat generated by the combustion process. The inner cavities of the cylinder head are made using chemically bonded sand cores. Many cylinder heads are made out of cast-iron, which is a highly resistant and relatively cheap material. However, cast-iron is heavy and not efficient in dissipating heat, so that aluminum, which is much lighter, is the preferred material for cars. In general, the production stages are different depending on the cast, the used process, the production rate... For aluminum cylinder head, which are mass produced in Montupet, these steps are:

- Tools fabrication (core-box and moulds);
- Core making (coring);
- Aluminum melting;
- Casting;
- Decoring, heat treatment, machining and controls.

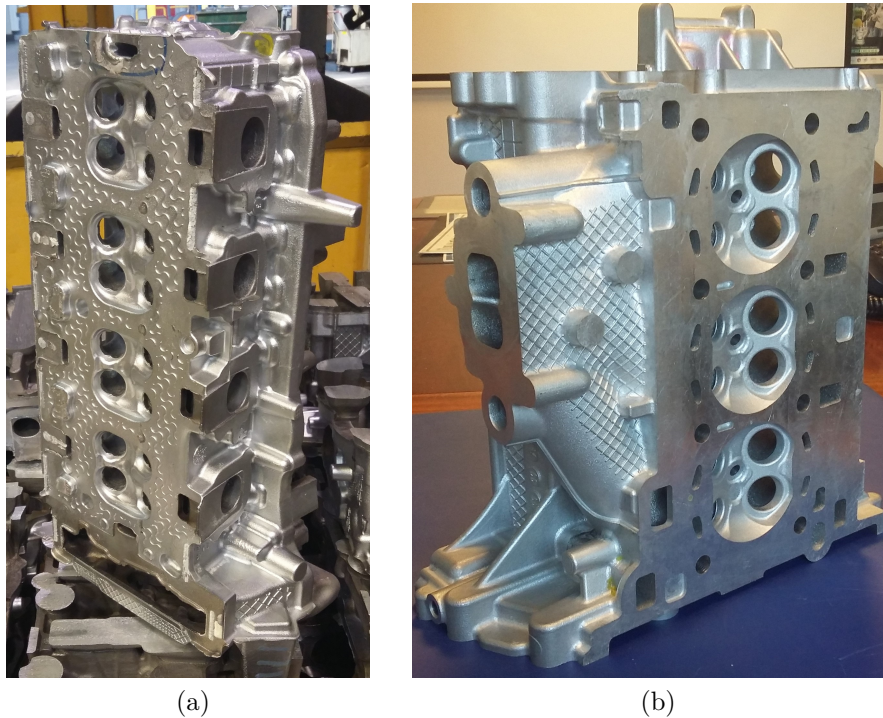


Figure 2.1: Cylinder head of (a) 4.0 liter V8-turbo BMW engine (b) 1.0 liter Ford engine with integrated manifold exhaust [Mon15].

2.1.1 Tools fabrication

In this stage, the tools needed for the process are produced. Their characteristics and the materials used are chosen depending on their function, production rate and the process itself. The main tools used are the mould and the core-box:

Mould. This part serves to obtain the external shape of the cast. Depending on whether these moulds can be reused again and permanent or not, we distinguish two types of moulds:

- *Permanent mould:* it is a metallic mould. It is obtained by machining the target cast shape on a metallic block. This type can be reused many times and is destined to light metal casting with low melting temperature such as aluminum [Mar06]. An example of a metallic mould is given in Figure 2.3.
- *Non-permanent mould:* It is made of a refractory matrix typically silica particles and is destructed after casting [Mar06]. This type of moulds is used in general for iron or steel big sized parts with high melting temperature.

Core box. This is a part used to form the resin bonded sand cores that allow to obtain the cavities in the cast. Depending on the complexity of the cavities in the cylinder head, many cores are needed and therefore many boxes can be designed for producing the different parts (oil passage, water jacket core-boxes...). The box can be made out of a metal (steel in general but it is costly) or a polymer (plastic, polyurethane...). A schematic representation of a cylindrical core and its corresponding core-box is given in

Figure 2.2.

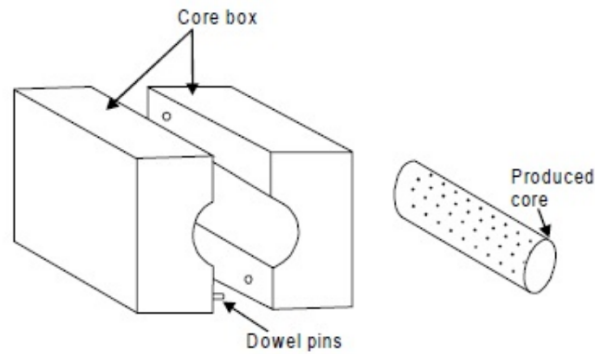


Figure 2.2: A representation of a cylindric core and its core-box.

2.1.2 Coring

The core is the part used to obtain the internal cavities in the cast. Examples of sand cores manufactured at Montupet are shown in Figure 2.3. The core is made of a mixture of a refractory matrix (zircon, bauxite, silica. . .) and a polymer which works as a binder between particles. This binder is usually added in small percentages going from 0.25 to 5 wt% [Gar86]. The core is placed in the mould just before casting. During this operation, the binder undergoes a thermal decomposition process at high temperature which may lead to the core destruction and allows its extraction from the cooled cast. Meanwhile, depending on the binder percentage and the core thickness, some parts might stay intact and additional operations are then added to remove it from the cavities, as discussed in paragraph 2.1.5. The main steps for the core preparation are the following:

- Mixing the sand with the binder;
- Filling the core-box with the mixture;
- Extraction of the final core.

In industry, many coring processes exist. This will be discussed in detail below in paragraph 2.2.3 .

2.1.3 Melting

At this stage, aluminum ingots are melt inside a furnace (it can be a resistive, conduction or combustion furnace [Cam15]). The furnace must enable to:

- ensure a good control of the metal temperature during fusion;
- Avoid any side reaction between the molten metal and the atmosphere;
- Quickly meltdown the ingot.

2.1.4 Casting and solidification

Once the core is placed inside the mould, the molten metal is poured. The filling step depends on the type of mould. For non permanent moulds, gravity filling is mostly used ([Mar06]), while for permanent moulds, gravity filling, pressure filling (low, high and counterpressure) as well as filling by centrifugation can be applied ([Cam15]). Once the liquid aluminum is poured and the mould is filled, solidification begins. The solidification kinetics are dependent on the alloy (its composition, melting temperature), the cast size and the materials in the molding system. After solidification, the metallic part is cooled down. Figure 2.3 shows an example of gravity casting.

2.1.5 Decoring, heat treatment, machining and controls

Once the cast is cooled down, comes the decoring stage. This consists in extracting the decomposed sand core from the cavities in the metallic part. It can be done by hammering over the feeder heads and vibrate the casting in order to remove the burned core parts. There can be a major difficulty sometimes in decoring. This is the case when the molten metal temperature is low (aluminum alloys) and if the core is thick, some parts in the core may not properly decompose and are difficult to break. After decoring, the feeder heads are removed.

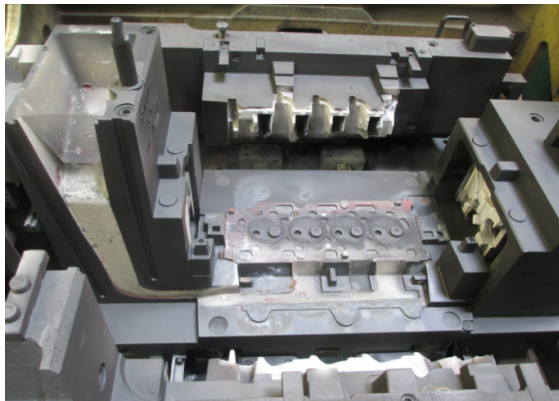
The cylinder heads might go then through heat treatment process in order to improve its thermomechanical properties. ([Cam15]). Depending on the customer's specifications, the metallic part may go through machining process in order to meet the requirement in terms of high dimensional precision and quality. This includes milling, turning and drilling operations. A final dimensional control is performed.

2.2 Sand casting

According to the different binders, foundry sand used for moulding can be divided into two main, categories, namely green sand and chemically bonded sand. Each binder is employed for a specific process. In ferrous casting, inorganic binders such as clay are used for sand moulds. For certain types of casting, due to the large production of parts made of light metals such as aluminum and thanks to the development of organic binders, foundries opted for processes such as the Polyurethane Cold box and the hot box for core production, with different types of resins as binders. These processes offer a high precision in sand core production.

2.2.1 Green sand (clay sand) for sand moulds

Green sand is a mixture of silica sand, bonding clays, carbonaceous materials and water. The term "green" denotes the presence of moisture in the casting sand, meaning that the binder is not baked or dried, does not harden or cure but stays moist. It is generally used for making casting sand moulds. Green sand, is a porous mixture of approximately 87 wt% of silica grains, 7 wt% of clay, 3 wt% of black carbon and 3 wt% of free water. More precisely two phases can be identified, the silica grains and a plastic binding phase formed of clay and carbon. Of course, depending on the compaction of the sand, the pores are



(a)



(b)



(c)



(d)

Figure 2.3: Casting process in Montupet of a Daimler cylinder head showing (a) the metallic mould (b), an example of water jacket and exhaust sand cores (c), the assembly of the different cores (d) gravity casting [Mon15].

more or less filled with water. When subjected to the thermomechanical loading, first by the liquid metal then by the solidified metal, several phase transformations can be observed in the sand, namely vaporisation of free water, coking of carbon black and burning of clay [Azz95].

2.2.2 Chemically bonded sand, for sand cores

In here, the casting is cured using a chemical binder system used to bond the grain matrix particles [Pil10]. The curing process is established through a chemical reaction either during mixing the sand and binder, while other processes may require gassing of the sand mixture, or heating the mixture to complete the cure. The simplicity of the system usually makes quality control less complex and results more consistent. It is mainly used in the manufacture of complex geometries of sand cores.

2.2.3 Sand cores manufacturing processes

The coremaking is of high complexity due to standards to which the core must respond [Hol15], [Pil10]. Before pouring, the core must have a very good strength during transportation and storage. Just after pouring, the core hot tensile strength must be very high to resist to the metallostatic pressure but must also fall rapidly afterwards to offer good collapsibility so that it can be extracted from the solidified cast. The resin cure and its reactivity condition the type of process used. We can find curing under temperature resins in hot curing processes also called hot box process, and cold curing at room temperature where a catalyst is added in a liquid or gaseous state. During casting, the thermal degradation of the resin at very high temperature may leads to the core destruction, so a low amount of resin is added and must be stricly monitored (between 0.25 and 5 wt% of the sand weight) to allow the core destruction, the extraction of the the metallic part, and to prevent defects caused by degassing which depend on resin quantity [Mon08].

When manufacturing sand cores, there are several requirements regarding the core quality to be respected, namely [Mon14]:

- The lifetime of the mixture sand and binder before coring must be sufficiently long. The mixture must not harden before filling the corebox;
- During coring, the hardening of the mixture must be instantaneous (a catalyst is usually used);
- The permeability of the core must allow the evacuation of the gases emitted during the binder cure (granulometry must be controlled);
- The shape of the sand particles is important in order to control the cast surface quality (in general, regenerated sand is used since this helps obtain round particles and remove the sharp edges);
- The core must be hard enough to be easy to manipulate during demolding, storage, placing it in the metallic mould and during casting without failure;
- The core must have a good hardness at medium temperatures during casting but also an easy decomposition at high temperatures to allow its extraction from the cooled cast during the decoring operation.

Hot curing processes

In this method, heating is used for the resin cure and the sand mix hardening. We distinguish two main processes “Hot box” process and “Croning” process. Phenolic novalak-hexa blends and modified as well as unmodified resoles, where the modifier can be furan resins, monomeric and polymeric furfuryl alcohol and urea resin are used [Gar88].

1. Hot box process: furan resin is used as a binder for aluminum casting. Sand is mixed with liquid resin and a curing agent. The mix cure takes place in heated sand box [War94].
2. Croning process “Shell process”: in this process, resin precoated sand is used. The sand is coated under temperature with phenolic novalak-hexamine resin and then cured at 200 °C to 300 °C forming then shells or cores. Curing time can vary depending on the thickness and shape of the core or shell [Rob71], [Ber81].

Cold curing with direct addition of a curing agent (No-Bake process)

Sand cores are made of self-setting sand at room temperature by addition of a curing agent as a liquid, usually acid as a catalyst. A well known process is the Urethane No-Bake (PUR No-Bake) where a phenolic resin is mixed with polyisocyanates and tertiary amine catalyst [Car95].

Gas curing processes: Polyurethane Cold Box (PUCB) process

In this process, a gas or vapor is introduced and works as a catalyst to cure and solidify the mix of sand and resin. Poly-Urethane Cold-Box process is the most common process for core manufacturing. It is widely used for delicate and thin sand cores such as water jacket for cylinder heads.

The binder represents a two-component system chemically composed of a polyol with a polyisocyanate hardener mixed with silica sand and introduced into the corebox by shooting. Liquid Amine at room temperature is vaporized using heat and sprayed into the corebox by means of a neutral gas (nitrogen) vector. It works as a catalyst to accelerate the condensation of the Polyurethane. Residual amine is purged out using air [Tri99].

In the following paragraph, we are going to develop more in detail the Cold Box Process “PUCB”. In fact, this process is chosen by the company Montupet for manufacturing sand cores which we are studying in the present work. We will then describe the types of binders and sand matrix and how they are manufactured.

2.3 PUCB process

2.3.1 The binder

The development of the phenolic urethane coldbox (PUCB) binders has known many advancements through the years. Their form, composition and properties have evolved and as a consequence the core making and casting quality has greatly improved.

In foundries, depending on the type of the phenolic resin and the isocyanate, different

phenolic urethane polymers can be obtained. The hardener polyisocyanate is a linear or oligomeric diphenylmethane-4-4'-diisocyanate, known as MDI. Its choice influences the humidity resistance, strength development, high temperature strength of the cured core and bench life of the mix. Both phenolic resin and the polymeric isocyanate are dissolved in organic solvents. The choice of the solvents is very important as it is necessary for a complete curing of the binder and enhances its speed. It determines the amine evaporation throughout the core [Lai85].

Some additives are introduced. Generally binders suppliers work on the resin chemistry to adapt its properties to the customer's needs. These additives are usually introduced to improve bench life, core extraction from the metallic box. In general, organic acid chlorides are selected and are always added to the hardener.

Binders influence throughout the foundry process has been underestimated for years simply due to the fact that Silica sand represents 99wt% of the sand core while the binder represents 1wt% of the sand weight assuming then that the core behavior and the casting quality are governed by the sand properties. Researches were focalized on the binder composition, types and chemical properties [Gar13],[Lad13], [Mar81],[Pri14],[Sch14] and [VH10] and their influence on the casting quality or compounds used in coating for preventing casting defects [Sto10]. Recently, works have been centered on defects related to gas emissions during the binder pyrolysis as in [Jom15],[Sta11], [Sta09b] and [Sta09a] with models for resin decomposition, gas emissions and the evolution of the gas pressure in the core.

2.3.2 The sand

Refractory matrices that are used in foundry can be introduced in the Coldbox process, essentially silica sand, chromite and zircon sand.

Silica sands are the most common sand grades in this process due to their chemical purity, they are compatible with the different binder systems and have advantageous thermal properties with high fusion temperature (around 1690 °C). A high quality Silica sand contains minor amounts of accompanying minerals. The presence of agents such as Calcium, Potassium and Iron can drastically depress the silica sintering point down to 1200 °C [Pil10]. Silica sand undergoes a phase change at around 570 °C from Alpha Quartz to Beta Quartz with an important thermal expansion as shown in Figure 2.4.

This thermal expansion can lead to casting defects such as veining (the occurrence of a sheet like casting defect, produced by molten metal penetration into a sand casting mould or core), as studied in [Thi07]. The required binder level needed is directly related to the particle size and shape and has major effects on the core bending and tensile strength. In fact, a larger amount of binder is needed when using small silica sand particles. On the other hand, coarse particles help evacuate the released gases during polymerization and resin pyrolysis while small silica sand particles give a higher compaction density and a smooth surface but difficulties in degassing. Regarding the mechanical properties, when using coarse particles less resin bridges are obtained. This leads to a loss in the mechanical performance of the core when compared to small sand particles made cores which are more compact. Edged sand particles are to be avoided since their arrangement gives rise to more voids in the core and non homogeneous resin coating. Foundries choose particles with smooth surface and homogeneous sizes for better mechanical properties. The temperature of the sand is very important, it must be around 20 °C, since temperature is a catalyst for the resin polymerization. A higher temperature would cause premature poly-

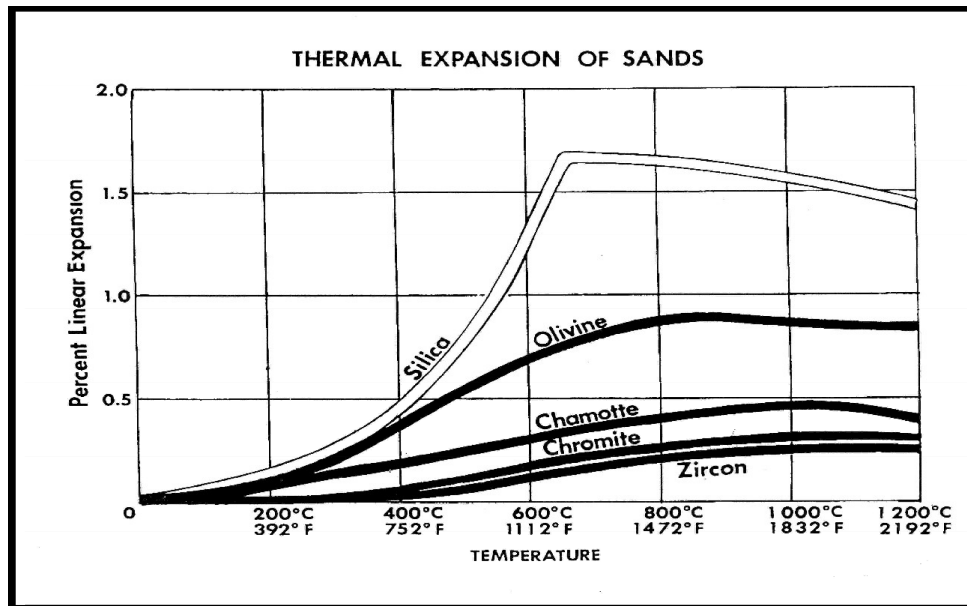


Figure 2.4: AFS handbook sand expansion chart

merization and resin bridges formation during mixing that will be broken during shooting and filling of the sand core box. Very cold sand on the other hand inhibits the resin polymerization [Mon14].

The sand used in the coldbox process is a dry sand (water content <math><0.1\%</math>) since the hardener polyisocyanate reacts with water to form CO_2 and inhibits the polymerization. After sand extraction, the impurities are eliminated, the fineness indicator AFS is regulated with elimination of small or big particles, the sand is washed and dried. In fact humidity during core conservation is a critical factor that is strictly controlled in foundries.

Other sand types as chromite and zircon are also able to fight veining defect especially due to their low thermal expansion and high density. Bauxite sand is an alternative for improving the bonding power due to its specific surface shape as shown in Figure 2.5. But finally only chromite is used in aluminum foundry because of its higher density together with improved thermal conductivity.

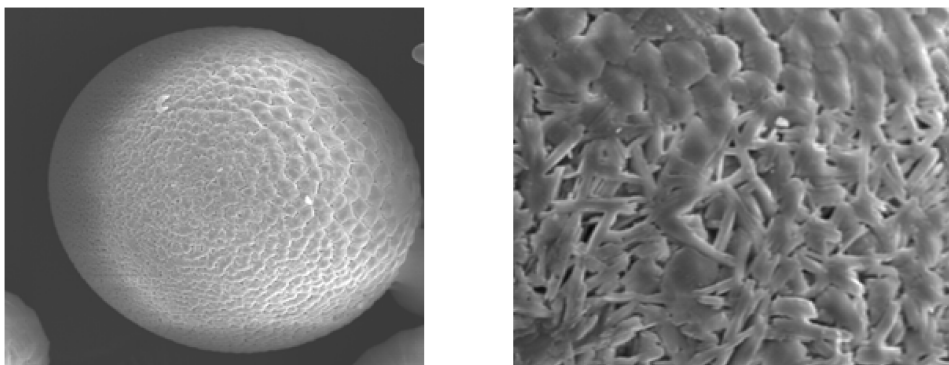


Figure 2.5: Bauxite sand and its surface texture [Ide12]

2.3.3 Structure of the PUCB sand

The structure of the PUCB bonded sand has been well studied and controlled in foundries. After mixing the sand and the binder, resin bridges between grains are formed as a result of the polymerization process with the addition of the catalyst. This is shown in Figure 2.6 presenting a SEM observation we performed on a core sample in the present work. In

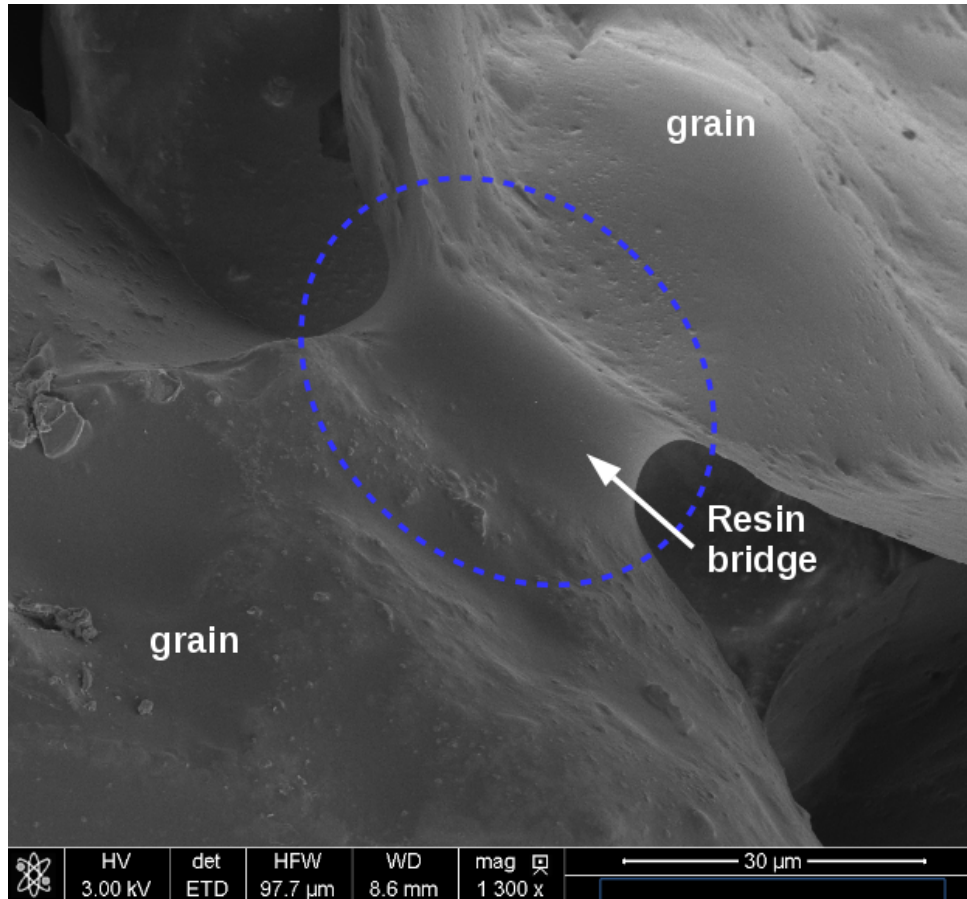


Figure 2.6: Resin bridges between two sand particles [Bar17]

[Boe85], the study showed that the binder has a thick layer and an internal global structure with cavities. In [Ide12], observations of Polyurethane bridges showed the presence of various phases with different densities (Figure 2.7). Four different phases can be observed. According to [Ide12] their formation and structure depends on the directional hardening caused by the catalyst gassing, the reaction rate and the solvents used.

- Phases 1 and 2 form a slightly porous dense layer with a rapid hardening and the solvent is dispersed to the outside.
- Phase 3 corresponds to the presence of a porous layer presenting a slower reaction.
- In phase 4 the material has a highly porous to coral-shaped microstructure with a very slow reaction and solvent surplus.

The different reaction rates throughout the bridge cross section are assumed to be caused by the gaseous amine advancement from the edge to its center and the displacement of the solvent into the edge occurring during Polyurethane transition from liquid to solid. The catalyst itself whether it is more or less reactive has an influence on the binder hardening. In the coldbox process where tertiary amine is used, dimethyl ethylamine “DMEA” has shown to be more reactive giving a larger layer of phase 2 and much less of phase 3 thanks

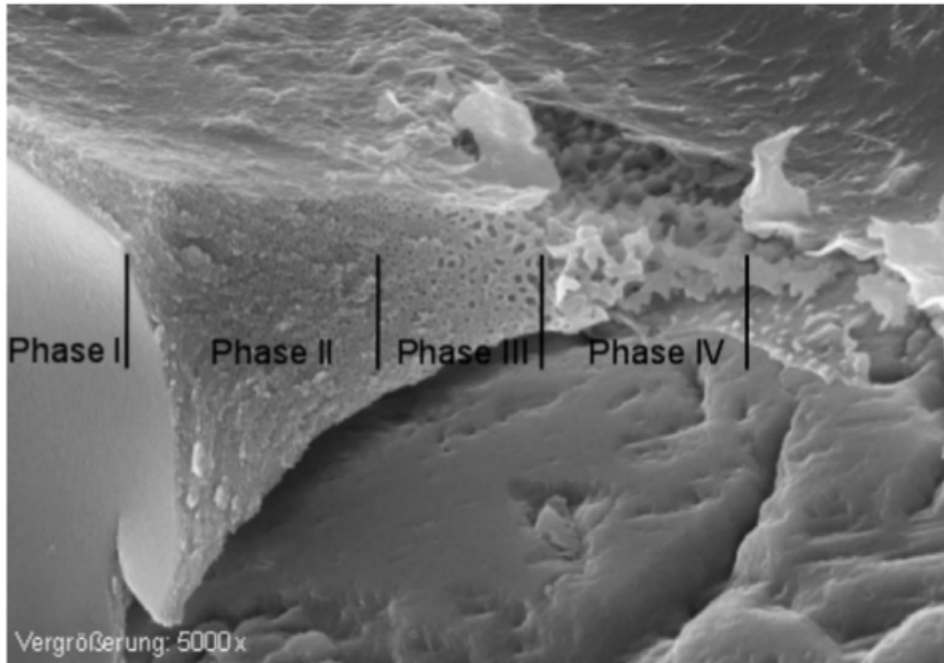


Figure 2.7: Cross section observation of PU bridge [Ide12]

to its molecular structure [Ide12]. This structure is totally different from that obtained by the PU-No-Bake process where the liquid catalyst is equally distributed in the binder giving rise to a uniform structure with simultaneous activation of the hardener different groups and therefore a simultaneous hardening across the bridge cross section as shown in Figure 2.8

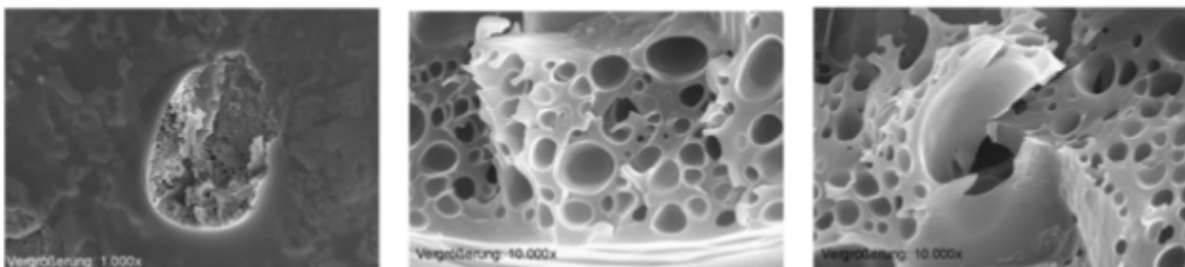


Figure 2.8: Bridge structure with the PU-No-Bake process [Ide12]

On the other hand, a higher sand temperature also accelerates the reaction, as shown in Figure 2.9 where phase 1 has risen from 27 to 43% for respectively 20 °C and 30 °C and phases 3 and 4 were reduced by 8%.

In the Coldbox process, about 20 to 40% of solvents are added. The percentage of solvent is an important factor regarding the binder hardening. Variations of the solvent rate used in coldbox process give rise to more or less cavities. The structure of a solvent-free binder introduced in the shell process is different. It is a massive bridge, dense and slaty with very few inclusions given in Figure 2.10.

According to [Ide12], the solvent is responsible for the inclusion formation. It is displaced, then remains trapped in the structure and forms pores which shape and size depend on the solvent and its properties. After demolding, it was found in [Ide12] that the core strength is increasing with the storage time. The final strength giving the optimum

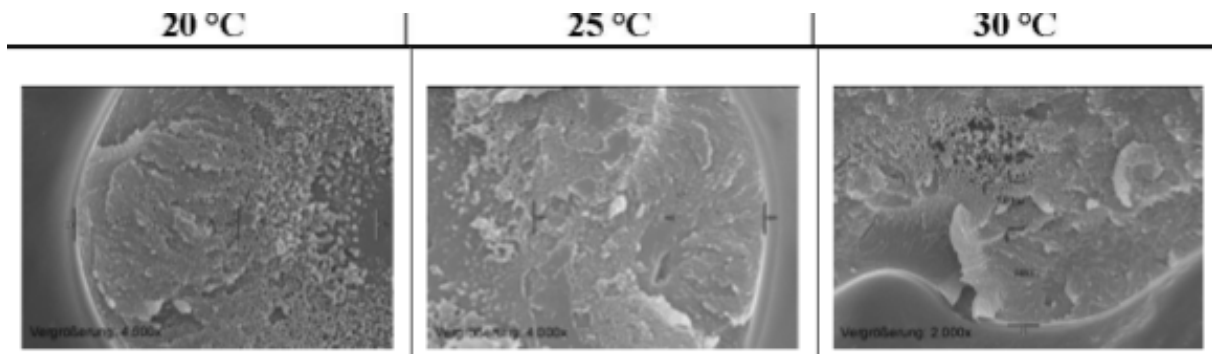


Figure 2.9: Variation of the different phases when increasing sand temperature [Ide12]

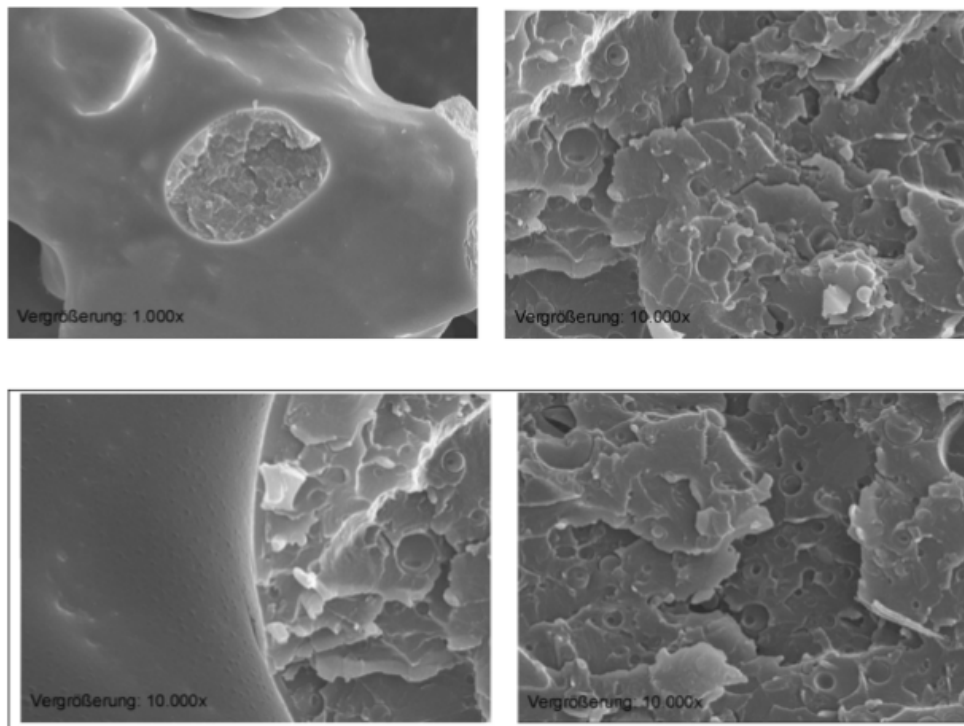


Figure 2.10: Binder bridge of a shell-moulding core [Ide12]

core quality and no casting defects was reached in 24 hours. Unwanted post-hardening was obtained with 20% strength increase within a week. This effect was assumed to be independent from the basic components but linked to polyurethane post-hardening.

2.4 Characterization of the molding material

2.4.1 Green sand characterization

Modeling the whole casting process is far from being completely resolved or documented. The computation process involves a fluid mechanics code, thermal computations and solid mechanics and structures code. Classical works were mainly focused on modeling the filling and solidification of the metal in order to predict the feasibility of the cast (correct filling, porosity control) and to examine the properties resulting from the thermal history in the metallic cast (dendrite size, precipitates). Codes such as MAGMA¹, Thercast²,

Procast/Quickcast³ are used for this purpose.

Thirty years ago [Sam85], works done in industry enabled to make progresses towards incorporating the exchanges at the sand-metal interface [Met01] or to take into account an large number of parameters influencing casting quality [Kar07]. More recent developments result in different filling strategies, allowing to detect impurities and defects, to control the duration of the exposition to air and oxide growth [Pan14]. Besides from these numerical aspects, recent studies highlight the importance of experiments to validate the numerical models. Industrial examples of the use of test bench for thermal measurements were made in [Sul12] and are now available in the academic field ([Mot12,Mot13a]. However, the interaction of the liquid and then the solid metal with the sand mould is far from being easy to understand. In [Kov12], efforts were made to take into account the thermal properties while in [Mot13b] and [Ino13], dynamic measurements of the applied load by the mould and the contraction of the solid were carried out.

In order to improve the design, that is being able to realise complex and thin wall castings, it becomes crucial to qualify high-quality performance of the mold or the core, then to incorporate mould and core characterization and modeling into a foundry casting process optimization system. Up to now, the characterization and finite element modeling of the thermomechanical behavior of the mould-cast set are often unsuccessful except from [Mon09]. The study of the behavior of sand moulds and cores is still the main obstacle.

It is surprising to see that twenty years ago ambitious attempts were made but not pursued. In these works, humid clayey sand (green sand) is tested (formed by mixing: silica particles 88.7%, clay 6.73 %, water content 3.36%, mineral carbon: 1.2%). The objective was to investigate and take into account the different thermal, hydric and mechanical mechanisms. In [AS96], uniaxial compression tests were performed on green sand specimens at different strain rates. The results showed no sensitivity to strain rate up to 600 °C. An elastoplastic behavior model derived from the soil mechanics formalism was used. It will be detailed in the next section. For the calibration of the model, triaxial tests, uniaxial compression tests, isotropic compression tests and die pressing tests were carried out. The model was developed, calibrated and the needed physical parameters were obtained in the temperature range 20-300 °C. An original triaxial apparatus has been built allowing a temperature of 800 °C and a pressure of 4 MPa to be reached and used to perform tests for the model validation.

In [Azz95], a phenomenological approach was adopted. The initial composition of each phase and the mould compaction were investigated. The evolution of the thermomechanical parameters as a function of temperature and moisture content were studied using different thermophysical and thermomechanical analyses. An elastic non-linear model was adopted. A triaxial test procedure was developed in order to perform experiments up to 1000 °C. The effect of temperature, hygrometric degree and compaction on the material reponse and its microstructure were studied and supported by a series of tomographic analyses. The initial hygrometric degree was taken into account in the model, the evolution of the hydric and anelastic deformations as a function of temperature as well as the damage development, due to the evolution of the different material phases and material properties, were presented.

In fact, the sand type and the wall thickness influence the final casting quality as

¹<https://www.magmaflow.de/en/>

²<http://www.transvalor.com/fr/cmspages/thercast.6.html>

³<https://www.esi-group.com/fr/solutions-logicielles/fabrication-virtuelle/fonderie/procast-quickcast>

shown in [Sai12] and [Sun12] for steel castings. This interaction with the metal is established through the thermomechanical properties of the foundry sand and still needs to be fully investigated during casting while taking into account the eventual transformations in the material.

2.4.2 Characterization of the resin bonded sand cores

2.4.2.1 The mixture sand-binder characterization

Among all these experimental and numerical advances, the mechanical, thermo-physical properties of resin bonded sand cores and their evolution as a function of temperature remain a too-often neglected part when dealing with sand molding. Very few studies were published about experimental characterization of the sand core, apart from unpublished studies developed by binder suppliers for their own products or foundries.

For chemically bonded sands, the existing works focus mainly on varying the type of binder and its amount as in [Gon11]. In [Sta06], a statistical study was made on silica sand core from different origins, different solvents, phenolic base resins, resin percentages and testing laboratories. The resulting impact on the final sand core strength was investigated.

The evolution of mechanical properties such as the elastic modulus and high temperature strength of various types of bonded sands has been investigated by [Thi08]. Bonded sand cores using epoxy acrylic resin, Polyurethane cold-box and resin coated sands were tested under uniaxial compression on standard cylindrical specimens and tensile tests were performed on a standardized geometry developed by the American Foundry Society (AFS), the so called “dog bone” given in Figure 2.11. They observed a decrease of the core strength up to 200 °C which was related to the solvent evaporation from the resin. It is followed by an increase between 200 °C to 300 °C which they supposed to be due to a possible secondary polymerization of the degraded urethane polymer chains. A further heating causes a decrease of the material strength. A higher strength in the compression tests was obtained in comparison to the results of the tensile tests which is a typical characteristic of granular materials. They concluded that the epoxy system has the fastest loss of strength with temperature. The coated sand showed an initial strengthening and was continuously degrading during heating while the polyurethane resin sand core maintains its strength longer and presents a secondary strengthening stage.

In the same perspective, researchers were interested in the elastic behavior of the bonded sand core. An evaluation of the elastic modulus for Polyurethane No-Bake (PUNB) sand was done in [Tho10] during heating and cooling using three point bending specimens. They found a dependence of the measured elastic modulus in heating rate for temperatures above 125 °C as shown in Fig.2.12. The elastic modulus decreases drastically during heating up to 100 °C and then increases until 350 °C which they believe can be related to the chemical reactions in the binder.

Having in view solidification modeling, [Cay10] performed an experimental investigation of the thermomechanical behavior of Polyurethane No-bake cold-box cores (addition of a liquid catalyst to the silica particles and the phenolic part of the resin, mixing and addition of the hardener art). Tensile tests on dog bone specimens were performed at room temperature with different strain rates. A higher force was obtained with a high strain rate showing then a strain rate dependency. Uniaxial compression tests were also

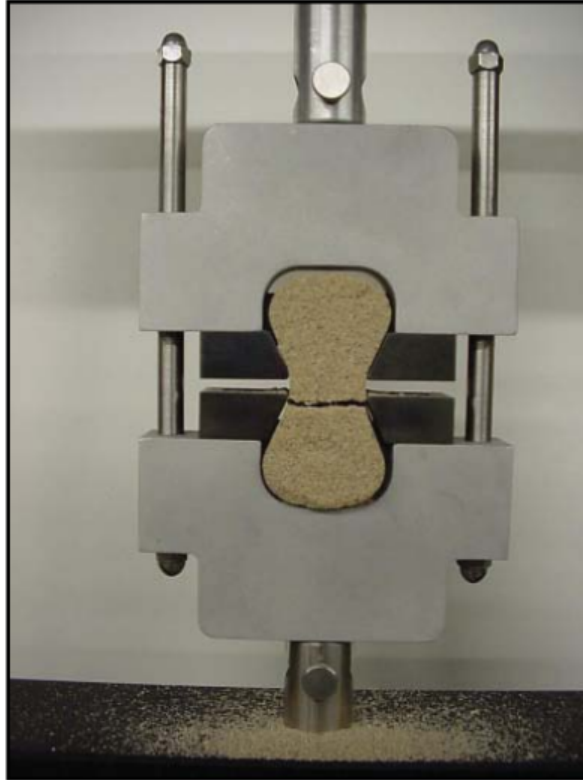


Figure 2.11: “Dog bone” sand core specimen developed by the American Foundry Society

performed at different temperatures up to 600 °C but without any investigation of the material behavior mechanisms. The specimens were heated using an inductor as shown in Figure 2.13 instead of an oven in order to reach the reference temperature as quickly as possible. This enabled to apply a heating rate of approximately 10 °C /min. The maximum strength was found to decrease down to 200 °C followed by a small increase up to 500 °C as summarized in Figure 2.14. An other decrease is observed at higher temperature . The same trend is found in [Thi08] but with a difference in the temperature range. This is probably due to the differences in the resin compositions, solvents. . .

In a recent study, [Sta16] investigated the properties of sand cores with four different types of binders. They were focused on the core behavior at room temperature and different storage times. Three point bending tests were used to evaluate the core strength and elastic modulus. The obtained results show an elasto-plastic behavior prior to fracture with dependence to the loading rate.

The majority of these studies were developed for the No-Bake proces used essentially in steel castings. In this context, the effect of the sand core expansion on the casting was investigated. It was found that the expansion of bonded silica sand causes a volume increase sharply until 570 °C , temperature at which a phase transformation of the silica particles from alpha quartz to beta quartz takes place causing then a distorsion of the cast. With further heating, the sand tends to shrink due to softening at the surface of the sand grains that causes veining defects. While in our study, for aluminum casting the maximum temperature reached in the core is 450 °C only, these transformations are not to be taken into account.

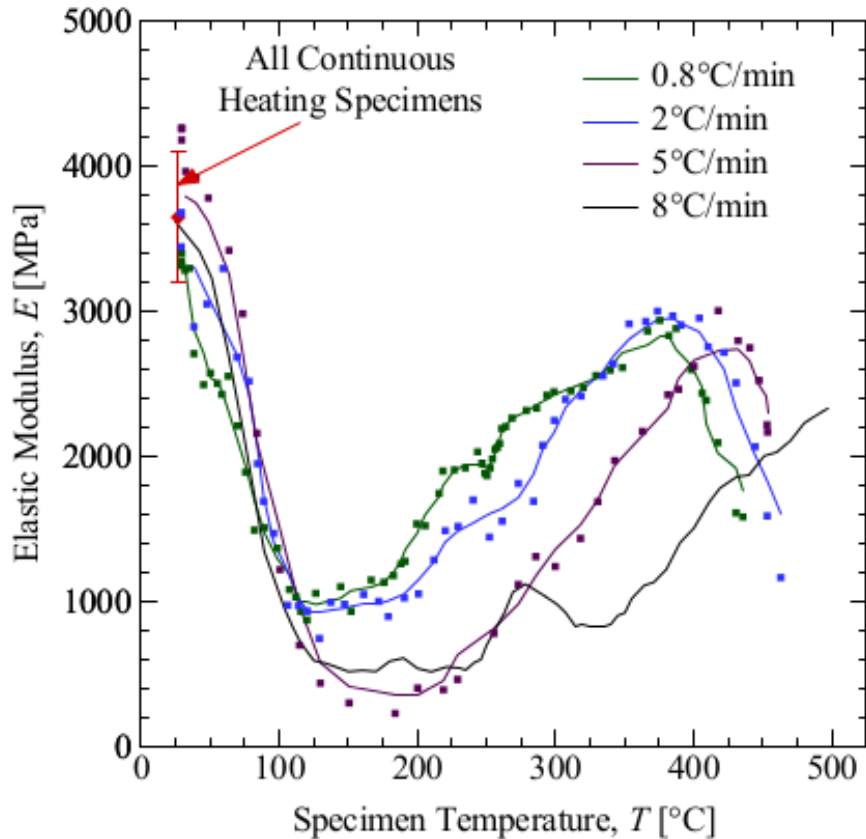


Figure 2.12: Variation of the elastic modulus with the temperature and heating rate for PUNB process[Tho10]

2.4.2.2 Binder characterization

The interest of the authors in the thermal behavior of the phenolic binders is recent. [Gie09] performed a thermal analysis of the phenolic binders used in PUNB process by means of a Dynamic Scanning Calorimetry (DSC) analysis under a Nitrogen atmosphere and a heating rate of 10 °C/min. They found that the resin undergoes a decomposition process up to 420 °C. Other works dealt with defects due to gas emission and binder cure during casting. Blowholes and pinholes are the most common as seen in [Rah93] and [Gib08]. In commercial simulation softwares, there are models which have been incorporated in order to take into account gas emissions during binder cure [Sta09a]. However, the evolution of the mass and the molecular weight as a function of temperature are still missing data. Recently, a step forward was made thanks to a simulation of the binder gas evolution with experimental data [Sam12,Jom14]. For this purpose, chromatography and thermogravimetric analyses were conducted on PUCB and PUNB binders.

2.5 Generalities about polymers

In this section a review about polymeric materials is presented, specifically polyurethane polymer.

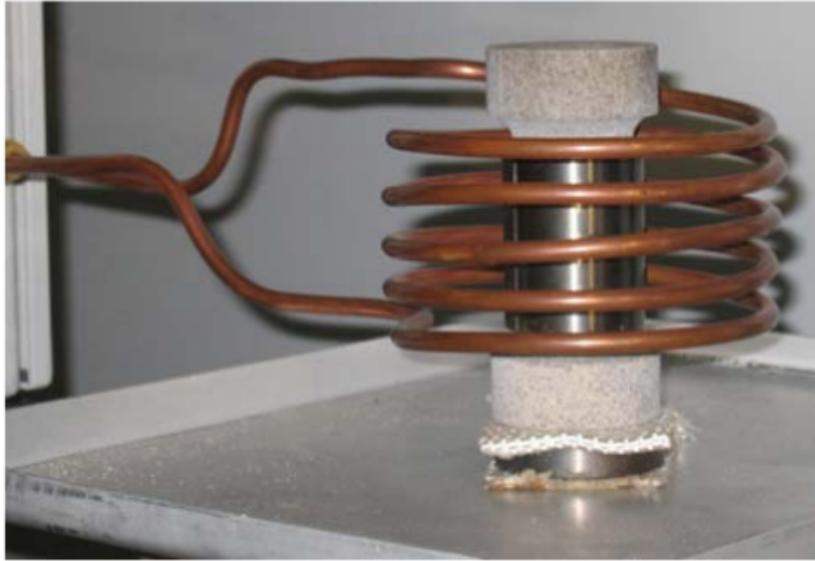


Figure 2.13: Heating of a sand core specimen using an induction coil [Cay10]

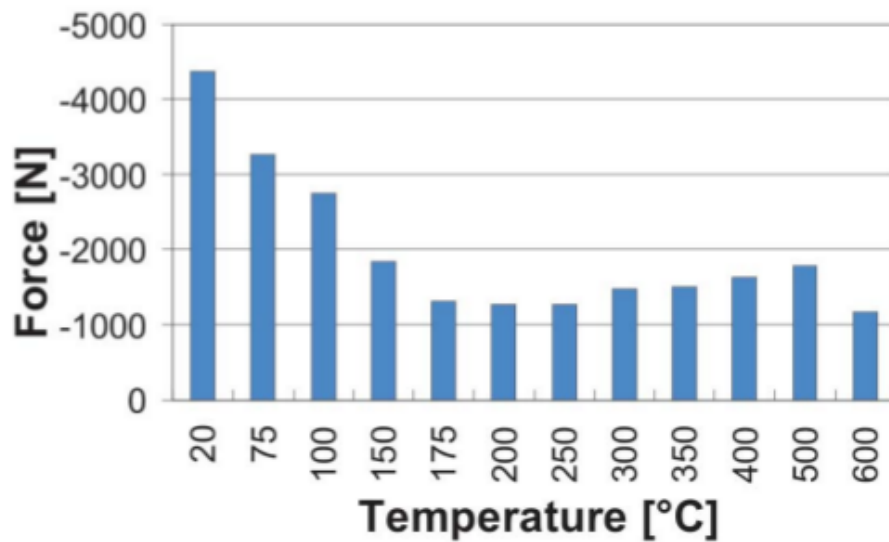


Figure 2.14: Maximum strength in compression test up to 600 °C [Cay10]

In general, polymers differ in characteristics because of their structural complexity. By definition, polymers are linkages of repeating structural units, peeled monomers. The chemical structure, the functionality of the patterns, or the type of polymerization are all ways of classifying them. However, the most used criterion is based on the response of these materials to temperature, thermoplastics group on one side and thermosetting group on the other, so that the properties of individual members in the same group may present large variations. A new nature of the pendant groups, of the arrangement of the monomeric units or a modification in the reaction conditions or the catalysts may tremendously change the properties. Specifically, the various transitions during heating and the thermomechanical properties are specific to each polymer binder.

2.5.1 Thermoplastic polymers

A thermoplastic has a linear structure of monomers bonded by Van der Waals, dipole-dipole or hydrogen links. They are generally linear polymers which may have sometimes ramifications [Tho99] and a high molecular weight. For increasing temperatures, the loss of strength of the connections causes a drop of the rigidity [Par11], reaching a behavior close to a fluid above a certain level. This is an important characteristic since the reversibility of the thermoplastics allows its heating and cooling several times during molding. They are used in the molten or softened state and are referred to as thermostable when they retain their mechanical properties at a temperature greater than 150 °C [Bri16]. As a result, they can be used over a wide temperature range. During thermal degradation, they emit very small gas quantities which is also an advantage. There is two types of thermoplastics: amorphous and semi-crystalline.

Amorphous thermoplastics. Amorphous thermoplastics can be considered as a solid having no molecular order at large distances [Par11]. They have only one characteristic thermal transition, glass transition. Before this transition, the polymer is in the vitreous state; after this transition, it is in the rubbery state [Hau01]. When the amorphous thermoplastics are thermostable, the glass transition is located at high temperatures. Although these thermoplastics present interesting thermal and mechanical properties, their low resistance to solvents due to the lack of crystallinity limits their use.

Semi-crystalline thermoplastics. The semi-crystalline thermoplastics have an amorphous phase and a crystalline phase, so that they present two transitions, vitreous transition and fusion. The crystallinity of a polymer strongly depends on the thermal history it has undergone, which can considerably alter its thermomechanical properties. Indeed, the cooling rate and annealing may modify the degree of crystallinity or the morphology of the crystal structure. Namely the crystallinity rate increases when the cooling rate decreases, which implies an increase in the elasticity modulus and a decrease in impact resistance [Bri16].

2.5.2 Thermosetting polymers

Thermosets are the most frequently used because of their mechanical properties and their stability once processed. In contrast to thermoplastics, a thermoset hardens during the polymerization by forming a three-dimensional network of monomers linked by covalent bonds [Bri16]. The transformation is unique and gives rise to the final piece [Pas02]. More precisely, the formation of the three-dimensional network is a function of the reactivity of the monomers. Ideally, a complete polymerization (that is a reaction of all the functional groups) ends with the best chemical stability and optimum mechanical properties. In reality, it is difficult to obtain a complete cross-linking (formation of linkages, entanglements between segments or groups) due to the remoteness of reactive groups during the reaction. The topology of the reticulated network thus comprises spatial heterogeneities, that is to say nodes with variable cross-linking densities embedded in a matrix where the polymerization rate was different. Nevertheless the reaction remains irreversible, and the only way to change the resulting structure is to break the molecules during thermal degradation as described in [Par11].

2.5.3 Polyurethanes

In this section we are interested in Polyurethane since it is the binder chosen for the sand cores studied in the present study. Polyurethane, usually referred to as PU, comes from the family of chemicals known as the urethane polymers. It is formed of two principal raw materials: isocyanates and polyols, brought together with catalysts and a variety of additives [Efs11].

In practice, several phenolic compounds can be employed to produce the polyol (phenolic resin) used to prepare the polyurethane resin, for instance phenol, cresol and xyleneol ([Lai85,Gar86]). According to [Mar81], a mixture of phenol and alkylphenols is most often used for the preparation of the phenolic resin in the PUCB process.

On the other hand, isocyanates, characterized by the group NCO, are the key products required for the formation of polyurethane polymers. Isocyanate may be aliphatic, alicyclic or aromatic. Polyisocyanate means that many functional groups are introduced. In the PUCB process, it is preferable to use polyisocyanates which contain up to five functional groups [Lai85,Gar86]. Among this variety, the aromatic polyisocyanates are the most used, essentially diphenylmethane diisocyanate (MDI) and toluene diisocyanate (TDI) [Lai85,Gar86]. The reason is that materials in the aromatically linked isocyanate group are much more reactive and cheaper. According to [Tri99] the MDI polyisocyanate is the most frequently used in the PUCB process.

Catalysts have a key role in PU production as they maintain the balance between the reaction of the isocyanate and polyol. Polyurethane catalysts can be classified into two categories, amine compounds and organo-metallic complexes. Tertiary amine catalysts are generally used for isocyanate-based polymers.

Apart from the basic raw materials, polyisocyanate and polyol, additives are also required for producing polyurethanes. Crosslinking agents and chain extenders which are both low molecular weight diols or triols and diamines are introduced. The network density of the PU polymer can be controlled using crosslinking agents and chain extenders. Urethane structures are obtained with *OH* crosslinking agents. The general formula of a urethane unit is given in Figure 2.15.

A broad spectrum of properties gives polyurethanes their versatility. This is achieved

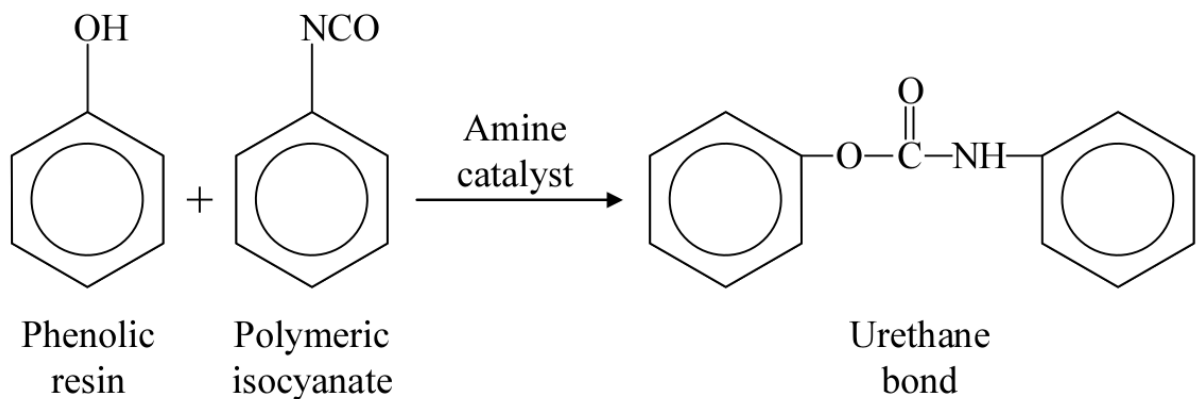


Figure 2.15: General structure of a urethane polymer [Efs11]

thanks to the selected components as shown in [Efs11]. Polyurethanes vary from flexible to rigid and solid by suitable combination of the starting materials. The variations of the chain length and the degree of branching or crosslinking determine the molecular structure. The polyaddition of MDI with long chain diols for example produces linear, segmented

polymers. Reversible crosslinking takes place by crystallization of the rigid segments consisting of MDI as shown in Figure 2.16, while polyols (*OH* groups) with polyisocyanates lead to a crosslinked polymer structures typical of thermosetting polyurethane. The high network density is usually further increased by using excess isocyanate, which results in additional crosslinking points as presented in Figure 2.17. The polyols form the flexible segments in polyurethane, while the polyisocyanates, combined with chain extenders or crosslinkers, constitute the rigid segments.

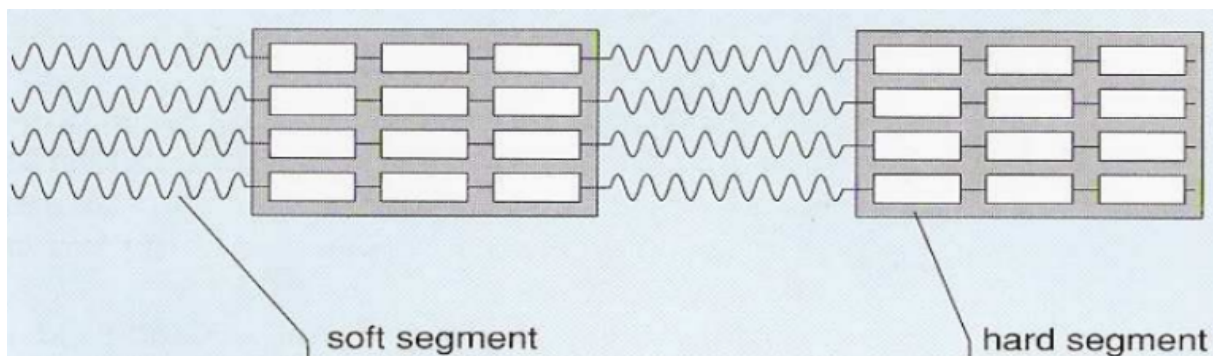


Figure 2.16: Morphology of thermoplastic polyurethane [Efs11]

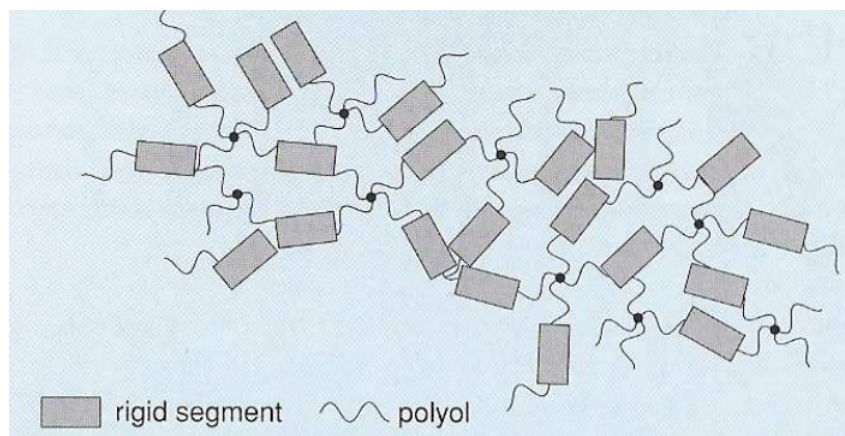


Figure 2.17: Morphology of thermosetting polyurethane [Efs11]

2.5.4 High temperature properties of polymers

When a polymer is exposed to high temperature, its stiffness and its resistance decrease with increasing temperature due in particular to heat softening. The common behavior of linear amorphous polymers is presented in Figure 2.18. Four regions of viscoelastic behavior are found, namely the glassy region, characterized by a very high value of the modulus, the transition region from glassy to rubbery-like consistency, the rubbery plateau at much lower modulus values, and finally a flow region at high temperature (see [Bri91,Bri16] and also [Pas02]). These areas may be explored by means of “Dynamic Mechanical Analysis (DMA)”. The behavior of polymer molecules in each of these regions is very different. In a polymer, the atom motion is related to their “free volume”, which is small for low temperatures and increases dramatically above the glass transition temperature. In thermoplastic

polymers, the bonds between individual chains are secondary and the free volume is sufficient for local chain motion. In thermosetting polymers, interchain interactions between crosslinked sites are also secondary bonds and motion of these segments is similar.

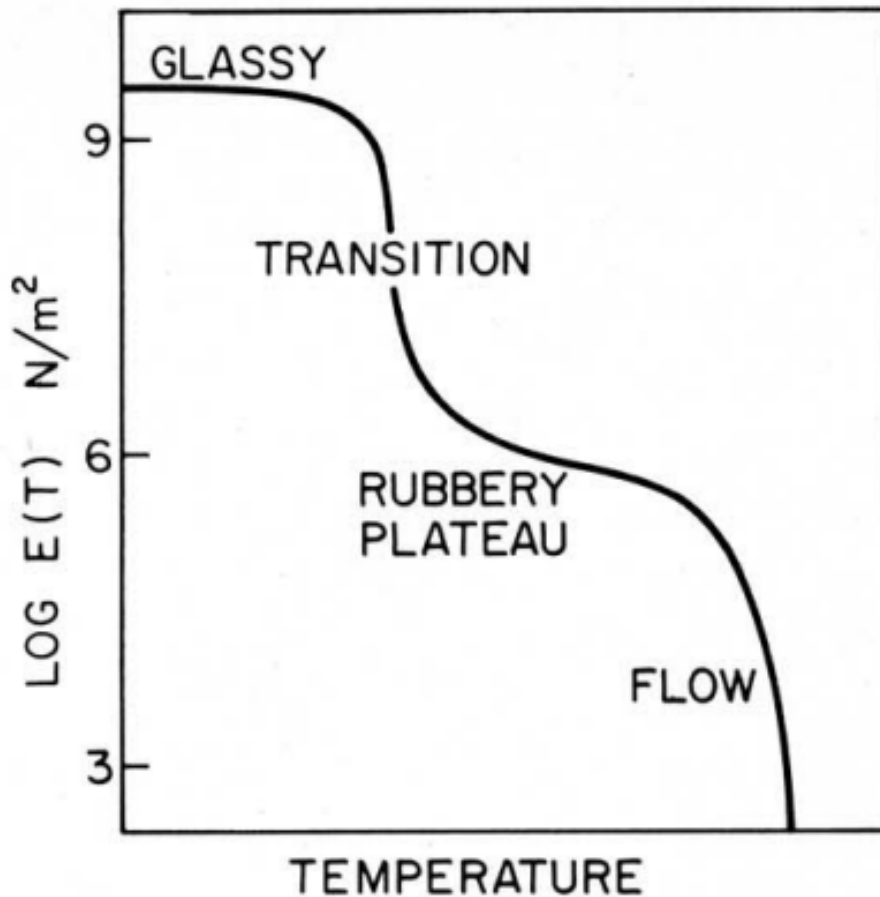


Figure 2.18: General schematic modulus-temperature curve showing the four regions of polymer behavior.

Glass transition. In the glassy domain the relatively low values of temperature result in limited extents of molecular motion. Short range motions of side chains on the polymer backbone or perhaps limited backbone motions involving short segments of chains take place. Below the glass temperature (T_g) the mobility of the molecules is strongly curbed by intermolecular interaction [Bri16,Efs11]. Position change is not possible, and only restricted thermal induced movements of chain segments or side chains are present. At the glass temperature, micromobility of chain segments and side chains starts to occur and the material becomes softer but it is still mechanically stable. Before reaching the glass temperature, second-order relaxation processes are possible, thanks to a restricted mobility of single-molecule segments. Then, as temperature increases, the segments of polymer chains have enough energy to overpass the local barriers which prevent molecular motion to occur. In this range, motions at a scale of ten monomer units may occur.

Flow regime. At higher temperatures, even longer range motion involving large chain segments becomes possible. However, as long polymer molecules are entangled, whole scale translational motions of polymer chains are forbidden, leading to the well known

rubbery plateau. The hindering influence of intermolecular interaction decreases until flow temperature (T_f), where complete macromolecular chains can slip against each other [Bri16]. At higher temperatures, molecular motion is so extreme that even chain entanglements are no longer effective in restricting molecular flow, and a liquid-like regime is obtained. This is specific to amorphous structures. They become softer and softer and start melting. No chemical degradation of the macromolecules of the plastic will occur in this state.

Crosslinking. Crosslinking, that is covalent bonding of one chain to another, results in permanent restrictions to flow which do not slacken with increasing temperature. Thus, a crosslinked polymer does not exhibit a flow regime [Efs11,Pas02,Bri16]. In crosslinked thermosets, the modulus depends on the number of chains that must be deformed to lengthen the specimen. In Figure 2.19, an example of the evolution of the modulus is given, for various polymer structures. Structure A is for a crystalline polymer. Structure C represents the behavior of an amorphous polymer, while structure B corresponds to a crosslinked polymer. In the latter case, for a highly crosslinked polymer, the density of network chains is high and thus the modulus becomes large.

Moreover in thermosetting polymers additional crosslinking may take place. Two cases are found. First, after the glass transition, a molecular chain gain in mobility and additional crosslinking may appear. In the second case, when a polymer is heated, and if there is an incomplete cure during forming, additional crosslinking can be obtained. In fact, this is because temperature is considered as a polymer curing catalyst [Bri16].

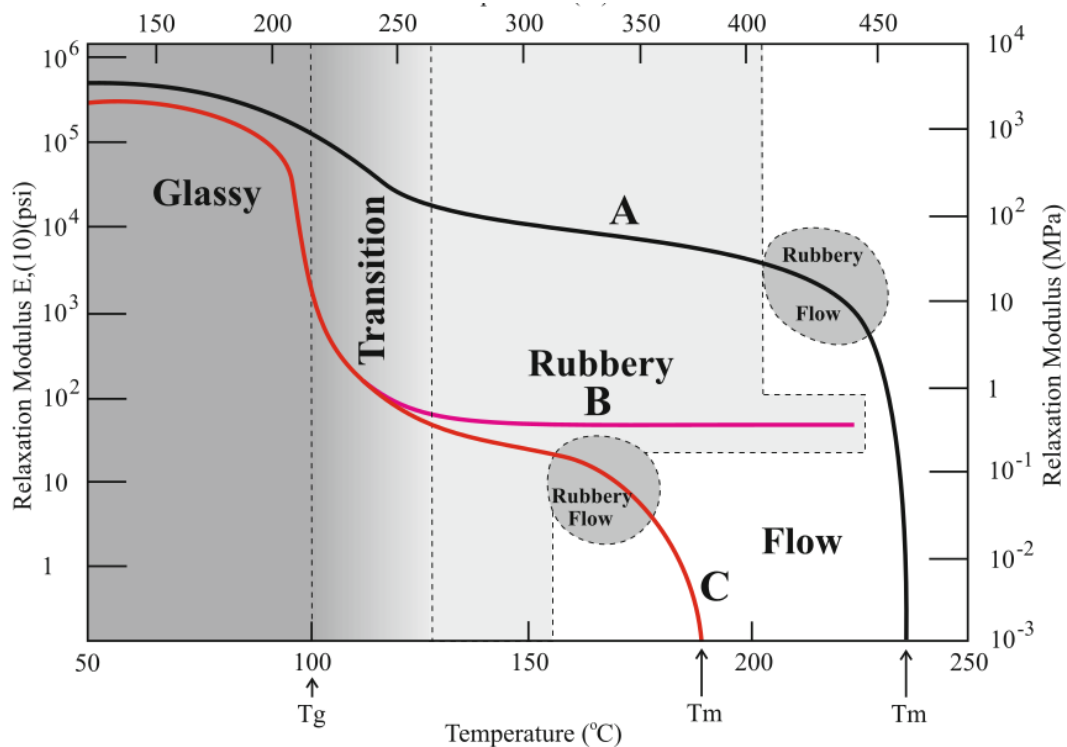


Figure 2.19: Changes in the schematic representation of modulus-temperature behavior of a polymer caused by cross-linking and crystallization [Bri16].

Thermal degradation. When exceeding the decomposition temperature, the macromolecules start to decompose. The corresponding chemical changes are irreversible. These phenomena are referred to as “aging”, either chemical or physical [Bri16]. Chemical aging comes in the case of changes in molecular weight or extent of crosslinking, breaking or forming of chemical bonds, while physical aging suggests structural and property changes. No change in chemical structure occurs during physical aging. At high temperatures, there are changes in molecular weight or crosslink density which result from the exposure to elevated temperatures. At a certain temperature, chemical changes may also be affected by other factors such as moisture, radiation, applied stress... The relation between time, temperature, and chemical structure for thermosets was developed by [Aro86], who present the time-temperature-transformation (TTT) cure diagram. Physical aging results in decrease in the specific volume and in molecular mobility. As a consequence, there are changes in mechanical properties such as increasing modulus and yield strength and decreasing toughness [Tan81,Str77,Kon86]. This has been investigated when dealing with high temperature reponse of a polymer matrix composite. The authors found that this may affect the mechanical properties of the overall composite [Kon86,Sul90].

Thermomechanical Properties of Polymers. Up to the onset of thermal decomposition, the thermomechanical properties of polymers have been extensively studied [Fay08,Joh13,Lie12,Bri91,Bri15,Joh05,Tob60,Joh10]. In general authors consider tests like stress relaxation, creep, or dynamic mechanical analysis [War93,Bri08,Bil03]. Some of them were interested in studying the behavior during material processing in order to estimate the material properties and aging prior production [Joh13], while in [Lie12], the authors worked on the simulation of the curing-induced viscoplastic deformation taking into account chemical shrinkage and thermal expansion. The response of polymers under high temperature service has been also investigated in composite parts for aerospace applications. At moderate temperatures, chemical and physical aging alters the viscoelastic behavior. Aging-induced changes in viscoelastic properties have been studied and discussed in [Bri16]. Critical problems related to aging and degradation of the matrix are observed. In fact, when submitted to high temperatures, weight loss, variation of properties, damage may take place. It is still difficult to quantify the degradation of the polymer matrix and its effect on composite properties. This is a limiting point when using composite materials in these applications. As discussed before, this temperature range is a domain where mass loss (“pyrolysis”) is present, so that it is necessary to take into account energy and mass balances, gas release and flow. Since years works have been made to model mass loss empirically by using Arrhenius law [Gra93] and combining the diffusion of oxygen with chemical reaction rate equations [Hip94]. Degradation of the matrix and crack propagation have been modeled by affecting the degraded layers different properties [Ped92].

Only recently works were made to model the pyrolysis with incorporating experimental thermogravimetric data as in [Sam12] with application to foundry sand cores and binders.

2.6 Summary

To conclude regarding the polymer aspects, the existing studies regarding the thermomechanical behavior were essentially developed for thermoplastic polymers presenting several transitions unlike thermosets. They are limited to temperatures slightly above glass transition, while thermochemical properties, mass loss and degassing are the main subjects

when dealing with high temperature effects. We can safely consider that the chemical aging subject is not as mature as physical aging. Most importantly, the relation between pyrolysis and its effect on the material thermomechanical properties is still an important topic that has not been fully investigated [Bri16]. This is a major limitation in our work since no data are available on the evolution of the resin thermomechanical properties during thermal decomposition and mass loss.

More generally, in this section, we made a review regarding core composition, structure and the approaches for its thermomechanical characterization. We have observed that the amount of studies about this subject at high temperature is low. In the next section, the experimental protocol used by the company Montupet to characterize the cores is presented and discussed. Then, the new protocol we developed in the present study is detailed.

2.7 Résumé en français

Pour conclure sur les propriétés des polymères, les études existantes sur le comportement thermomécanique ont été essentiellement développées pour des polymères thermoplastiques présentant plusieurs transitions. Contrairement aux thermodurcissables, ils sont limités à des températures légèrement supérieures à la transition vitreuse, tandis que les propriétés thermochimiques, la perte de masse et le dégazage sont les principaux sujets à traiter lorsqu'il est question d'effets à haute température. Nous pouvons ainsi considérer que le sujet du vieillissement chimique n'est pas aussi mature que le vieillissement physique. Plus important encore, la relation entre la pyrolyse et son effet sur les propriétés thermomécaniques du matériau reste un sujet important qui n'a pas été complètement étudié [Bri16]. Ceci est une limitation majeure de notre travail car il n'existe aucune donnée sur l'évolution des propriétés thermomécaniques de la résine lors de la décomposition thermique et de la perte de masse.

Plus généralement, dans cette section, nous avons passé en revue la composition, la structure et les approches utilisées en matière de caractérisation thermomécanique du noyau de fonderie. Nous avons observé que les études sur ce sujet à haute température sont peu nombreuses. Dans la section suivante, le protocole expérimental utilisé par la société Montupet pour caractériser les noyaux sera présenté et discuté. Ensuite, le nouveau protocole que nous avons développé dans la présente étude est détaillé.

Chapter 3

Experimental characterization

Contents

3.1	Sand core thermal history	38
3.2	Study of the industrial sand cores at Montupet	39
3.2.1	Manufacturing of PUCB sand cores	39
3.2.2	Experimental characterization: bending creep tests	41
3.3	Creep bending tests at CDM introducing laser measurements .	46
3.4	Synthesis of the pre-existing tests	48
3.5	Development of a new testing protocol: Experimental methods for resin characterization	50
3.5.1	Differential Scanning calorimetry (DSC)	50
3.5.2	Thermogravimetric analysis (TGA)	50
3.5.3	Dilatometry	50
3.5.4	Dynamic Mechanical Analysis (DMA)	51
3.5.5	Tensile tests	52
3.5.6	Creep tests	52
3.6	Development of a new testing protocol: Experimental methods for sand core characterization	53
3.6.1	Dilatometry	53
3.6.2	DMA tests	53
3.6.3	Compression tests	54
3.6.4	Four-point bending tests	54
3.6.5	Four-point bending tests for temperatures above 300 °C	58
3.7	Results and discussions	61
3.7.1	Resin and core thermophysical characterization	61
3.7.2	Resin thermomechanical characterization	71
3.7.3	Sand core thermomechanical characterization	78
3.8	Summary	89
3.9	Résumé en français	90

This chapter is dedicated to an in-depth experimental investigation of the evolution of the material properties, including bonding resin, which has been neglected so far, and of the damage or physical mechanisms which are involved in the material deformation. The first section is dedicated to the starting point of our work, namely the approach that Montupet recommended to characterize the sand core behavior during casting. In the second section, we show the experimental protocol we defined to study the material and its subsequent evolution.

3.1 Sand core thermal history

In order to determine the temperature range which will be used in the present study, five thermocouples have been positioned on the water jacket core of a "DAIMLER" cylinder head as shown in Figure 3.1.

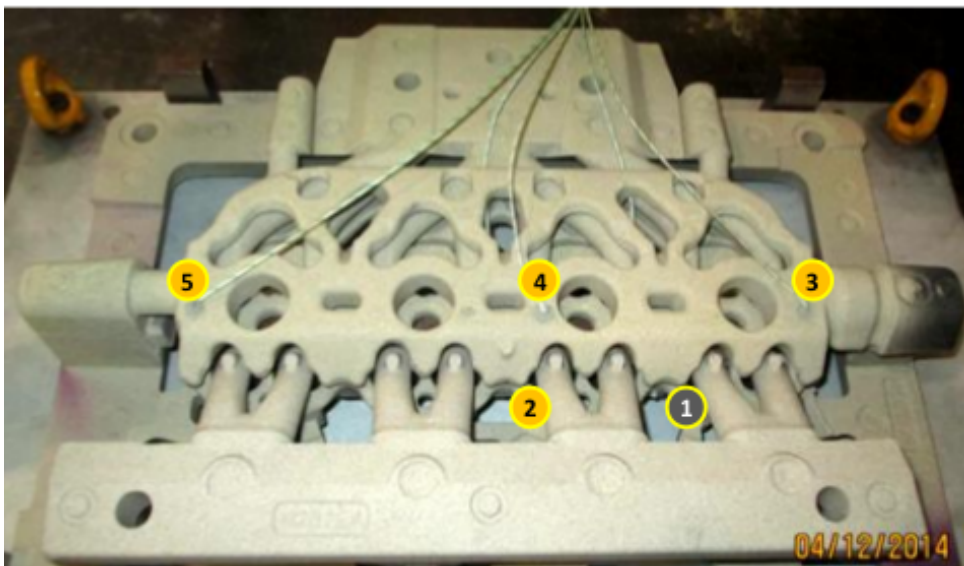


Figure 3.1: Water jacket sand core instrumented with thermocouples prior to casting.

The first thermocouple was used to measure the temperature of the aluminum. The thermocouples 2 and 4 were located respectively at the superior and inferior regions of the core at the center, while the thermocouples 3 and 5 were placed at the edges, close to the metal mold. The temperature was measured during ten minutes after casting. The evolution of the temperature as a function of time is plotted in Figure 3.2.

The temperature of the liquid aluminum is $660\text{ }^{\circ}\text{C}$ before casting. During the filling operation, the temperature drops at $600\text{ }^{\circ}\text{C}$ while the temperature in the sand core reaches its maximum value of $450\text{ }^{\circ}\text{C}$ in about two minutes. The highest temperatures were obtained in the thinner area, at the center of the core, with a thermal gradient of $80\text{ }^{\circ}\text{C}$ between the center and the edges. This information will then be used to determine the temperature range applied in the tests that will be carried out during this study.

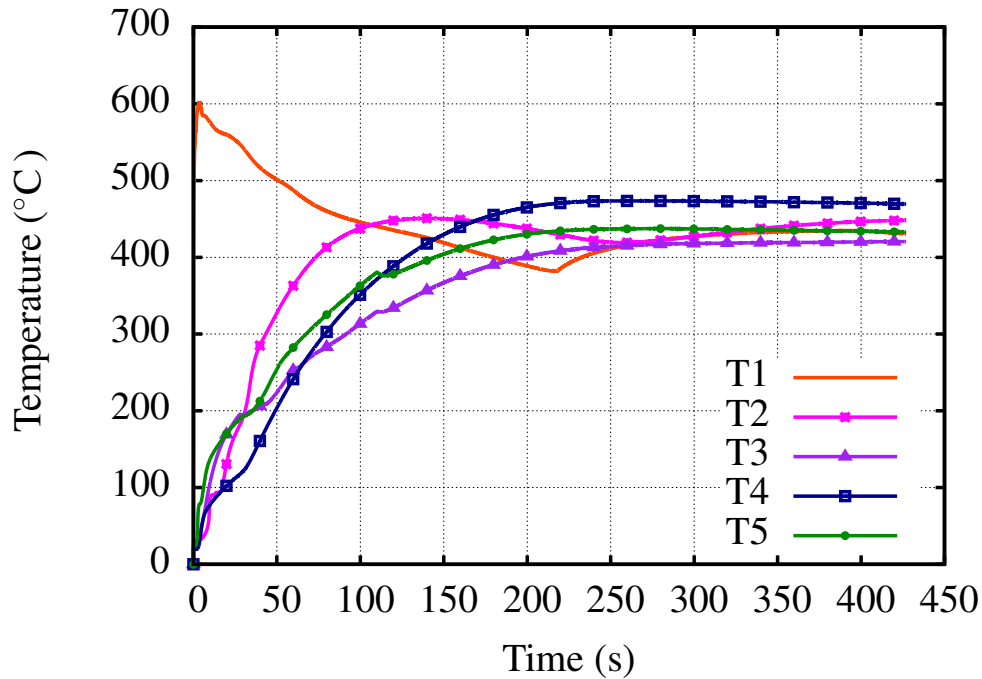


Figure 3.2: Temperature evolution of the aluminum and inside the sand core during casting

3.2 Study of the industrial sand cores at Montupet

3.2.1 Manufacturing of PUCB sand cores

The binder: Avecure 331/631. The coldbox process is used by Montupet Laigneville for sand core manufacturing. Polyurethane resin is used as a binder. There is only limited information about the binder, its composition or properties because of the confidential aspects. The available data are provided by the supplier (see Avecure 331/631 in Appendix A).

A percentage of 1%wt binder is added to the sand (namely 0.5% of phenolic resin and 0.5% of hardener). SEM observations of sand cores (Figure 3.3 showed the structure identified in paragraph 2.3.3 with resin bridges showing dense phase at the edge and more porous phases towards the center. The catalyst used is DMEA in the gaseous state.

The sand: Silica sand. The Silica sand used in Montupet Laigneville is provided by SIBELCO. This is a pure dry sand with 99.5% of Silica (SiO_2). The size of sand particles is a critical parameter, since it determines the final quality and the rugosity of the final core (see paragraph 2.3.2) that will facilitate degassing and impact the quality of the cylinder head. Sand particles are considered as large when their mean size is larger than 2.5mm, fine for sizes smaller than 0.106mm. and average between the two. New sand (not reclaimed) is used in the R&D department, the corresponding grading curve is given in Figure 3.4.

Preparation of bonded sand specimens. Representative specimens of resin bonded sand for the experimental characterization are prepared according to the following procedure:

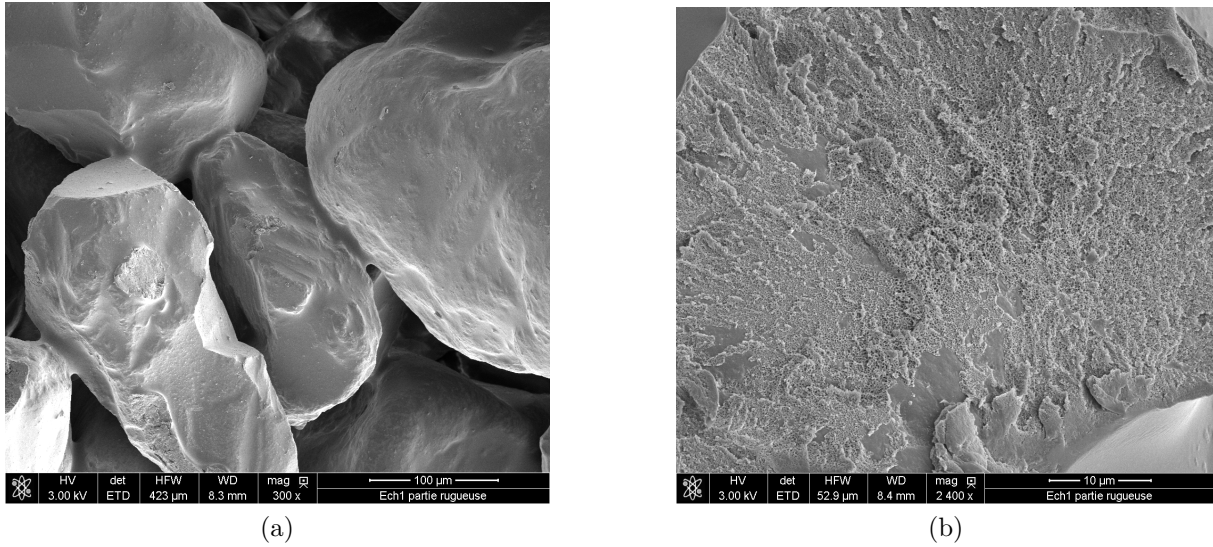


Figure 3.3: (a) Structure of resin bonded sand developed at Montupet (b) Polyurethane resin bridge [Bar17]

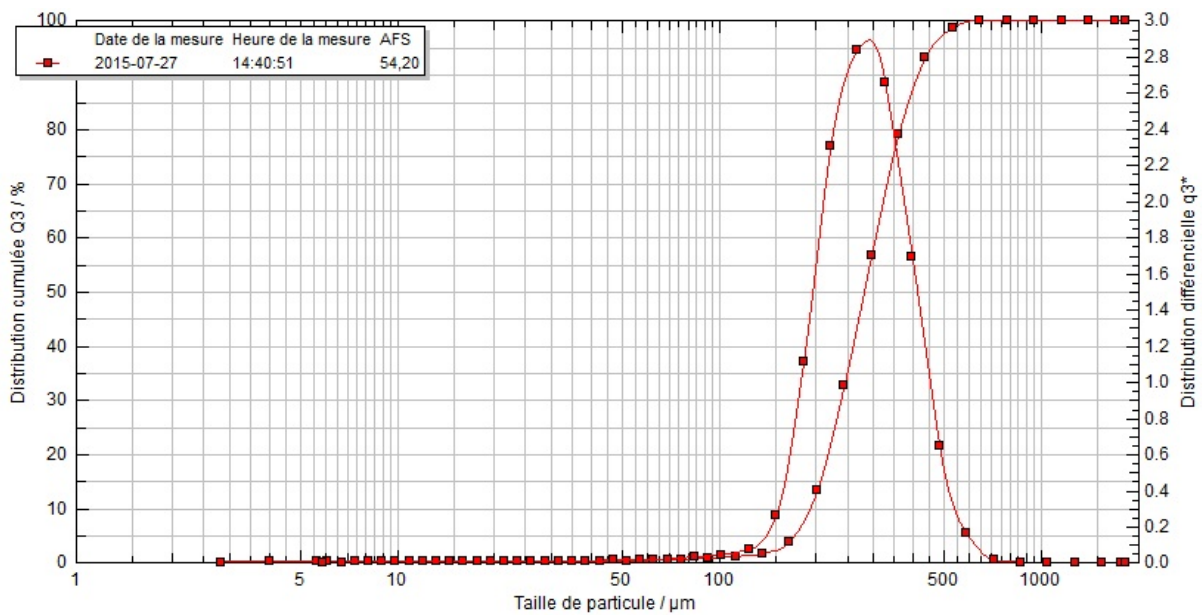


Figure 3.4: Grading curve of new silica sand

1- The basic components are new sand, phenolic resin and hardener in liquid state (Figure 3.5).

2- The sand is mixed with the phenolic resin during 90 seconds. The hardener is added and mixed during 90 seconds. The final mixture (sand, resin and hardener) is blended again during 90 seconds. (Figure 3.6).

3- The mixture is introduced into the container shown in Figure 3.7, then injected

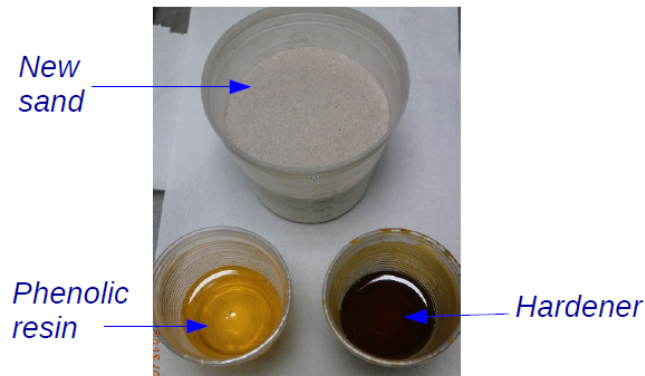


Figure 3.5: Basic components for specimen preparation



Figure 3.6: Basic components mixing

into the core box at a pressure of 3 bars. The amine at gaseous state is sprayed using the gassing plateau and air later on to ensure a homogeneous distribution of the catalyst and evacuate the gases emitted during polymerization.

The total polymerization of the resin takes 24 hours at the end of which the material reaches its optimal strength and a constant porosity. As discussed in paragraph 2.3.3, the material presents some post hardening with increasing storage time and is sensitive to humidity. This is why the specimens are tested 24 hours after coring and kept in a dry environment.

3.2.2 Experimental characterization: bending creep tests

The industrial laboratory of the R&D department of Montupet has developed a four-point bending creep test to study the thermomechanical response of sand core specimens at different temperatures. The experimental procedure is presented below. The results obtained are discussed together with the successive steps proposed to improve our knowledge of the material behavior.

Experimental procedure. Four-point bending isothermal creep tests are performed, with the following operations:

- A specific “dog bone” geometry developed at Montupet is used (Figure 3.8). The

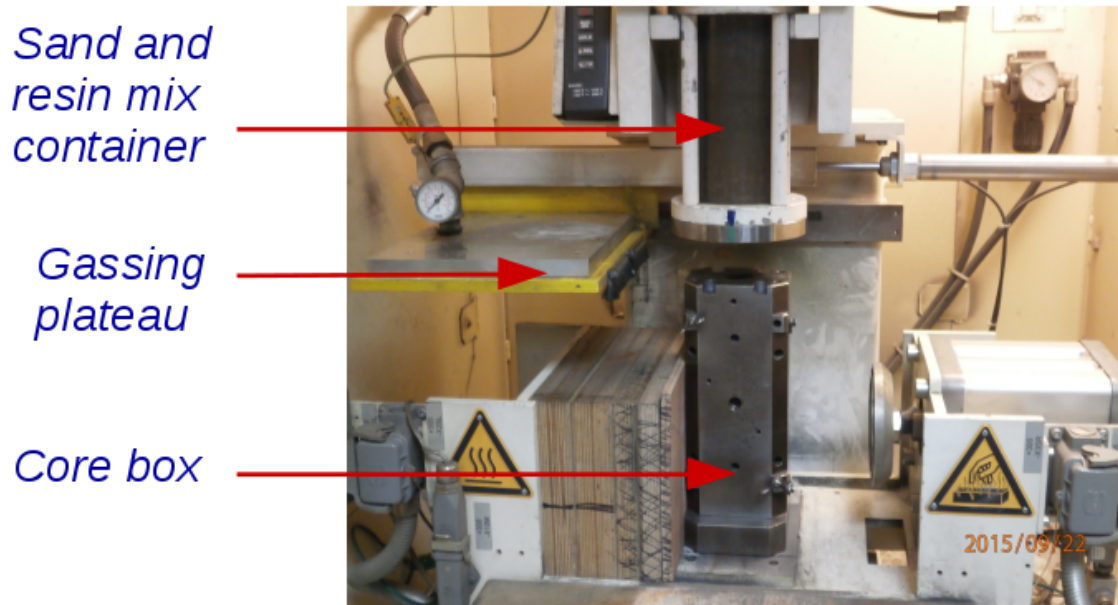


Figure 3.7: The experimental setup for specimen preparation

specimen presents massive parts of 20 mm high and 30 mm wide. It is placed on a metallic support, so that the contact is a surface rather than a point, as is traditionally in bending tests;

- A metallic mass of 75 g is applied to the system. As shown in Figure 3.8, its width is 18 mm only, while the specimen width is 30 mm, so there is no uniform load distribution across the sample;
- A Nabertherm furnace is used. It is calibrated for temperatures up to 1340 °C (Figure 3.9). It can be observed that the furnace volume is way too big compared to specimen size;
- The aluminum melting point being about 660 °C, the temperature range studied goes from 200 °C to 500 °C;
- The temperature indicated for the test is the one given by the furnace and not the specimen temperature;
- Once temperature reaches the target value, the furnace is opened and the specimen is introduced;
- The deflection is measured with an LVDT sensor placed at the top of the furnace from the outside. It is in contact with a ceramic rod placed directly on top of the specimen as shown in Figure 3.9. The ceramic rod weighs 13 g.

Experimental results. Bending tests were performed by Montupet before the present study started. Different temperatures were considered: 100 °C, 200 °C, 300 °C, 400 °C and 500 °C, as illustrated by Figure 3.10, that shows the deflection evolution as a function

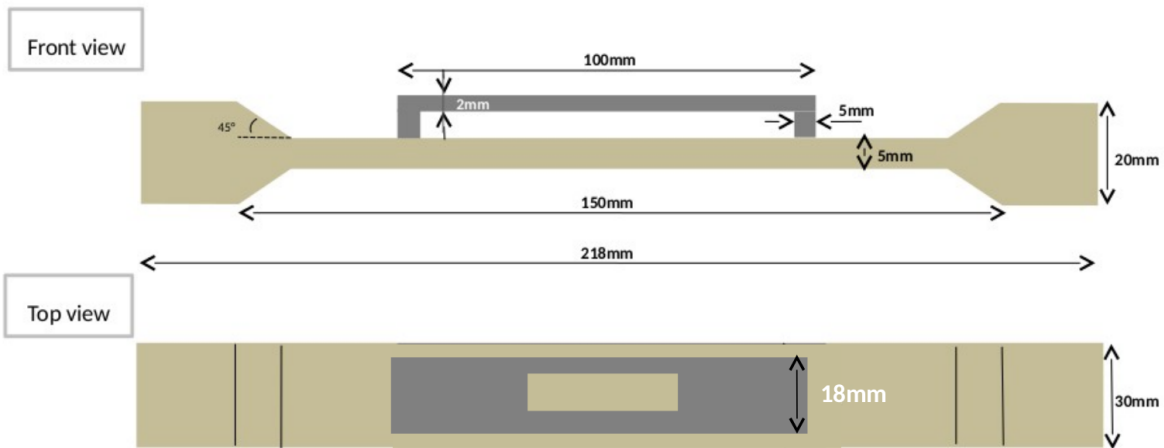


Figure 3.8: Four point bending creep specimen geometry.

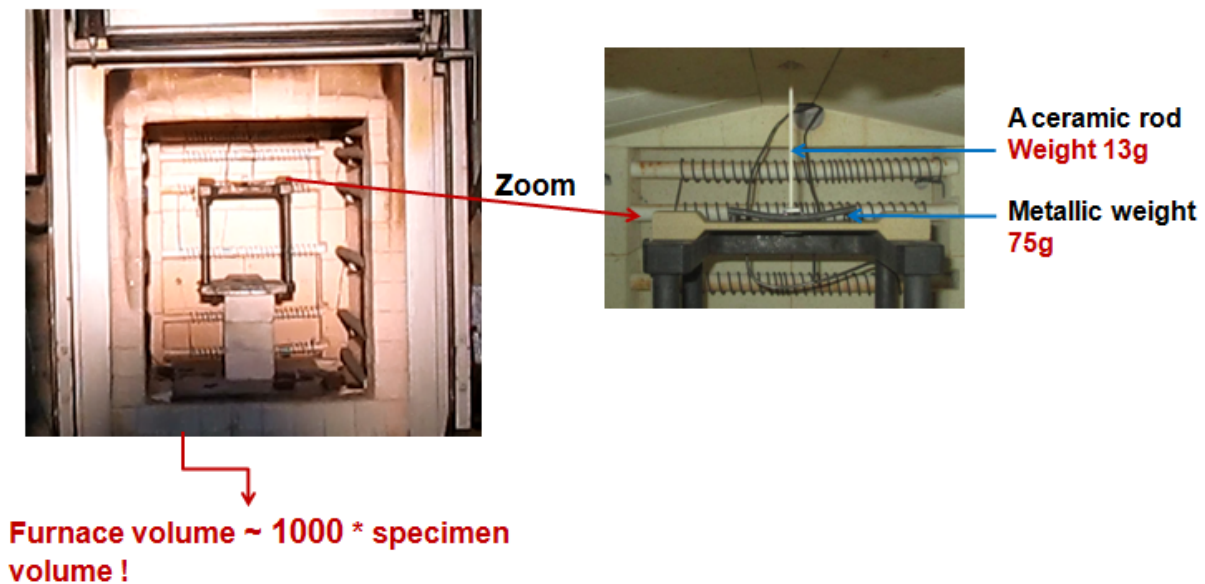


Figure 3.9: Experimental setup for bending tests used at Montupet.

of time.

Based on these results, it seems that the tertiary evolution of the curves reveal creep damage. However, a careful analysis of the results shows that (1) the mechanical loading is not the same for all the test, (2) there is no information about specimen temperature. Regarding the first point, at 100 °C and 200 °C, the specimen was loaded with a metallic weight of 75g, while the tests at higher temperatures in Figure 3.10 were carried out under self-weight without any additional applied external load (but the ceramic rod and the LVDT sensor do apply a significant-but-unknown load). The results can hardly be compared. The second point is more critical, since, knowing that the test is performed as soon as the specimen is introduced in the furnace, there is not enough time for it to reach an homogeneous temperature (test duration is very small, for example 18s for the test at 500 °C).

It therefore became essential to revise this experimental protocol.

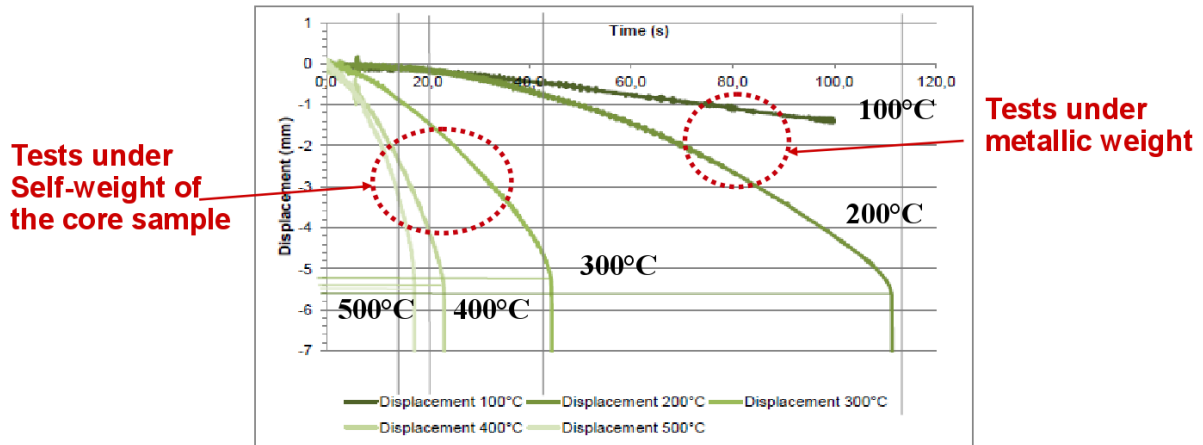


Figure 3.10: Evolution of the deflection at different temperatures in bending tests performed by Montupet’s R&D department.

Modifications of the experimental procedure and observations. Several points are to be fixed, namely:

- The applied load must be uniformly distributed across the specimen width. For this purpose, a new metallic mass of 37 g was designed (half of the previous one). It is presented in Figure 3.11. This will enable us to follow all creep stages;
- The temperature of the specimen must be measured to check its homogeneity, given that the furnace volume is way too large, and to be used instead of the temperature in the furnace. A sample has been equipped with three thermocouples, type K and diameter 2 mm, located at different locations, as shown in Figure 3.12 ;
- A continuous recording of the evolution of the deflection and of the sample temperature must be available from each test.

The results of two tests for which the reference temperatures in the furnace are respectively 400 °C and 200 °C are presented Figures 3.13 and 3.14.

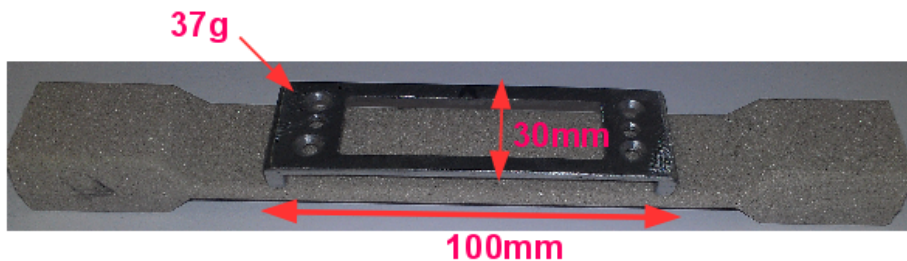


Figure 3.11: Bending creep test specimen with new weight dimensions.

The conclusions are the following (Figure 3.13):

- The setpoint temperature decreases by 80 °C when opening the furnace to introduce the specimen.

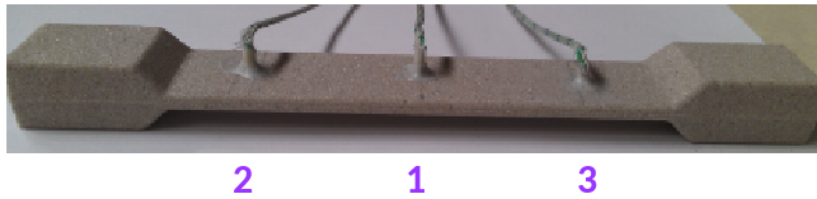


Figure 3.12: Bending creep test specimen instrumented with three thermocouples.

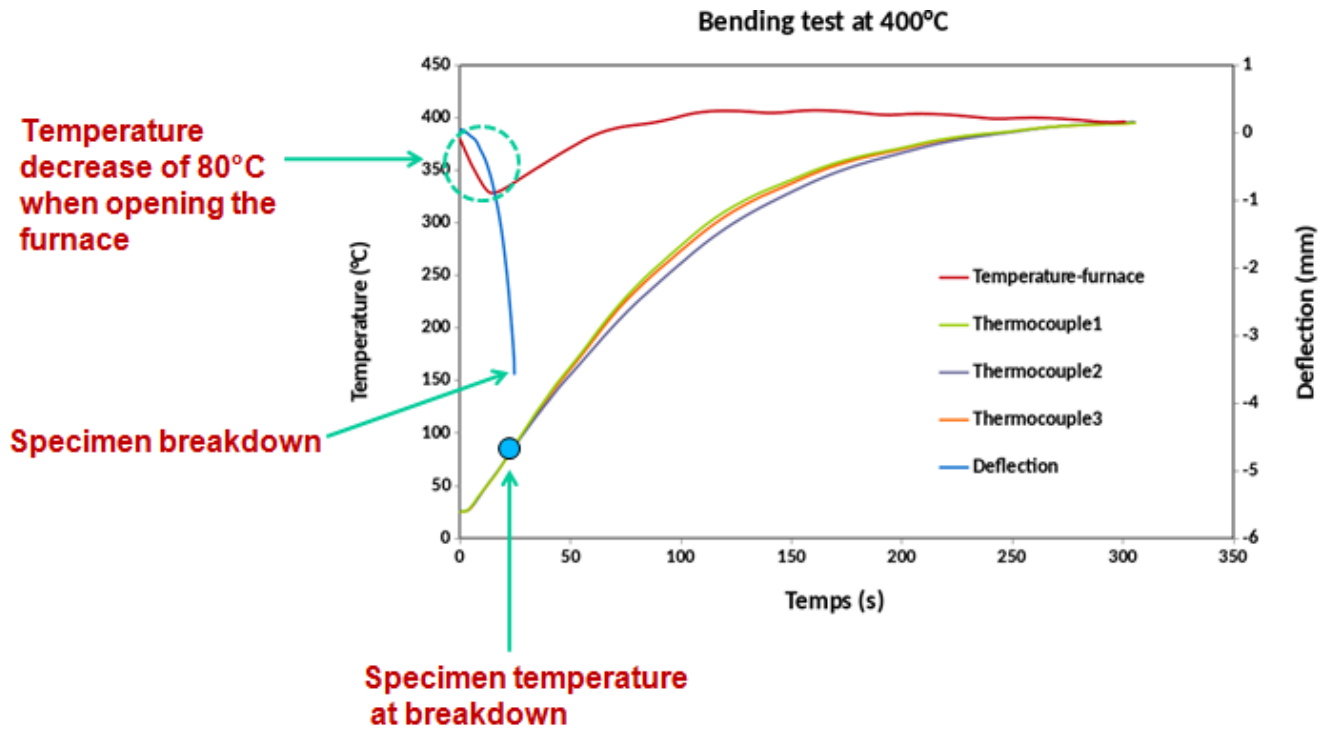


Figure 3.13: Deflection and temperature evolution during a creep test at 400 °C .

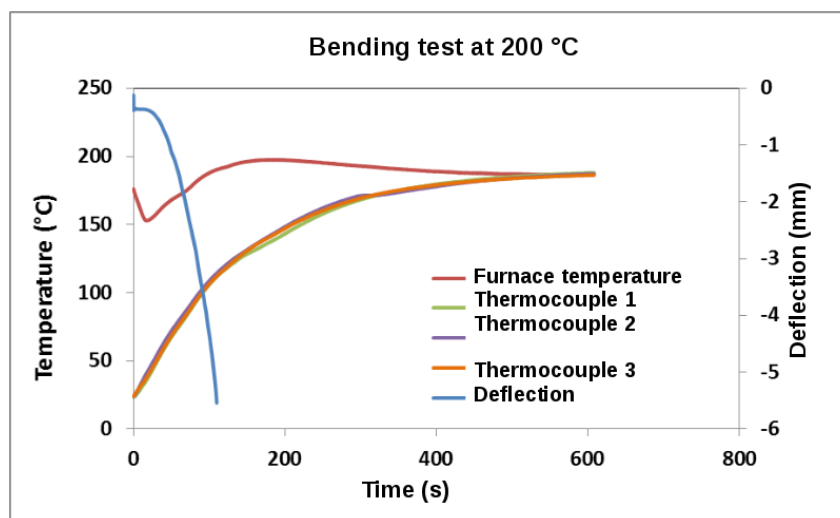


Figure 3.14: Deflection and temperature evolution during a creep test at 200 °C .

- The temperature is homogeneous throughout the specimen. It reaches the setpoint temperature (400 °C) after 5 min. Hence, the comparison between the evolution of the deflection and of the specimen temperature as a function of time shows that the specimen failed after 25 s, when the temperature is only equal to 70 °C. The same results is observed in Figure 3.14.
- It is then not possible to control the specimen temperature. There is an evolution of the furnace temperature when introducing the sample.
- The LVDT sensor does not provide a reliable deflection measurement. It is not well calibrated, and, together with the ceramic rod, it applies a load the value of which is not controlled to the 5 mm thick specimen, causing premature failure.

A significant improvement was needed, in particular with regard to temperature measurement, which must be made on the specimen, and the measurement of the deflection. This is why it was decided to redefine the experimental procedure and develop an experimental procedure at Centre Des Matériaux (CDM), as detailed in the following sections.

3.3 Creep bending tests at CDM introducing laser measurements

The new experimental procedure is defined as follows:

- We modified the specimen geometry and got rid of the massive parts. We opted for a simple rectangular bending geometry as shown in Figure 3.16;
- The mass of 37 g is still in use;
- We took a furnace with a high heating capacity (capable of rising to a temperature of 1600 °C for application to ceramic materials);
- We measured the deflection by means of laser sensors as presented in Figure 3.15.

Temperature measurement. The first step was to measure the sample temperature, to check its homogeneity and validate the chosen furnace. Five type K thermocouples of 0.8 mm were used to measure the specimen temperature during the test. They were placed at different locations on the sample as summarized in Figure 3.17.

The temperature field is not very uniform in the specimen, with a difference of 20 °C between the center and the edges. At 450 °C, the specimen broke down into pieces (brittle and friable as shown in Figure 3.18). Moreover, as illustrated in Figure 3.17, the temperature regulation is difficult for low temperatures (20 to 200 °C) because the furnace is intended for the temperature applications. Unfortunately, this temperature range corresponds to the target of the present study.

Deflection measurement. In order to make a comparison with the deflection measured in Montupet's tests, the same weight of 37 g was used. Since temperature regulation is now stable at 300 °C (see Figure 3.17), the new test was carried out at this temperature. A constant load is applied at room temperature and then the specimen is introduced into the furnace, heated at 2 °C/min until 300 °C and held for 25 hours. The deflection is

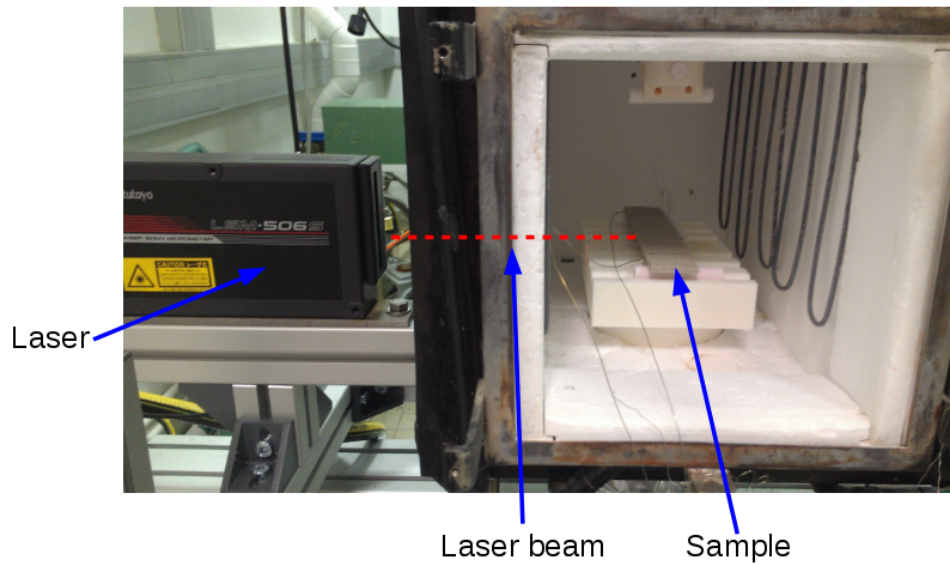


Figure 3.15: Experimental setup for bending tests with laser measurements.

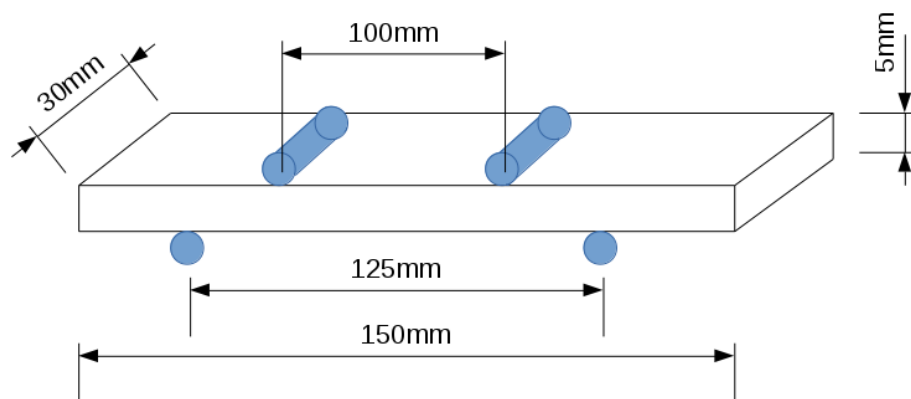


Figure 3.16: New specimen dimensions for creep tests with laser measurements.

measured at the center (location of thermocouple 3 in Figure 3.17) during both heating and the isothermal part of the test. The corresponding creep curve at is given in Figure 3.19.

During heating, a deflection of 0.7 mm was obtained. Once the temperature reaches 300 °C, there is a deflection inversion of 0.1 mm. The specimen breaks down after about 27 hours.

Compared to Montupet's test (Figure 3.10), the maximum deflection is now ten times smaller, and it increases only during heating, with no subsequent evolution once temperature remains constant.

At this stage, the phenomena that come into play are still difficult to analyze, due to the rather strong contrast between Montupet and CDM test results.

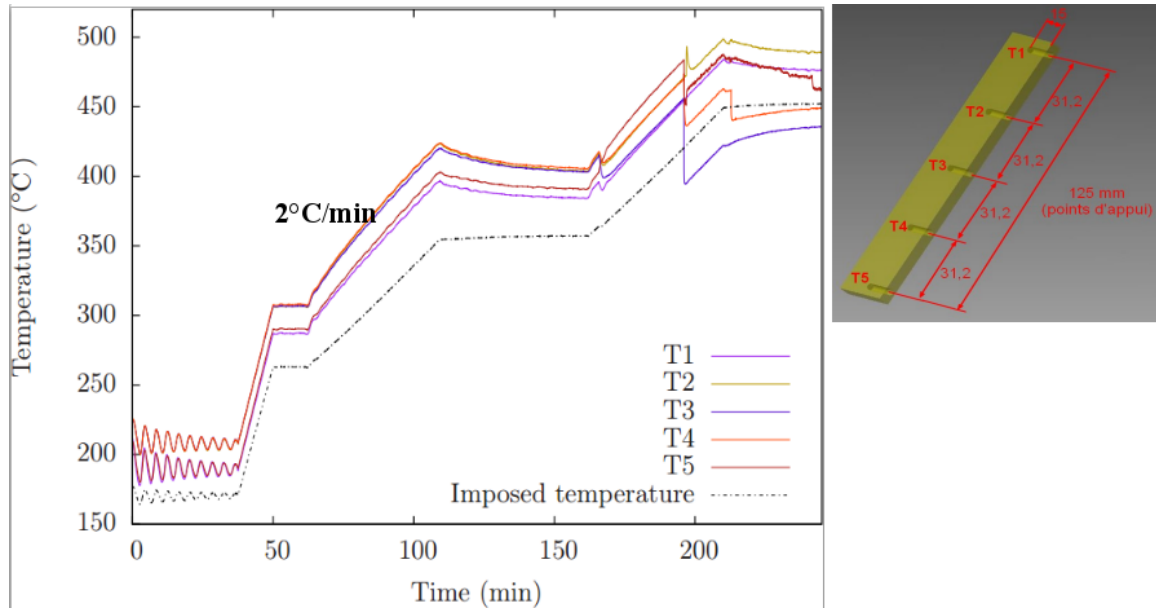


Figure 3.17: Specimen instrumentation with thermocouples.



Figure 3.18: Sand core specimen heated up to 450 °C during the instrumentation.

3.4 Synthesis of the pre-existing tests

The first two attempts to characterize the material behavior confirm the limitation of the present knowledge, as previously discussed in 2.4.2 and 2.5.4. While the objective of the present work is to develop a predictive model for the cores behavior, there is certainly a need to redefine the experimental protocol and investigate properly the mechanical and

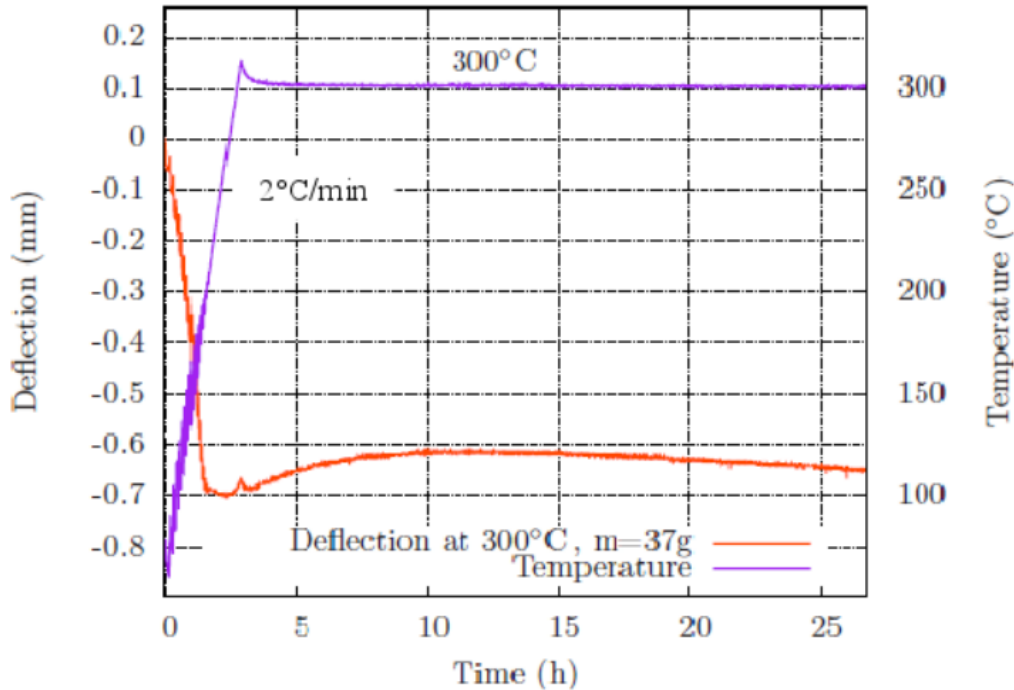


Figure 3.19: Creep test at 300 °C under a constant uniaxial load of 37 g.

thermal properties and dependent parameters. The following items have to be addressed:

- The type of binder must be identified;
- The binder contribution to the overall material response must be qualified;
- The experimental protocol must be redefined, with a clear control of the test conditions;
- The mechanisms that govern the sand core deformation must be characterized. This information is essential for the model development;
- The asymmetric behavior of the core in tension/compression needs to be taken into account.

The new experimental procedure considers possible interactions taking place in the core during casting as follows.

Thermo-mechanical coupling. The mechanical properties of the material depend on temperature.

Microstructure and thermal coupling. During heating, possible transformations may take place in the binder (depending on the binder nature). These phenomena and the evolution of the core internal structure must be investigated and taken into account.

Microstructure and mechanical behavior coupling. Resin bonded foundry core is a heterogeneous material, its behavior is fundamentally different from pure silica sand particles. The transformations in the resin and the evolution of the core overall structure have an impact on the mechanical properties. The identification of these phenomena,

their influence and the temperature range at which they take place are, however, difficult to identify separately. Moreover, the core is subjected to triaxial loading during casting, meaning that multiaxial effect must be investigated.

From the results of our first tests made in comparison to those carried out at Montupet (see paragraph 3.2), we were unable to understand the material response and the contribution of the binder to the overall material deformation. In addition to that, we do not know the composition of the binder and its behavior at high temperature. This is why we decided to restart everything from scratch, introducing a specific study of the binder and a study of the sand core on its own. The results will be analyzed in order to determine the physical mechanisms that cause core deformation and the contribution of each parameter and component.

The series of tests applied to bonding resin and sand core consist in thermophysical analyses (DSC, TGA and dilatometry) and thermomechanical tests (DMA, tensile tests, creep tests, four-point bending tests). The experimental methods are first detailed and then the results are presented, analyzed and discussed.

3.5 Development of a new testing protocol: Experimental methods for resin characterization

3.5.1 Differential Scanning calorimetry (DSC)

The DSC analysis consists in measuring the temperature differential between a reference sample and the studied material when submitted to a temperature cycle. This technique allows to quantify the energy loss or gain in a material during a transformation. This analysis was applied to the binder only, since there is no transformation in silica sand under 450 °C. The setup used is a Tzero Q2000 TA differential calorimeter (Figure 3.20). Small rigid polyurethane disks, weighing 10 mg, were prepared. They were machined from small resin blocks manufactured at Montupet with a mass ratio 1:1 between the phenolic resin and the hardener. An empty crucible was used as a reference. The specimens were heated continuously at different heating rates (2 °C/min, 5 °C/min and 10 °C/min) under nitrogen atmosphere.

3.5.2 Thermogravimetric analysis (TGA)

The thermogravimetric analysis (TGA) is used to evaluate the mass loss during heating. The sample is maintained in a flow of inert gas. Depending on the nature of the transformation, the mass variation can either be negative (combustion, pyrolysis) or positive (oxidation. . .). In the present work, Polyurethane (PU) samples weighing 5 mg were tested using Netzsch STA 449 F3 Jupiter analyzer, as shown in Figure 3.21. The sample was heated under inert Argon atmosphere at two heating rates, 2 °C/min and 10 °C/min.

3.5.3 Dilatometry

The investigation of the thermal expansion was conducted using a horizontal dilatometer NETZSCH DIL402 DC (Figure 3.22). Cylindrical specimens 20 mm long and 5 mm in diameter were used. Measurements were done under Argon atmosphere in a temperature range of 25-450 °C at different heating rates.

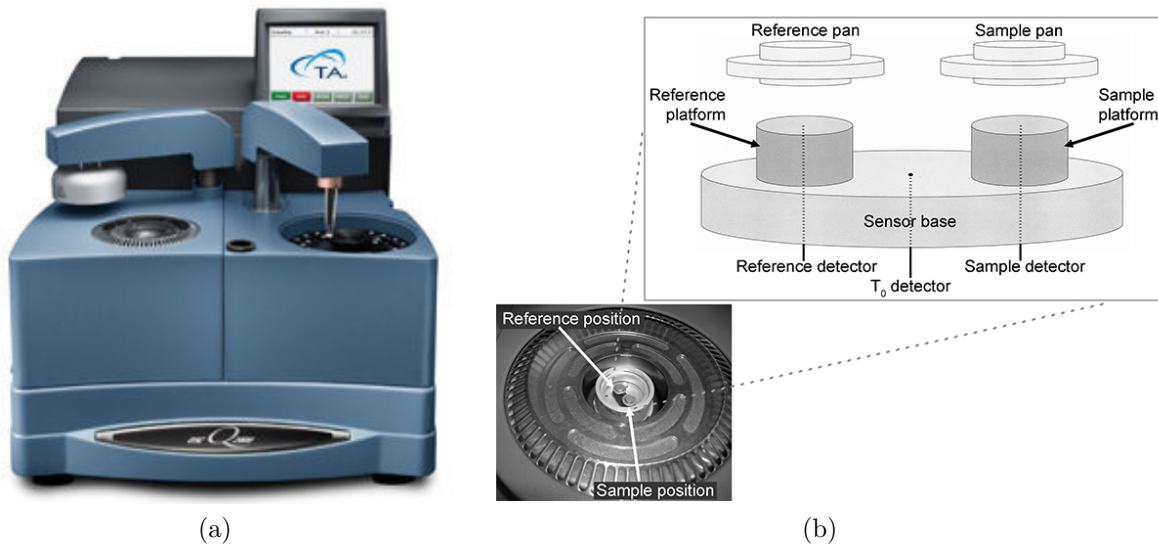


Figure 3.20: DSC machine showing (a) a cell controller (b) sample platform and sensors.

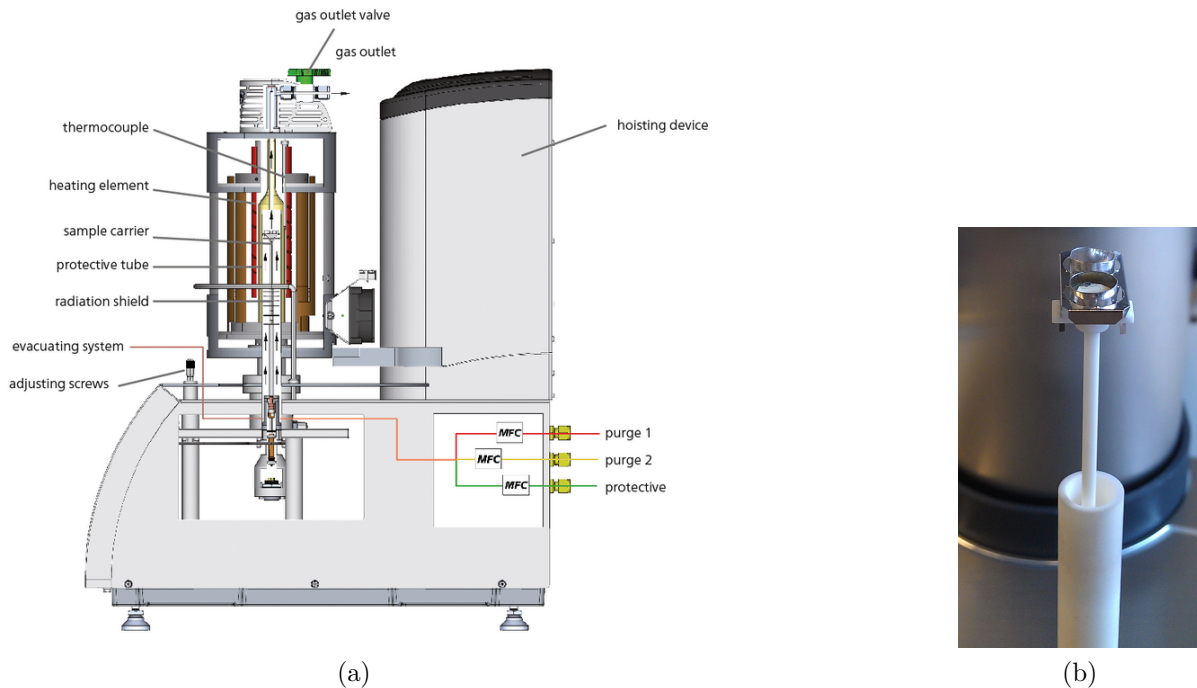


Figure 3.21: TGA machine showing (a) a cell controller (b) sample platform and sensors.

3.5.4 Dynamic Mechanical Analysis (DMA)

It is a technique based on the material's response to sinusoidal stresses, which makes it possible to characterize the elastic behaviour and the viscosity, through a complex Young's modulus, the variation of which determines the transitions undergone as a function of temperature. These measurements give access namely to the elastic modulus E' , the loss modulus E'' , the dynamic elastic modulus E and the phase lag between stress and strain defined by $\tan \delta = E''/E'$. Various loading types can be applied, such as three-point bending, tension, torsion, or shear between parallel plates depending on the transitions and the temperature range considered. In our study, tensile DMA analysis was

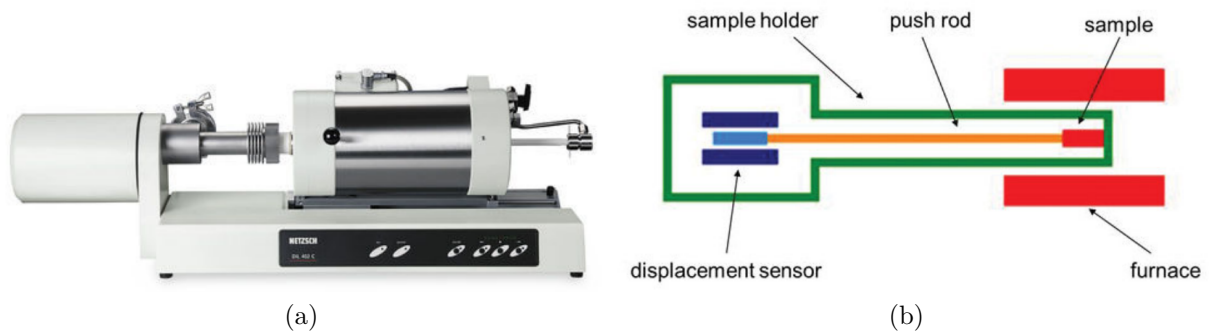


Figure 3.22: Horizontal dilatometer showing (a) a cell controller (b) sample platform and sensors.

conducted on solid polyurethane samples which dimensions are $20\text{ mm} \times 4\text{ mm} \times 1.5\text{ mm}$, using a “METRAVIB VA 4000” (Figure 3.23). The specimens were heated up to $200\text{ }^\circ\text{C}$ at a rate of $2\text{ }^\circ\text{C}/\text{min}$ and tested at a frequency of 5 Hz .

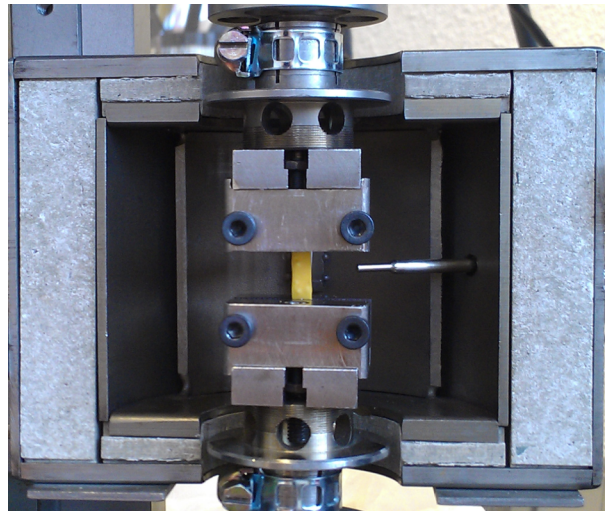


Figure 3.23: Experimental setup for Dynamic Mechanical Analysis (DMA).

3.5.5 Tensile tests

Tensile tests were carried out at different temperatures on standard tensile specimens shown in Figure 3.24. An Instron machine with a 1 kN cell load was used. As shown in Figure 3.25, an Advanced Video Extensometer system provides a measurement of the local displacement and of the strain fields. The machine is equipped with a resistive furnace and a temperature controller with a type K thermocouple. The effect of several parameters, such as the temperature, aging and strain rate was investigated. The specimen was heated at $2\text{ }^\circ\text{C}/\text{min}$ up to different reference temperatures under zero stress control.

3.5.6 Creep tests

Tensile creep tests were performed at different temperatures using the specimen geometry given in Figure 3.24 and the experimental setup shown in Figure 3.25. The machine

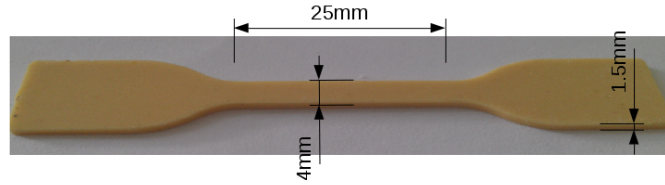


Figure 3.24: Resin specimen for tensile tests.

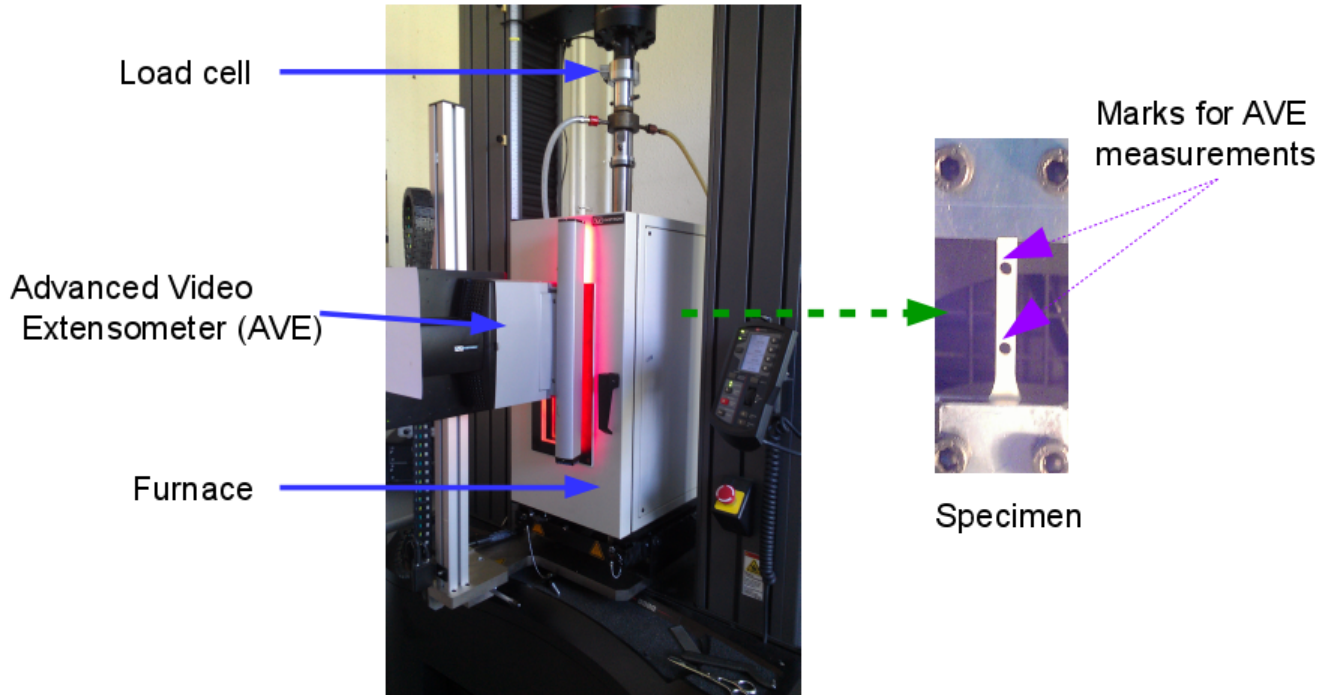


Figure 3.25: Experimental setup for tensile tests.

enables to switch mode from stress control during heating to strain control until a target stress, and finally stress control again to perform the creep test. The strain measurement was made by means of a video extensometer. The specimens were heated up to different temperatures, 70 °C, 200 °C and 210 °C at zero stress. They were next loaded at a strain rate of 10^{-3}s^{-1} up to a stress level of 1.1 MPa, slightly above the yield stress.

3.6 Development of a new testing protocol: Experimental methods for sand core characterization

3.6.1 Dilatometry

The procedure is the same as for resin, as detailed in paragraph 3.7.1.3.

3.6.2 DMA tests

The procedure was applied to a rectangular specimen submitted to three-point bending in order to measure an “apparent” value of the Young modulus of the sand core represented by the dynamic elastic modulus E . The dimensions of the specimen are 5 mm in height,

13 mm in depth and 130 mm in length. A "METRAVIB VA 4000" setup was used (Figure 3.26). The specimens were heated up to 200 °C at a heating rate of 2 °C/min and tested at a frequency of 5 Hz.

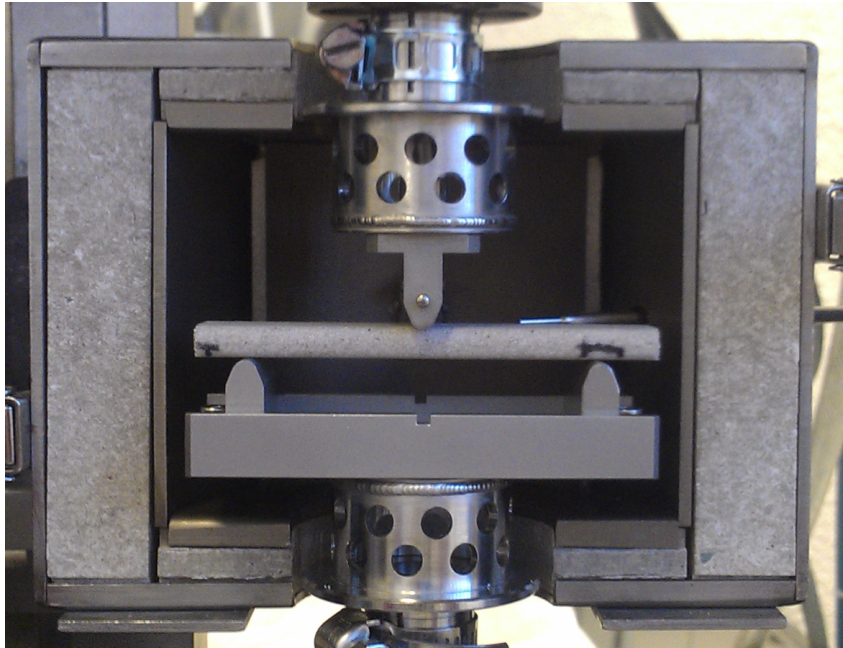


Figure 3.26: Three point bending DMA test on sand core.

3.6.3 Compression tests

Despite our efforts, it was not possible for us to carry out tests on a triaxial compression machine such as in [AS96,Azz95]. Nevertheless, we have had an access to an INSTRON machine at Centre des Matériaux, allowing us to perform uniaxial compression tests. A resistive furnace enabling to reach temperatures up to 200 °C is used. A 0.8 mm diameter type K thermocouple was placed at the specimen center at a width of 15 mm to measure the temperature evolution. Cylindrical samples must have a diameter of 30 mm and a 2:1 ratio between height and diameter. They were cut from 45 mm long pawns prepared in the only 30 mm diameter-225 mm long sand core box available at Montupet. Unfortunately, there is a risk that the preparation process will lead to the breakage of the resin bridges especially at the edges, weaken the material and distort the results.

3.6.4 Four-point bending tests

This new experimental campaign allowed us to introduce a new specimen geometry together with more complex temperature and loading conditions. The details of the experimental procedure are given below.

Specimen geometry and preparation The sand cores were prepared by mixing silica sand with a 1:1 phenolic resin:polyisocyanate mass ratio in total of 1 wt% of the whole sand mass. A granulometric analysis was made on silica particles by means of the *QICPIC&PICTOS* image analysis system (see Figure 3.27). The system includes a fast camera (450 images/s) and a monochromatic laser source of variable frequency to

improve image sharpness. The software is based on an image analysis algorithm. Figure 3.28 shows the obtained sand size distribution varying between 0.3 mm and 0.9 mm. The highest proportion is around 0.35 mm with an average sphericity index of 0.86 in Figure 3.29.

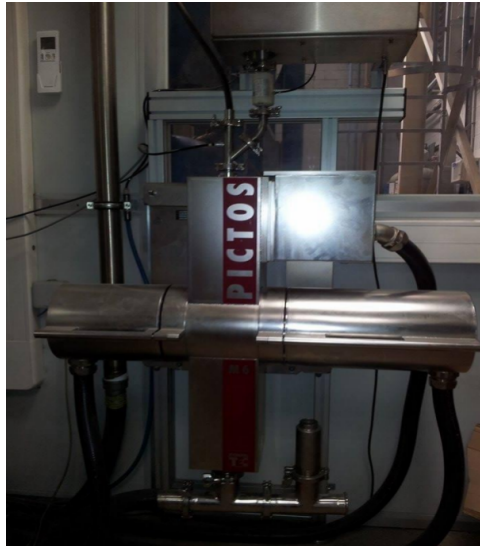


Figure 3.27: PICTOS machine for granulometric analysis.

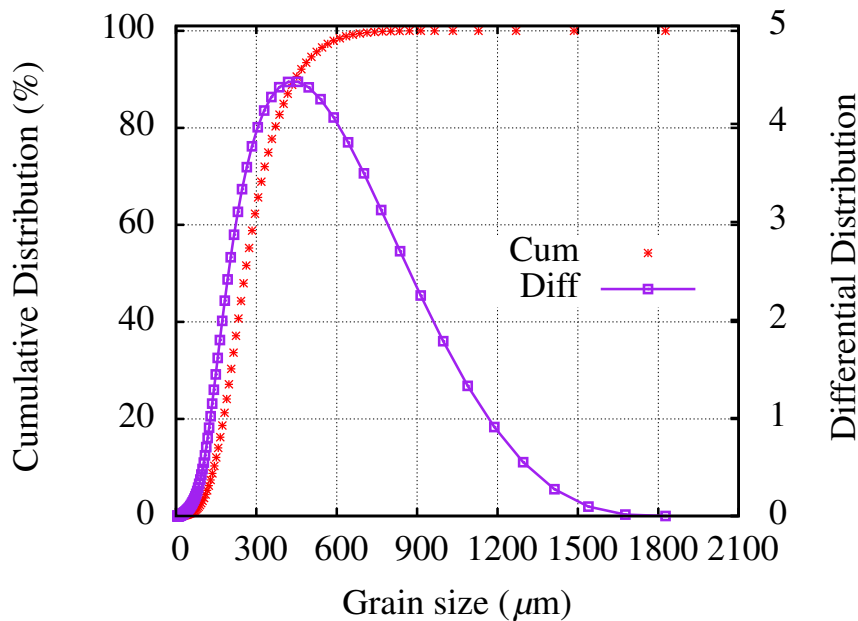


Figure 3.28: Grading curve for silica sand.

The specimens are manufactured 24 hours before testing so that the resin polymerization is completed and the strength can reach its optimum. An important parameter which may drastically affect material properties is moisture since the hardener in the resin may react with water to produce CO_2 and inhibit polymerization.

An X-Ray tomography inspection is performed before testing on a sand core cylindrical specimen 45 mm high and 30 mm in diameter, in order to examine the sample homogeneity and determine the porosity ratio. A typical image extracted from the reconstructed

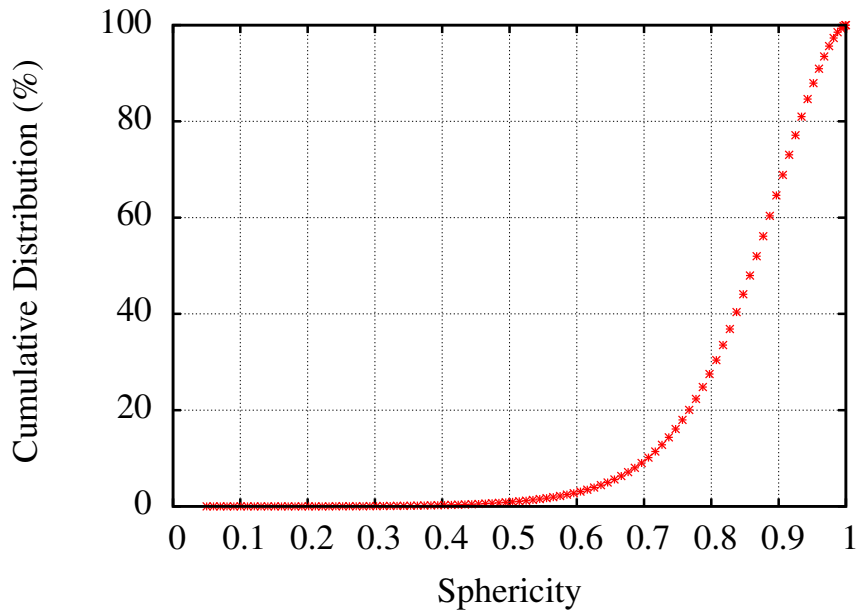


Figure 3.29: Grain sphericity distribution.

volume is given in Figure 3.30. The pixel size is $13 \mu\text{m}$. It was actually very difficult to distinguish the resin bridges from the silica particles. The fractal dimension of the set sand+resin (bright phase) is large, while the pore phase (dark phase) has a much smaller dimension. Based on color contrast, the porosity was calculated over the whole volume. It represents 32 % of the sample volume.

The samples are then kept in a dry atmosphere with controlled humidity. Standard parallelepipedic specimens are used. The dimensions are given in Figure 3.31. We modified the loading in order to respect a spacing ratio of $1/3$ between the support points and avoid shear development.

Experimental setup. Unlike the case of our first attempt (paragraph 3.2), a new experimental setup is now used, with a lower heating capacity but far better temperature control. It includes the items described below.

- The resistive furnace can reach a maximum temperature of $300 \text{ }^\circ\text{C}$. The precision of the regulation is $\pm 0.5 \text{ }^\circ\text{C}$. A calibration has been made with a sand core sample instrumented with two type K thermocouples of 0.8 mm (T1 and T3 in Figure 3.32), placed inside the specimen. The sample was heated up to $200 \text{ }^\circ\text{C}$ at a heating rate of $2 \text{ }^\circ\text{C}/\text{min}$. The evolution of temperature as a function of time is plotted in Figure 3.33. The specimen temperature seems to be homogeneous during the heating cycle and the regulation more effective than previously (see section 3.2). During the bending tests, the thermocouple T1 at the sample edge was kept and used as a control temperature. Low heating rates were chosen for the experimental characterization to assure a homogeneous temperature inside the specimen.
- The furnace is installed on an MTS machine equipped with four-point bending test plates presented in Figure 3.34. The minimum effort that can be applied by the load cell is 1 kN . It is way too important to apply for our material considered as a brittle one. For this reason, only the inferior plate was used. The sample was then placed on two cylindrical supports on the inferior plate and is loaded by means of

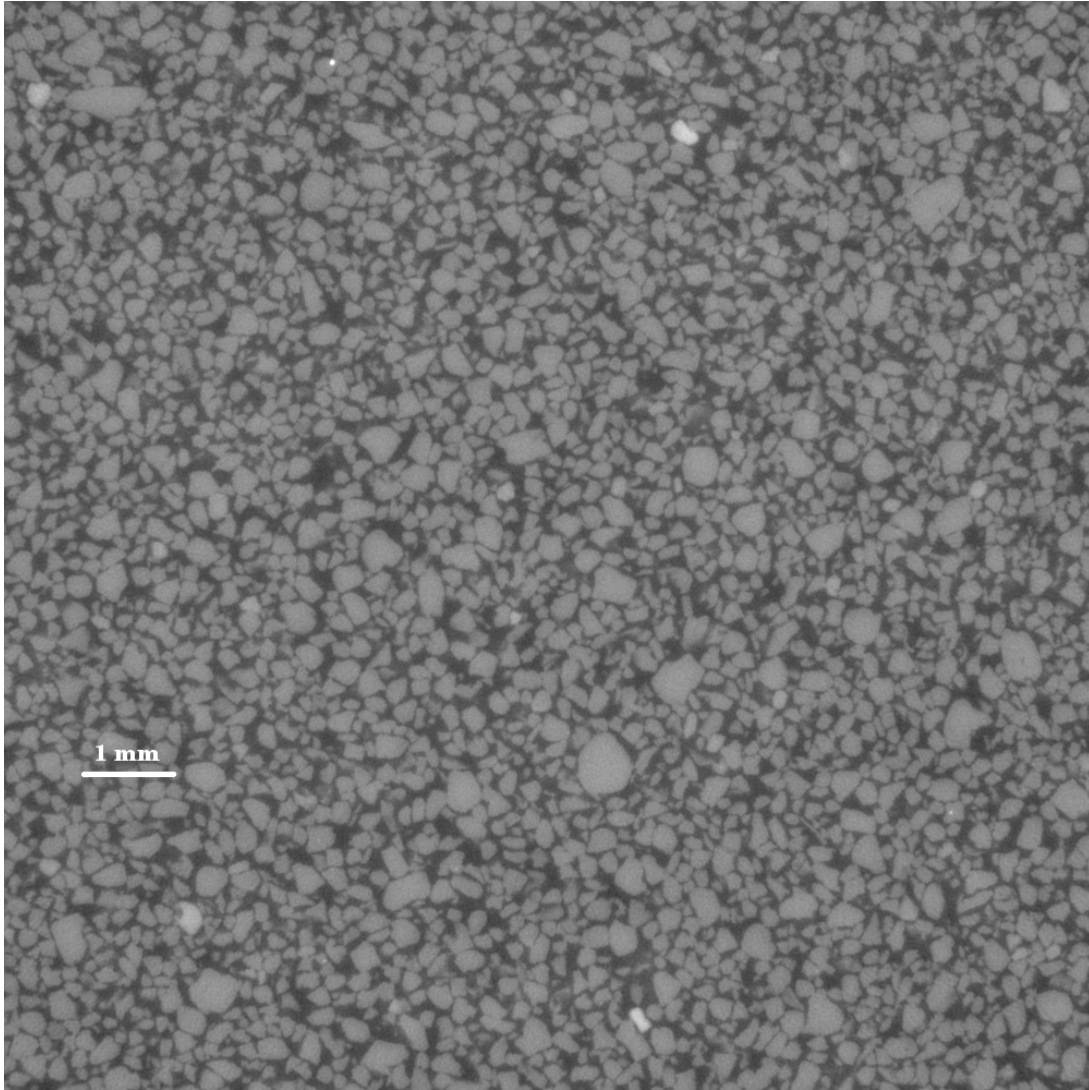


Figure 3.30: A two-dimensional image of a sand core sample using X-ray tomography.

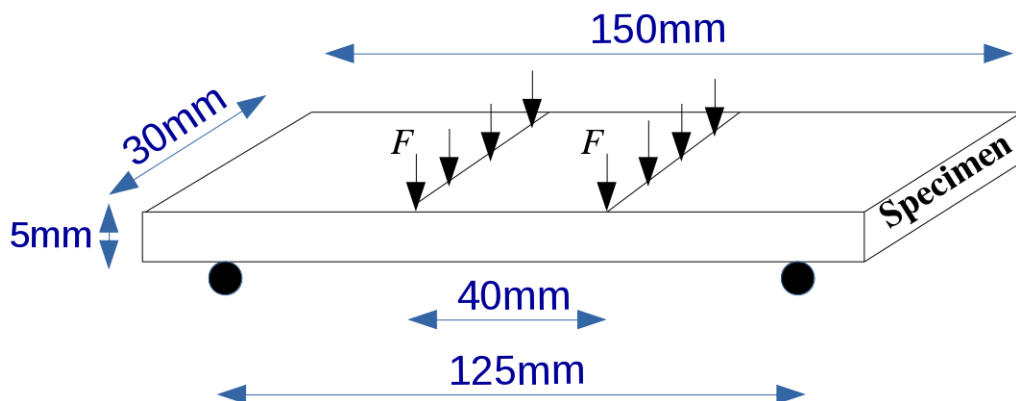


Figure 3.31: Parallelepipedic geometry of the four-point bending creep specimens.

a constant ceramic mass of 164 g. The tests consist in applying the mass at room temperature and then heating the specimen up to a target temperature.

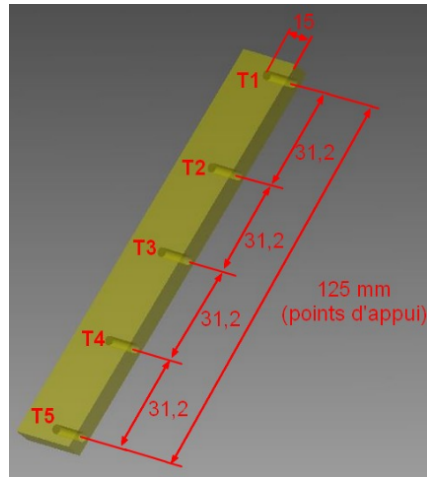


Figure 3.32: Parallelepipedic geometry for four-point bending creep tests indicating thermocouples positions.

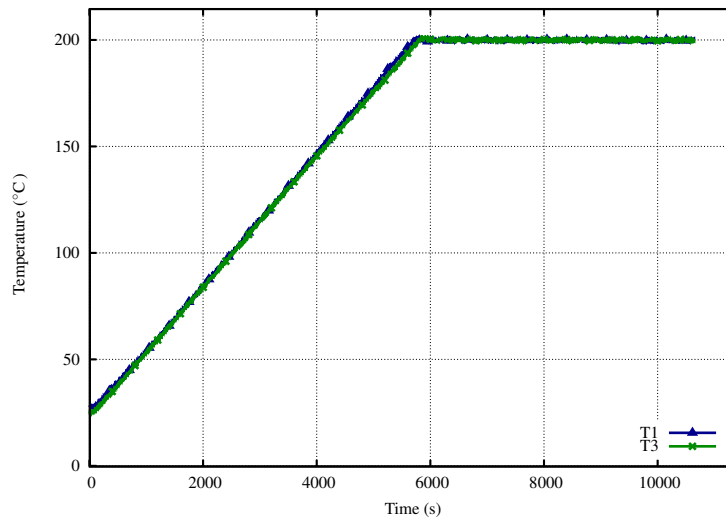


Figure 3.33: Evolution of temperature inside the bending specimen at the center and at the edge during heating up to 200 °C at 2 °C/min.

- The deflection of the specimen is measured at the center of the neutral axis where it reaches its maximum value. The measurement is done using an optical extensometer, a camera and digital image correlation technique. The reference point is placed on the inferior metallic plate and the measurement point at the center as shown in Figure 3.35. The data sampling frequency is 1 s. Figure 3.36 shows a specimen during a test.

Different factors which probably have an impact on the sand core behavior were examined, namely: temperature, heating rate, complex thermomechanical history, applied load, binder volume fraction.

3.6.5 Four-point bending tests for temperatures above 300 °C

The sand core thermal history has been recorded on an instrumented industrial water jacket core during casting. The results presented in paragraph 3.1 revealed that the maximum temperature reached is 450 °C. Since our bending creep test can work up

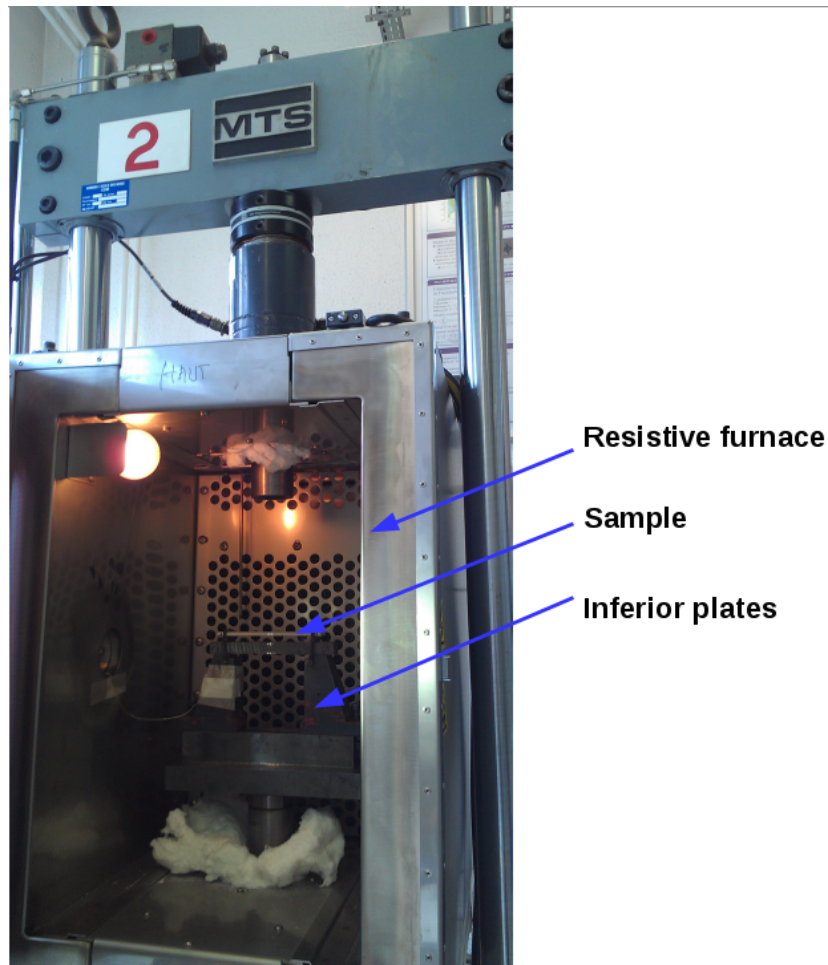


Figure 3.34: Experimental setup for bending tests showing the resistive furnace and the specimen placed on the inferior plateau.

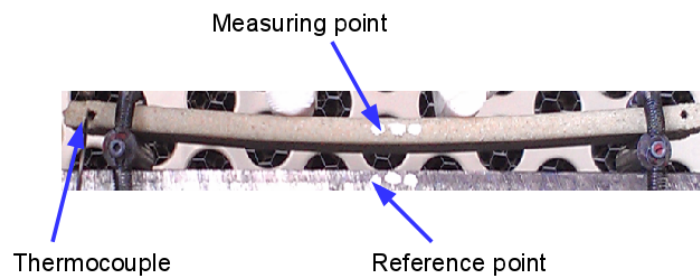


Figure 3.35: Deflection measurement by means of an optical extensometer.

to 300 °C only, we need an other solution to collect data in the 300 °C–450 °C range. We used an Instron machine equipped for creep–fatigue testing as presented in Figure 3.37. Two halogen lamps of 1500 W each provide enough power for the furnace (a tube-furnace) to reach a maximum temperature of 1200 °C. The walls of the furnace are water-cooled. In our tests, the furnace was placed horizontally. The geometry and the deflection measurement means are the same as in the previous section as shown in Figures 3.38 and 3.39. The deflection measurement point is at the specimen center along the neutral axis. The same experimental protocol is used. The sample is placed on two cylindrical

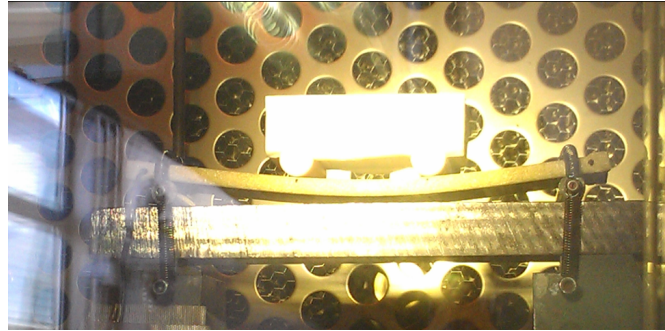


Figure 3.36: Specimen loaded in four-point bending creep test during heating.

supports on the inferior plate and is loaded by means of a constant ceramic mass of 164 g. The mass is placed at room temperature and then the specimen is heated up to a prescribed temperature. However the thermal regulation is controlled by a thermocouple placed in the furnace and not by the temperature of the specimen as for the tests with the resistive furnace.

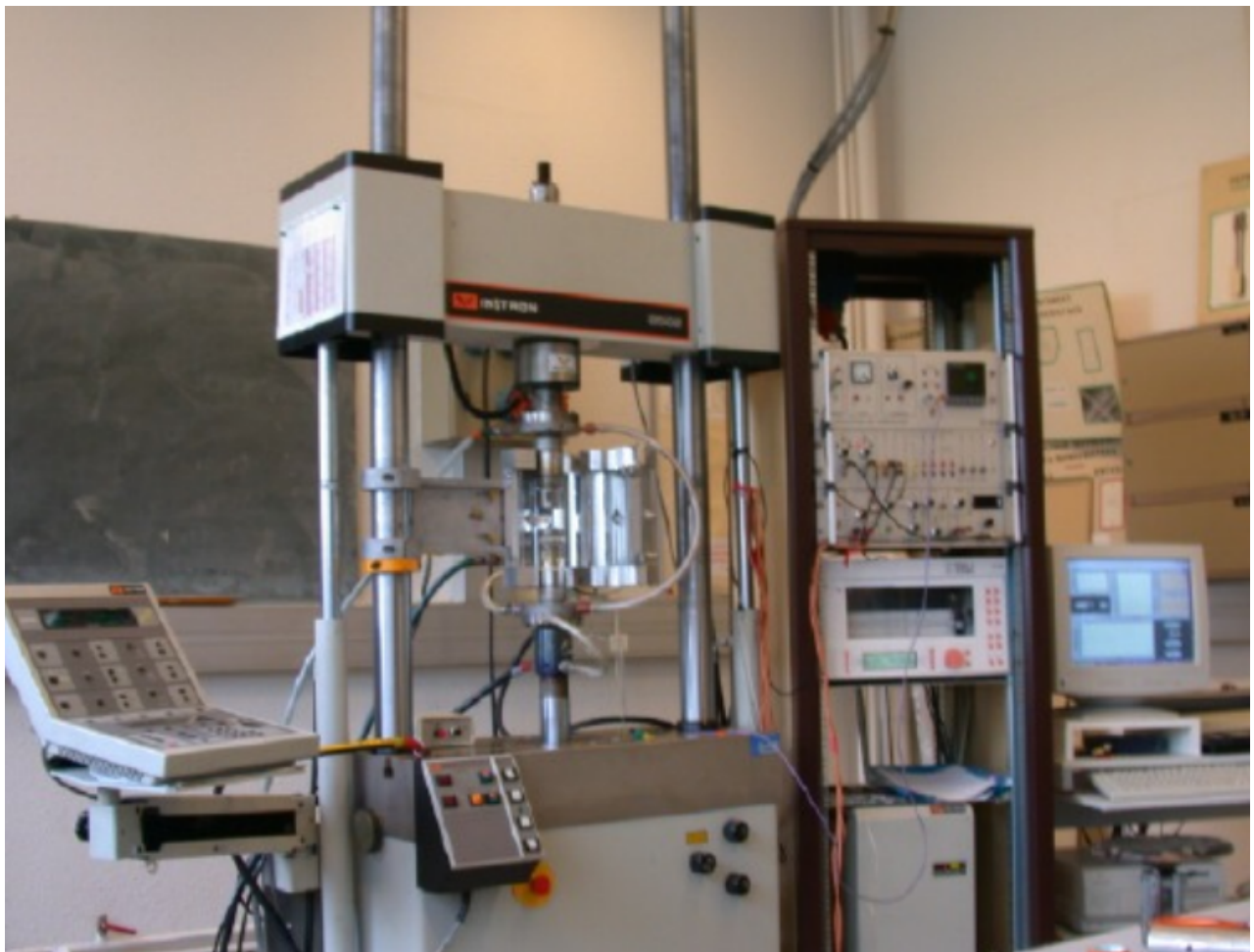


Figure 3.37: INSTRON hydraulic machine equipped with a tube furnace used for fatigue tests at high temperatures

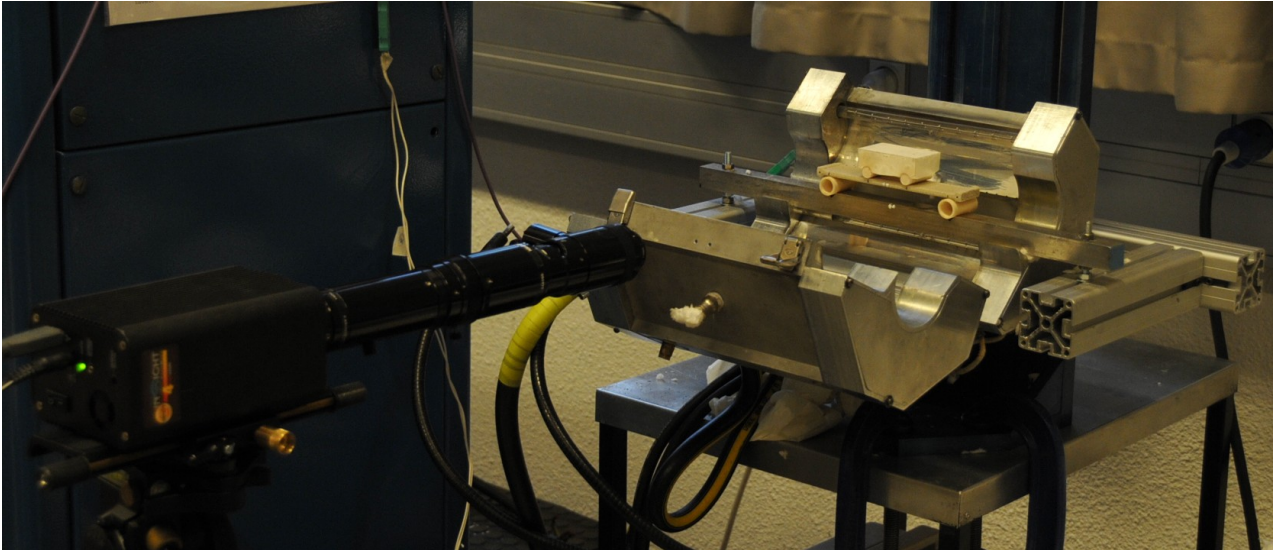


Figure 3.38: Bench equipped with tube furnace used for bending creep tests on sand core at high temperatures

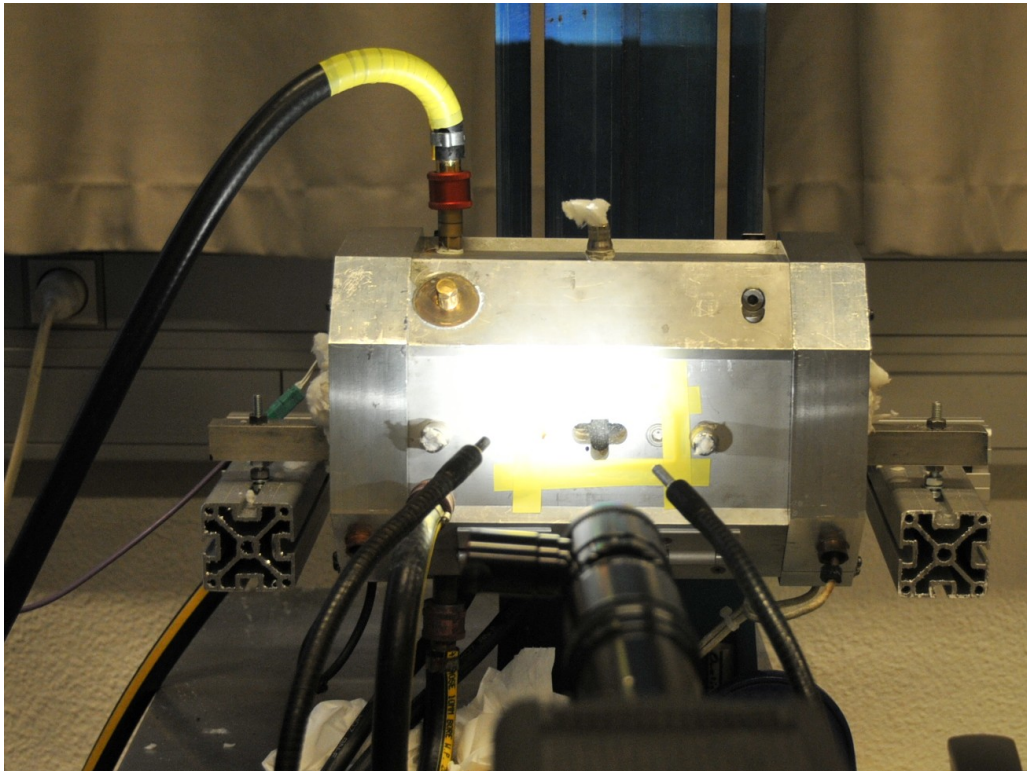


Figure 3.39: Deflection measurement during bending creep tests on sand core at high temperatures using tube furnace

3.7 Results and discussions

3.7.1 Resin and core thermophysical characterization

As shown in the next two sections the DSC and TG analyses performed on the Polyurethane resin revealed that during heating, the polymer goes through irreversible chemical transformations related to thermal degradation. This process is rate dependent

and takes place between 150 °C and 450 °C.

3.7.1.1 DSC analysis on resin

The results of the thermal analysis carried out on resin are given in Figure 3.40. The curves show a first endothermic reaction followed by two exothermic reactions. There is not endothermic reaction appearing at high temperatures which can be related to melting temperature. The absence of a melting point lead us to the conclusion that we are dealing with a thermosetting polymer. The corresponding temperatures for the observed reactions and the peak amplitudes depend on heating rate. In the case of a thermoset cure, three phases can be found, as discussed in [Gie09]:

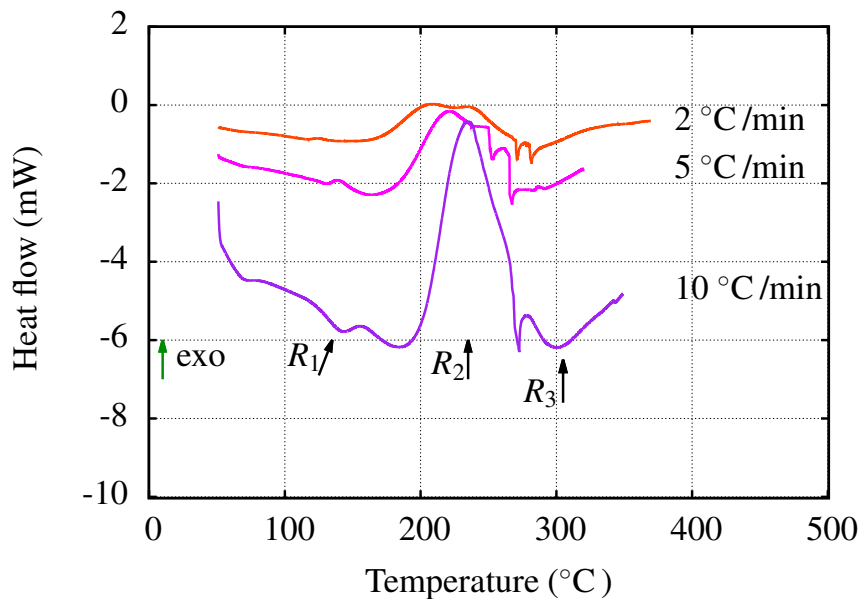


Figure 3.40: DSC thermal analysis on polyurethane at heating rates of 2 °C /min, 5 °C /min and 10 °C /min.

- Phase 1 : An endothermic reaction denoted (R1), related to the evaporation of solvents having low boiling temperatures (generally between 60 °C and 110 °C) along with glass transition where the molecular chains gain in mobility as explained in paragraph 2.5.4.
- Phase 2 : First exothermic reaction denoted (R2). There are two overlapping peaks. The first one corresponds to polyurethane additional crosslinking. The second one is an irreversible chemical reaction corresponding to urethane bond breakage.
- Phase 3 : Second exothermic reaction denoted (R3) corresponding to the breakdown of the phenolic part in the resin.

In this temperature range, the polymer exhibits only chemical reactions. The polyurethane resin used in the cold-box process was identified as a thermosetting resin which undergoes a thermal decomposition process and mass loss starting approximately at 60 °C with solvent evaporation.

3.7.1.2 TG analysis on resin

The phenomena related to thermal degradation observed in the DSC test were investigated by means of a thermogravimetric analysis. The thermogravimetric curve in Figure 3.41 shows that polyurethane decomposition at low heating rates starts with solvent release up to 150 °C. It is followed by two main reactions which correspond to two peaks in the DTG curve given in Figure 3.42. The first peak takes place between 150 °C and 250 °C. The second peak goes from 250 °C to 400 °C. The critical temperature for each step is shifted with increasing heating rate. A final residue is obtained. It represents approximately 30% of the initial mass. Recently, [Jom15] studied the pyrolysis of the same commercial polyurethane resin using non isothermal thermogravimetric analysis in nitrogen atmosphere. The specimens were heated at higher temperature rates (20 °C/min, 60 °C/min and 80 °C/min). Our results are in agreement with theirs where the resin was also found to go through a two-stage decomposition. Since the analysis was made at higher heating rates, the evaporation stage of the solvents could not be detected and the critical temperatures of the two decomposition stages were shifted to higher values compared to our results. The first step was found to take place up to 250 °C while in [Jom15] it extends until 300 °C.

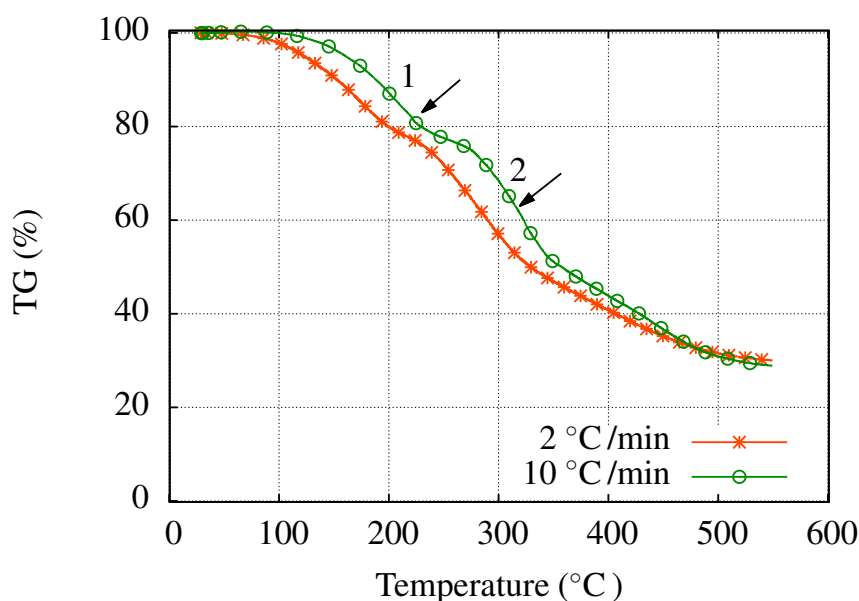


Figure 3.41: TG analysis on on polyurethane at heating rates of 2 °C/min and 10 °C/min.

The decomposition of polyurethane is particularly complex, since it is governed by several physical and chemical phenomena, with the formation of various gases [Nav15]. It depends on the chemical components, nature and complexity of the chemical structure, type of bonds and their nature. At high temperature, the covalent bonds break down to form new fragments or small molecules which may go through further fragmentation or recombine and it ends with the formation of a final char residue [Nav15]. Some authors [Gie09] studied the different decomposition stages and its influence on the polymer strength evolution at high temperature. They found that in the first step, urethane bond (called Hard segments "HS") breakage leads to a modification of the chemical structure of the polymer. This causes a decrease of the bonding strength. Nevertheless, the polymer

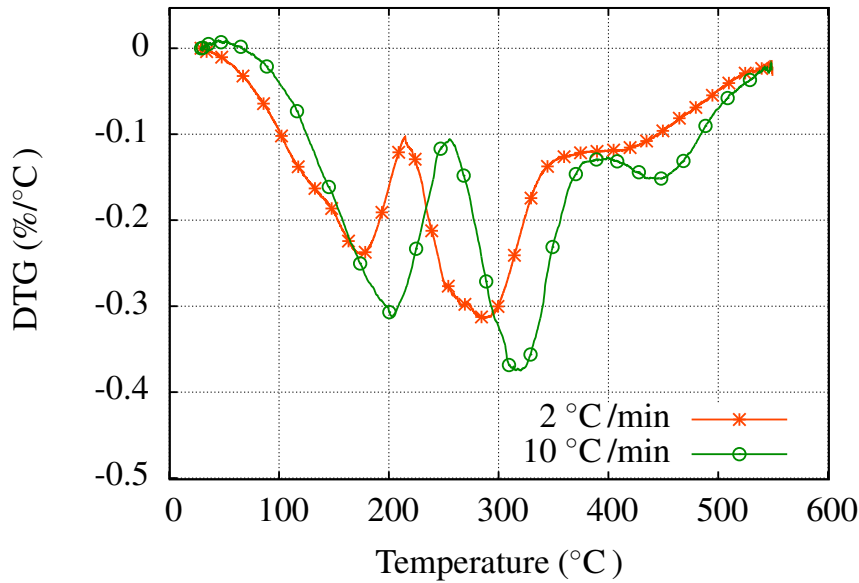


Figure 3.42: DTG curve in thermogravimetric analysis on polyurethane at heating rates of 2 °C/min and 10 °C/min.

strength remains, since aromatic compounds are still present in the complex three dimensional bonding network. From DSC and FTIR (Fourier Transform InfraRed spectroscopy) analyses, they concluded that the resin extensive bond network provides a resistance to thermal degradation and moderate temperature strength even with urethane bond failure. In the second step, the phenolic urethane rapidly decomposes into aromatic compounds and therefore there is a rapid strength loss. Similarly, [Cha09] and [Nav15] reported that polyisocyanate is rigid and exhibits high and complex inter-chain interaction. The urethane bonds are first broken leading to the degradation of the HS during the first stage, while polyol (referred to as the Soft Segment "SS"), which breaks down during the second stage, is flexible. During this step, random polymer chain scissions, chain-end scission and cross linking mechanisms take place. In contrast, other authors, looking at polyurethane pyrolysis, supposed that the polyol decomposition takes place at a first stage followed by the polyisocyanate decomposition in a second stage [Jom15].

3.7.1.3 Dilatometry

The aims of this analysis are, first to investigate the thermal behavior of the material (both the mix sand core and the binder) and second to measure the expansion coefficient which will be used in the structural computations. This is important since, as mentioned before, there is a poor database in the commercial softwares about sand core properties.

1. **Sand core.** The dilatometry curve of the sand core is given in Figure 3.43. The material exhibits a thermal expansion/contraction behavior. A linear expansion is observed between room temperature and 220 °C. A contraction is obtained afterwards within two steps. They correspond to the two decomposition stages identified in paragraph 3.7.1.2. A linear expansion regime is recovered at higher temperatures. The different thresholds as well as the contraction amplitude depend on heating rate. The different values of the thermal expansion coefficient at different temperatures are given in Tables 3.1, 3.2 and 3.3 for the heating rates 2 °C/min, 10 °C/min and 20 °C/min respectively.

2. **Resin binder.** The dilatometry analysis on pure solid polyurethane under the same experimental conditions (Figure 3.44) shows an expansion of the resin up to 150 °C with a first contraction corresponding to solvent evaporation, denoted Ev , and a second contraction corresponding to the glass transition, denoted T_g , while a significant contraction and swelling of the resin are obtained afterwards along with the additional crosslinking and thermal degradation at point D . These observations can be seen through the final aspect of the tested specimens in Figure 3.45.

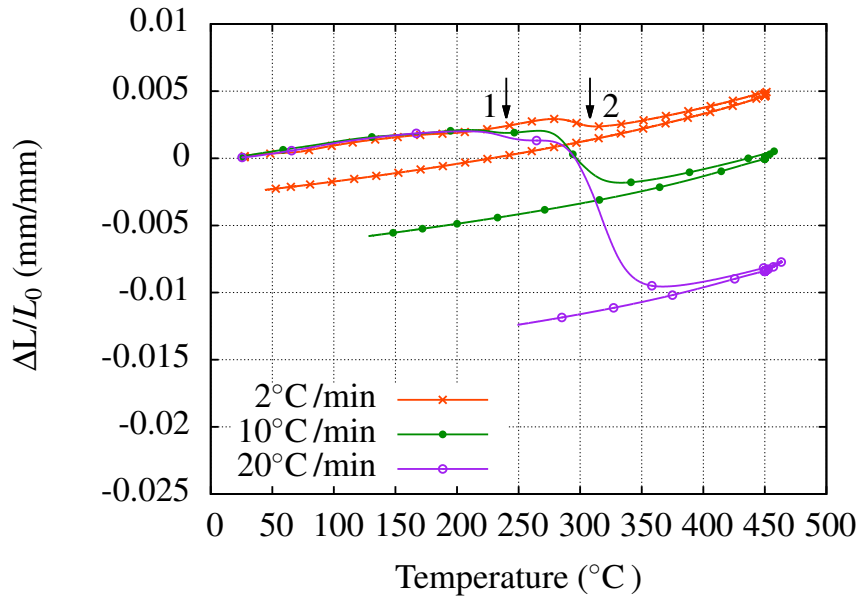


Figure 3.43: Dilatometry analysis on sand core at heating rates of 2 °C/min, 10 °C/min and 20 °C/min.

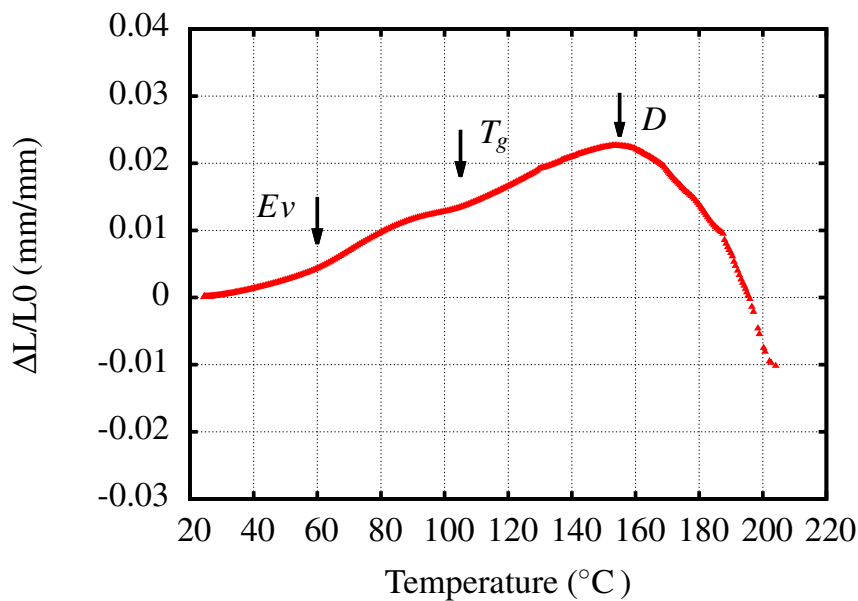


Figure 3.44: Dilatometry analysis on resin sample at 2 °C/min.

Table 3.1: Thermal expansion coefficient for a heating rate of 2 °C /min

temperature °C	Thermal expansion value (°C ⁻¹)
22	1.4e-5
100	1.2e-5
200	1.15e-5
250	1.1e-5
287	1.13e-5
310	0.78e-5
450	1.13e-5
550	1.13e-5

Table 3.2: Thermal expansion coefficient for a heating rate of 10 °C /min

temperature (°C)	Thermal expansion value (°C ⁻¹)
22	1.4e-5
100	1.4e-5
200	1.3e-5
250	0.95e-5
287	0.9e-5
310	-0.45e-5
450	0.88e-5
550	1.1e-5

Table 3.3: Thermal expansion coefficient for a heating rate of 20 °C /min

temperature (°C)	Thermal expansion value (°C ⁻¹)
22	1.4e-5
100	1.4e-5
200	1.3e-5
250	0.75e-5
287	0.58e-5
310	-0.26e-5
450	-1.1e-5
550	1.1e-5

Due to this combination of expansion and contraction effects, we believe that the sand core exhibits a structural modification and granular rearrangement up to 400 °C approximately when the thermal decomposition in reaction R2 stops (Figure 3.40). The silica sand expansion occurs afterwards. These modifications seem to be strongly dependent on the mechanical and chemical transformations in the resin binder.

Dependence on the heating rate was investigated furthermore, introducing a two-step thermal history, with a heating up to 250 °C at 2 °C/min followed by a temperature rate of 20 °C/min from 250 °C up to 450 °C. The corresponding dilatometry curve is given in Figure 3.46 and compared to the dilatometry curves obtained with a continuous heating up to 450 °C at 2 °C/min and 20 °C/min respectively. For the test at two temperature rates, the part between room temperature and 250 °C is in good agreement with the reference test at 2 °C/min showing a good reproducibility. Once the heating rate is switched to 20 °C/min, the sand core collapses and the resulting gap is between those obtained for the two reference curves. It shows that the contraction of the specimen depends on the current temperature rate, but on temperature history as well. The irreversibility of the observed phenomena was then investigated through the following test:

- phase 1: the specimen was heated up to 450 °C at 2 °C/min and cooled down at 2 °C/min.
- phase 2: the same specimen is reheated again up to 450 °C at 20 °C/min and cooled down at 20 °C/min.

The results in Figure 3.47 show that the slope of the curve is the same in phase 1 and in phase 2 above 350 °C. The material response during phase 2 becomes reversible. It means that the structure inherited from phase 1 is now frozen, and does not depend on temperature history anymore. The analysis of the results in Figure 3.46 and 3.47 suggests the following deformation mechanisms:

- For low temperature rates, the slow heating allows the binder to become stronger, due to crosslinking of the chains, so that the link between the sand particles remains rather stable.
- For high temperature rates, a degradation of the binder takes place, accompanied by a rearrangement of the particles, and the sand core structure collapses.

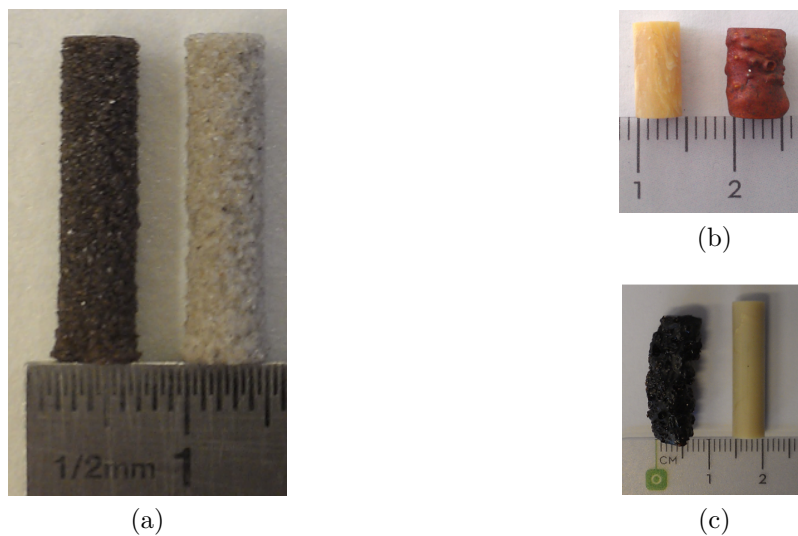


Figure 3.45: Dilatometry specimens (a) sand core specimen heated up to 450 °C (b) resin specimen heated up to 200 °C and (c) resin specimen heated up to 350 °C.

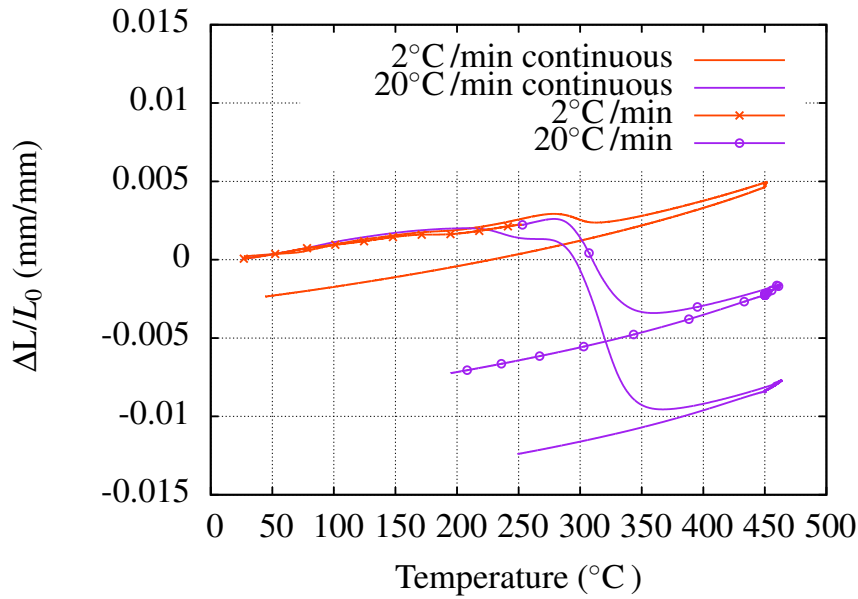


Figure 3.46: Dilatometry analysis on sand core specimen between room temperature and 450 °C showing reference tests with a continuous heating at 2 °C /min and at 20 °C /min and two level temperature rate test at 2 °C /min up to 250 °C and 20 °C /min up to 450 °C .

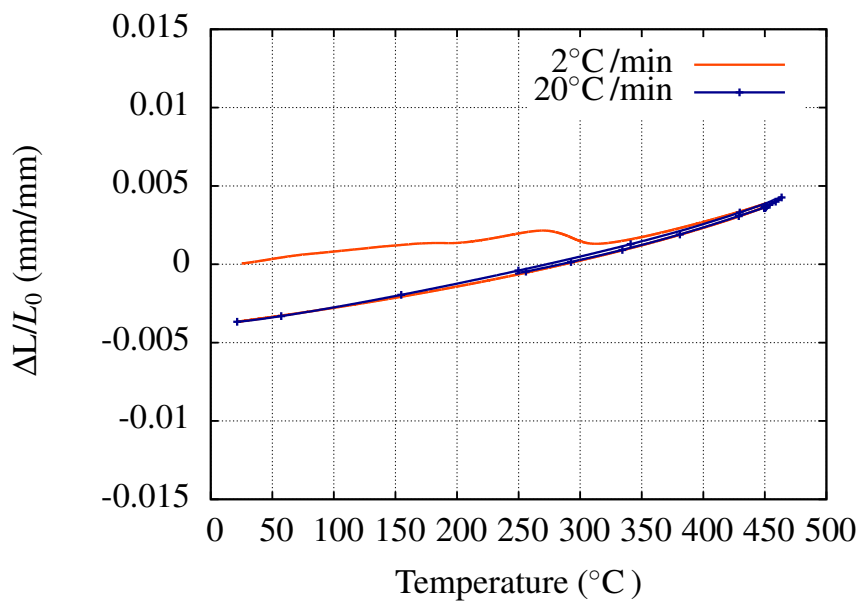


Figure 3.47: Dilatometry analysis on sand core specimen between room temperature and 450 °C showing cycle 1 at heating rates of 2 °C /min and cycle 2 at 20 °C /min up to 450 °C .

3.7.1.4 Specific heat capacity measurement

The specific heat capacity corresponds to the energy needed for a material unit mass to increase its temperature by one degree. This property is also important for the structural computations and is missing in the available database used by our industrial partner.

An experimental procedure had been set up to measure the resin bonded sand specific heat capacity and validated on Sapphire as a reference and also on the sand. Two

methods were used for the C_p measurement: Differential Scanning Calorimetry (DSC) and Modulated Differential Scanning Calorimetry (MDSC).

The DSC consists in measuring heat flow of the specimen during heating in comparison with a reference material having close C_p values and calibrated using an empty crucible. The standard DSC with continuous measurement method corresponding to a continuous temperature increase given in Figure 3.48 strongly depends on the stabilization of the baseline and the choice of the heating rate (in general very low heating rates for a good stability). The C_p value is deduced using the following equation:

$$C_{ps} = \frac{\Phi_s - \Phi_e}{\Phi_r - \Phi_e} \cdot \frac{m_r}{m_s} \cdot C_{pr}(T)$$

with the following notations:

Φ_s : The sample heat flow

Φ_e : The flow of the empty crucible (baseline)

Φ_r : The flow of the reference material

m_r : Weight of the reference material

m_s : Weight of the sample

C_{pr} : Reference specific heat capacity

C_{ps} : Sample specific heat capacity.

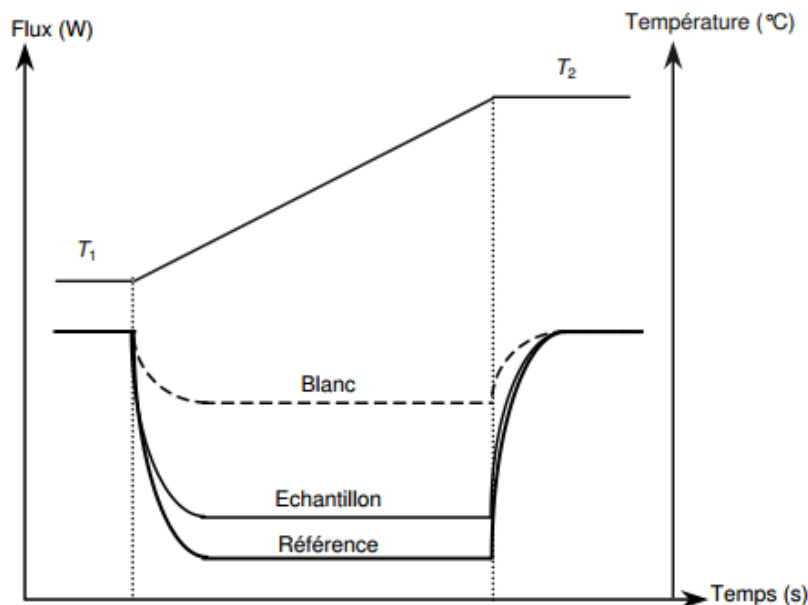


Figure 3.48: DSC continuous measurement method

The heating rate is about $0.01 \text{ }^\circ\text{C}/\text{min}$, which can take days for good and stable measurement. So the alternative is the MDSC technique, which consists in applying a modulated heat rate in order to separate the total heat flow of DSC into two parts based on the heat flow that does and does not respond to changing heat rate. In general, heat capacity responds to the changing heat rate and the MDSC gives then access directly to

the C_p value denoted C_{prev} .

The total heat flow reads:

$$\frac{dH}{dt} = C_p \cdot \frac{dT}{dt} + f(T, t)$$

where dH/dt is the total average DSC heat flow, C_p is the sample heat capacity, dT/dt is the heating rate and $f(T, t)$ is time and temperature dependent. Tzero Q200, TA instruments machine was used. The calorimetric precision is of 0.05% and the temperature precision is 0.01 °C.

In our analysis, the DSC standard measurement was done under Nitrogen atmosphere and a heating cycle from room temperature until 450 °C at a heating rate of 1 °C /min.

- Sapphire is used as a reference $m_r = 21$ mg
- Resin bonded sand specimen $m_s = 26$ mg

Modulated heating rate was applied at certain temperatures at 1 °C /min during 100 s. The experiment is summarized in Figure 3.49. Values of C_p using both DSC (C_p) and

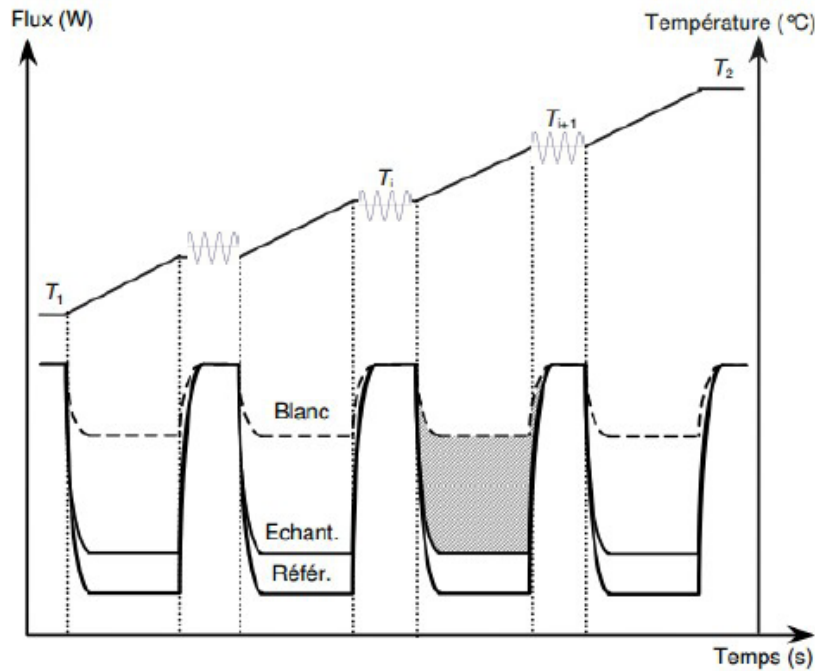


Figure 3.49: DSC and MDSC analysis for C_p measurement

MDSC (C_{prev}) techniques are given in table 3.4.

In a first stage, this experimental methodology was validated on the sapphire in comparison with values from the literature (TA instruments) and summarized in table 3.5.

In a second stage, the C_p values of silica sand particles was measured as well and compared to the resin bonded sand C_p values given in table 3.6 denoted respectively $C_{psilicasand}$ and $C_{presinbondedsand}$.

The C_p value of the resin bonded sand tends to that of the silica sand which can be related to the thermal degradation and possible vanishing of the resin. Therefore, the

Table 3.4: Sand core C_p values using the two techniques DSC (C_p) and MDSC (C_{prev})

Temperature (°C)	C_{prev} (J/°C.g)	C_p (J/°C.g)
100	0.856	0.819
200	0.955	0.92
260	0.99	0.94

Table 3.5: Sapphire C_p values

Temperature (°C)	C_p (J/°C.g)	$C_{pliterature}$ (J/°C.g)
100	0.871	0.902
200	0.97	1.01
260	1.01	1.065

Table 3.6: Comparison between heat capacity values of pure Silica sand particles ($C_{psilicasand}$) and resin bonded sand core ($C_{presinbondedsand}$)

Temperature (°C)	$C_{psilicasand}$ (J/°C.g)	$C_{presinbondedsand}$ (J/°C.g)
100	0.836	0.856
200	0.94	0.955
260	0.99	0.99

heat capacity to be used are those obtained by means of the MDSC technique. For higher temperatures, as no transformation takes place in the silica particles up to 500 °C, heat capacity remains a constant equal to 0.99 J/°C.g.

3.7.2 Resin thermomechanical characterization

3.7.2.1 DMA analysis on resin

DMA analysis was conducted on resin specimens to evaluate the viscoelastic properties during heating. The evolution of E' and E'' as a function of temperature is shown in Figure 3.50a, meanwhile E and $\tan\delta$ are in Figure 3.50b. The main observations are:

- There is an important decrease of the storage modulus E' due to the evaporation of the volatile elements and solvents. The values of the loss modulus E'' are lower than those of E' .
- The peak of $\tan\delta$ around 100 °C is linked to the glass transition.
- Figure 3.50b shows that with increasing strain rate (frequency), the peak $\tan\delta$ is shifted to a higher value.

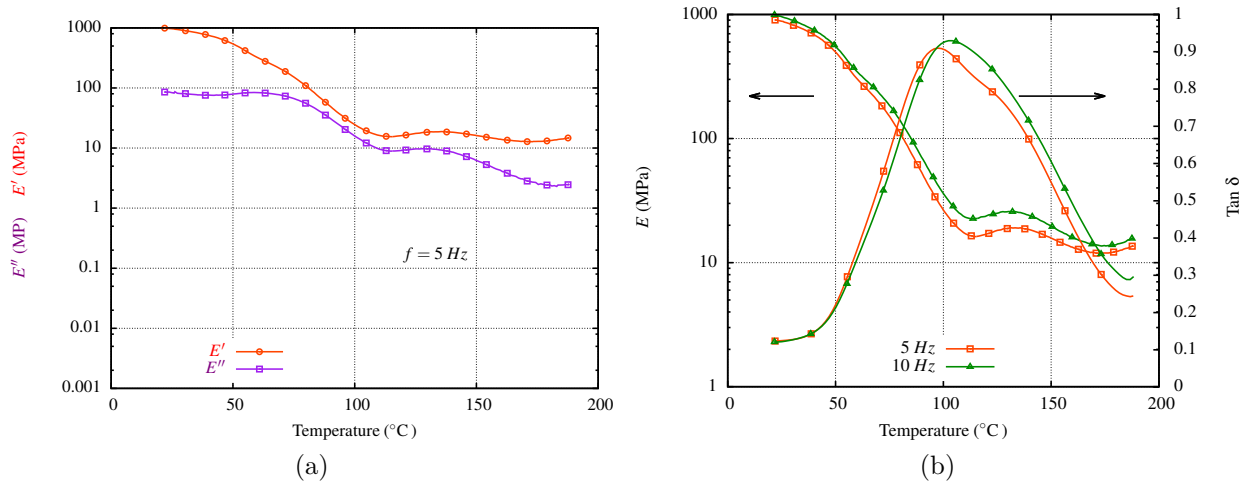


Figure 3.50: DMA analysis on Polyurethane (a) Loss modulus and storage modulus evolution (b) Elastic modulus and $\tan \delta$ evolution at different strain rates of 10^{-3}s^{-1} and 10^{-2}s^{-1} .

- The value of the elastic modulus decreases with temperature, and stabilizes at low values above the glass transition. These results are in agreement with the literature ([Tro14]). Also, the values of the elastic modulus and of the glass transition temperature depend on polyurethane type and composition.

The effect of heating rate on the mechanical response of the polyurethane was studied through DMA during heating up to 200 °C at 0.5 °C/min, 2 °C/min and 10 °C. The results illustrated in Figure 3.51 show a dependence of the apparent elastic modulus over heating rate. There is a further decrease of the elastic modulus with a higher heating rate. This supposes that a low heating rate gives rise to a harder resin and a stronger structure. This is probably due to the phenomena of additional crosslinking discussed in the previous paragraph 3.7.1.3 and strengthens the hypothesis made where the overall core structure depends on resin mechanical properties.

3.7.2.2 Tensile tests on resin

1. **Effect of temperature.** The temperature effect on the monotonic behavior of the Polyurethane resin for a strain rate of 10^{-3}s^{-1} is shown in Figure 3.52 for room temperature and in Figure 3.53 for five different temperatures, namely room temperature, 70 °C, 135 °C, 150 °C and 200 °C.

A large temperature dependence is observed below the chemical decomposition temperature at 150 °C, due to the physical aging (softening process and glass transition). In fact, the resin softens when increasing temperature [Bri16], which explains the loss of mechanical properties in tests from room temperature up to 150 °C. A material hardening is observed at 200 °C which we believe is due to crosslinking since it is known that thermosetting polymers do not meltdown due to crosslinking [Bri16]. The resulting behavior is then stronger for 200 °C than for 135 °C and 150 °C.

However, due to thermal decomposition and degassing, the specimen exhibits many defects with apparent gas cavities as shown in Figure 3.54 for a specimen heated up

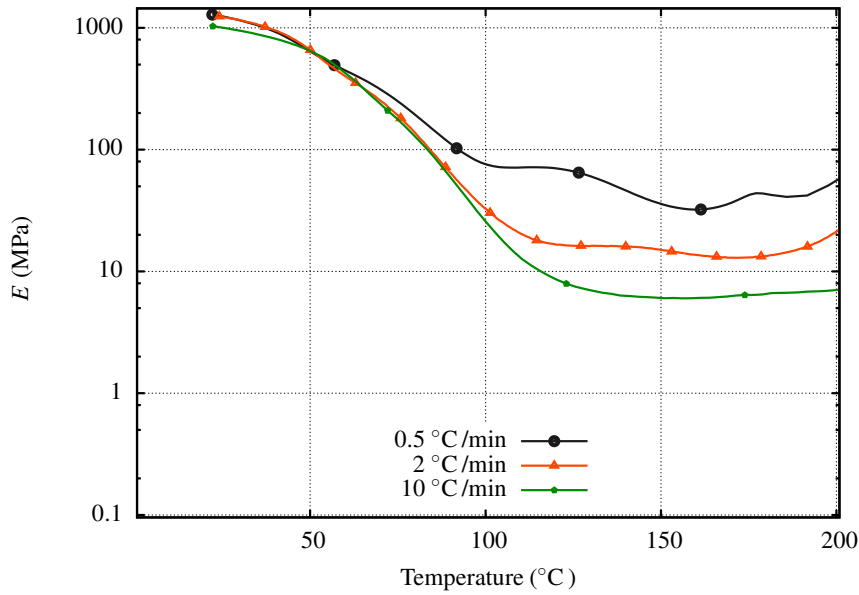


Figure 3.51: DMA analysis on Polyurethane during heating between room temperature and 200 °C at 0.5 °C/min, 2 °C/min and at 10 °C/min.

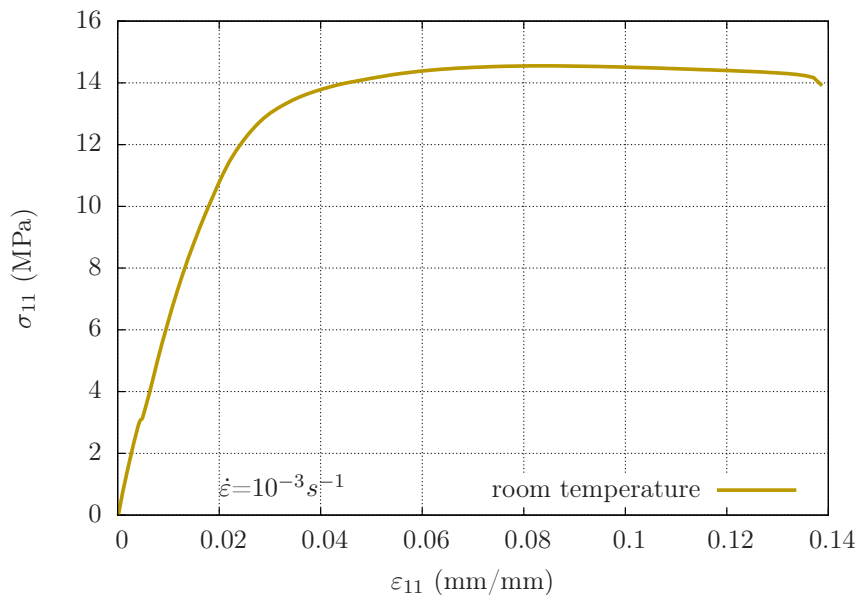


Figure 3.52: Tensile test at a strain rate of 10^{-3}s^{-1} at room temperature.

to 230 °C. It was then impossible to perform a mechanical characterization of the polyurethane at high temperature.

- Effect of aging time.** The effect of aging period at constant temperature on the mechanical response of the resin was studied through tensile tests at different temperatures and hold time. Tensile tests were performed at a strain rate of 10^{-3}s^{-1} at different temperatures (100 °C, 135 °C and 200 °C) and aging times ($T_{ag} = 1\text{min}$, 10 min and 20 min). The tests consist in heating the specimen up to a certain constant temperature at a heating rate of 2 °C/min. Once the selected temperature is reached, hold times of 1, 10 and 20 min are applied before the tensile loading. The curves obtained for the three temperatures are plotted in Figures 3.55a, 3.55b and

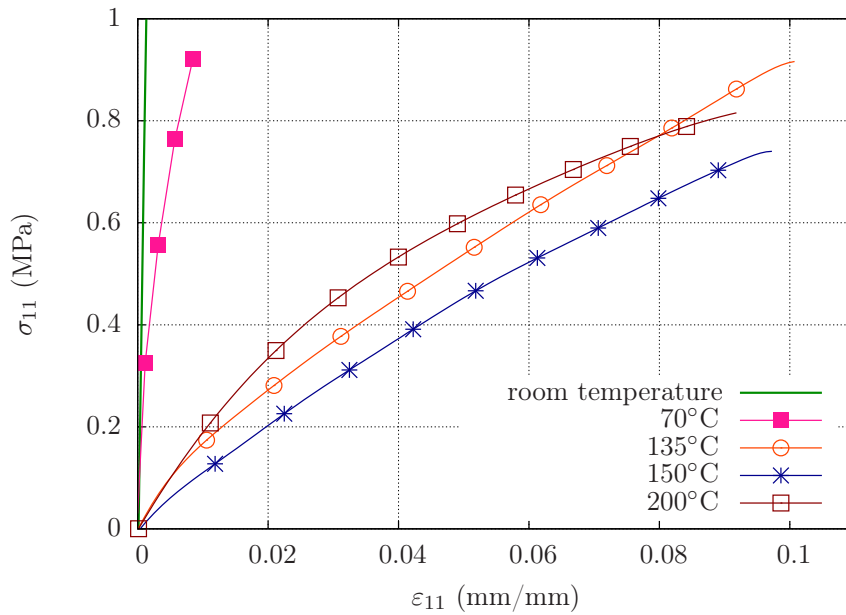


Figure 3.53: Tensile tests at a strain rate of 10^{-3}s^{-1} at room temperature, $70\text{ }^{\circ}\text{C}$, $135\text{ }^{\circ}\text{C}$, $150\text{ }^{\circ}\text{C}$ and $200\text{ }^{\circ}\text{C}$.

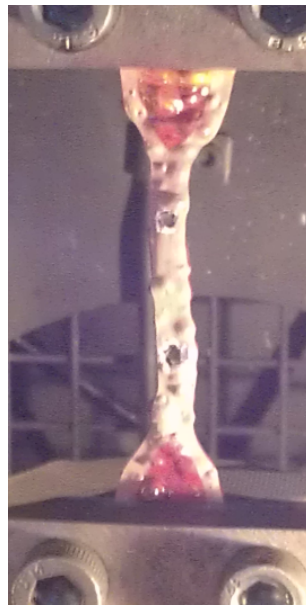


Figure 3.54: Specimen heated up to $230\text{ }^{\circ}\text{C}$ at $2\text{ }^{\circ}\text{C}/\text{min}$.

3.55c respectively for the different aging periods, until the specimen is broken. The failure was initiated by defects (either present in the material (air cavities trapped in the material during preparation) or developed during resin degradation) so that the strain to failure is not significant.

The material exhibits an elastic behavior at $100\text{ }^{\circ}\text{C}$ and $135\text{ }^{\circ}\text{C}$, while at $200\text{ }^{\circ}\text{C}$, the resin develops non linearities. When increasing aging time, the maximum stress reached increases. The material hardens but there was no significant difference in the material response when aged under isothermal conditions during 10 or 20 min before loading.

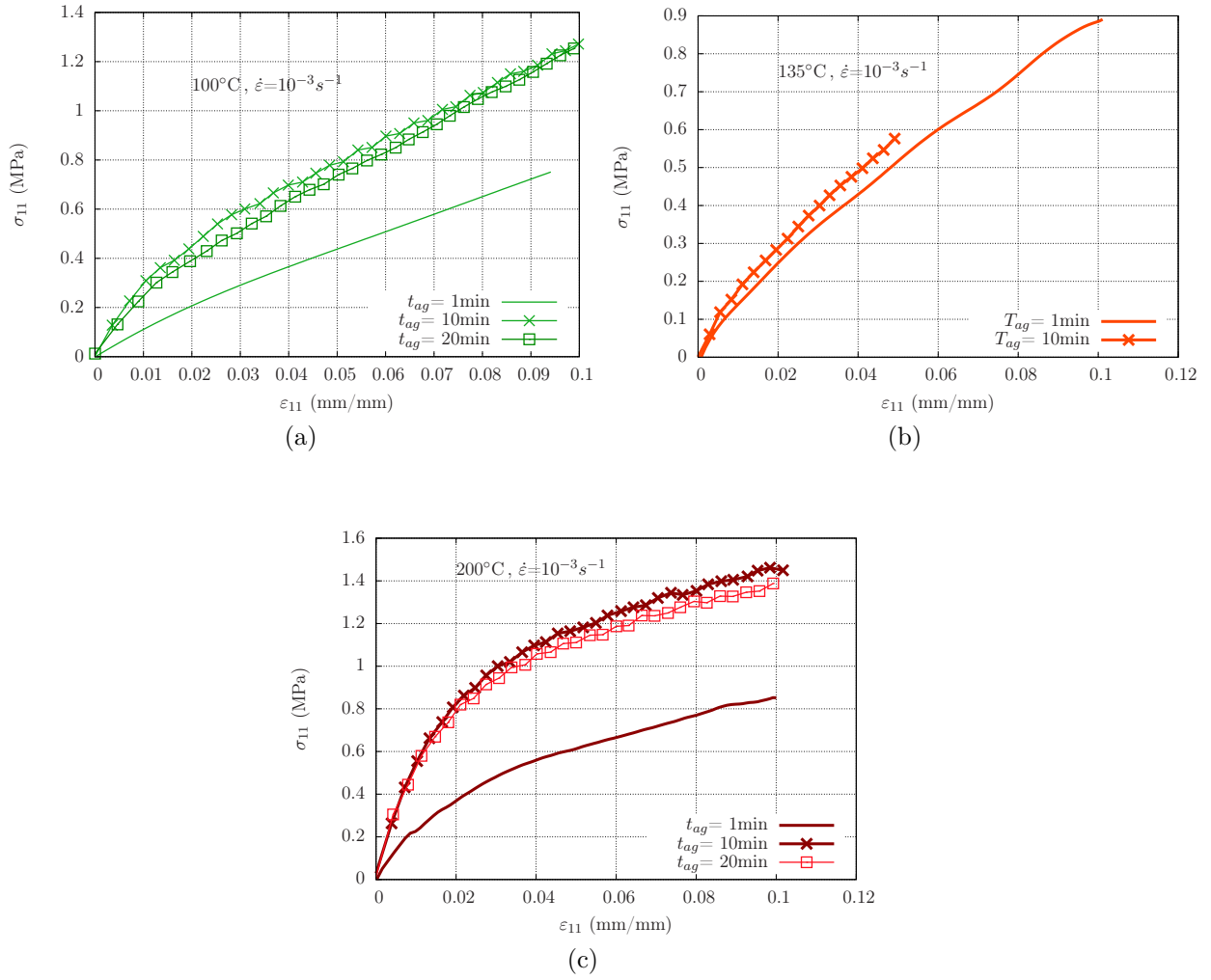


Figure 3.55: Tensile tests at different aging times $T_{ag} = 1, 10$ and 20 min at (a) $100^\circ C$ (b) $135^\circ C$ and (c) $200^\circ C$.

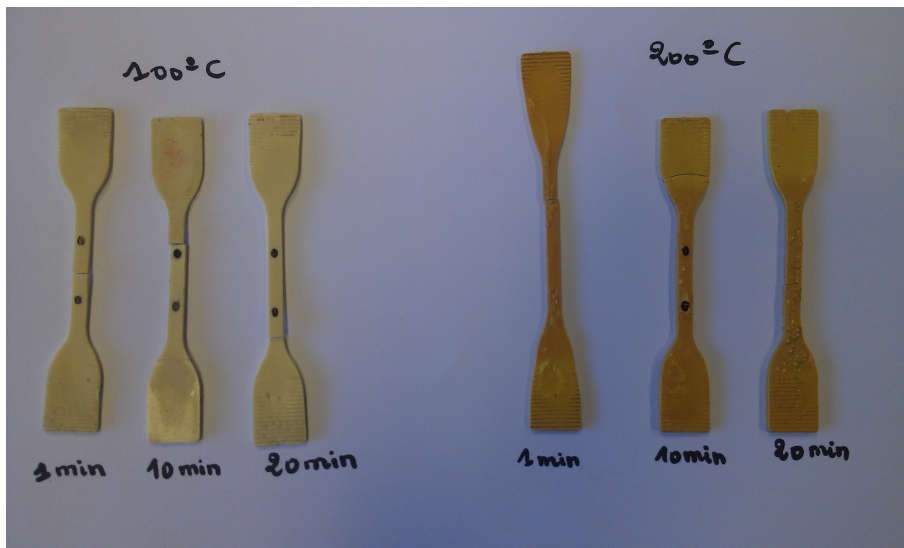


Figure 3.56: Resin specimens tested at different temperatures and aging times.

3. **Effect of applied strain rate.** Tensile tests at a strain rate of 10^{-2}s^{-1} at room temperature and $150\text{ }^\circ\text{C}$ were done in comparison to 10^{-3}s^{-1} tests in order to investigate the viscosity effect. The corresponding curves are given in Figure 3.57. At room temperature, viscosity is well pronounced in comparison to the test at $150\text{ }^\circ\text{C}$. These results are in agreement with the DMA analysis shown in paragraph 3.7.2.1 where the viscosity effect vanishes at high temperatures above the glass transition temperature.

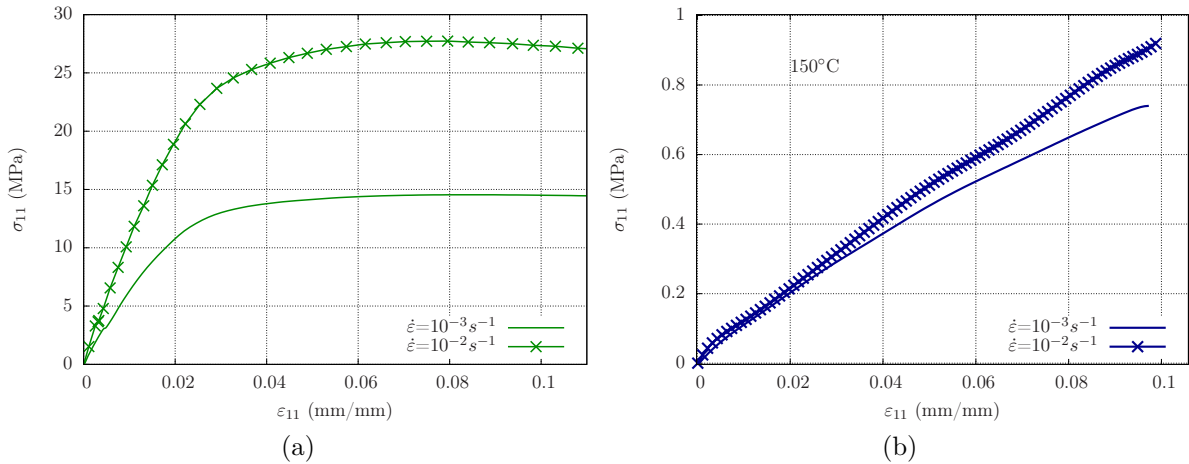


Figure 3.57: Tensile tests at a strain rate of 10^{-3}s^{-1} and 10^{-2}s^{-1} (a) at room temperature (b) at $150\text{ }^\circ\text{C}$.

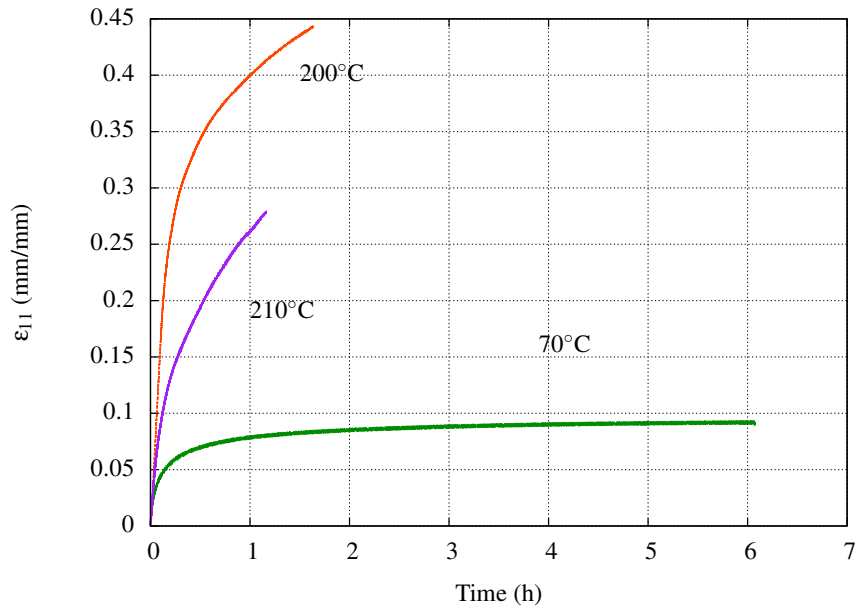
3.7.2.3 Creep tests on resin

Figure 3.58a shows the results of creep tests conducted on resin. Primary and secondary creep stages were observed in all tests.

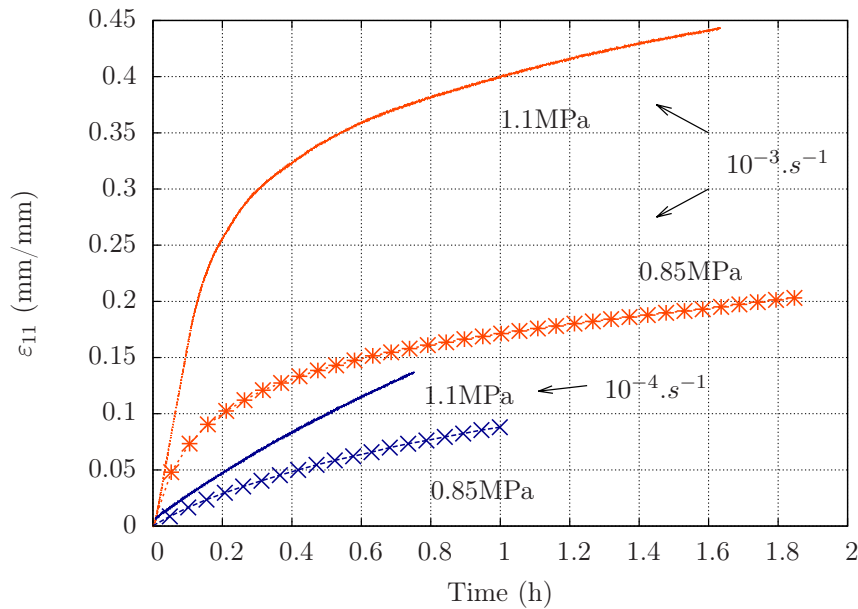
At $70\text{ }^\circ\text{C}$, a creep saturation is observed. At $200\text{ }^\circ\text{C}$, the creep strain is much larger, while the total strain observed at $210\text{ }^\circ\text{C}$ is smaller than for $200\text{ }^\circ\text{C}$. It is worth noting that during tests above $200\text{ }^\circ\text{C}$, the material presents defects due to degassing and its color changes indicating material degradation such that the test had to be interrupted. In order to characterize the influence of the loading history on creep response, the resin creep behavior was investigated at $200\text{ }^\circ\text{C}$ at strain rates of 10^{-3}s^{-1} and 10^{-4}s^{-1} with applied stresses of 1.1 MPa and 0.85 MPa . The specimens loaded at a strain rate of 10^{-3}s^{-1} show primary and secondary creep stages as seen in Figure 3.58b, while only primary creep was obtained with a loading strain rate of 10^{-4}s^{-1} . This is a clear demonstration that time allows the material to become stronger due to resin reticulation. For a given prescribed strain rate, the accumulated strain was found to increase with increasing stress level.

3.7.2.4 Discussion

The experimental results revealed a dependence of the resin behavior on temperature, temperature rate and aging time. However, we were limited in our mechanical analysis to $200\text{ }^\circ\text{C}$ due to thermal degradation. Unfortunately, the evolution of the mechanical



(a)



(b)

Figure 3.58: Total strain evolution as a function of time in creep tests (a) at 70 °C, 200 °C and 210 °C with a loading strain rate $\dot{\epsilon}=10^{-3}\text{s}^{-1}$ and an applied stress $\sigma_{creep}=1.1\text{ MPa}$ (b) at 200 °C under different applied stresses and loading strain rates.

properties at higher temperature due to the chemical transformations taking place could not be studied.

Meanwhile the mechanisms and properties related to the polymer behavior at low temperatures have been investigated in the literature. Rodriguez *et al* [Rod14] studied the softening and hardening phenomena in polymers. They describe the softening process as caused by a chain scission mechanism and the hardening (embrittlement) processes as due to the crosslinking process at higher temperatures. Tobolsky [Tob60] discusses further in his study the creep behavior and related cleavage mechanism (chain scission) and crosslinking for rubbers. In a more recent study [Joh05] the authors worked on elastomers

response subjected to finite deformation in a temperature range of 90–150 °C. They present a model for stress relaxation (viscoelasticity) and chemical relaxation (chain scission mechanism) under complex temperature histories and uniaxial loads. A method was also developed to further account for scission process and oxygen depletion. In [Ala07] and [Ala08], the authors study both deformation, thermally induced scission and crosslinking in the macromolecular chains. They describe these mechanisms as time and temperature dependent chemical changes occurring above a critical temperature in elastomers. However, the few existing studies were focused on the rubbery stage at temperatures slightly above the glass transition temperature.

To the best of our knowledge, the relation between the mechanical properties and the heating rate and hold time which was revealed in our study has not been previously described in the literature. We can safely consider that the chemical aging subject is not as mature as physical aging. Most importantly, at higher temperatures (above the temperature of thermal degradation which is 150 °C in our case), chemical aging (pyrolysis) and its effect on the material properties is still an important topic that has not been fully investigated [Bri15].

3.7.3 Sand core thermomechanical characterization

3.7.3.1 DMA tests

Three point bending DMA tests were conducted on sand core samples. This experiment provide an “apparent” value of the Young modulus (Table 3.7) that decreases with increasing temperature. Unfortunately, the specimen broke down at 200 °C so we do not have any measures above this temperature. We assumed that the Young modulus values will continue to decrease above 200 °C due to thermal decomposition.

Table 3.7: Sand core apparent Young modulus values

temperature (°C)	value (MPa)
20	3000
50	2910
100	1898
150	1216
200	180

3.7.3.2 Compression tests on sand core

Uniaxial compression tests were conducted at room temperature and 80 °C and a strain rate of 10^{-3}s^{-1} on 45 mm long and 30 mm in diameter cylindrical pawns. The specimens were heated at 2 °C/min. Once temperature reaches the setpoint, the load is applied. The temperature control curves are given in Figure 3.59. The specimen temperature is measured at the center of the specimen, at a width of 15 mm. The target temperature is reached in about 60 min. In fact, the furnace size is too big compared to the specimen size, so that makes the heating rate is hardly controlled, due to the porosity of the material and the inertia of the furnace.

The compression curves are given in Figure 3.60 using the LVDT data. All the curves

have a zero-stress bearing representing the loading step and more precisely the catch-up of the space between the plates and the sample (contact and granular rearrangement). A particular attention was given to the adjustment of the parallelism of the two plates. This zero stress bearing is followed by an increase of the stress to reach a maximum value and then it decreases. The maximum stress reached in the tests at room temperature presents some scatter. This may be related to the preparation of the specimens. The maximum stress drops from room temperature to 80 °C. The slope of the curves is difficult to analyse since at the beginning of the test, a near zero stress is obtained when bringing into contact the compression plateau to the specimen due to grain rearrangement. The aspect of the specimen at the end of the test is given in Figure 3.61. The specimens broke down from the top surface with an angle of 45 degree. This might be due to sample weakening coming from its cutting during preparation.

An attempt to study the local strain field for a test at 110 °C was made using an “Advanced Video Extensometer” (AVE) which allowed us to measure directly the local strain fields by means of an optical extensometer as shown in Figure 3.62. Figure 3.63 shows a comparison between the previous results (using LVDT sensor) and the local 2D measurements. It appears that the optical extensometer prevents errors related to grain rearrangement and the problem linked to the deficient parallelism of the plates. However the technique is too sensitive to the preparation of the specimen and the temperature control is not effective enough. More advanced experimental tests need then to be developed.

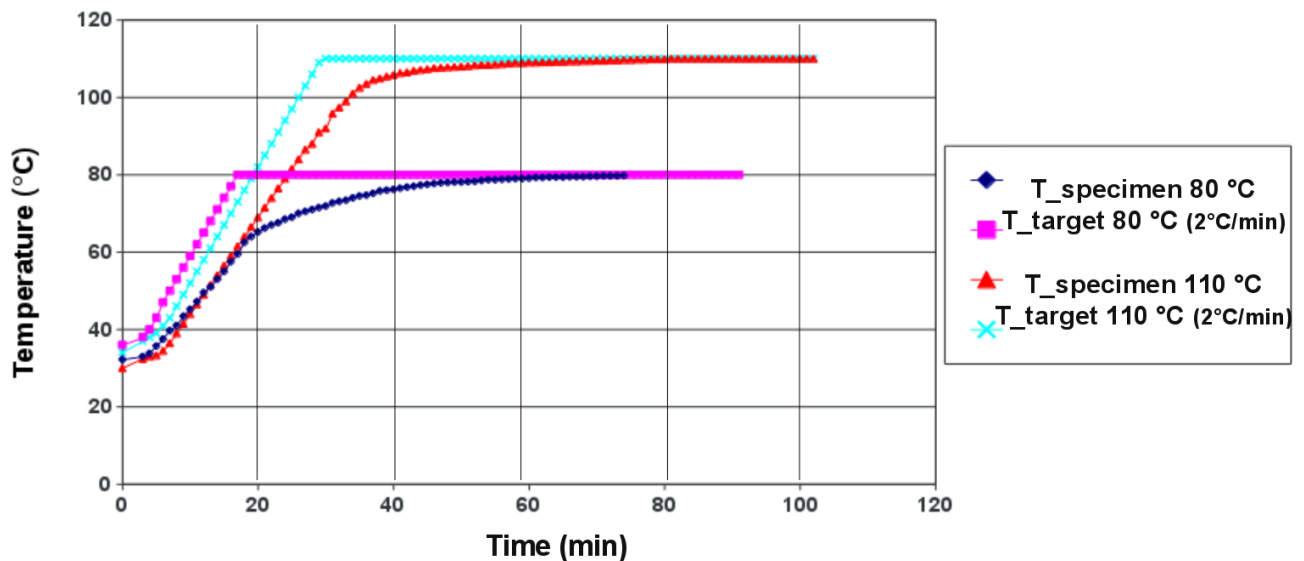


Figure 3.59: Temperature evolution of a compression specimen compared to the set temperature during heating.

3.7.3.3 Isothermal creep bending tests on sand core

Four-point bending tests were conducted at different temperatures. In Figures 3.64a and 3.64b, we compare the evolution of the measured deflection at a heating rate of 2 °C /min under respectively self weight up to 300 °C and with an applied mass of 164 g at different

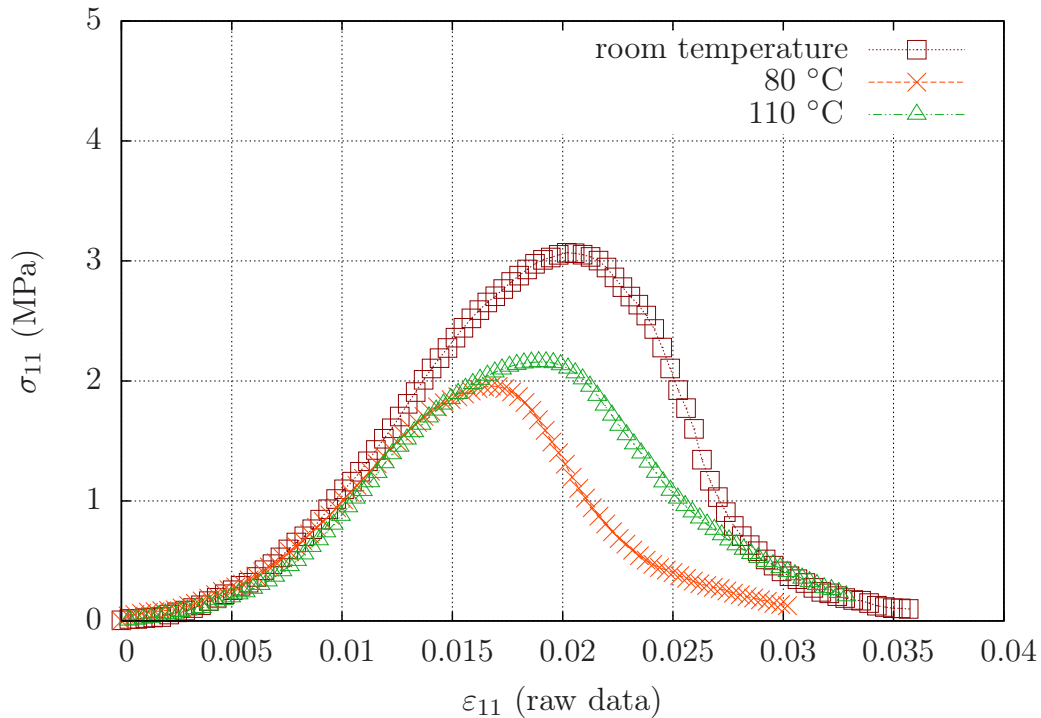


Figure 3.60: Uniaxial compression tests at room temperature and 80 °C and a strain rate of 10^{-3}s^{-1} .

reference temperatures.

Under both types of loading, there is an evolution of the deflection only during the heating phase. A displacement is observed above 50 °C, the temperature for which solvents start boiling, as discussed in section 3.7.1.1. When temperature becomes constant, there is a quick saturation of the deformation process. The maximum value reached seems to depend on temperature and probably on the resin decomposition stage.

Unless indicated otherwise, each test was performed twice in order to check the reproducibility. Figure 3.65 shows the results for bending tests with a maximum temperature of 200 °C and a temperature rate of 2 °C/min. It can be seen that the reproducibility is ensured, thanks to good preparation and preservation conditions, specifically against humidity. In general, each time scatter is observed, which might be due to the specimen preparation or the number of resin bridges present in the sample, the tests are repeated three times.

Temperature dependence was further investigated using Scanning Electron Microscopy (SEM). Observations were done on the tested specimens. The SEM samples were extracted at the center of the specimen in the region of maximum deflection. Micrographs of a reference specimen at room temperature and specimens tested at 200 °C and 300 °C are shown in Figure 3.66, 3.67 and 3.68 respectively. In Figure 3.66, the surface of a specimen, before the test shows a relatively smooth aspect with few cavities at the center of the resin bridge. In contrast, Figures 3.67 and 3.68 show a significant development of cavities in the resin bridges at high temperatures with more pores towards the center due to mass loss. Most importantly, these microscopic observations at high temperatures (Figures 3.67 and 3.68) show the presence of resin linking bridges between sand particles. The resin is not completely destroyed. The overall material deformation is possibly due to internal damage occurring in the resin. The thermal degradation (mass loss, irreversible

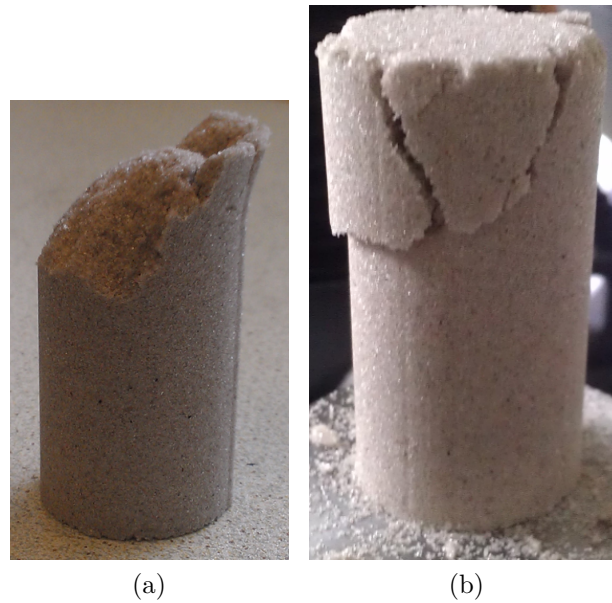


Figure 3.61: Sand core compression specimens tested at (a) room temperature (b) 80 °C .

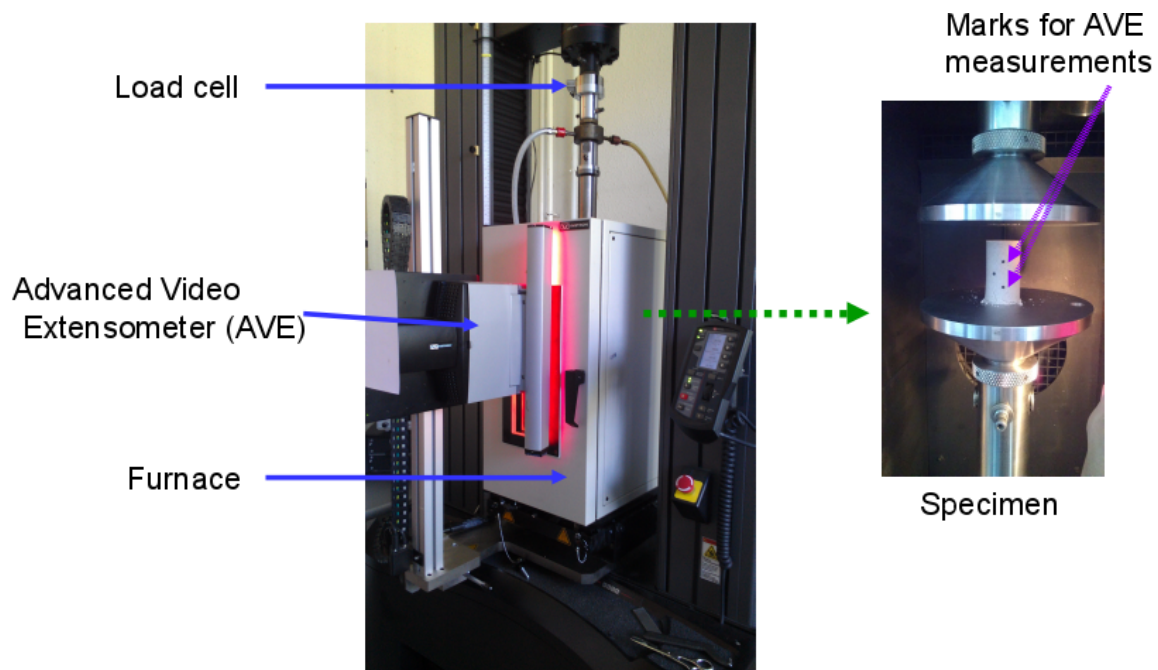


Figure 3.62: Compression apparatus equipped with Advanced Video Extensometer.

macromolecular changes) leads to a strength loss in the bonding resin which has an impact on the overall material response. We believe that these observations may explain further the expansion/contraction changes discussed in paragraph 3.7.1.3.

1. **Effect of heating rate.** Four-point bending specimens were tested at different heating rates (typically 0.5 °C/min, 2 °C/min, 10 °C/min and 20 °C/min). Figure 3.69 illustrates the evolution of the deflection as a function of temperature. The maximum deflection increases drastically with increasing heating rate. In case of temperature rates of 10 °C/min and 20 °C/min, the specimens lost their strength

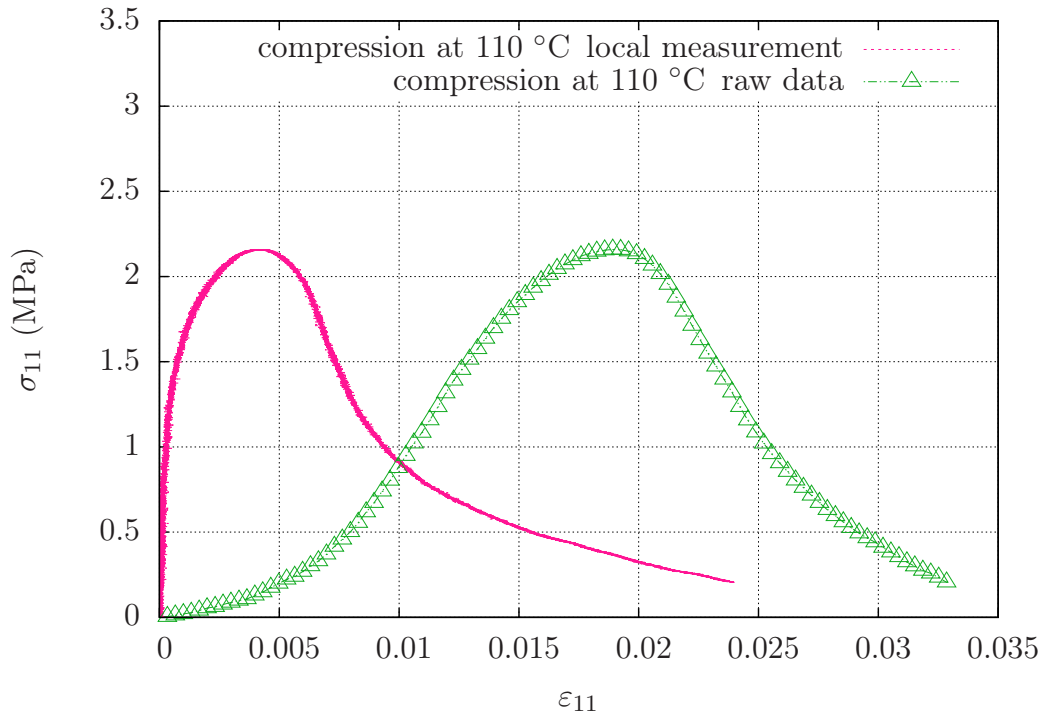


Figure 3.63: Comparison of uniaxial compression test results 110 °C between local strain measurements (AVE optical extensometer) and using the LVDT.

and broke down slightly above 200 °C.

We believe that the dependence on heating rate is directly related to the resin behavior. A faster heating leads to lower values of the elastic modulus. This is probably due to a chain scission mechanism which causes a strength loss, while crosslinking at low heating rates gives rise to a stronger resin.

2. **Effect of thermomechanical history.** The strong dependence of the material behavior on time, heating rate and temperature suggests a further investigation with more complex thermomechanical histories. Two configurations were tested:

(a) Configuration 1: Heating up to different temperatures with different hold times. Tests with complex heating cycle were performed as described in Figure 3.70a where $T_1 = 200$ °C, $t_1 = 2$ hours, $T_2 = 250$ °C and $t_2 = 1.5$ hour at a heating rate of 2 °C/min. The results are given in Figure 3.70b.

The maximum deflection measured at T_2 with a hold time at the intermediate temperature T_1 in Figure 3.70b is compared with result of the reference test presented before in paragraph 3.7.3.3 with a continuous heating up to 240 °C and recalled below in Figure 3.71. It can be seen that the value of the deflection obtained with an intermediate hold time is lower than the reference deflection reached with a continuous heating until T_2 .

The material state shows a dependence on the maximum temperature and the duration of the dwell period. As discussed in paragraph 3.7.2.2, the irreversible macromolecular change in the polymer structure and the additional crosslinking mecha-

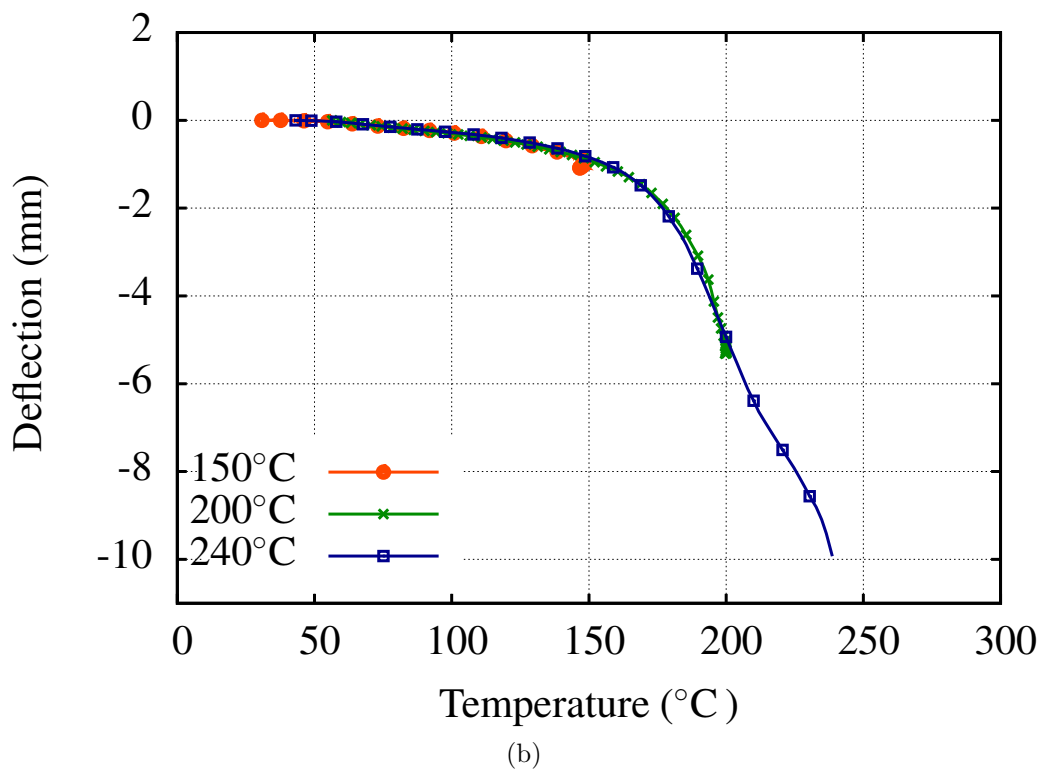
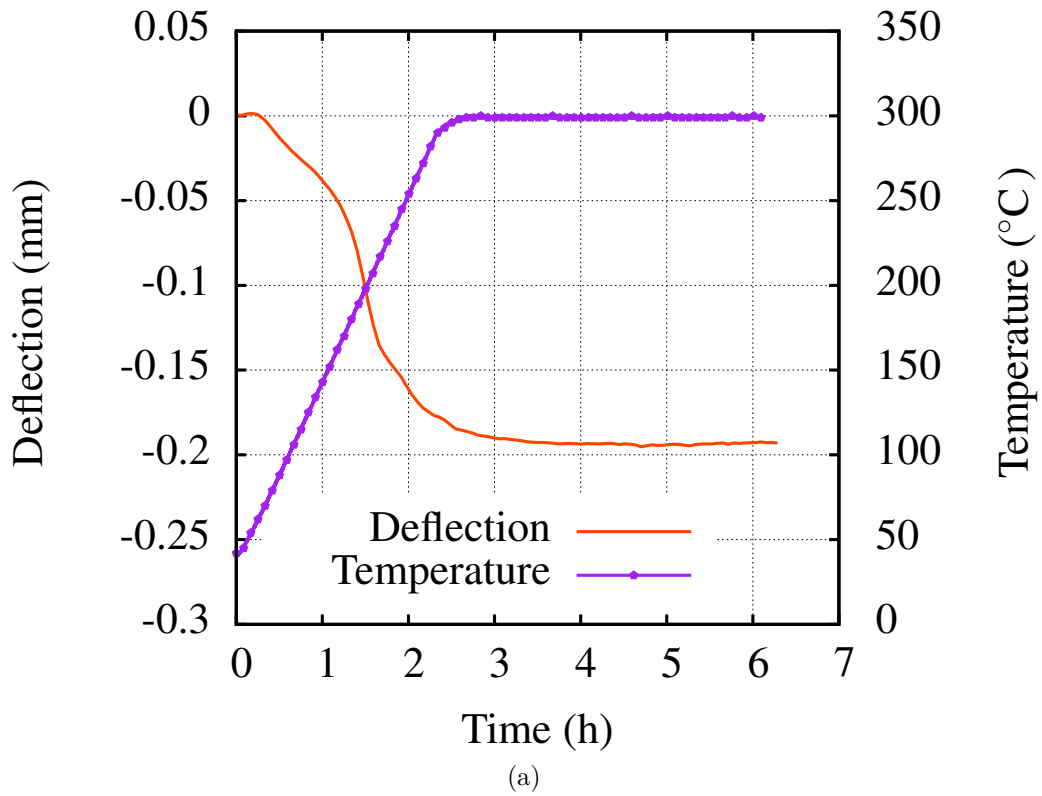


Figure 3.64: Bending test on sand core (a) under self weight at 300 °C (b) under a mass of 164 g at different target temperatures.

nism which induces hardening in resin may be responsible for hardening in the sand core structure.

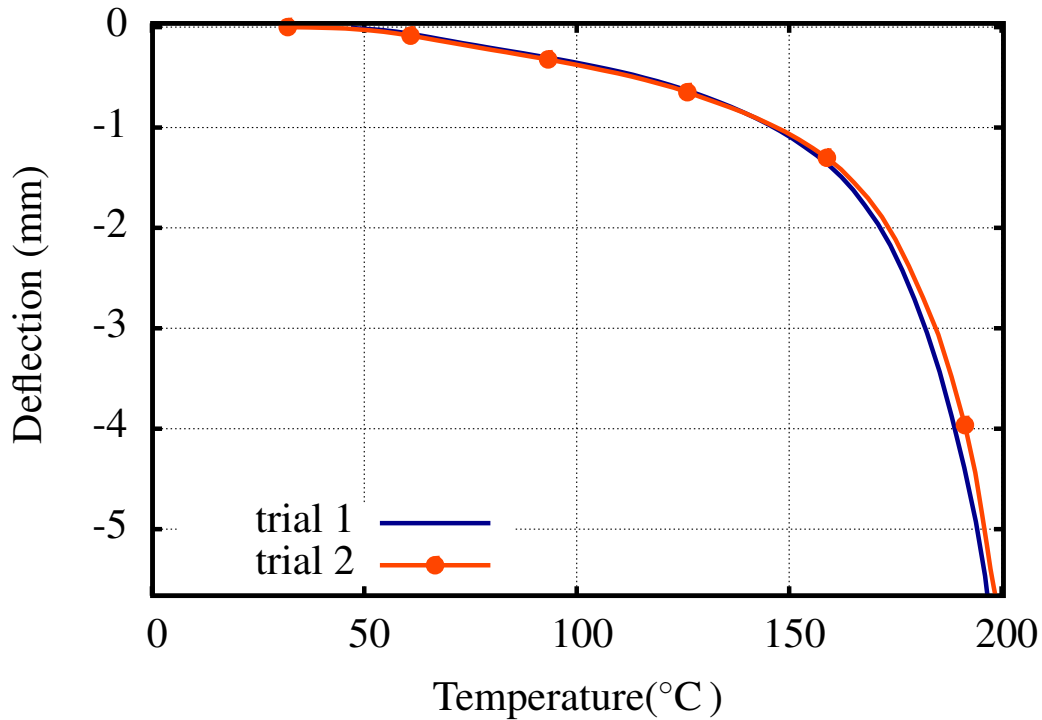


Figure 3.65: Comparison of bending test results under heating up to 200 °C at 2 °C /min for two different tests.

The influence of test parameters like the heating rate (typically 0.5 °C /min, 2 °C /min and 10 °C /min) and the hold time t_1 at T_1 (typically $t_1 = 30$ min and $t_1 = 2$ hours) were further investigated. Results are given in Figure 3.72. During heating from T_1 to T_2 , a longer hold time at T_1 slows down the deflection variation (additional crosslinking and hardening). Meanwhile, with a higher heating rate (Figure 3.72c), whatever the hold time at T_1 , the final state is close to the value obtained with a direct heating up to T_2 , and the specimen broke down. These results show an aging effect that is essentially dependent on resin degradation kinetics. Particularly, a higher heating rate was found to cause collapse of the sand core structure and hinder resin additional crosslinking (see paragraph 3.7.1.3).

(b) Configuration 2: Cyclic loading. This type of material is characterized by its asymmetric behavior in tension and compression. Since performing tensile tests on the sand core is not possible, tests were designed to apply a cyclic loading by turning upside down the specimen during the test using the same mass of 164 g as for the previous isothermal tests. The configuration of the mechanical loading applied in one cycle is shown in Figure 3.73. To the best of our knowledge, such configurations have not been tested yet.

A first specimen is heated up to 200 °C at 2 °C /min with a subsequent hold time of 45 min, which is enough to reach a stationary stage as shown in Figure 3.74a. At the point denoted *a*, the specimen is turned upside down without any temperature change.

The results show that once the specimen is turned, a reverse deformation takes place

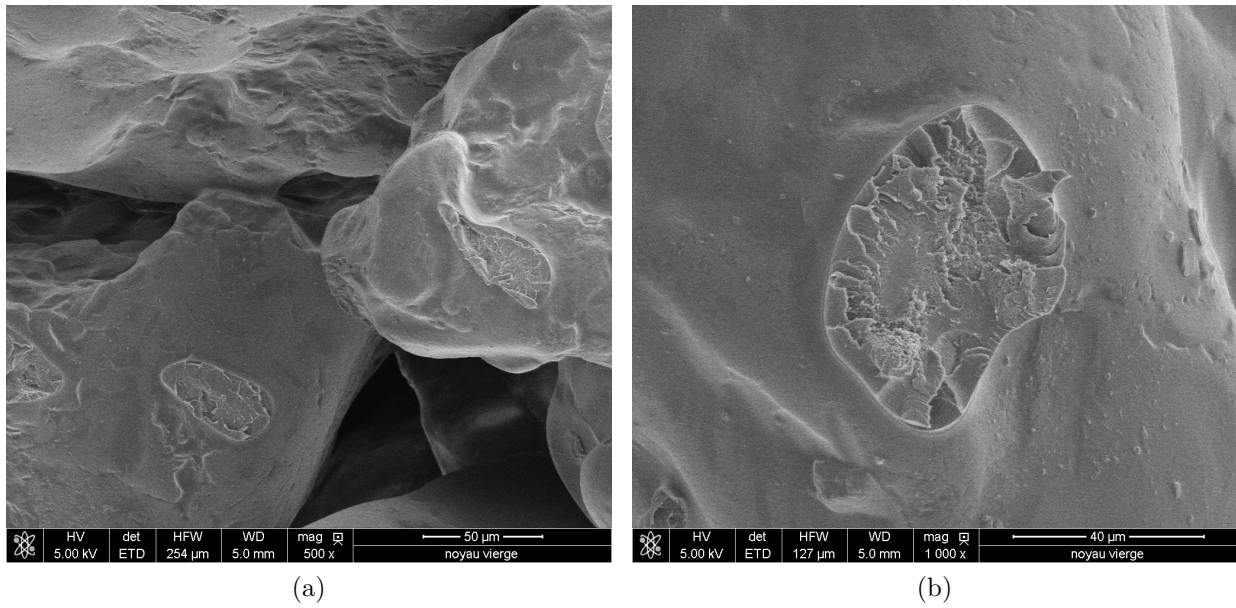


Figure 3.66: SEM image of a sand core at room temperature (a) global view (b) resin bridge

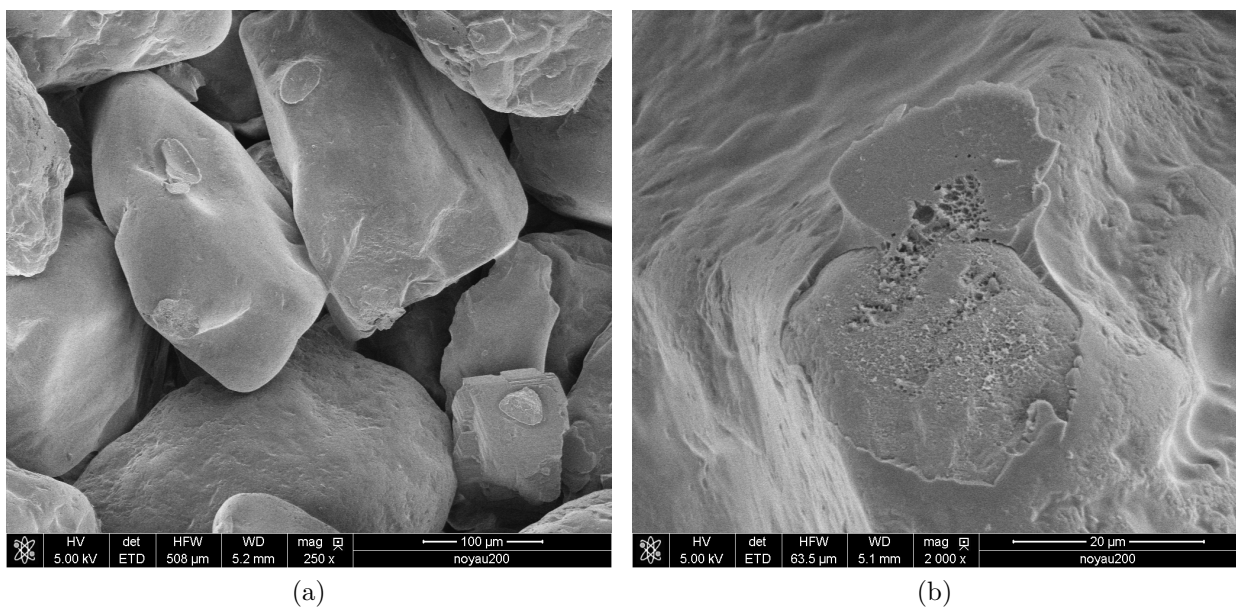


Figure 3.67: SEM image of a sand core tested at 200 °C (a) global view (b) resin bridge

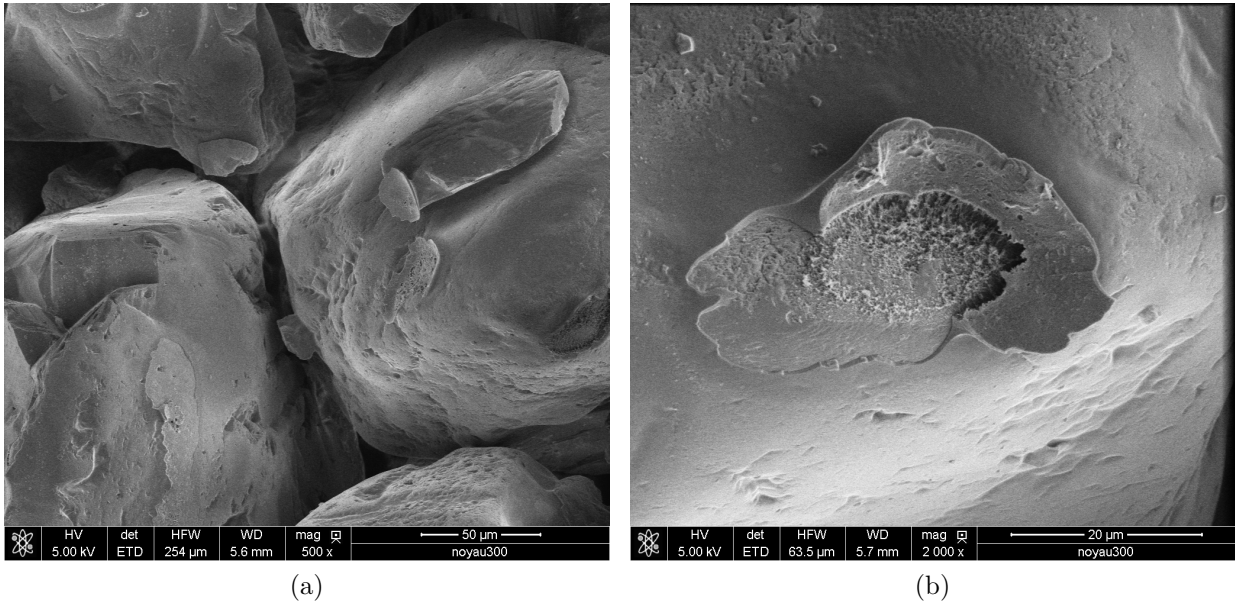


Figure 3.68: SEM image of a sand core tested at 300 °C (a) global view (b) resin bridge

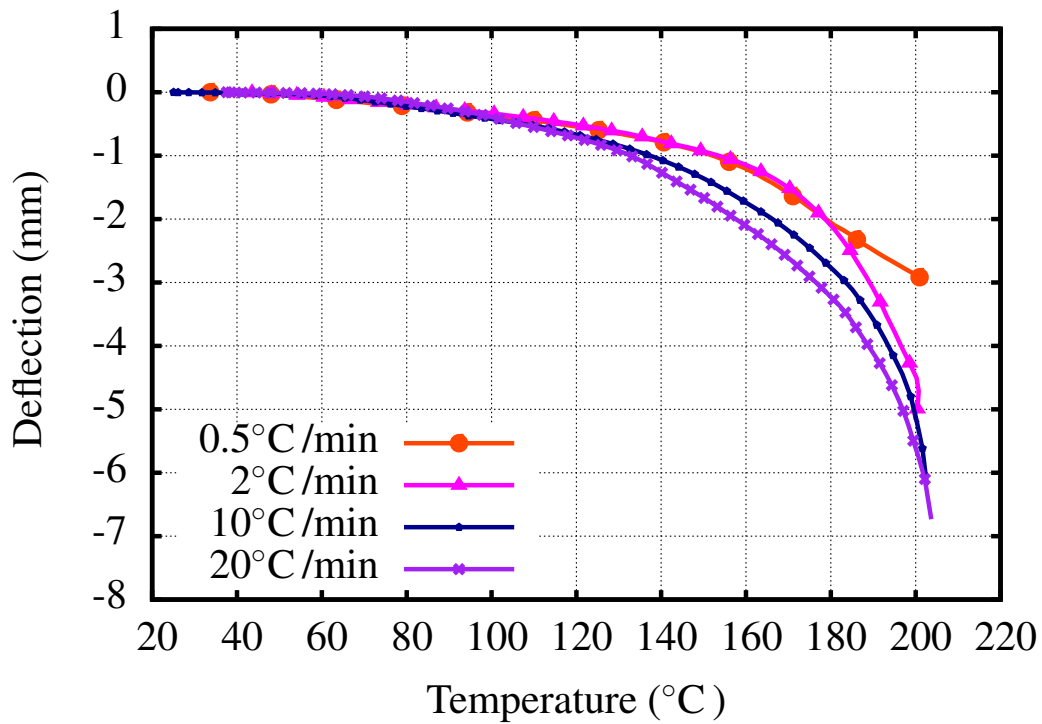


Figure 3.69: Four-point bending tests at heating rates of 0.5 °C/min, 2 °C/min, 10 °C/min and 20 °C/min.

and tends, again, towards a stationary stage due to resin crosslinking. This evolution may be related to the fact that the resin bridges initially loaded in compression are now loaded in tension with temperature conditions such that the thermal decomposition and crosslinking are still active. For a final stage with heating up to 250 °C, the deflection varies again.

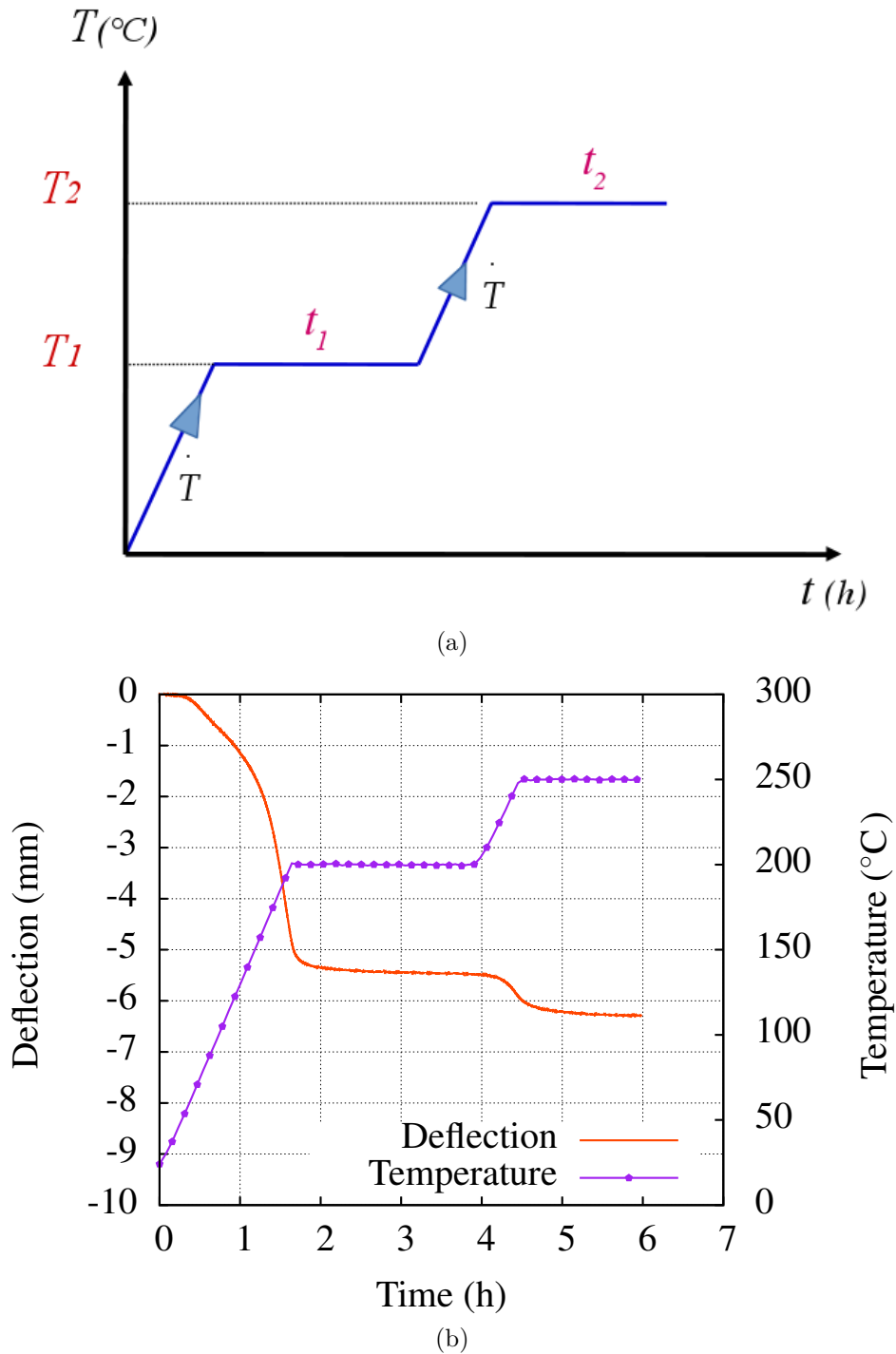


Figure 3.70: Four-point bending test (a) under heating cycle with a hold time t_1 at T_1 and then up to T_2 and a hold time t_2 . Deflection evolution (b) with a dwell time $t_1 = 2$ h at $T_1 = 200$ °C and then up to $T_2 = 250$ °C.

A second specimen (Figure 3.74b) was cooled down before being turned upside down. The test includes the following steps:

- **Step 1:** The sample is heated up to 150 °C. The temperature is kept constant during 45 min, then the specimen is cooled down;
- **Step 2:** At point a , the cooled sample is turned upside down, heated up again

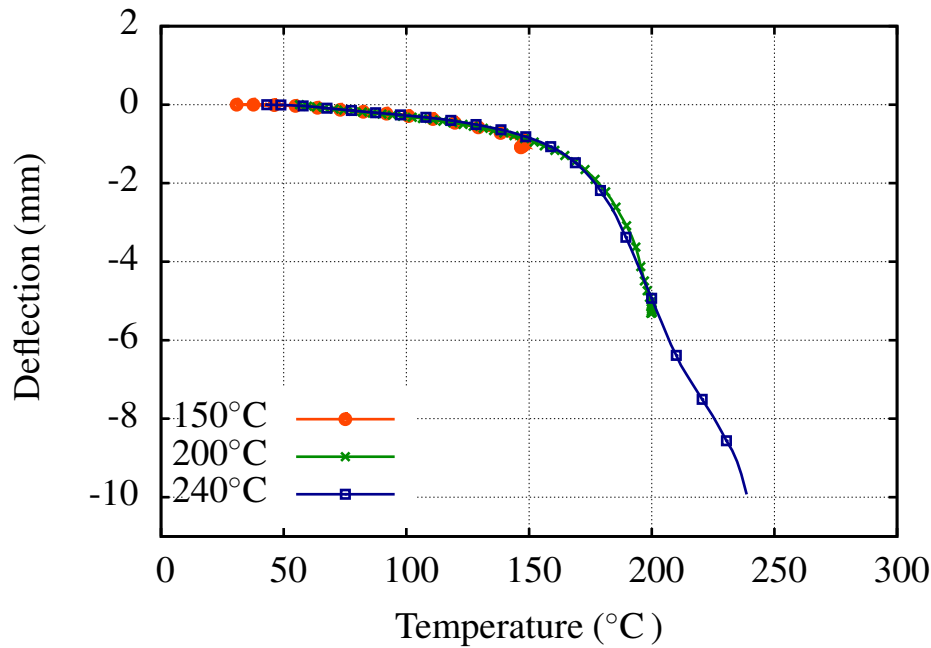


Figure 3.71: Bending test on sand core under a mass of 164 g at different target temperatures.

and maintained at 200 °C and then cooled down;

- **Step 3:** At stage denoted *b*, the cooled sample is turned upside down, heated up one more time up to 250 °C.

As seen in step 2 (Figure 3.74b), once the specimen is turned over and reheated, the deflection remains constant until 150 °C. The deformation obtained in step 1 is then irreversible. This is possibly related to the irreversible chemical reactions as discussed in paragraph 3.7.1.1. Even when turning upside down the specimen, there is no deformation of the material if the decomposition process is no longer active and the resin structure becomes highly crosslinked. Above 150 °C, the deflection varies again with the activation of the thermal degradation process. The same results are obtained in step 3 where the deflection varies above 200 °C.

These cyclic loading tests enabled to trigger the compression and tension areas. The results confirm that the sand core deforms only during an active thermal decomposition process which is governed by irreversible chemical reactions.

3. **Effect of applied load.** The sand core was tested under four-point bending tests with two different constant loads (100 g, 164 g) during heating up to 200 °C. Figure 3.75 shows the evolution of the deflection as a function of the temperature. The deformation under a mass of 164 g is larger compared to the one observed under a mass of 100 g. The resin viscosity effect is very strong here.
4. **Effect of resin proportion.** The effect of the resin decomposition on material behavior raises the question of the influence of the resin percentage present in the sand core. An investigation was then made with total binder percentages of 0.8 wt%, 1 wt% and 1.3 wt%. The specimens were tested under four-point bending at heating rates of 0.5 °C/min and 2 °C/min up to 200 °C.

The results given in Figure 3.76 show that the sand core is stronger for the case of high resin contents, while the specimens broke down at approximately 180 °C with the lowest resin percentage of 0.8 wt%.

Based on these results, a higher resin percentage seems to provide better mechanical properties. In contrast, this causes difficulties when extracting the core from the cooled metallic part, and more gases are emitted during casting due to the resin decomposition. These gases could be trapped inside the cast part, and may cause defects in the final product. The choice of 1 wt% seems to be a good compromise then.

3.7.3.4 High temperature isothermal bending creep tests

The sand core reaches temperatures up to 450 °C during casting. While the maximum temperature which could be applied by means of the resistive furnace in the previous tests is 300 °C. Another setup has been used to extend the domain of study using a tube oven.

A sand core specimen was first instrumented with two type K thermocouples of 0.8 mm (T2 and T3 in Figure 3.77), placed inside the specimen, in order to validate the experimental protocol and check the temperature homogeneity. The sample was heated up to 200 °C at a heating rate of 2 °C/min. The evolution of temperature as a function of time is plotted in Figure 3.78. The specimen temperature is not homogeneous during the heating cycle. There is a gradient of 35 °C approximately, with a higher temperature in the center. In fact, the heating lamps are too close to the specimen. Moreover, the lamps are too powerful and we faced many difficulties regarding temperature regulation. The furnace is adapted for very high temperatures, extremely high heating rates (100 °C/min to 200 °C/min) and much smaller specimens. It was impossible to obtain an homogeneous temperature inside the specimen for our isothermal characterization.

Despite these difficulties four-point bending creep tests were conducted under an imposed heating rate of 2 °C/min with an applied mass of 164 g at different reference temperatures using this tube oven. In Figure 3.79, we compare the evolution of the measured deflection during heating up to 200 °C in tests 1 and 2 and 230 °C in test 3 at a heating rate of 2 °C/min with a reference test up to 240 °C conducted using a resistive furnace (see paragraph 3.7.3.3). It can be seen that there is scattering in the results. The difference becomes more pronounced above 150 °C where the thermophysical transformations and thermal degradation start in the binder as explained in paragraph 3.7.1. In tests 1 and 2, we continued recording the deflection evolution during the hold time at 200 °C, the specimen was found to continue to deform during the isothermal.

3.8 Summary

In this chapter, an original experimental protocol was implemented to characterize the sand core behavior. In the first part, the approach by Montupet was described, together with the limitations of the experiment. In the second part, a new approach was proposed. It consists in decoupling the study of the sand core and the binder in order to investigate the deformation mechanisms and depending parameters. Various tests were presented. In table 3.8 we summarize the mechanical tests performed on the sand core.

The main difficulty was to find the right device for our study in terms of temperature range and loading. Only the tests for the temperature range between room temperature

and 300 °C were conclusive. Unfortunately, it was not possible to explore the material through tomography because we could not distinguish the resin bridges from the silica particles due to the important difference in absorption between the resin and the silica phases. This would have given an important information about the resin proportion evolution under heating and the eventual structure evolution.

The different experimental analyses conducted on the sand core and the bonding resin revealed that the overall behavior of sand cores is governed by the resin aging. Up to 220 °C, the resin goes through solvents evaporation and softening leading to an important decrease of the core rigidity. At higher temperature, the thermal decomposition of the solid components (hardener and phenolic resin) takes place. During the latter stage, an irreversible contraction, characteristic of materials presenting microstructure variation, that is dependent on temperature history, was observed through the thermal tests and it was linked to resin aging. The thermal decomposition was found to cause complete loss of strength of the core. While heating at slow heating rates leads to resin hardening effect due to crosslinking and a stronger overall core structure, a higher heating rate fosters the elimination of the bonding resin and causes core structure collapse.

As a conclusion, the study of the sand core thermomechanical behavior revealed

- The dependence on temperature T ;
- The dependence on temperature rate;
- The dependence on applied load:
- The non classic thermal expansion behavior (expansion/contraction effect) with dependence on the heating rate;
- The resin physical and chemical aging;
- The asymmetric behavior in tension/compression;
- The sand core aging and structure collapse caused by the resin aging and strength loss.

3.9 Résumé en français

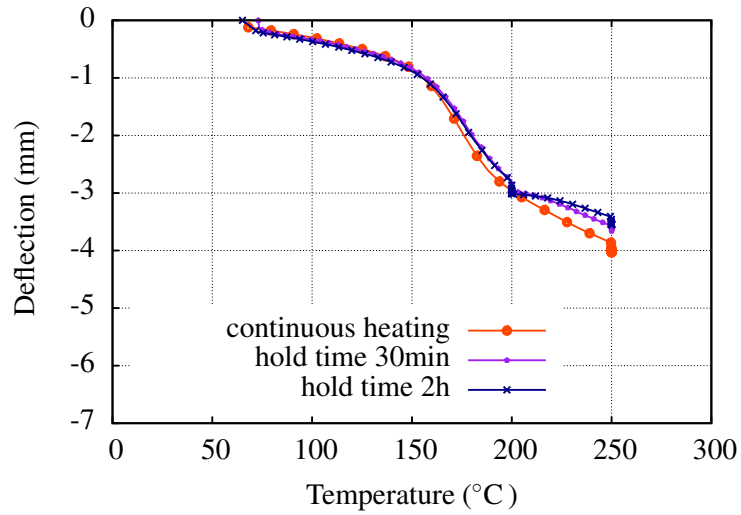
Dans ce chapitre, un protocole expérimental original a été mis en place pour caractériser le comportement et les propriétés du noyau de fonderie. Dans la première partie, l'approche utilisée par la société Montupet a été exposée, les difficultés rencontrées et les limites des expériences ont été discutées. Un accent particulier a été mis sur les informations nécessaires au développement d'un modèle de comportement thermomécanique et qui doivent être déterminées à travers des différents essais expérimentaux. Dans la deuxième partie, une nouvelle approche a été mise en place. Elle consiste à découpler l'étude du noyau de sable et du liant afin d'étudier les mécanismes de déformation et les paramètres dépendants. Différents essais de flexion 4 points variés et riches en informations ont été présentés.

La principale difficulté qu'on a rencontrée était de trouver les appareils adaptés à notre étude en termes de plage de température et chargement. Les essais thermophysiques nous

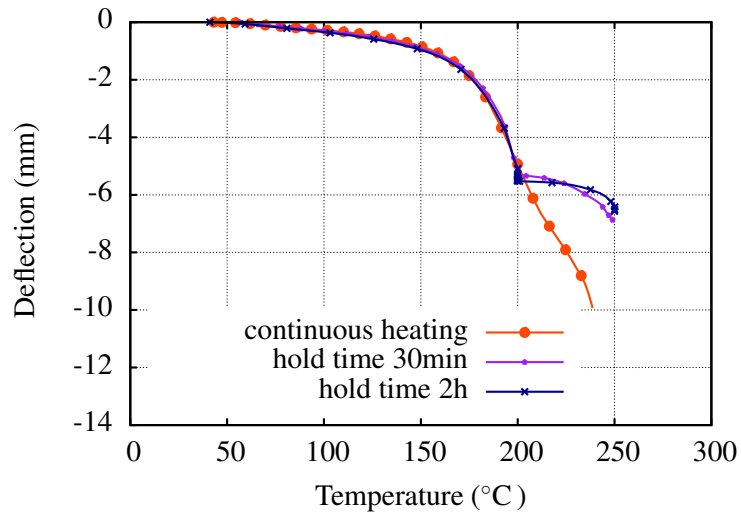
ont permis d'étudier les propriétés du noyau et de la résine jusqu'à 450 °C. Quant aux essais thermomécaniques, seuls ceux dans la plage de température entre la température ambiante et 300 °C se sont avérés concluants. Malheureusement, il n'a pas été possible d'explorer le matériau par tomographie car nous ne pouvions pas distinguer les ponts de résine des particules de silice en raison de la différence importante d'absorption entre les phases de la résine et de la silice. Cela aurait donné une information importante sur l'évolution de la proportion de résine sous l'effet de la température et l'évolution éventuelle de la structure du noyau.

En conclusion, l'étude du comportement thermomécanique du noyau de sable a révélé :

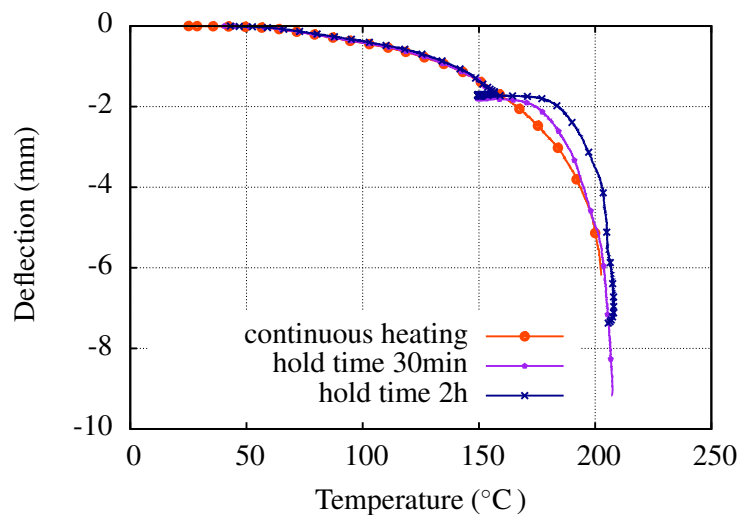
- La dépendance à la température T ;
- La dépendance à la vitesse de la température ;
- La dépendance à la charge appliquée :
- Le comportement de dilatation thermique non classique (effet de dilatation/contraction) en fonction de la vitesse de chauffage ;
- Le vieillissement physique et chimique de la résine ;
- Le comportement asymétrique en tension/compression ;
- Le vieillissement et l'effondrement de la structure du noyau de sable causés par le vieillissement et la perte de résistance de la résine.



(a)



(b)



(c)

Figure 3.72: Four-point bending test with hold times of $t_1 = 30$ min and $t_1 = 2$ h at an intermediate temperature $T_1 = 200$ °C (a) at 0.5 °C/min and (b) at 2 °C/min and $T_1 = 150$ °C (c) at 10 °C/min.

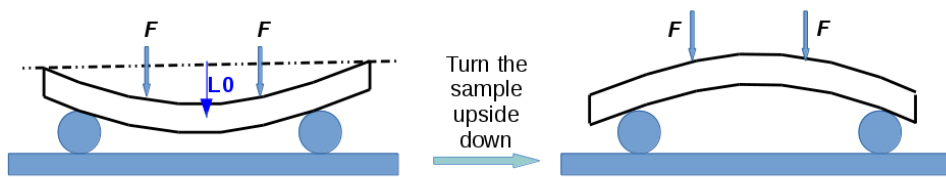
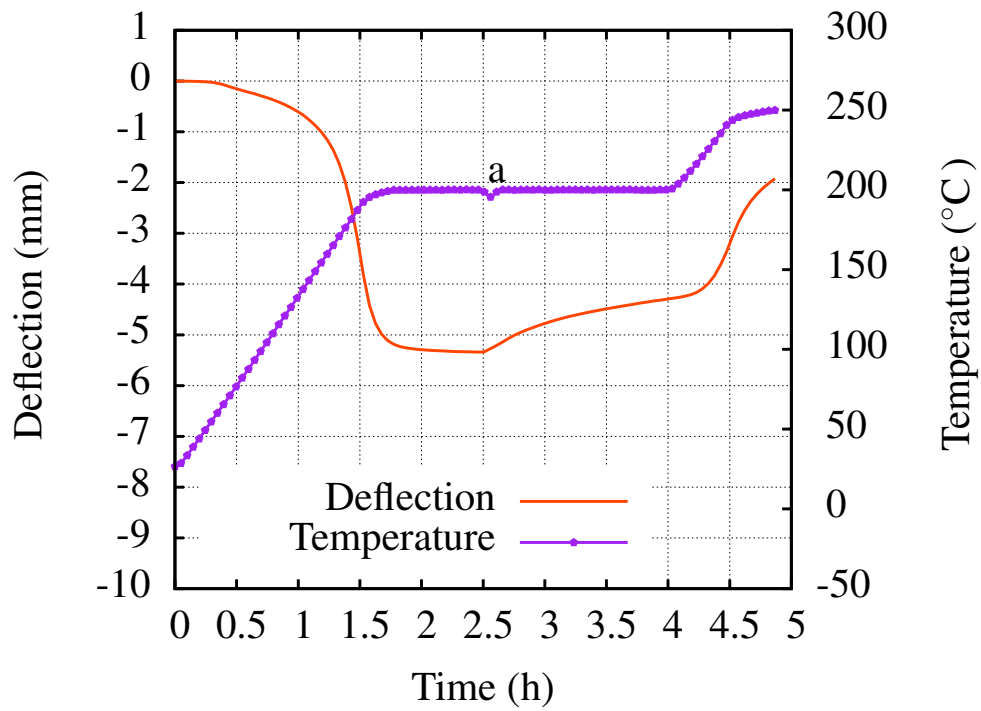
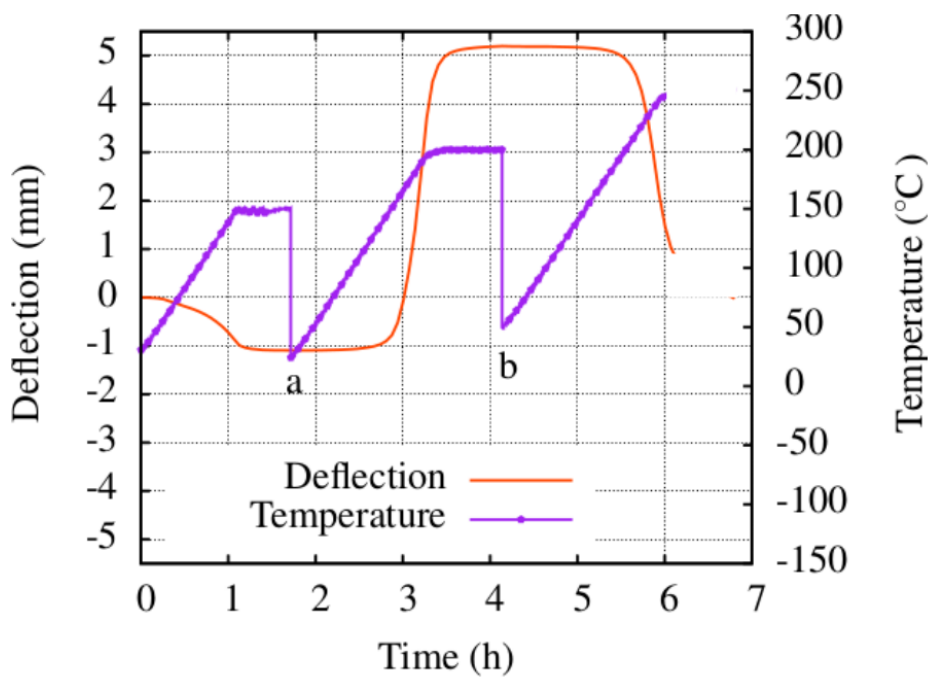


Figure 3.73: Configuration of four-point bending creep tests with turning upside down the specimen.



(a)



(b)

Figure 3.74: Four-point bending tests at a heating rate of 2 °C/min with turning upside down the specimen (a) at 200 °C at the stage denoted *a* (b) with heating, cooling and turning upside down the specimen at stages denoted *a* and *b*.

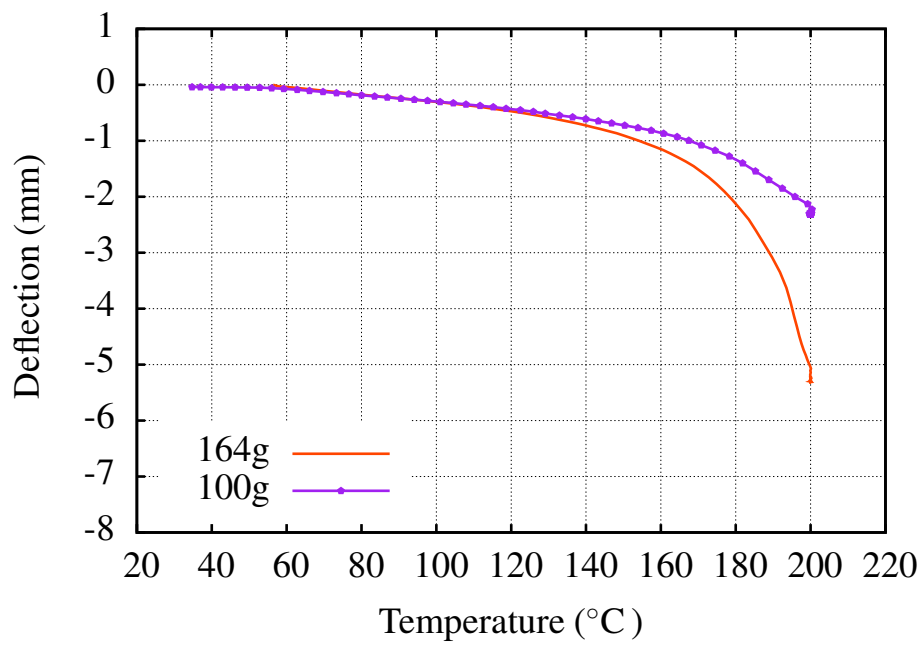


Figure 3.75: Four-point bending tests at a heating rate of 2 °C /min at different applied loads.

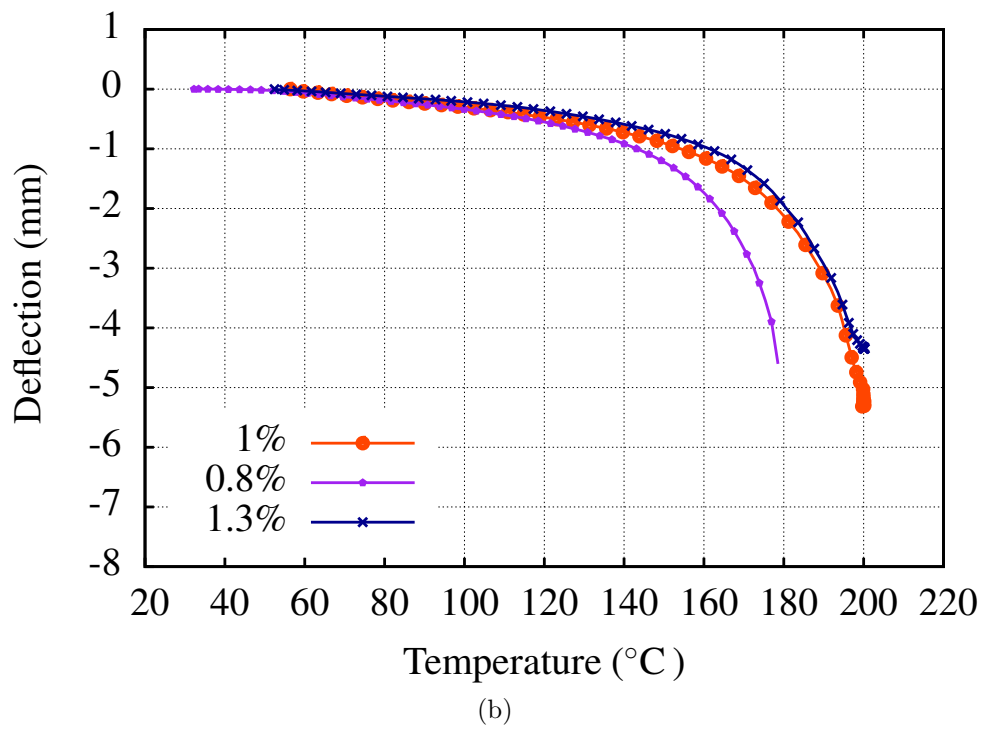
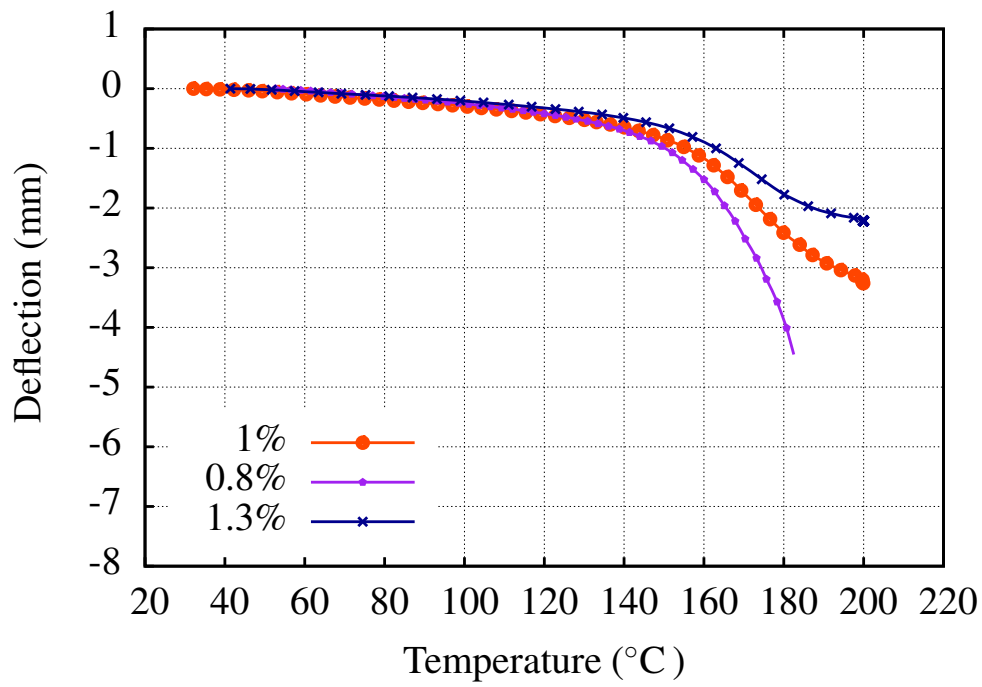


Figure 3.76: Four-point bending tests on sand core samples with binder percentages of 0.8 wt%, 1 wt% and 1.3 wt% with a heating rate of (a) 0.5 °C/min (b) 2 °C/min

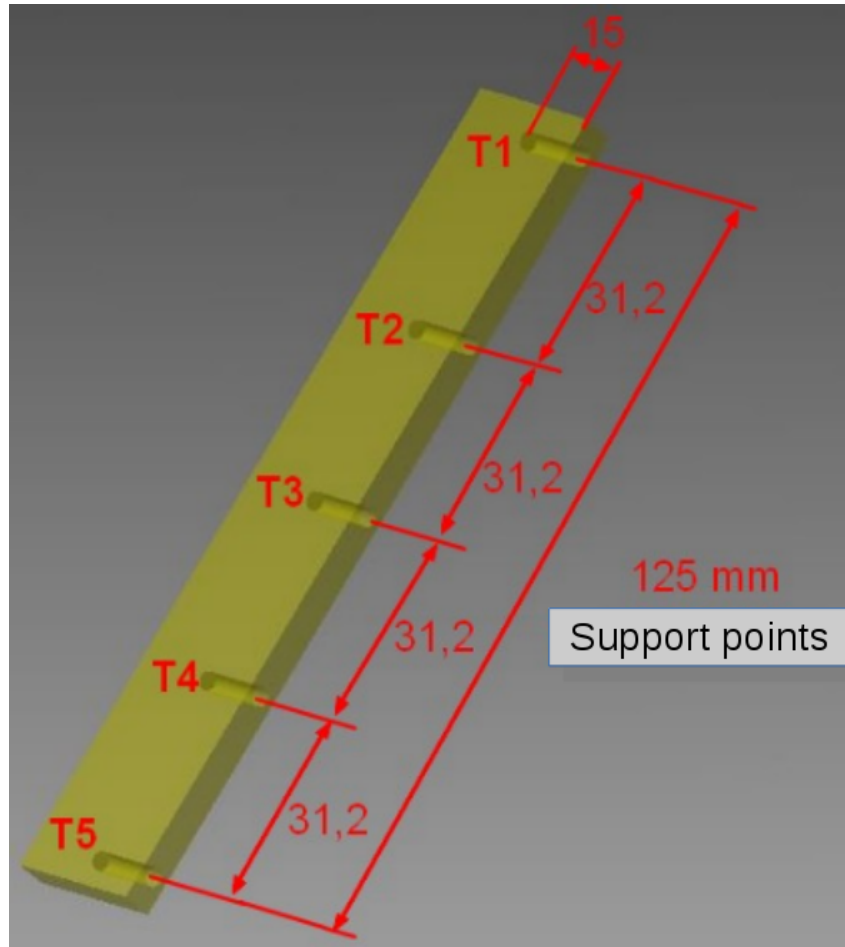


Figure 3.77: Temperature evolution inside a sand core specimen during heating up to 200 °C in tests 1 and 2 and 230 °C in test 3 at a heating rate of 2 °C/min using a tube oven.

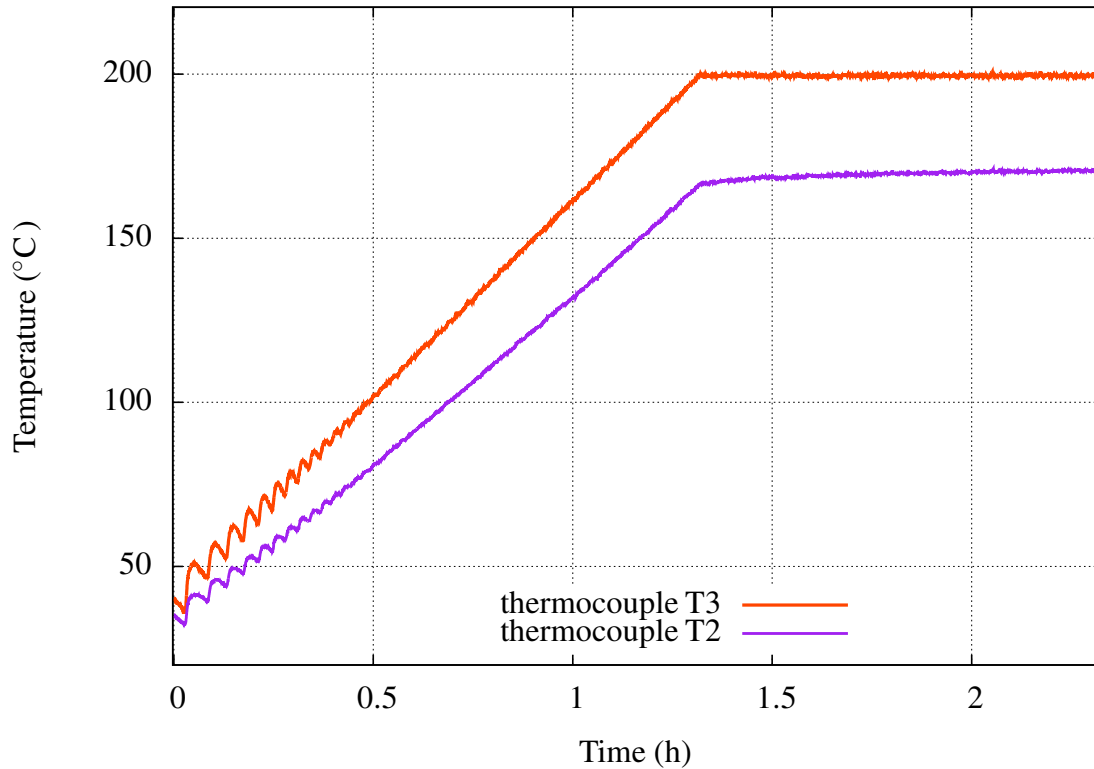


Figure 3.78: Temperature evolution inside a sand core specimen during heating up to 200 °C at 2 °C/min using a tube oven measured with two thermocouples T2 and T3.

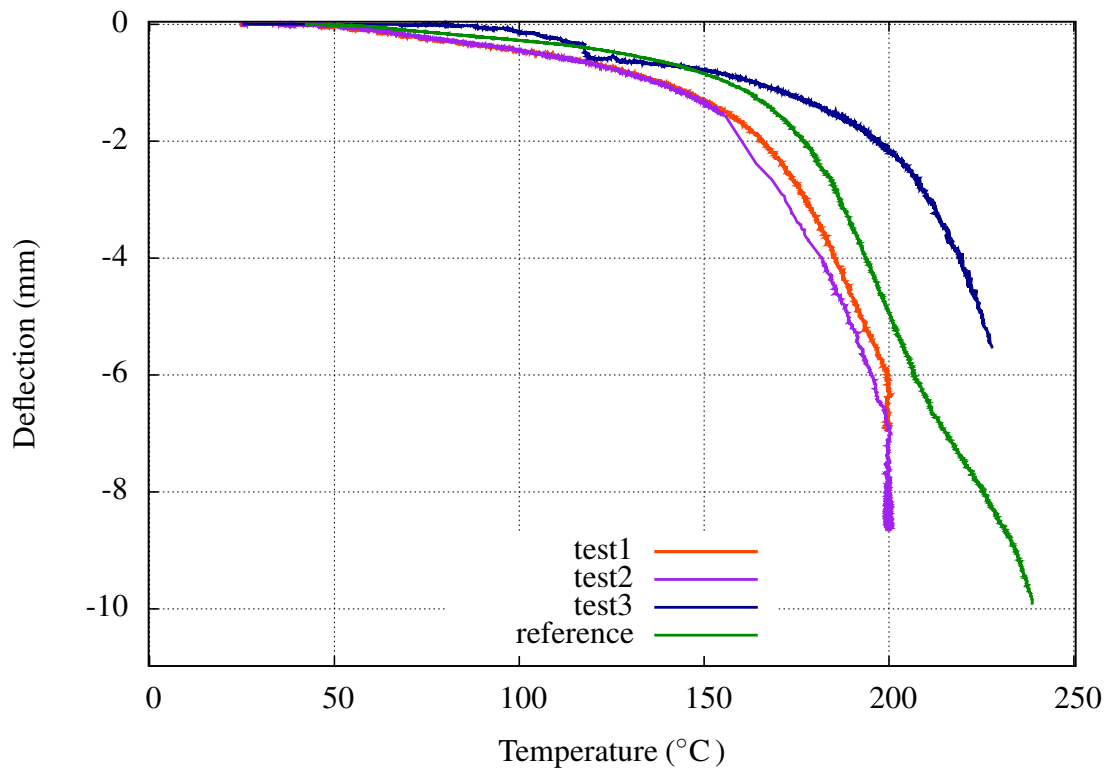


Figure 3.79: Deflection evolution during heating up to 200 °C at a heating rate of 2 °C/min using a tube oven in three tests compared to a reference test using a resistive furnace.

Table 3.8: Sand core thermomechanical tests

Type of test	Temperature	Temperature rate	Load	Comments
Compression tests	room temperature, 80 and 110 °C	2 °C/min	164g	Study the effect of temperature Non concluding tests (non adapted experimental setup)
Isothermal bending creep tests	150, 200 and 240 °C	2 °C/min	164g	Study the effect of temperature
	200 °C	0.5, 2, 10 and 20 °C/min	164g	Study the effect of temperature rate
High temperature Isothermal bending creep tests	250 °C	2 °C/min and different intermediate hold time during isothermal	164g	Study the effect of a complex thermal history
	250 °C	2 °C/min and different intermediate thermomechanical loading	164g	Study the effect of a complex thermomechanical history
	200 °C	2 °C/min	100 and 164g	Study the effect of the applied load
	150 and 200 °C	0.5 and 2 °C/min	164g	Study the effect of the resin proportion
	200 and 230 °C	2 °C/min	164g	Study the effect of temperature Non concluding tests (non adapted experimental setup)

Chapter 4

A thermomechanical model of resin bonded sand core behavior

Contents

4.1	Generalities about material modeling	102
4.2	Plasticity criteria for geomaterials: monophasic materials	103
4.2.1	Mohr-Coulomb criterion	103
4.2.2	Drucker-Prager criterion	103
4.2.3	Cam-Clay and Modified Cam-Clay criteria	104
4.2.4	Discussion	106
4.3	Models for granular materials: multiphase materials	106
4.3.1	Models for cemented geomaterials	106
4.3.2	Models for foundry green sand	107
4.3.3	Micropolar elasto-plasticity model for Cold-Box sand	111
4.3.4	Discrete elements method	111
4.3.5	Summary	112
4.4	A new model for resin bonded sand core	112
4.4.1	General framework	112
4.4.2	Modeling of the binder behavior	112
4.4.3	Modeling of the core behavior	114
4.4.4	Summary	116
4.5	Model calibration	117
4.5.1	Introduction	117
4.5.2	Model calibration strategy	117
4.5.3	Simulation of the resin behavior	117
4.5.4	Simulation of the behavior of the sand core	118
4.6	Summary	123
4.7	Résumé en français	124

The present chapter focuses on the thermomechanical behavior of resin bonded sand cores. In the first section, a literature review of the different existing models for geomaterials is presented. Their hypotheses and capability to predict the behavior of sand cores are discussed. The second section proposes a new model and shows its implementation within the framework of small strain formalism in the Zmat library of the Zset code. The model parameters are determined on the experimental data base of the previous chapter.

4.1 Generalities about material modeling

The study of the mechanical behavior of materials (metal, polymer, concrete, soil, rock. . .) requires to define the conditions associated with the different material states. Several criteria, generally expressed in the stress space, are used, to represent:

- the limit of the elastic domain and transition to inelastic regime (plasticity criterion);
- the critical state (corresponding to the critical void ratio when no volume change occurs);
- the plastic potential (which serves to define inelastic deformation);
- the failure strength (associated with the maximum peak stress);
- residual strengths.

Beyond the elastic limit, the material behavior depends on the deformation mechanisms, which may induce hardening. Consolidated or cemented materials (rock, concrete, soils, powder. . .) exhibit brittle behavior. The inelastic deformation is generated under drained conditions by frictional sliding and crushing up to a critical state (iso-volumetric) condition.

The criteria used to define the elastic domain are usually expressed by a scalar function of the stress state. In elastoplasticity or viscoplasticity, the introduction of a (visco-)plastic potential is a convenient solution to define plastic strain evolution [Bes09]. Functions are also used to describe the peak strength (failure criterion), the threshold for crack initiation (damage criterion), and the critical state condition (where a constant void ratio is reached). In fact, most of the models employed for porous metals and metallic compounds (including metal powders) have kept their roots in the von Mises criterion which has been extended to describe pressure sensitive yielding (Drucker-Prager) and the evolution of voids in porous materials [Gur77,Tve84,Tve90]. Coulomb's criterion has also served as a starting point for geomaterials like soils and rocks (Mohr-Coulomb, or the Cambridge critical state models [Ros68]). The experimental study of the behavior needs to carry out triaxial tests starting from different confining pressures and initial void ratio to investigate hardening, densification, dilatation or combination of these behaviors [Dor08]. The difficulties related to the development of the models and the determination of the material parameters are then linked to the strong coupling between the different thermal and mechanical mechanisms responsible for deformation and failure.

The sand core is a porous material mixture of silica particles and resin binder that can be considered as a geomaterial. Various models exist in the literature that take into account the critical mechanisms observed in the behavior of geomaterials

[Dar95,Sha03a,Sha06]. Our experimental analysis revealed that the behavior depends on applied stress, temperature, temperature rate, humidity... The formalism used to develop the model can be micromechanical (multiscale) or macroscopic phenomenological. For reasons of numerical efficiency, we will be interested by the second solution. In the next part, we will first discuss the most used geomaterials models for industrial applications in a chronological order. Then, the model we developed in the present PhD thesis will be detailed.

4.2 Plasticity criteria for geomaterials: monophasic materials

The most simple models taking into account the plasticity mechanisms are perfectly plastic. In this case, the same function is used to define the yield limit and the failure criterion. The expression retained can be either Mohr-Coulomb [Che82] or Drucker-Prager [Dru52].

4.2.1 Mohr-Coulomb criterion

The Mohr-Coulomb criterion [Che82] is a generalization of Tresca's criterion, based on Coulomb's friction equation. It introduces two material parameters, the cohesion c and the angle of internal friction ϕ . As shown in Figure 4.1a, it can be expressed in the Mohr plane shear-normal stress (τ - σ_n) in the form:

$$|\tau| = c - \sigma_n \tan \phi \quad (4.1)$$

Figure 4.1b shows its form in terms of eigenstresses:

$$(\sigma_1 - \sigma_3) = 2c \cos \phi - (\sigma_1 + \sigma_3) \sin \phi \quad (4.2)$$

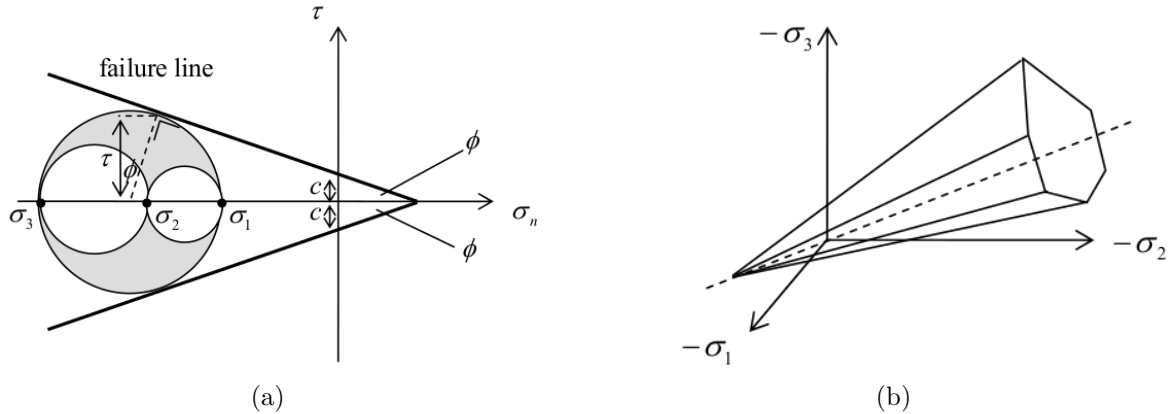


Figure 4.1: The Mohr-Coulomb yield surface (a) in the (τ, σ_n) plane (b) in the eigenstress space.

4.2.2 Drucker-Prager criterion

Here and in the following, the first invariant the stress tensor $\underline{\sigma}$ will be denoted by I_1 , such as, $I_1 = tr(\underline{\sigma})$. The deviatoric part \underline{s} of the stress tensor $\underline{\sigma}$ reads:

$$\underline{s} = \underline{\sigma} - \frac{1}{3}I_1\mathbf{I} \quad (4.3)$$

where $\underline{\mathbf{I}}$ is the identity of the symmetric tensors of order 2.

Its second invariant J_2 is defined as:

$$J_2 = \frac{1}{2} \underline{\mathbf{s}} : \underline{\mathbf{s}} \quad (4.4)$$

It is sometimes more convenient to use J defined by: $J^2 = 3 J_2 = \frac{3}{2} \underline{\mathbf{s}} : \underline{\mathbf{s}}$.

Drucker–Prager criterion is an extension of the von Mises criterion, which includes the effect of first invariant, which a linear relationship between I_1 and J [Dru52].

$$f(\underline{\boldsymbol{\sigma}}) = (1 - \alpha)J(\underline{\boldsymbol{\sigma}}) + \alpha I_1(\underline{\boldsymbol{\sigma}}) - \sigma_y = 0. \quad (4.5)$$

The material parameters are σ_y and α . The yield stress under uniaxial tension is σ_y [Bes09]. The Drucker-Prager yield surface in the $(I_1, \sqrt{J_2})$ plane is given in Figure 4.2a and in the eigenstress space in Figure 4.2b.

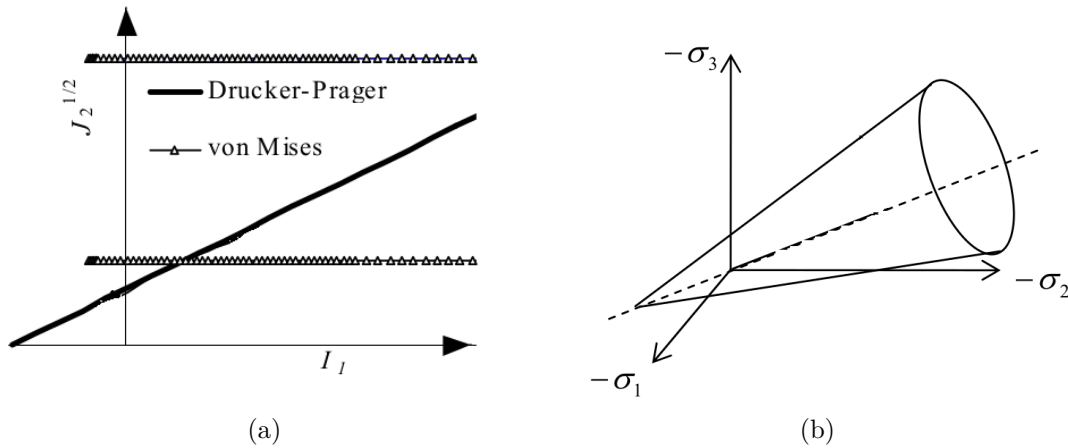


Figure 4.2: The Drucker-Prager yield surface (a) in the $(I_1, \sqrt{J_2})$ plane (b) in the eigen stresses space.

Despite the many other developments, Drucker–Prager criterion is still often used due to its simplicity. Nevertheless it is known that it is not representative of many aspects of porous material behavior, considering its linearity in the $(I_1, \sqrt{J_2})$ plane and the fact that it generates a volume increase, whatever the applied load [Bes09]. Among the existing multiaxial criteria, some include a dependence on the initial (or actual) porosity of the material. This is the case with the Gurson model.

The main issue with Drucker–Prager model is that it is “open” in triaxial compression, offering an infinite reversibility domain in this direction, which is not representative of the experimental behavior. In order to reflect possible collapse of the porous matrix for this loading type, a series of models introduce a “Cap”, ensue from the work of [Ros68] for soils and of [Gur77] for metals. Examples of criteria with a closed yield surface are described below.

4.2.3 Cam-Clay and Modified Cam-Clay criteria

The way a closed (capped) yield surface is introduced is illustrated in Figure 4.3.

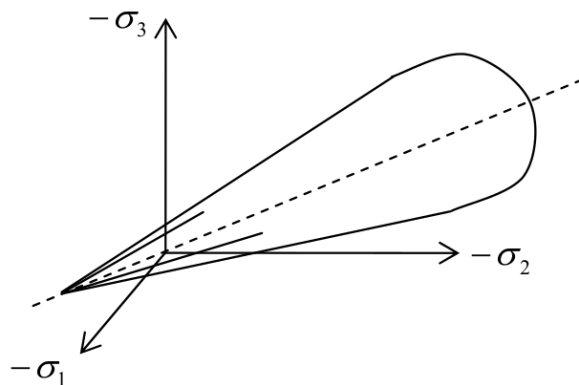


Figure 4.3: A capped yield surface

This class of models, such as Cam-Clay (CC) and Modified Cam-Clay (MCC) were formulated by researchers at Cambridge University ([AS96], [Azz95] [Ros68]). Both models describe three important aspects of soil behavior:

- (i) Strength
- (ii) Compression or dilatancy (the volume change that occurs with shearing)
- (iii) Critical state M at which soil elements can experience unlimited distortion without any changes in stress or volume.

A large amount of the volume occupied by a soil consists of voids that may be filled by fluids (primarily air and water). As a result, deformations in soil are accompanied by significant, and often non-reversible, volume changes. A major advantage of cap plasticity models is their ability to correctly account for volume changes. They are controlled by two variables, the effective mean stress p and the deviatoric (shear stress) q . The specific volume ν is defined as $\nu = 1 + e$, where e is the void ratio.

The models assume that when a soft perfectly drained soil specimen is slowly compressed in triaxial stress conditions ($\sigma_1 = \sigma_2 = \sigma_3 = p$), the relationship between the specific volume, ν , and $\ln p$ reduces to a straight virgin consolidation line (also known as the normal compression line) and a set of straight swelling lines. Swelling lines are also called unloading-reloading lines. Sustained shearing of a soil specimen eventually leads to a state in which further shearing can occur without any changes in stress or volume. This means that at this condition, known as the critical state, the soil distorts at constant state of stress with no volume change. This state, called the Critical State, is characterized by the Critical State Line (CSL). The critical stress state M defined by $M = q/p$ is used in both CC 4.6 and MCC models 4.7:

$$\text{Cam-Clay:} \quad q + Mp \ln\left(\frac{p}{p_0}\right) = 0 \quad (4.6)$$

$$\text{Modified Cam-Clay:} \quad \frac{q^2}{p^2} + M^2\left(1 - \frac{p_0}{p}\right) = 0 \quad (4.7)$$

In the (p, q) space, the CC yield surface has a logarithmic shape while the MCC yield surface is as an elliptical surface (Figure 4.4). The parameter p_0 (known as the yield stress or pre-consolidation pressure) controls the size of the yield surface. The parameter M is the slope of the CSL in (p, q) space. A key characteristic of the CSL is that it intersects the yield curve at the point at which the maximum value of q is reached.

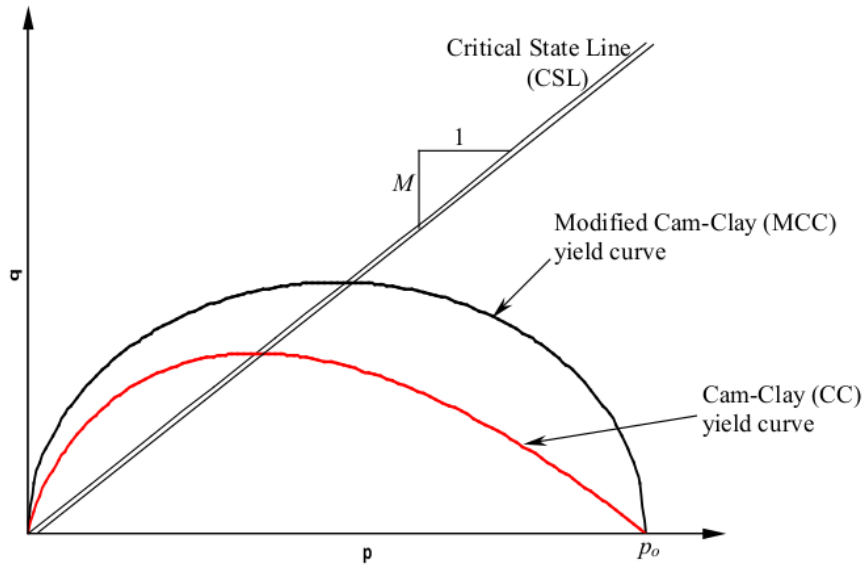


Figure 4.4: Cam-Clay and Modified Cam-Clay yield surfaces in (p, q) space

4.2.4 Discussion

We presented in this part several plasticity criteria that can be used for geomaterials where deformation is governed by frictional sliding and crushing up to a critical state. However, the sand core is a two-phase material (silica particles+resin (+voids)), so that its behavior is governed by more complex physical phenomena due to resin aging. A specific model needs to be developed based on the concepts developed for geomaterials and completed to take into account the sand core deformation mechanisms.

4.3 Models for granular materials: multiphase materials

4.3.1 Models for cemented geomaterials

Model presentation. In many types of soil based materials, the soil particles may become cemented, the cementing agent being present around particles, at particle contacts and precipitated in the pore space forming nodules [Rin08]. They resulting properties are very different from those of the original uncemented material. They present an additional strength due to the specific interactions between the grains. Under mechanical loading, these bonds may be damaged particularly under cyclic loading. [Sha03b] studied the effect of cementation degradation using triaxial compression tests. They found that the progressive degradation of the bond results in significant decrease in stiffness and at the same time a possible change in the size of the elastic domain. [Vau03] considered the bond as a brittle material, its damage leading to a structure deterioration. They used the MCC model and proposed a coupled formulation between the elastic strains of bond and the total elastic strain of soil.

Some authors ([Arr12], [Rio16]) were interested in modeling the behavior of cemented clay. They used a bonded elasto-plastic criterion based on the works of [Yu98]. Inspired from CC model, this approach introduces a critical state. They assume that initializing the main state variables can be done only by measuring the porosity, the unconfined

compression strength and the amount of cement in the mixture. The model is modified by introducing a scalar history variable b called the bonding variable. The authors consider the variable b to be representative of the bonding effect which causes the yield surface to enlarge with increasing the amount of bonding in the soil. The yield surface shown in Figure 4.5 reads :

$$f = \left(\frac{q}{M_0(p' + p'_t)} \right)^n + \frac{1}{\ln r} \ln \frac{p' + p'_t}{p'_c + p'_t} = 0, \quad (4.8)$$

where:

$$p'_c = p'_s(1 + b) \quad (4.9)$$

$$p'_t = p'_s(\alpha_t b) \quad (4.10)$$

and p'_c controls the yielding of the bonded soil in isotropic compression and p'_t the cohesion and tensile strength of the material; α_t is a material parameter. p'_s is the equivalent pre-consolidation pressure, or preconsolidation pressure of the unbonded reference material. It is related to the void ratio, while the plastic potential function has a similar form to the yield surface using a non-associated behavior.

Bonding decreases with plastic strain damage called h :

$$b = b_0 e^{-h} \quad (4.11)$$

$$\dot{h} = h_1 |\dot{\varepsilon}_v^p| + h_2 |\dot{\varepsilon}_s^p| \quad (4.12)$$

where h_1 and h_2 are material parameters defining the degradation rate. A schematic representation of the tests needed to calibrate the model is given in Figure 4.6. The study showed that the mechanical behavior of the mixture is mostly controlled by the ratio between the current void ratio and percentage of bonding cement. One of the shortcomings of the initial model is that the elastic parameters do not depend on bonding. A formulation has also been proposed to introduce the parameter b in the elastic bulk modulus.

Discussion. In the most recent works on cemented geomaterials ([Arr12], [Rio16]), a unified stress state for clay and cement was used. The main assumption is that the only effect the bonding cement has on the material response is the expansion of the yield surface. This was introduced by means of a scalar variable b which depends on the cementation rate and damage development. Either at room temperature or during heating, the bonding properties of the grains in cemented clay and sand cores are different since the cement behavior is quite different from the resin. While the experiments showed also a dependence to many variables affecting both the resin properties and the sand core. In here, the introduction of the scalar b is not enough to describe the physical phenomena, damage and mechanisms leading to the irreversible deformation of sand cores.

4.3.2 Models for foundry green sand

Soil mechanics approach for foundry green sand. Green sand, as prepared and used in foundries, is a fine porous mixture of approximately 87 wt% of silica grains, 7 wt% of clay, 3 wt% of black carbon and 3 wt% of free water. More precisely, each silica grain

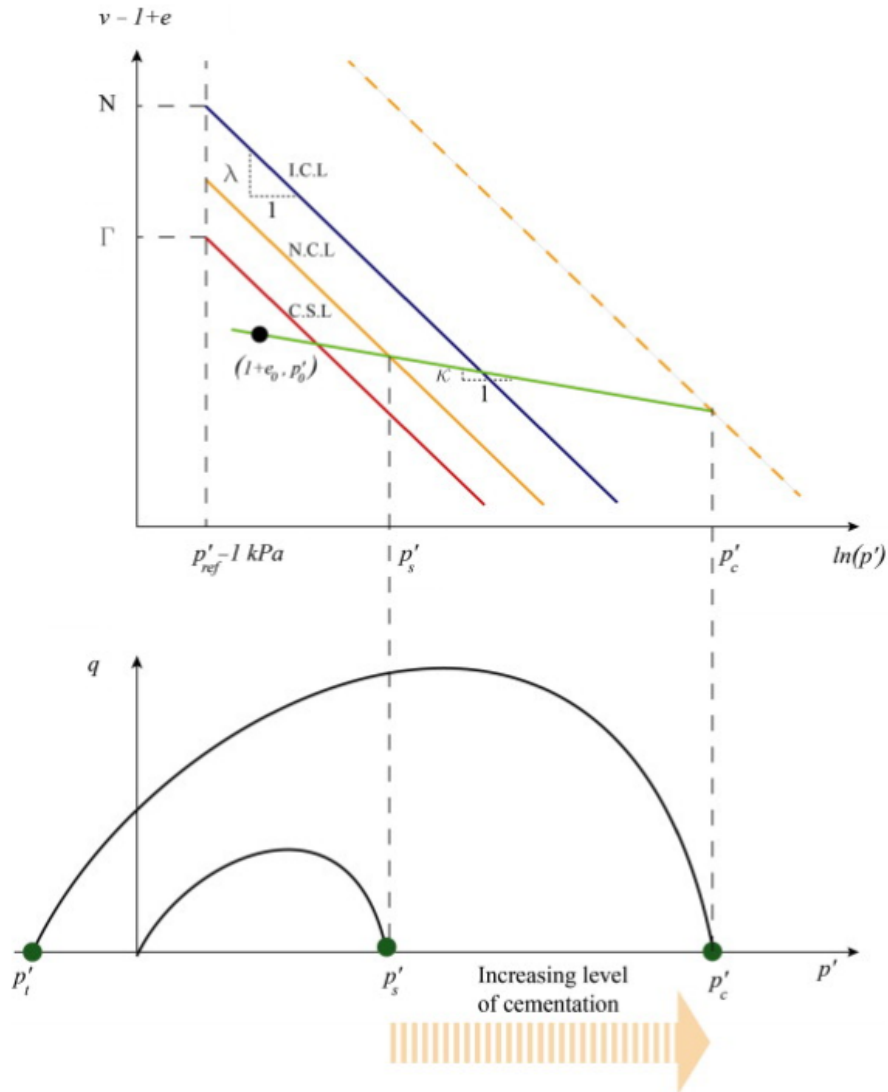


Figure 4.5: Yield surface for bonded and unbonded materials [Arr12]

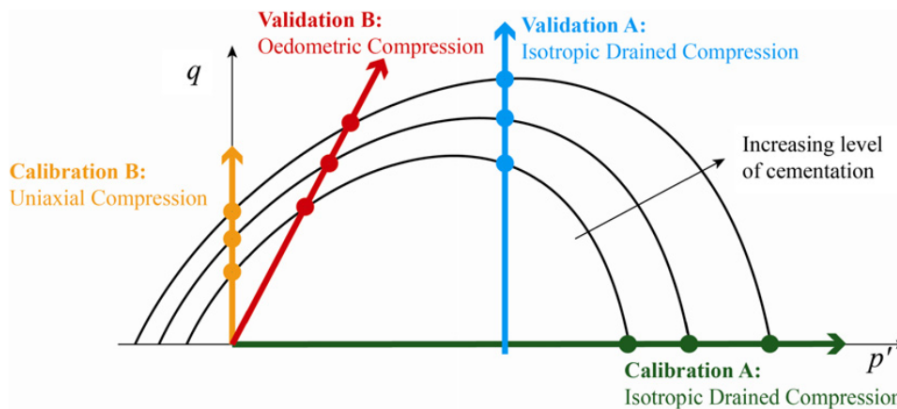


Figure 4.6: Schematic approach showing the approximate stress paths of the tests employed in the calibration and validation of the model [Arr12]

is embedded in a plastic binding phase composed of clay and carbon black. Depending on the compaction level, the pores are more or less partially filled with water. The green

sand composition is quite different from the sand core which is a mixture of 99 wt% of silica sand and 1 wt% of resin binder.

A thermo-mechanical model based on soil mechanics approach was developed by [AS96] for green casting sand. It introduces an elasto-plastic formulation inspired from the Cam Clay model [Ros68] [Ros58]. In fact, the Cam Clay was compared to other models: a “Modified Cam Clay” model which yield surface has an elliptical shape and a “Revised Modified Cam Clay” model where the plasticity is related to a second yield surface incorporating the deviatoric plastic strain. In order to study the material response, triaxial compression tests, uniaxial tests, isotropic compression tests and die pressing tests were used. In the triaxial compression tests, the material behavior exhibits a load increase with a peak followed by a load drop. The load increase was explained by the material expansion. The compression, cyclic tests showed that there is a continuity and recovery, between the starting and final points in the stress-strain curves. In order to account for temperature, all the model parameters were supposed to be temperature dependent.

In their work, the authors [AS96] determined the critical state and the cohesion strength from the Mohr circles representation while an optimization process was used to identify the others parameters based on isotropic compression and die pressing tests. Among these models, the “Revised Modified Cam Clay” provides the best fit of the triaxial tests and enables to reproduce the material expansion (see Figure 4.7).

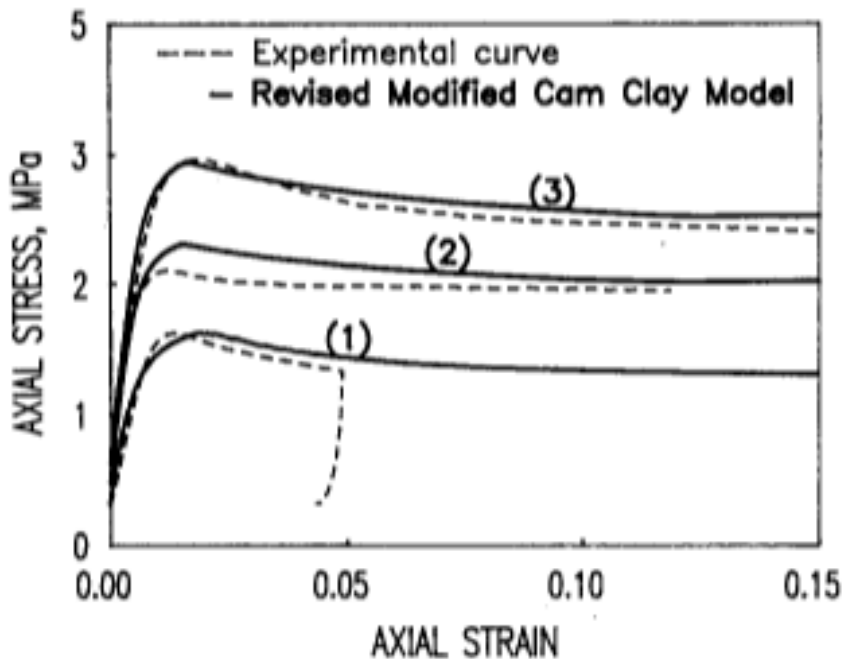


Figure 4.7: Results for drained triaxial tests at $T=300\text{ }^{\circ}\text{C}$ and various lateral pressures, (1) $\sigma_3 = 0.4\text{ MPa}$, (2) $\sigma_3 = 0.6\text{ MPa}$, (3) $\sigma_3 = 0.8\text{ MPa}$. Comparison with theoretical prediction using revised modified Cam Clay model [AS96]

Thermo-hydro-mechanical model for foundry green sand. As shown in a previous study [Azz95], the temperature history imposed to green sand during the foundry process by the metal (liquid then solidified), induces several phase transformations, namely the vaporisation of free water, coking of carbon black and burning of clay.

Based on the thermodynamics of irreversible processes, a phenomenological approach including damage was developed by the author. The different physical aspects governing the material behavior were represented by internal variables, namely the pore evolution and the hydrometric degree. In fact, the suction effects due to the presence of water in the mixture are taken into account using a scalar internal variable in the volumetric hydric strain part. The behavior is supposed to be governed by the porosity evolution, clay and black carbon nature and the evaporation of water during complex thermomechanical loading histories. The degradation of black carbon and clay are temperature dependent. The internal scalar variable d that is introduced to represent damage influences both volumetric and deviatoric plastic strain evolution. The yield surface reads:

$$f(\underline{\sigma}, \underline{\varepsilon}^w, d) = \frac{I_1^2}{18K(1-d)^2} + \frac{J_2}{2G(1-d)^2(1-ad)} + \frac{b_1(1+b_2d)}{(1-d)} I_1 - b_3d(1-d)b_4 - b_5, \quad (4.13)$$

where $\underline{\varepsilon}^w$ is the hydric strain, b_1 , b_2 , b_3 , b_4 and b_5 are material parameters. K is the compressibility modulus, G is the shear modulus.

The calibration of the parameters was done using thermo-mechanical triaxial compression tests in a specifically developed setup. The material response under different temperatures, water content and compaction ratio was studied. The model was successfully validated and implemented as a UMAT in the finite element code Abaqus. The evolution of the hydric strain as a function of water ratio and temperature is given in Figure 4.8.

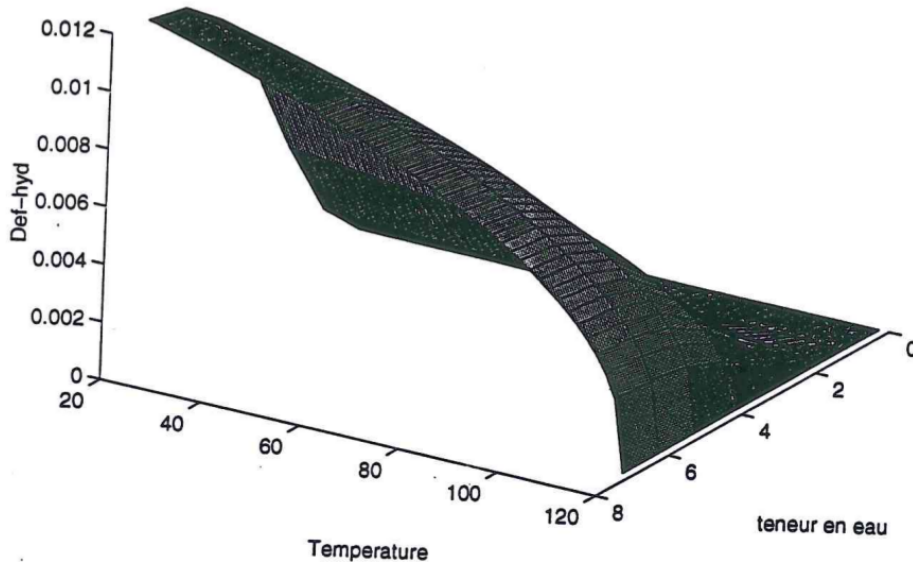


Figure 4.8: Evolution of the hydric strain as a function of water ratio and temperature [Azz95]

Discussion. This model developed for foundry green sand is in good agreement with the material behavior. The mechanisms were identified and exposed through a wide

experimental database. A plasticity criterion taking into account the asymmetric behavior and dependence to I_1 and J_2 was used. Internal variables clearly represent the physical phenomena revealed through the experiments (irreversible deformation due to porosity evolution, water evaporation and depending parameters). However, the deformation mechanisms are not the same in green sand and resin bonded sand. In foundry sand cores, the deformation is governed by the resin behavior while in green sand there are suction effects, degradation of black carbon and clay. This justifies the need for a more specific model for the sand core.

4.3.3 Micropolar elasto-plasticity model for Cold-Box sand

Model presentation. One of the few studies on chemically bonded sand was made in [Mah11]. The behavior was investigated through uniaxial compression and tension tests up to 600 °C and triaxial compression tests at room temperature. Shear band development was investigated through image correlation technique at room temperature.

The authors proposed a mechanical model in the framework of micropolar continua. This framework is a special case of microcontinuum field theories introduced by [Eri12]. The difference with the classically known linear and non-linear field theories is that each material point possesses additional degrees of freedom [Pab05] (rotations in addition to translations). Introducing rotations is needed as soon as internal friction is present.

In this framework, the authors [Mah11] were also able to account for the asymmetry between tension and compression. The model parameters have not been identified and it was not applied to real materials.

Discussion This is one of the few studies in the literature dealing with sand core modeling. The influence of temperature history was not considered. There was no investigation of the deformation mechanisms. Moreover, the practical implementation of micropolar theory is rather complex. The main difficulty lies in the experimental calibration, as mentioned in [Eri12,Pab05].

4.3.4 Discrete elements method

Model presentation. The discrete methods consist of assemblies of elements, deformable or not, linked together by simple laws that represent the very local interactions in the material [Fra08]. These methods are widely used for granular materials since they naturally present the kinematics of these materials and their possible discontinuous behavior. At the macroscopic scale the material is seen as a continuum whose behavior and failure result from discontinuous phenomena [Hen04]. In the Discrete Element Method, a set of distinct elements interact by contact or cohesion laws. The discrete elements are rigid and the stiffness is defined by the conditions of contact [Cun71,Cun79,Fra08]. The method has been used for granular materials [Cun71] and also geomaterials [Cam00].

Discussion. This type of approach is dedicated to the investigation on a material element, since the numerical model introduces a large number of elements and a tricky algorithm for contact management. The purpose of the method is just to generate mechanical responses at the macroscopic level for predefined microstructures and interactions rules. Its use in structural computation would lead to unacceptable CPU time.

4.3.5 Summary

In this part, a review of the main existing approaches for geomaterials behavior modeling was presented. First, different plasticity criteria used to define the elastic domain were detailed. The irreversible deformation is basically due to mechanisms such as crushing and sliding of particles, generating volume changes, crack initiation and propagation. . . In this context, some of the most known models were described. A comparison was made between the existing studies and the required characteristics for the modeling of foundry sand cores. In this last case, there are coupled physical, chemical and mechanical mechanisms in the resin which must be taken into account.

4.4 A new model for resin bonded sand core

Sand core, as prepared and used in foundries, is a fine porous mixture silica sand particles and 1 wt% of resin. More precisely, each silica grain is embedded (totally or partially) in a plastic binding phase (the resin), forming bridges between particles. Depending on the compaction of the sand, there are more or less pores in the final material. The proposed constitutive equations are intended to be applied to the thermomechanical behavior of the core during casting process and not to the compaction of the sand core during the manufacturing process. This is why an hypothesis of small strain is appropriate. Moreover, for the sake of simplicity, it is assumed that the sand core is initially isotropic.

4.4.1 General framework

The tensor $\underline{\underline{\xi}}$ is split into a thermal part $\underline{\underline{\xi}}^{th}$ and a mechanical part which is composed of the elastic and the inelastic strains denoted respectively $\underline{\underline{\xi}}^e$ and $\underline{\underline{\xi}}^{in}$ so that:

$$\underline{\underline{\xi}} = \underline{\underline{\xi}}^{th} + \underline{\underline{\xi}}^e + \underline{\underline{\xi}}^{in} \quad (4.14)$$

The inelastic strain itself is decomposed into two parts, the classical viscoplasticity $\underline{\underline{\xi}}^{vp}$ linked to resin and some strain induced by the rearrangements in the grain microstructure, $\underline{\underline{\xi}}^{res}$:

$$\underline{\underline{\xi}}^{in} = \underline{\underline{\xi}}^{res} + \underline{\underline{\xi}}^{vp} \quad (4.15)$$

- **Viscoplastic inelastic strain $\underline{\underline{\xi}}^{vp}$**

In here, the expression of the deformation takes into account the effect of the resin viscoplastic behavior. As explained before in chapter 3 in paragraph 3.7.2, this may develop in the resin during the rubbery plateau at intermediate temperatures and is more pronounced at slow temperature rates. It was also observed through the cyclic loading tests and will be discussed in details in the next section.

- **Inelastic strain induced by resin thermal decomposition $\underline{\underline{\xi}}^{res}$** In this part, the thermal degradation mechanism is taken into account. For this, the resin pyrolysis will be simulated and calibrated based on the thermogravimetric tests.

4.4.2 Modeling of the binder behavior

Description of the thermal degradation. The thermal behavior including thermal degradation (pyrolysis under inert atmosphere such as during casting) s been studied

extensively in works dealing with powders manufacturing processes ([Thi01], [Hwa92], [Man92]). In particular the debinding stage where the material is submitted to a thermal treatment in order to eliminate the binder.

In general, resin pyrolysis can be described as the solid components conversion by heat in absence of oxygen which results in the production of gas and a final char residue. Kinetic analyses are useful for understanding the thermal degradation process and providing information for a pyrolysis process. The kinetic modeling of the decomposition is crucial for an accurate prediction of the material behavior under different working conditions [Nav15]. The pyrolysis of polyurethane resin is a chemically complex process in which several reactions occur simultaneously. The study of degradation process is mostly done by means of the thermogravimetric analysis performed in the present study in paragraph 3.7.1.2 since it gives informations about the temperatures of degradation, degradation rates and material thermal stability. The investigation of the derivative curve is important to determine the amount of each decomposed component or the degradation rate by considering the highest value in this curve. The degradation kinetics can be quantified by mathematically studying the TGA data. Because of this complexity, a large number of papers in the literature assume different approaches to describe the thermal degradation. Some use equations to describe reactions such as nucleation and growth, diffusion and phase boundary as in [Cri89] and [Núñ00]. However, empirical models are usually used to describe thermal degradation without considering these physical mechanisms [Won10], first order or n-order models.

Kinetics. The thermal degradation is controlled by the conversion rate $\dot{\alpha}$, defined as:

$$\dot{\alpha} = k(T) H(\alpha) \quad (4.16)$$

where $H(\alpha)$ is the reaction function and k is a material parameter.

We will adopt the approach based on independent reactions developed in [Jom14]. The solid material is considered to be made of different pseudo-components which decompose separately. For a pseudo-component i in the solid material, the conversion ratio α_i of the pyrolysable part can be determined as follows:

$$\alpha_i = \frac{M_{0_i} - M_{m_i}}{M_{0_i} - M_{f_i}} \quad (4.17)$$

For each pseudo-component i , the initial mass is M_0 , the final mass is M_f , and the current value is M_m

The conversion rate then of the pseudo-component i is given by:

$$\dot{\alpha}_i = k_i(T) f(\alpha_i) = Z_i \exp \frac{-E_{ai}}{RT} f(\alpha_i) \quad (4.18)$$

where:

n_i is the reaction order.

E_{ai} is the activation energy of the decomposition reaction of the pseudo-component i .

Z_i is a frequency factor.

R is the universal gas constant.

For a n -component system, the total conversion ratio α_m and conversion rate $\dot{\alpha}_m$ are respectively given by:

$$\alpha_m = \sum_{i=1}^n c_i \alpha_i \quad ; \quad \dot{\alpha}_m = \sum_{i=1}^n c_i \dot{\alpha}_i \quad (4.19)$$

where c_i is the mass fraction loss due to component i , so that.

$$\dot{\alpha}_m = \sum_{i=1}^n c_i Z_i \exp\left(\frac{-E_{ai}}{RT}\right) (1 - \alpha_i)^{n_i} \quad (4.20)$$

The first reference to these equations dates back to the 60s [Fly66], [Oza65], while for foundry applications, only recently works were carried out to study the resin binder decomposition, and specifically the degassing process during cure, which causes defects in the final product when gas is trapped [Sam12], [Sta09a] and [Jom14].

In the present work, we will consider two pseudo-components (corresponding to the phenolic resin and the hardener), so that:

$$\dot{\alpha}_m = c_1 \dot{\alpha}_1 + c_2 \dot{\alpha}_2, \quad (4.21)$$

4.4.3 Modeling of the core behavior

Deformation due to thermal degradation. The solid binder decomposition into gas induces an irreversible transformation in the sand core. The pyrolysis is a thermally activated process. When heating is applied, the process is triggered causing weight loss, defects and variations of the material properties. The resulting effect is an irreversible deformation process which can be described in the framework of macroscopic plasticity.

The elastic domain is an elliptic function of the first invariant of the stress tensor I_1 and the second invariant of its deviator J with a parameter P_0 to account for the asymmetry of the behavior in tension and compression:

$$f(\underline{\sigma}) = \sqrt{J^2 + \alpha_c (I_1 - P_0)^2} - \sigma_s \quad (4.22)$$

The rate $\dot{\underline{\epsilon}}^{res}$ is normal to the equipotential defined by f , and is driven by the conversion rate $\dot{\alpha}_m$, according to:

$$\dot{\underline{\epsilon}}^{res} = k_{res} \dot{\alpha}_m g_r \left(\frac{\frac{3}{2} \underline{\mathbf{s}} + \alpha_c (I_1 - P_0) \underline{\mathbf{I}}}{\sqrt{J^2 + \alpha_c (I_1 - P_0)^2}} \right) \quad (4.23)$$

where k_{res} and α_c are two material parameters, and g_r is a function that accounts for temperature rate dependence. Our experiments showed that a decreasing temperature rate induces a hardening effect in the resin binder, giving rise to a stronger material structure. This effect is represented through the following expression for g_r :

$$\dot{g}_r = \dot{T} - \frac{g_r}{\tau} \quad (4.24)$$

where τ is a parameter that allows a deviation from the stabilized conditions during temperature transients to be introduced.

Deformation due to viscoplastic flow. The deformation can leave the elastic domain unchanged, produce a shrinkage (isotropic softening), an expansion (isotropic hardening), or a shift of the domain (kinematic hardening), depending on the class of material. Some materials may even present hardening followed by softening under a cyclic loading. In order to be able to decide the question of the type of hardening to be introduced, we performed a test on a sand core specimen that was turned up-side down to activate viscoplastic flow in the reverse direction, the result of which is shown in Figure 4.9. During the period at constant temperature, before turning upside down the specimen at

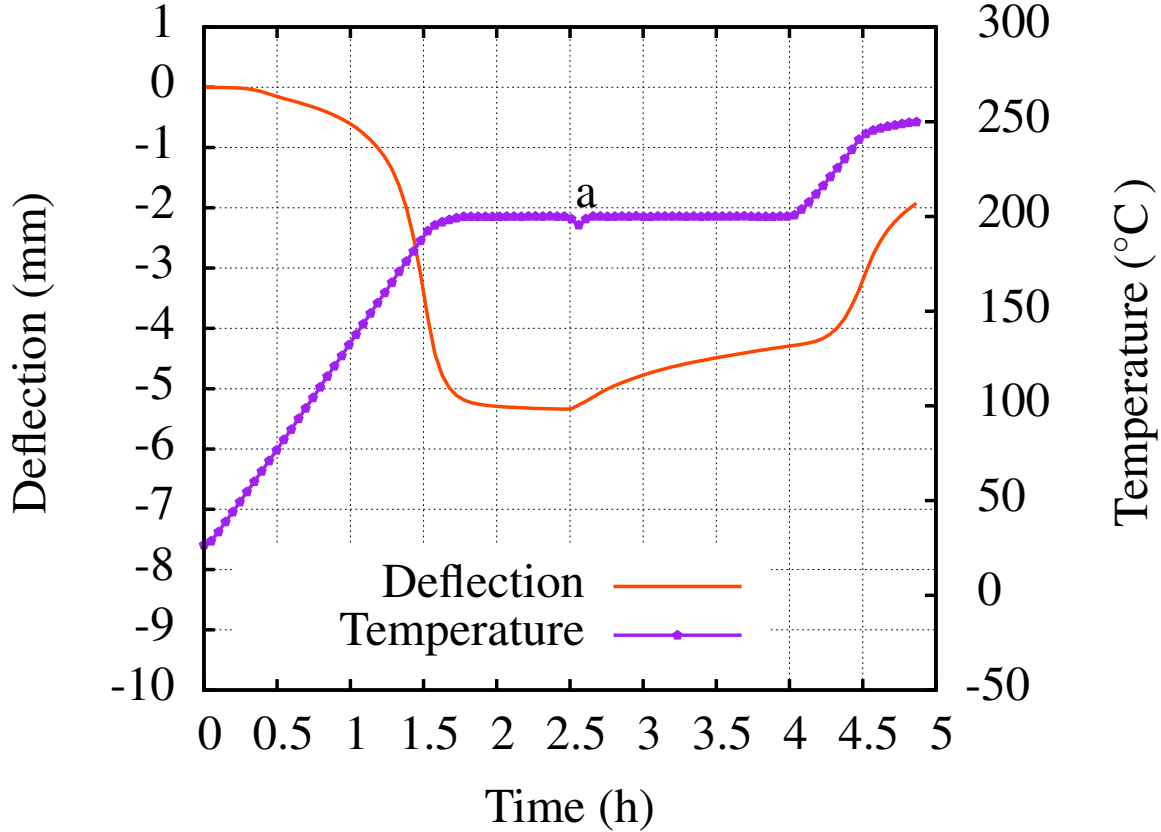


Figure 4.9: Four-point bending creep test at a heating rate of 2 °C/min with turning upside down the specimen at 200 °C at the stage denoted “a”

point denoted a , there is a progressive saturation of the deformation due to crosslinking and resin hardening. After reloading in the opposite direction, there is an increase of the deformation in the opposite direction. This evolution was related to the viscoplastic behavior of the resin bridges in tension and compression. This has to be modeled by means of a back stress, the evolution of which is supposed to be linear (Prager law). The viscous effect is assumed to be deviatoric, so that the viscoplastic deformation rate is expressed by:

$$\dot{\xi}^{vp} = \left(\frac{J(\underline{\sigma} - \underline{\mathbf{X}}) - \sigma_y}{K} \right)^n \frac{\partial J}{\partial \underline{\sigma}} \quad (4.25)$$

where K and n are material parameters, with:

$$J(\underline{\sigma} - \underline{\mathbf{X}}) = \sqrt{\frac{3}{2} (\underline{\sigma}_{eff} : \underline{\sigma}_{eff})} \quad ; \quad \underline{\sigma}_{eff} = \underline{\sigma} - \underline{\mathbf{X}} \quad (4.26)$$

and:

$$\underline{\mathbf{X}} = \frac{2}{3} C \underline{\xi}^{vp} \quad (4.27)$$

4.4.4 Summary

Table 4.1 contains a summary of the main constitutive equations of the sand core model.

Table 4.1: Constitutive equations of the foundry sand core model

Strain partition

$$\underline{\xi} = \underline{\xi}^e + \underline{\xi}^{in} + \underline{\xi}^{th}$$

Stress partition

$$\underline{\sigma} = \underline{\mathfrak{s}} + \frac{1}{3} I_1 \underline{\mathbf{I}}$$

Yield function

$$f(\underline{\sigma}) = \sqrt{J^2 + \alpha_c (I_1 - P_0)^2} - \sigma_s$$

Resin conversion rate

$$\dot{\alpha}_m = \sum_{i=1}^n c_i Z_i \exp \frac{-E_{ai}}{RT} (1 - \alpha_i)^{n_i}$$

where α_i is the conversion ratio of a component i

Inelastic strain

$$\underline{\xi}^{in} = \underline{\xi}^{res} + \underline{\xi}^{vp}$$

$$\dot{\underline{\xi}}^{res} = k_{res} \dot{\alpha}_m g_r \left(\frac{\frac{3}{2} \underline{\mathfrak{s}} + \alpha_c (I_1 - P_0) \underline{\mathbf{I}}}{\sqrt{J^2 + \alpha_c (I_1 - P_0)^2}} \right)$$

where $g_r = \dot{T} - \dot{T}_r = \dot{T} - \frac{g_r}{\tau}$

$$\dot{\underline{\xi}}^{vp} = \left(\frac{J(\underline{\sigma} - \underline{\mathbf{X}}) - \sigma_y}{k} \right)^{n-1} \frac{\partial J}{\partial \underline{\sigma}}$$

where $J(\underline{\sigma} - \underline{\mathbf{X}}) = \sqrt{\frac{3}{2}} (\underline{\sigma}_{eff} : \underline{\sigma}_{eff})$

and $\underline{\sigma}_{eff} = \underline{\mathfrak{s}} - \underline{\mathbf{X}}$

4.5 Model calibration

4.5.1 Introduction

The finite element code Zset¹ was used to implement the constitutive equations and perform parameter identification. This is a set of numerical tools dedicated to material modeling and structural calculations.

Zmat: This module provides a wide library of constitutive equations, as well as specific language ZebFront allowing the user to develop his own model.

Zsimopt: This module contains a material driver (Zsim) for Zmat and a series of optimization methods (Zopt) to simulate point loading (in terms of stress and/or strain) and to calibrate the material parameters from test data.

Zsolve: This is the finite element code. It is perfectly compliant with Zmat, so that the same material files can be used for the optimization process and for the subsequent structural calculation.

The constitutive equation set shown in the preceding section has been implemented in Zmat by means of the language ZebFront.

4.5.2 Model calibration strategy

The identification process consists of three steps.

1. The identification of the parameters related to the resin binder thermal degradation was performed first, based on the thermogravimetric tests;
2. The mechanical tensile tests performed on the resin were simulated in order to obtain an initial estimation of the parameters of viscoplastic strain part;
3. The bending tests conducted on the sand core were the used to calibrate the full model.

The next paragraphs detail the different results of the simulations made on the resin, then on the sand core.

4.5.3 Simulation of the resin behavior

Thermal degradation. The thermogravimetric tests conducted on the resin were simulated for the two heating rates 2 °C/min and 10 °C/min. The process is assumed to take place with two distinct reactions. The initial values for the activation energy was set to 80000 kJ/mole. The other values are 20000 s⁻¹ for the pre-exponential factor, 0.5 for the coefficient c and 2 for the reaction order n based on the studies made in [Sta09a] and [Jom14].

The values of the parameters are given in Table 4.2. It can be checked that the sum of the lost mass fraction c_i is equal to 1. The first reaction was found to be order 2 and the second reaction is order 3.

Figures 4.10 and 4.11 show respectively the results for the two tested heating rates of 2 °C/min and 10 °C/min. The model is in good agreement with the experiment during the heating period.

¹<http://www.zset-software.com/>

Table 4.2: Arrhenius law parameters

Reaction (i)	c_i	Z_i (s^{-1})	E_{a_i} ($kJ\ mole^{-1}$)	n_i
1	0.45	7.9e+02	54.9	2
2	0.55	1.5e+06	106	3

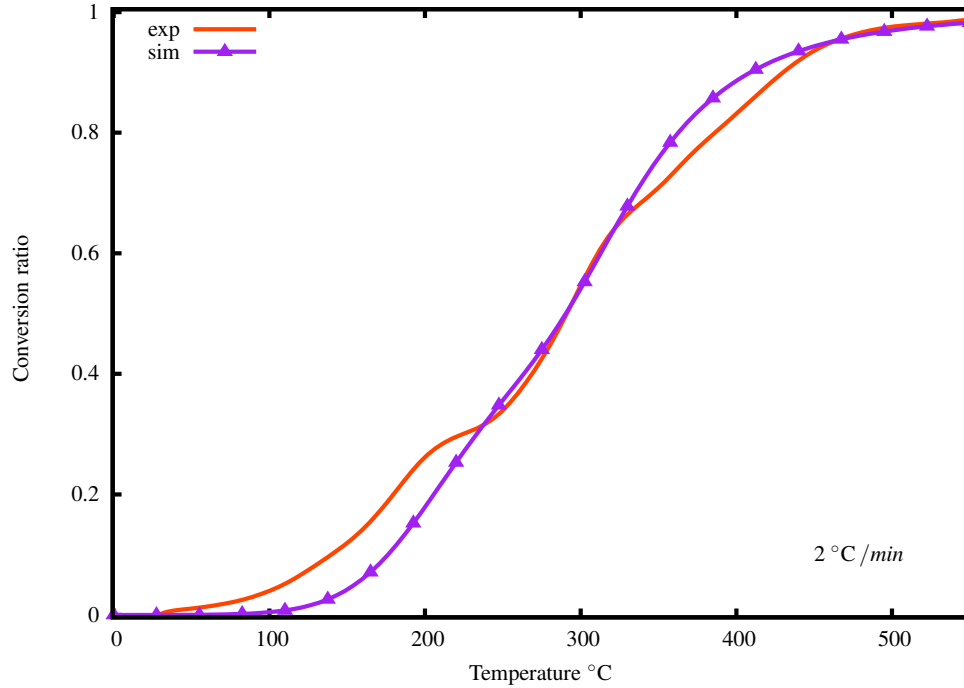


Figure 4.10: Comparison between the simulation of the conversion ratio and the TGA results during heating at 2 °C/min

Mechanical behavior of the resin. In this section, the viscoplastic behavior of the resin is simulated. The deformation is defined by Eq.4.25.

The parameters to identify are n , C and K . The tensile tests performed at different temperatures under strain rates of $10^{-3}\ s^{-1}$ and $10^{-2}\ s^{-1}$ and a heating rate of 2 °C/min were used. This enables to calibrate the parameters of the viscoplastic law and to obtain a set of parameters for this part of the deformation. Unfortunately, there are only two tests available, which were performed at room temperature and 150 °C presented (see section 3.7.2.2). The simulated curves are in good agreement with the experimental results (Figures 4.12).

4.5.4 Simulation of the behavior of the sand core

4.5.4.1 Specimen geometry and mesh.

The specimen must be considered as a structure. It is therefore no longer possible to perform a simulation on a material element. It is a finite element calculation that is required. Exploiting the symmetry of the specimen geometry and loading conditions, only one-half of the specimen is meshed (Figure 4.13). The computations are made in generalized plane strain. A constant load is imposed in the vertical direction and the vertical displacement is fixed at the support point. The left edge is fixed in the horizontal

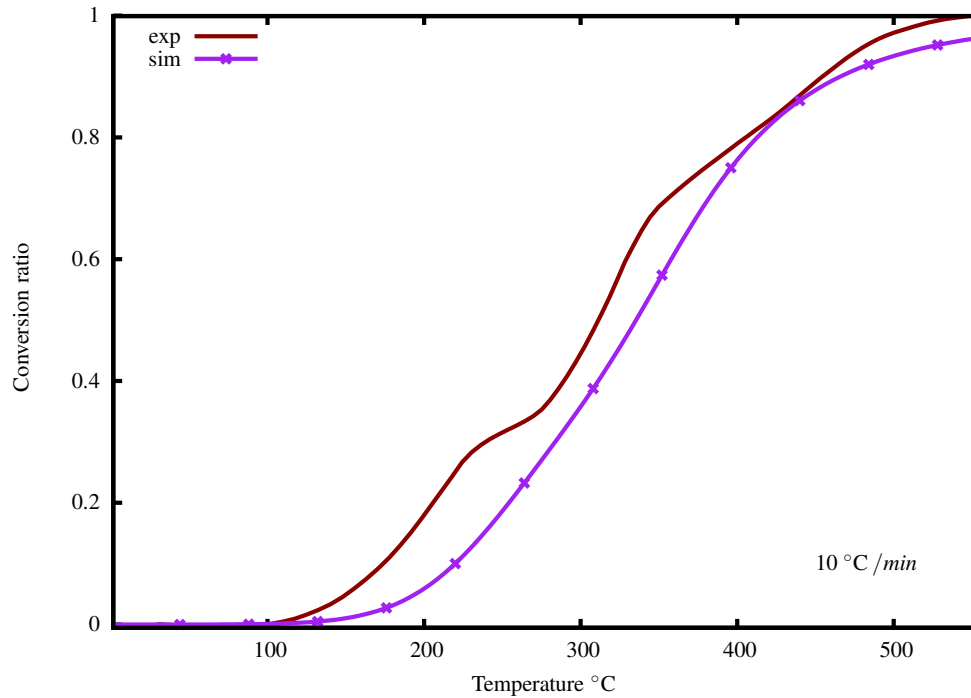


Figure 4.11: Comparison between the simulation of the conversion ratio and the TGA results during heating at 10 °C /min

direction to represent the symmetry. Eight-node quadratic elements (C2D8) were selected. The mesh contains 420 elements. This choice results from a convergence study that is shown in Appendix B: three meshes with quadratic elements (C2D8) and a mesh with linear elements (C2D4) were used.

4.5.4.2 Parameter identification methodology.

The parameters to identify at this stage are: k_{res} , α_c , P_0 , τ , σ_y . The model calibration was performed following these steps:

- In the material data file, the thermal expansion coefficient as well as the Young modulus values for different temperatures, obtained through the experiments are introduced;
- An initial set of parameters is defined. For a given heating rate, the isothermal bending tests performed at different target temperatures of 150 °C, 200 °C and 240 °C are simulated and an automatic identification process is carried out using the `Simopt` module;
- The coefficient τ which operates during the temperature transients is then readjusted by fitting the curves of the bending tests at a target temperature 200 °C and different heating rates 2 °C /min, 10 °C /min and 20 °C /min;
- The parameters related to the viscoplastic model, namely C , n , k and σ_y , are adjusted using the tests where specimen is turned upside down.

In the next section we are presenting the results of the simulations for the dilatometry tests and then the bending tests carried out on the sand core.

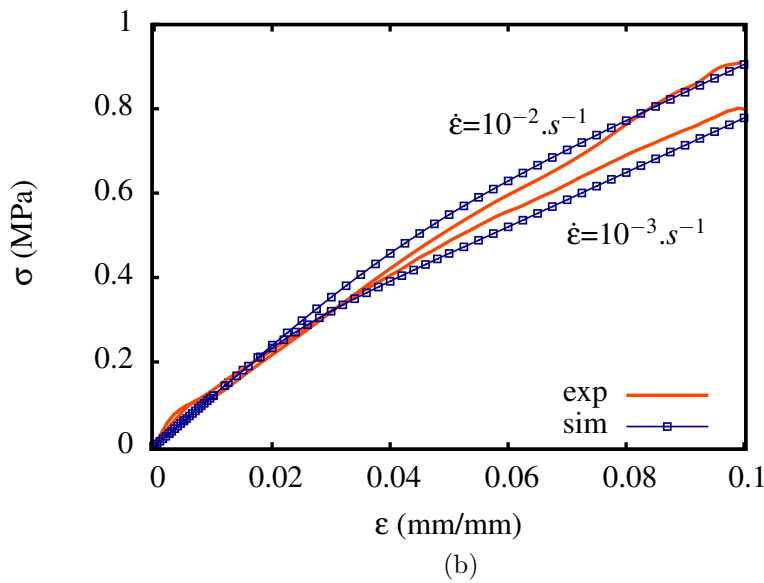
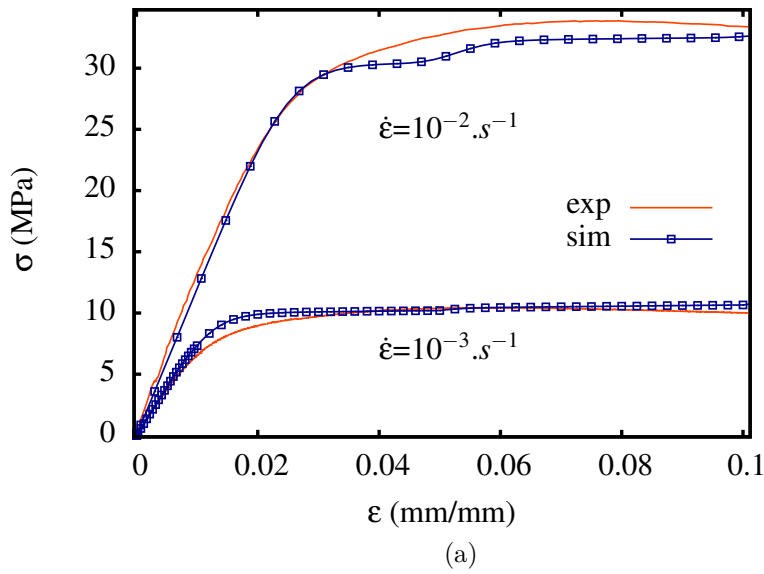


Figure 4.12: Comparison of the computations and experimental results of the tensile tests performed on the resin at (a) room temperature and (b) 150 °C

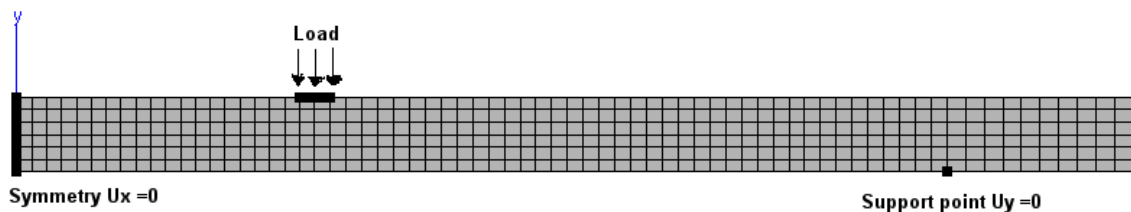


Figure 4.13: Mesh used for the specimen computation

4.5.4.3 Thermal behavior.

The thermal response of the sand core was computed using the developed model under zero stress. The results of the tests at different heating rates of 2 °C/min, 10 °C/min and 20 °C/min are shown in Figures 4.14 and 4.15. The values of the secant thermal

expansion coefficient are given in tables 4.3, 4.4 and 4.5 for the heating rates of 2 °C /min, 10 °C /min and 20 °C /min respectively. Three values of the thermal expansion include negative values. This is a non classic behavior, representative of the observed contraction due to thermal degradation. However, it can be seen that the model describes well the sand core thermal behavior, that is the expansion/contraction observed due to thermal degradation.

Table 4.3: Secant thermal expansion modulus for a heating rate of 2 °C /min

temperature	Secant modulus value (°C ⁻¹)
22	1.650×10^{-5}
250	1.650×10^{-5}
270	-2.96×10^{-5}
320	-2.96×10^{-5}
340	1.70×10^{-5}
400	$2. \times 10^{-5}$
550	$2. \times 10^{-5}$

Table 4.4: Secant thermal expansion modulus for a heating rate of 10 °C /min

temperature	Secant modulus value (°C ⁻¹)
22	1.650×10^{-5}
255	1.650×10^{-5}
275	-2.37×10^{-5}
330	-4.09×10^{-5}
330	-0.6×10^{-5}
445	2.5×10^{-5}
550	2.5×10^{-5}

Table 4.5: Secant thermal expansion modulus for a heating rate of 20 °C /min

temperature	Secant modulus value (°C ⁻¹)
22	1.4×10^{-5}
200	1.4×10^{-5}
210	1.2×10^{-5}
248	-1.35×10^{-5}
360	-1.18×10^{-5}
450	1.65×10^{-5}
550	1.65×10^{-5}

4.5.4.4 Thermomechanical behavior.

In this section, the results of the simulations of four point bending tests performed on the sand core with the final set of parameters are presented. The data base include investigations about complex loading paths, temperature and temperature rate effect.

1. **Effect of temperature.** The applied loading in these tests is a mass of 164 g and a heating rate of 2 °C/min up to different target temperatures of 150 °C, 200 °C and 240 °C.

In the experiments, the deformation of the core observed during heating was found to be dependent on the maximum temperature reached. In Figure 4.16, the results of the computations of these tests are shown. The model describes reasonably well the evolution of the deformation and delivers a good estimation of its final value. In fact, with temperature increase, the deformation increases as well.

Examples of the deformed specimens at the end of the test, heated at 2 °C/min respectively up to at 150 °C, 200 °C and 240 °C are given in Figures 4.17, 4.18 and 4.19. It can be seen that the maximum deflection is obtained at the central area of the specimen as observed in the tests.

2. **Effect of temperature rate.** The bending tests carried out under a constant mass of 164 g and during heating up to 200 °C at different heating rates of 2 °C/min, 10 °C/min and 20 °C/min were simulated as well. The experimental analyses revealed that a higher heating rate fosters thermal degradation, strength loss and causes a structure collapse. In the computations, the resulting deflection given in Figure 4.20 describes the effect of heating rate. Its evolution is more important with a higher temperature rate. However, it is important to note that the maximum computed deflection value is higher than in the experiment for the tests at 10 °C/min and 20 °C/min. But actually, the specimen broke down at 200 °C at these testing temperature rates, while the model is not designed to represent material failure. Examples of the deformed specimens at the end of the test, heated respectively at 2 °C/min, 10 °C/min and 20 °C/min are given in Figures 4.21, 4.22 and 4.23. The maximum deflection is observed at the central area of the specimen and is higher with increasing heating rate.

3. **Complex thermomechanical loading and asymmetry tension/compression.** The sand core presents a dissymmetry in tension/compression. This is taken into account by the plasticity criterion (Eq.4.22). The parameter P_0 represents the shift of the hydrostatic stress. Cyclic tests with turning upside down the specimen under various thermal loadings and a heating rate of 2 °C/min were performed to trigger different areas in the specimen in tension and then compression and observe this difference. The simulations, shown in Figure 4.24, demonstrate the good quality of the model prediction.

The main observations are as follows:

- There is an evolution of the deformation during continuous heating;
- In Figure 4.24a, during the isothermal period at 200 °C, the computed deformation tends towards a steady state and after turning upside down the specimen, a renewed evolution of the deflection is obtained. When heating again up to 250 °C, we observe an increase of the deflection with a different slope. This is also captured in the simulations;

- In Figure 4.24b, there is an evolution of the deformation during continuous heating up to 150 °C. When cooling down to room temperature, the deformation does not change. At this stage, the specimen is turned upside down and reheated up to 200 °C. During this stage, there is no evolution of the deformation until 150 °C. This is linked to the irreversible character of the chemical reactions governing thermal degradation. These phenomena are well described by the model. Above 150 °C, a new evolution of the deflection is obtained in the simulation. The magnitude of this deformation predicted by the simulation is smaller than the one obtained in the experiment. This is probably due to the fact that during the isothermal period, before turning upside down the specimen, there is a hardening effect due to resin crosslinking.

An important point which needs to be investigated is the asymmetric behavior in tension/compression of the sand core. This analysis was performed through the above discussed test with turning upside down the specimen during the isothermal reminded in Figure 4.25.

In this test, the tension and compression areas before stage denoted a are submitted to compression and tension respectively after turning the specimen. The stress and strain evolution were then investigated in the central zone shown in figure 4.26. The computed stress and strain were extracted at Gauss points in elements 1 and 6.

In Figure 4.27, the evolutions of the stress and strain as a function of time during the test are presented on the left. When the specimen is heated up to 200 °C, the element 1 is in compression and the element 6 is in tension. A steady state is reached during the isothermal. At stage a , once the specimen is turned, the evolution restarts during the next isothermal period.

The stress-strain curves are plotted in the right hand side of the Figure. During heating, the maximum compression stress reached at element 1 is higher than the maximum tensile stress at element 6. When the specimen is turned upside down at stage a , the previous tensile zone is now submitted to compression and the previously compressed area is submitted to a tension. Again, the maximum compression stress is higher than the tensile level. The dissymmetry of the behavior is verified in here.

4.6 Summary

This chapter presents the development and the identification of the sand core model.

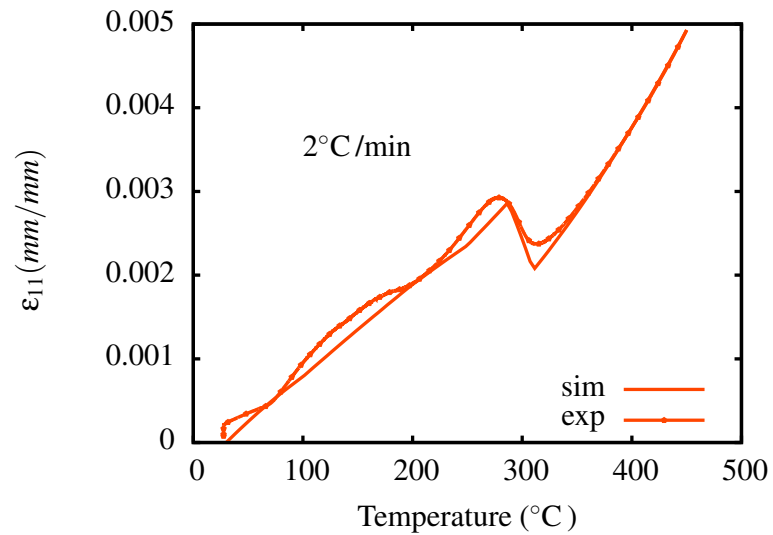
- The expression of the deformation accounts for the different physical governing mechanisms and depending parameters;
- The parameters of the thermal degradation model were identified based on the thermogravimetric tests, which showed a good agreement with the experiments;
- The model parameters were identified from the bending tests on the sand cores. The numerical simulations demonstrated that the model describes all the effects linked to temperature, temperature rate and complex thermomechanical loadings. Both thermal and thermomechanical behaviors were investigated;
- The deformation computed in the complex loading configurations with turning upside down the specimen still needs to be improved. We believe that the gap between

the simulations and the experiments are due to sand core aging during the isothermal period. However, the main purpose of the work is to develop a model for the sand core during casting which can be used easily in an industrial context. Briefly speaking, the most important aspects, namely the physical mechanisms, and the deformation process are well described by the model.

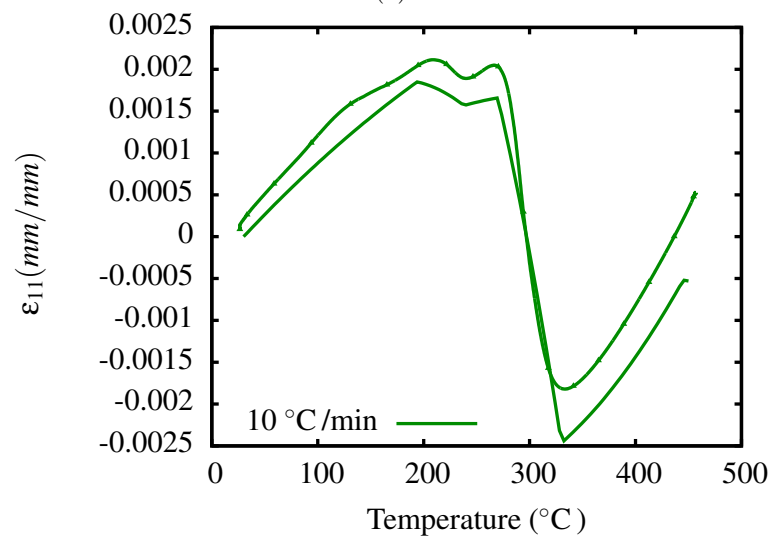
4.7 Résumé en français

Ce chapitre présente le développement et l'identification du modèle développé pour les noyaux de fonderie.

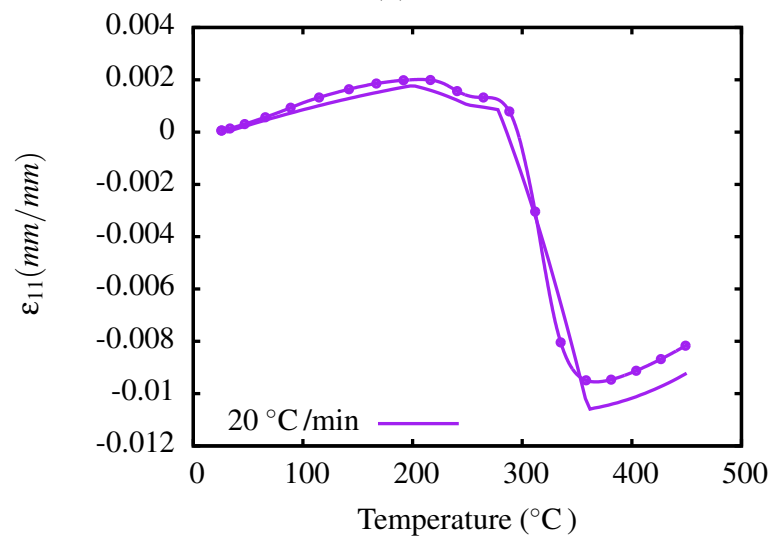
- L'expression de la déformation a été construite de manière à prendre en compte les différents mécanismes physiques qui gouvernent le comportement du matériau.
- Les paramètres de la loi de dégradation thermique ont été identifiés sur la base des essais thermogravimétriques, qui ont montré un bon accord avec les expériences.
- À partir des essais de flexion effectués sur les noyaux de sable, les paramètres du modèle ont été identifiés. Les résultats numériques ont montré que le modèle décrit les effets de la température, de la vitesse de chauffe et des chargements thermomécaniques complexes. Les comportements thermiques et thermomécaniques ont été étudiés.
- Enfin, la déformation calculée dans les configurations de chargement complexes avec retournement de l'échantillon doit encore être améliorée. Nous pensons que l'écart entre les simulations et les expériences est dû au fait que le noyau de sable vieillit pendant le palier isotherme à cause de la réticulation de la résine. Son effet sur les propriétés du noyau ne sont pas encore pris en compte dans le modèle. Cependant, les aspects les plus importants, qui sont les mécanismes physiques et le processus de déformation sont correctement décrits par le modèle, et nous avons un bon accord entre les simulations et les résultats expérimentaux.



(a)



(b)



(c)

Figure 4.14: Comparison of the computations and experimental results of the thermal tests performed on the sand core with heating up to 450 °C at (a) 2 °C/min (b) 10 °C/min and (c) 20 °C/min

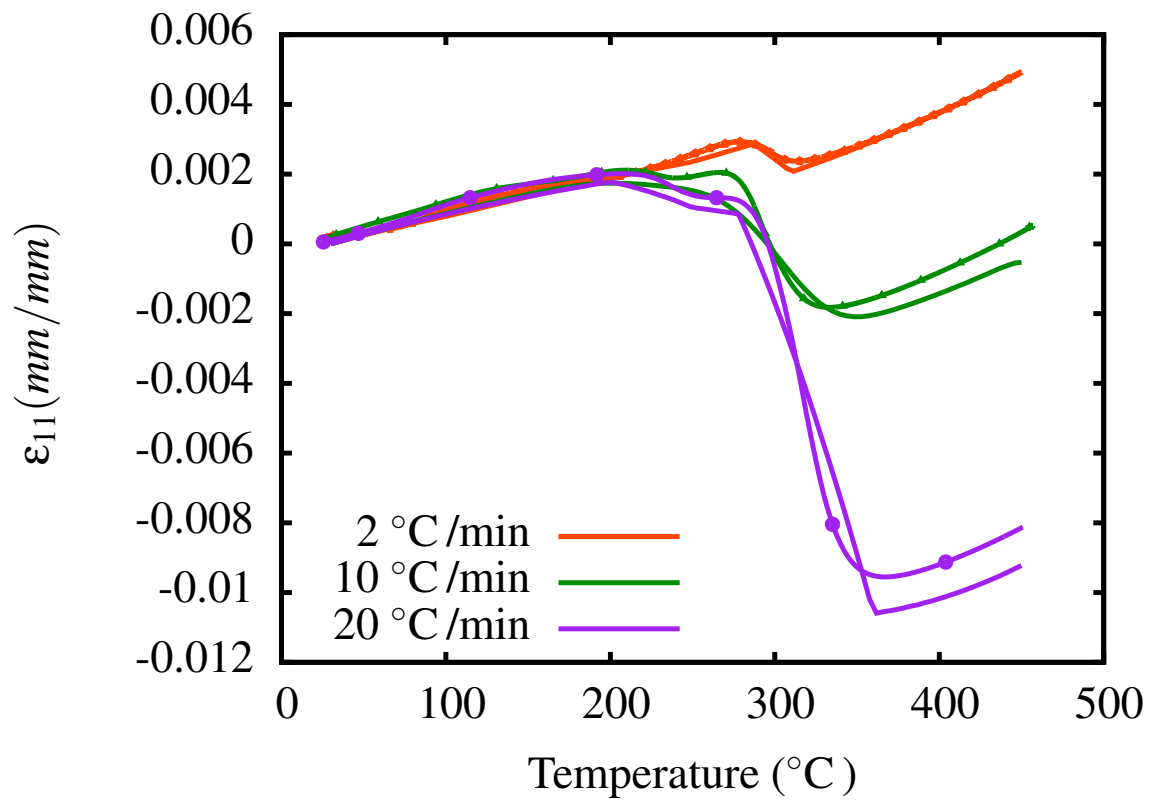
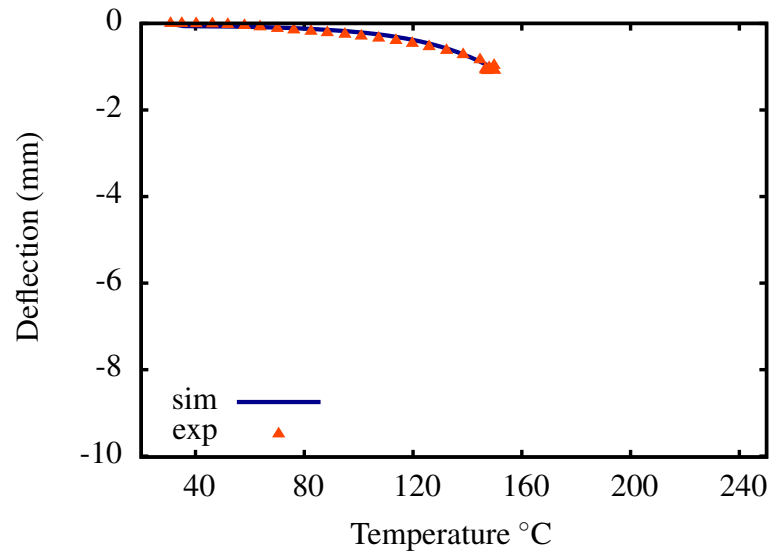
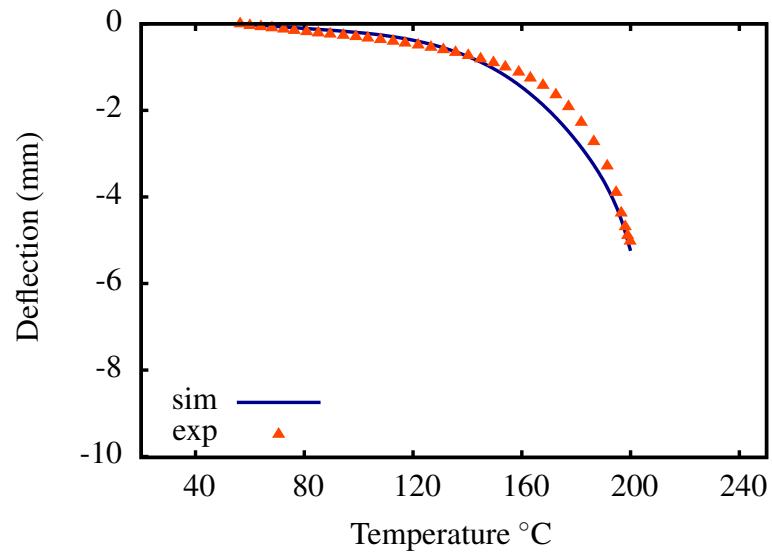


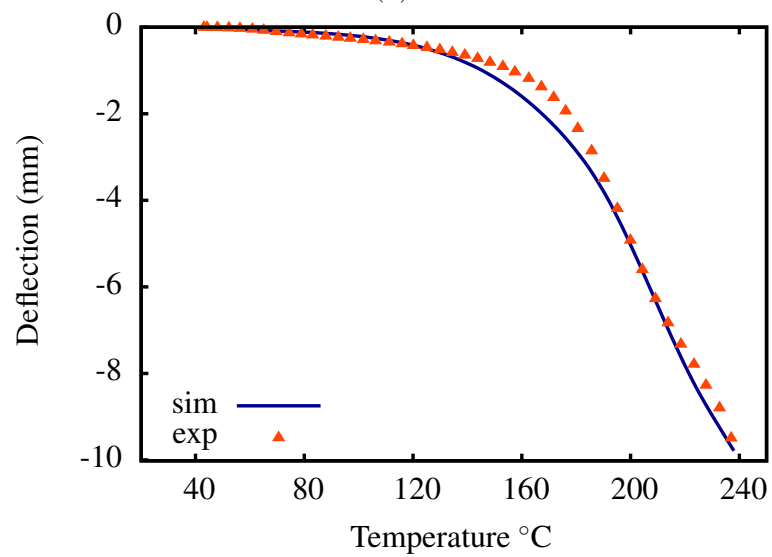
Figure 4.15: Comparison of the three tested heating rates



(a)



(b)



(c)

Figure 4.16: Comparison of the computations and experimental results of four-point bending tests performed on the sand core with heating up to (a) 150 °C (b) 200 °C and (c) 240 °C

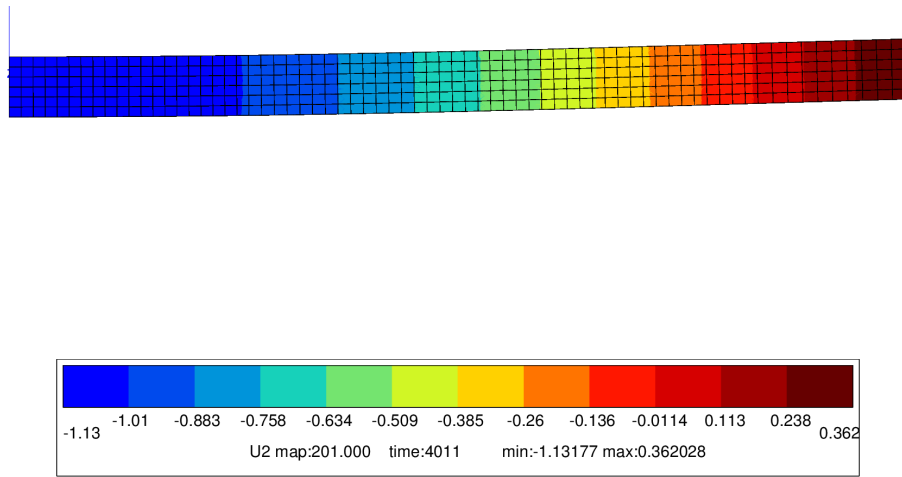


Figure 4.17: Specimen maximum deflection at 150 °C

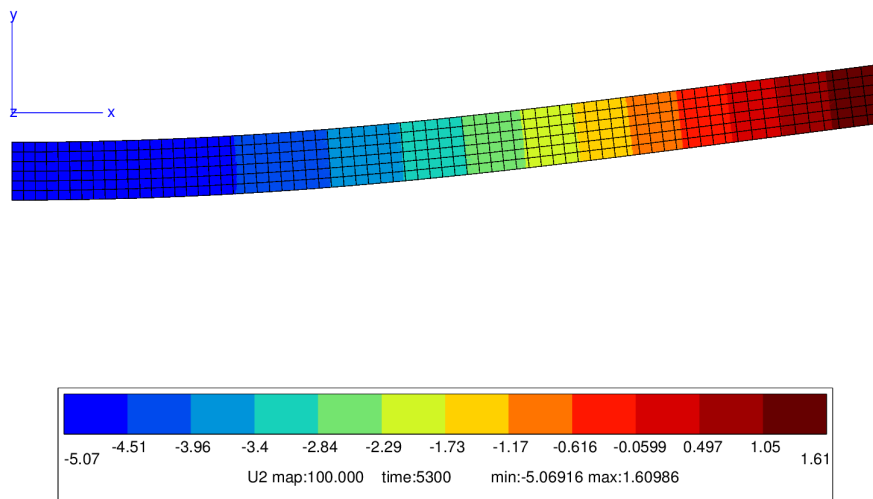


Figure 4.18: Specimen maximum deflection at 200 °C

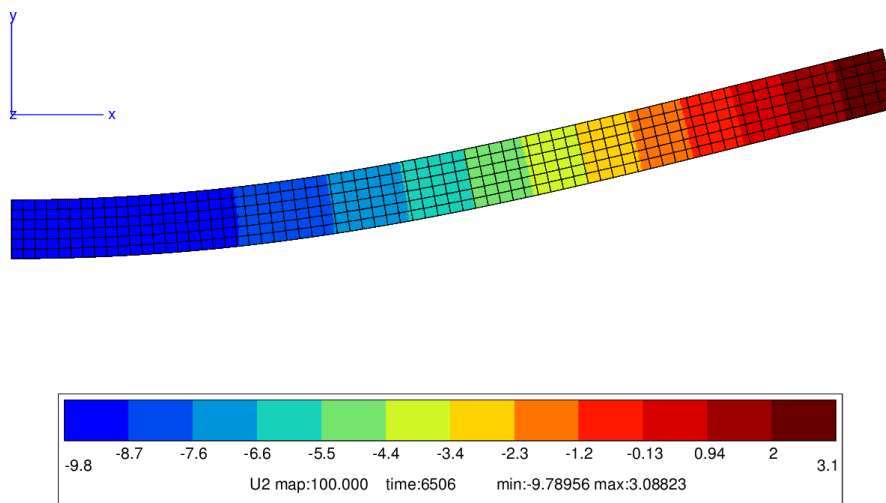
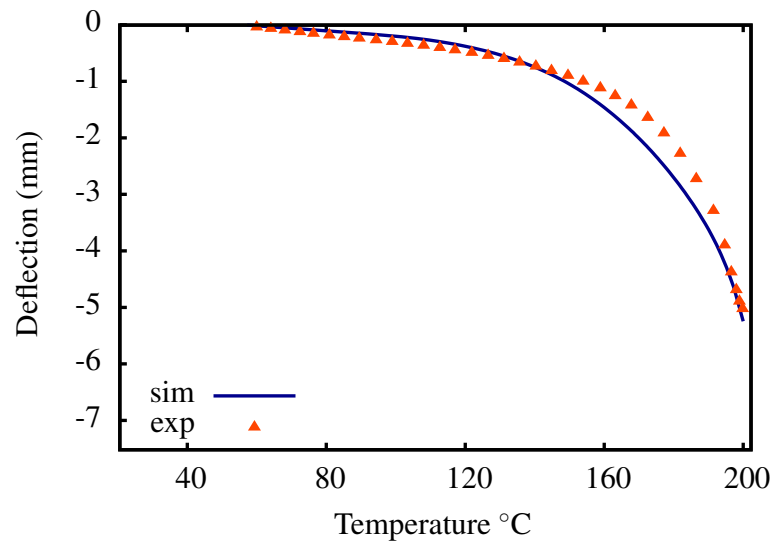
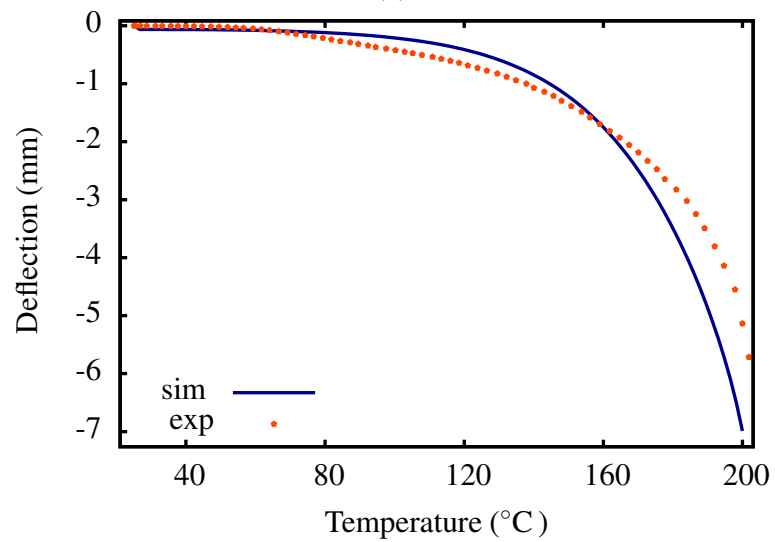


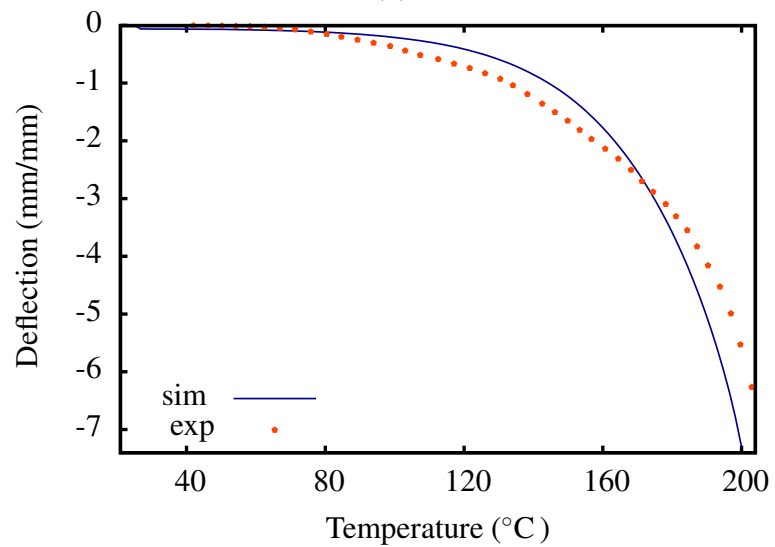
Figure 4.19: Specimen maximum deflection at 240 °C



(a)



(b)



(c)

Figure 4.20: Comparison of the computations and experimental results of four-point bending tests performed on the sand core with heating up to 200 °C at temperature rate of (a) 2 °C/min (b) 10 °C/min and (c) 20 °C/min

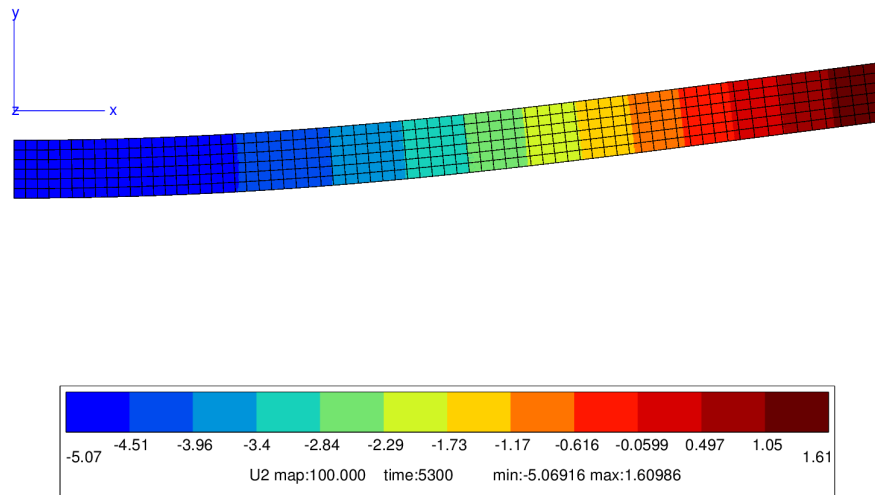


Figure 4.21: Specimen deflection at 200 °C during heating at 2 °C/min

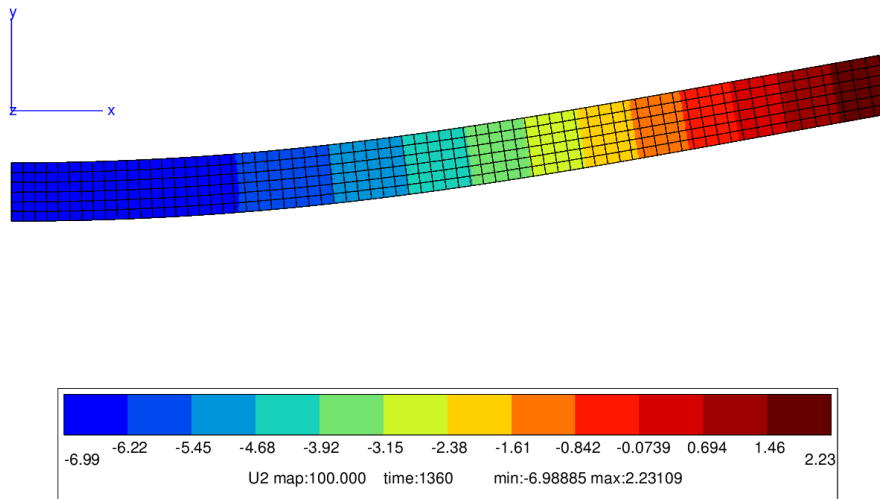


Figure 4.22: Specimen deflection at 200 °C during heating at 10 °C/min

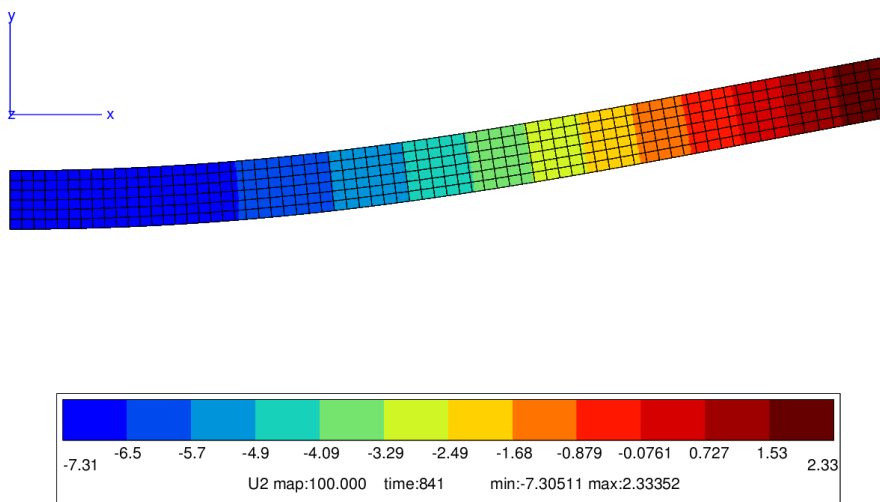
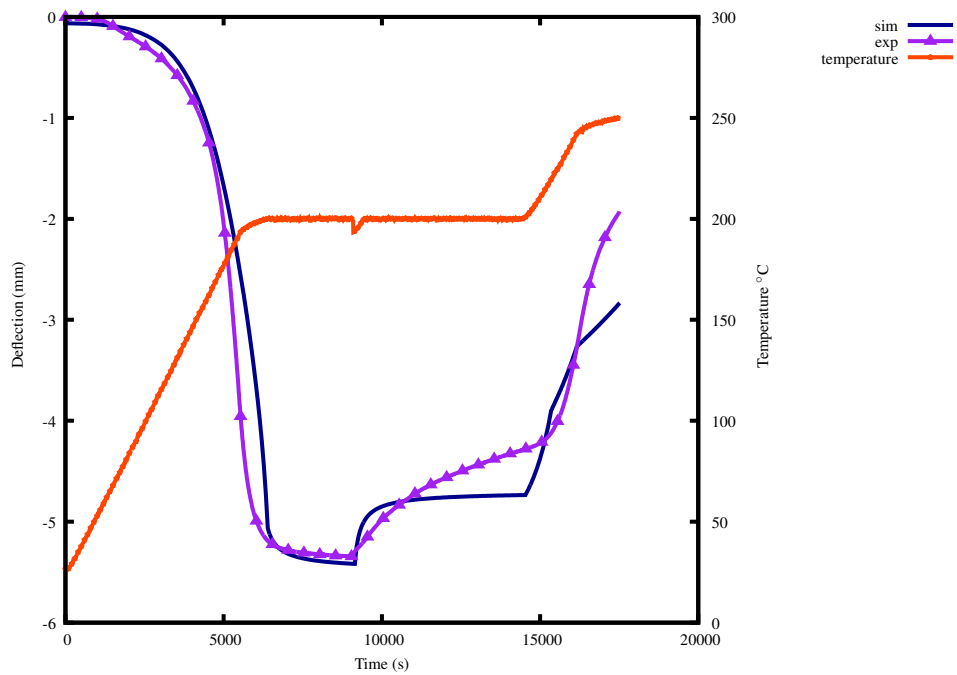
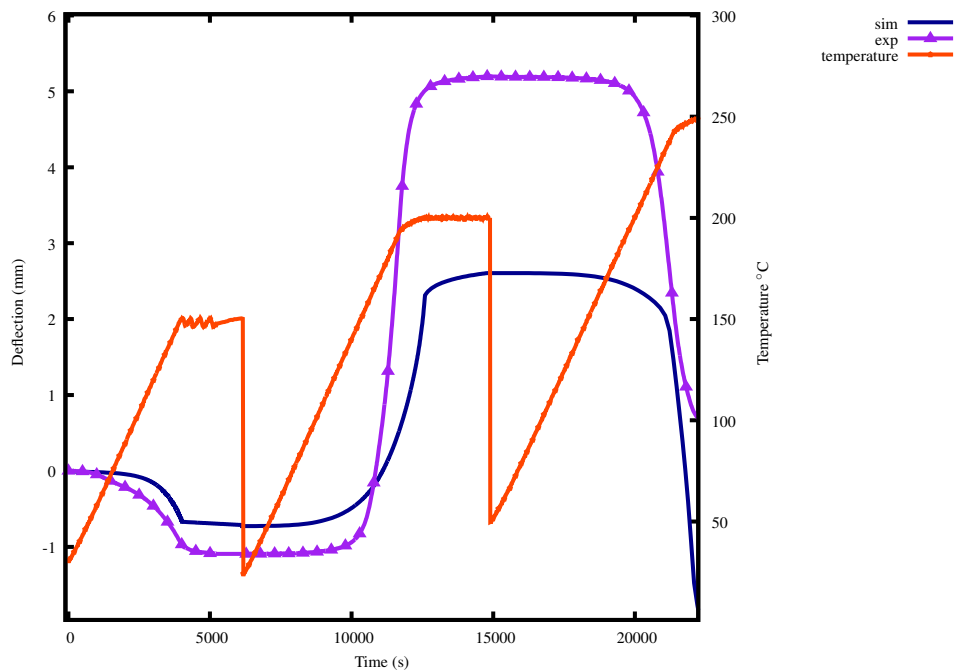


Figure 4.23: Specimen deflection at 200 °C during heating at 20 °C/min



(a)



(b)

Figure 4.24: Comparison of the computations and experimental results of four-point bending tests with turning upside down the specimen in (a) at 200 °C without temperature change and in (b) with temperature change

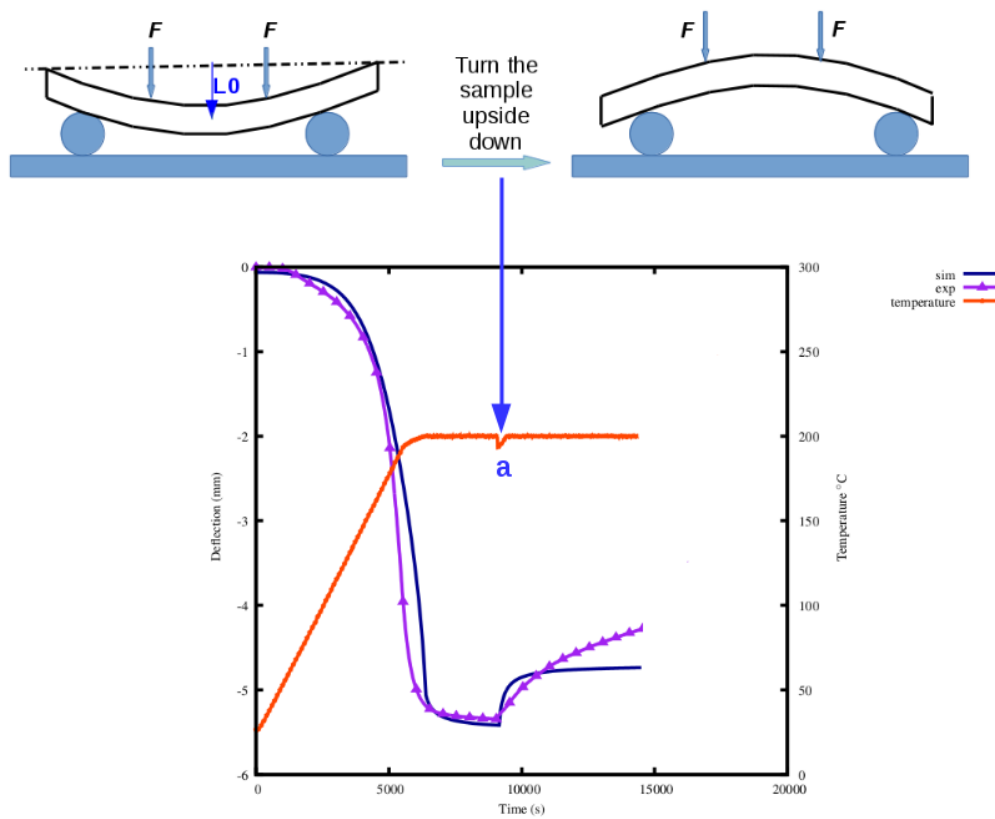


Figure 4.25: Cyclic loading configuration with turning upside down the specimen at 200 °C and experimental results

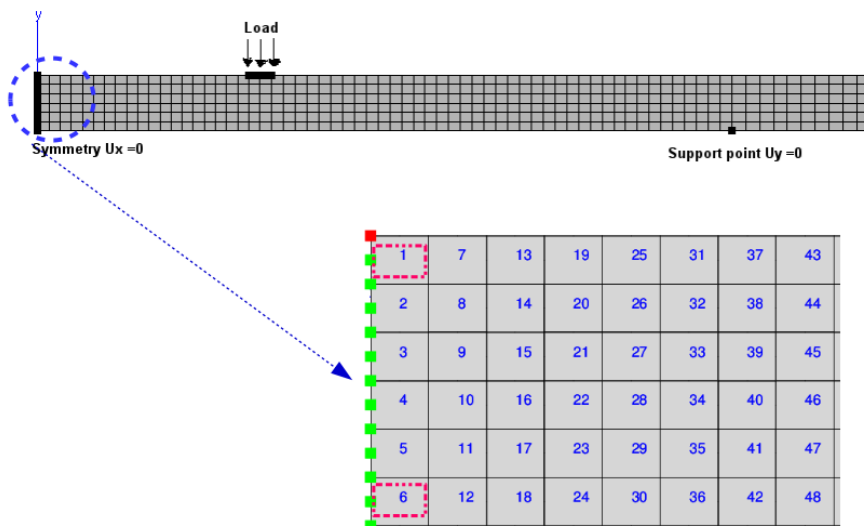


Figure 4.26: Initial specimen mesh showing the stress and strain analysis zone at elements 1 and 6 highlighted in red

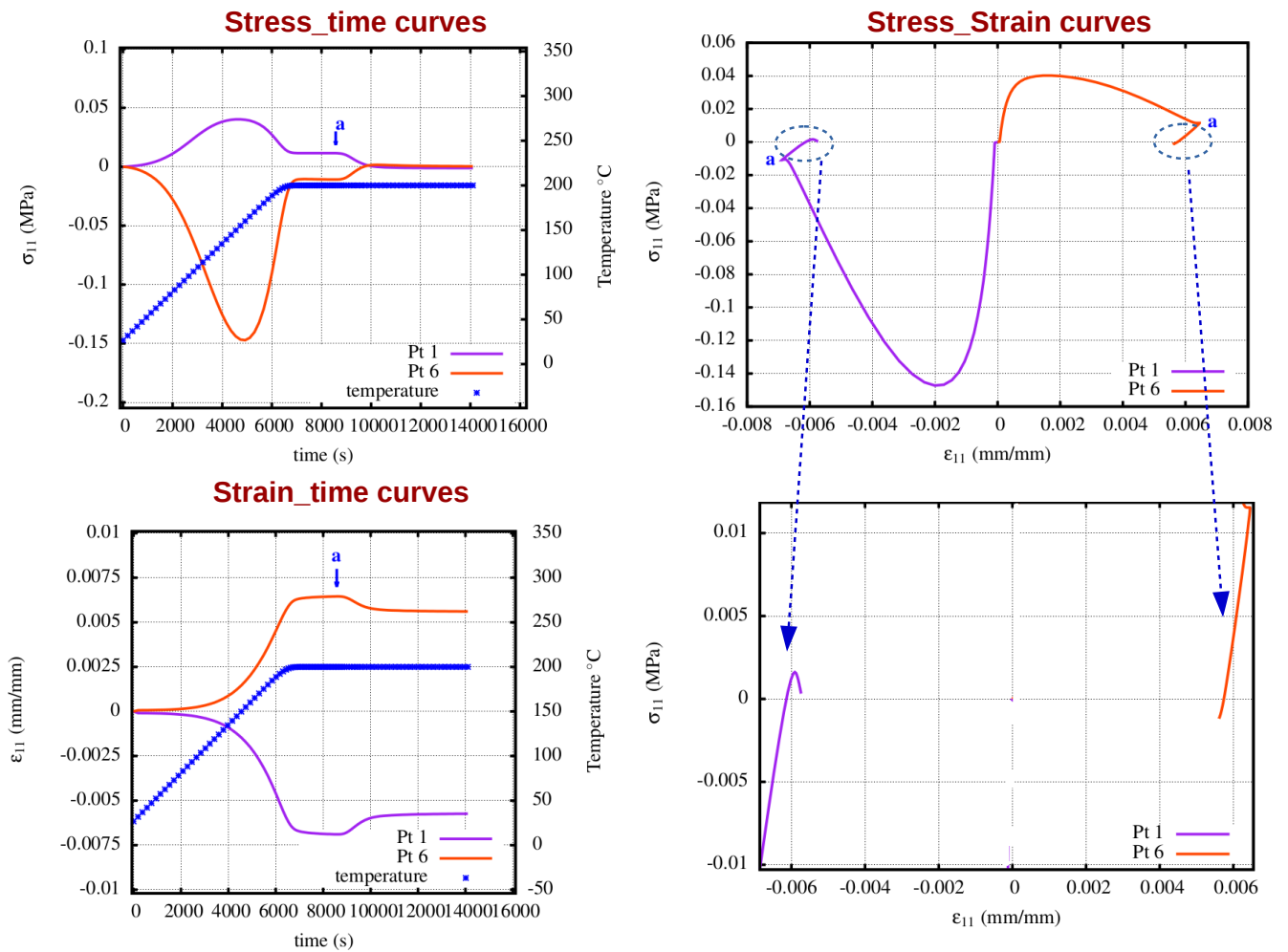


Figure 4.27: Stress and strain evolution at elements 1 and 6 during test with turning upside down the specimen. Top left: stress vs time. Bottom left: Strain vs time. Top right: Stress vs strain. Bottom right: Zoom on the stress strain curve when turning upside down the sample.

Chapter 5

Model validation on a technological specimen

Contents

5.1	Design and instrumentation of the technological specimen	136
5.1.1	The metallic mold and aluminum cast	136
5.1.2	Aluminum alloy	137
5.1.3	Technological specimen designs	137
5.1.4	Measurement techniques	139
5.2	Instrumentation protocol	140
5.2.1	Specimen preparation	141
5.2.2	Instrumentation stages	142
5.3	Instrumentation results	144
5.3.1	"Dog bone" design	144
5.3.2	"CDG" design	154
5.4	Numerical validation of the model on "CDG" design	161
5.4.1	Mesh of the specimen	161
5.4.2	Numerical simulation	161
5.4.3	Results and discussion	163
5.5	Summary	164
5.6	Résumé en français	165

The present chapter deals with the design and instrumentation of a technological specimen in order to validate the model developed.

In general, the basic approach when studying a material behavior remains the experimental method, while models draw on the results of the experimentation and new developments. On the other hand, for real industrial applications, we now recognize the interest of “technological tests”, intermediate structures between the simple laboratory test specimen and the real component. These tests enable to give a feedback on the performance of components and structures operating under extreme thermal and mechanical loading conditions and validate the experimental and numerical approaches developed with laboratory specimens.

In the present work, the four-point bending tests carried out on the small sand core specimen were used to feed the behavior model presented in Chapter 4. In fact, during casting, the core is subjected to a more complex loading (triaxial stress state and higher temperatures) which might generate deformation mechanisms that are not revealed by simple tests. Between the too simple laboratory test and the too expansive test on full size sand cores, a technological specimen representative of the core has been developed. It is a question of verifying the validity of the model outside its initial identification domain.

The results of an extensive test program performed on two technological specimens are presented. First, the experimental procedure developed for measuring the core deformation during casting is detailed. Second, the computations performed on the selected specimen design are shown and compared to the experimental results obtained from the industrial instrumentation.

5.1 Design and instrumentation of the technological specimen

The purpose of the instrumentation is to measure both temperature and displacement during casting. Temperature measurement is a routine operation that is done at Montupet on industrial cores using embedded thermocouples, while the displacement measurement has never been performed before.

The criteria that prevailed for the design of the specimen are as follows:

- The design geometry must be representative of the new developed sand cores;
- The core must be thin enough so that when submitted to the metallo-static pressure and the high temperature field during casting, a deformation can be obtained but also thick enough to enable its extraction from the corebox after manufacturing;
- There is only one laboratory testing mold at Montupet *R&D* department, which will be presented in the following paragraph. It enables to cast metallic parts called “clarinet”. The chosen specimen must fit inside.

5.1.1 The metallic mold and aluminum cast

The mold available at Montupet *R&D* department is presented in Figure 5.1. It is basically suitable for the production of cores with a cylindrical shape. Only gravity casting can be performed using manual pouring technique. The so called “clarinet” is presented in grey in Figure 5.2.

Mold “clarinette”

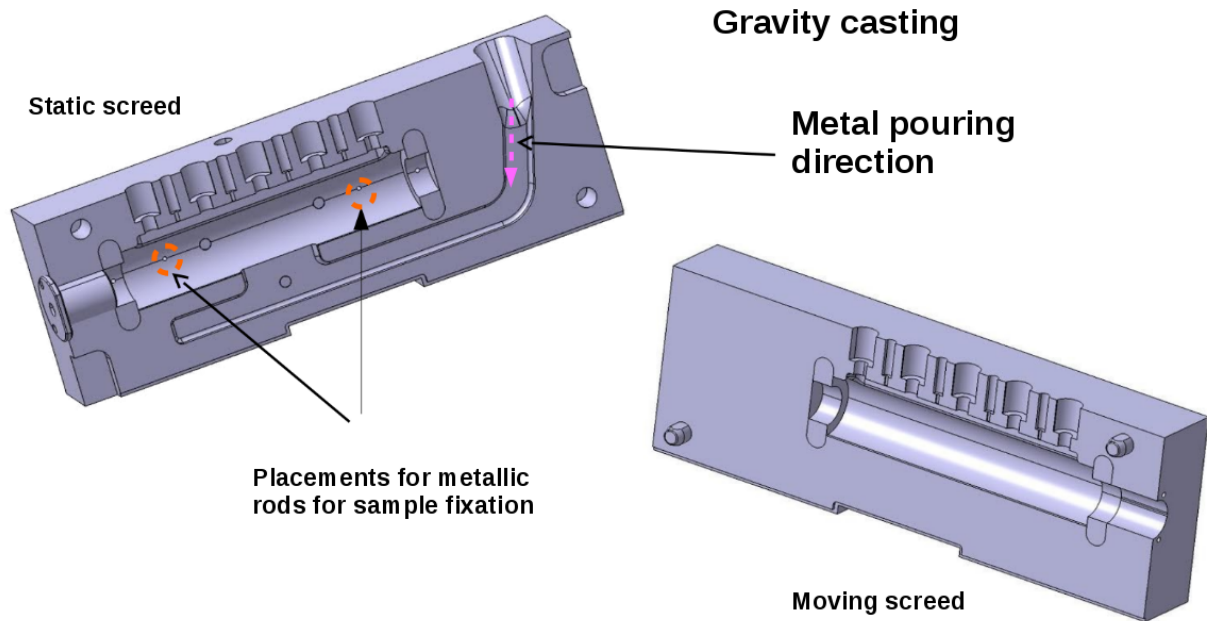


Figure 5.1: View of the “clarinet” mold

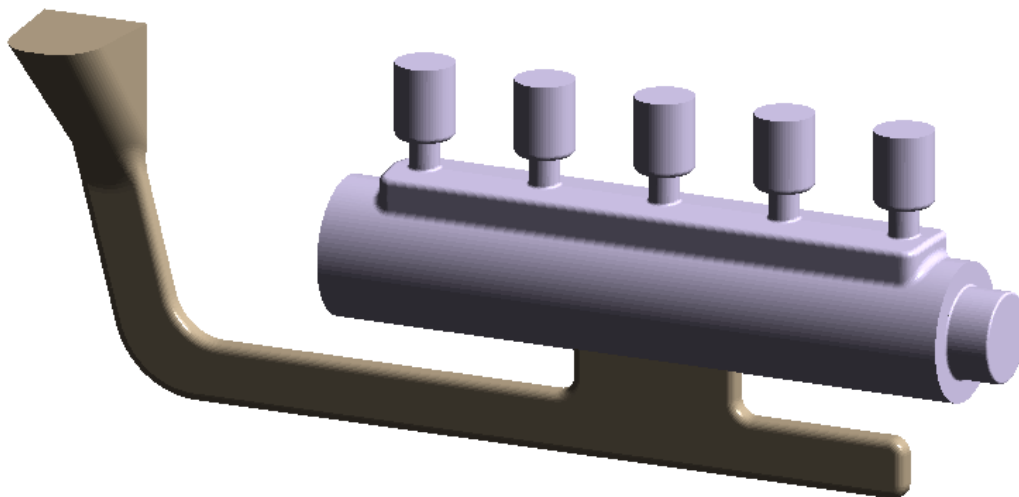


Figure 5.2: Metallic part obtained with the “clarinet” mold

5.1.2 Aluminum alloy

The selected alloy is *AS7U3*, which presents a large solidification domain between 502 and 607 °C (Figure 5.3). This large range enables to follow specimen deformation during the solidification.

5.1.3 Technological specimen designs

Two designs were tested in this study denoted: “dog bone” and “CDG”. The “dog bone” specimen was mainly used to define the protocol for instrumentation and casting. In fact, displacement measurements were not conclusive on this specimen. The second design (“CDG”) was created in order to be able to correctly measure the core deformation: it is

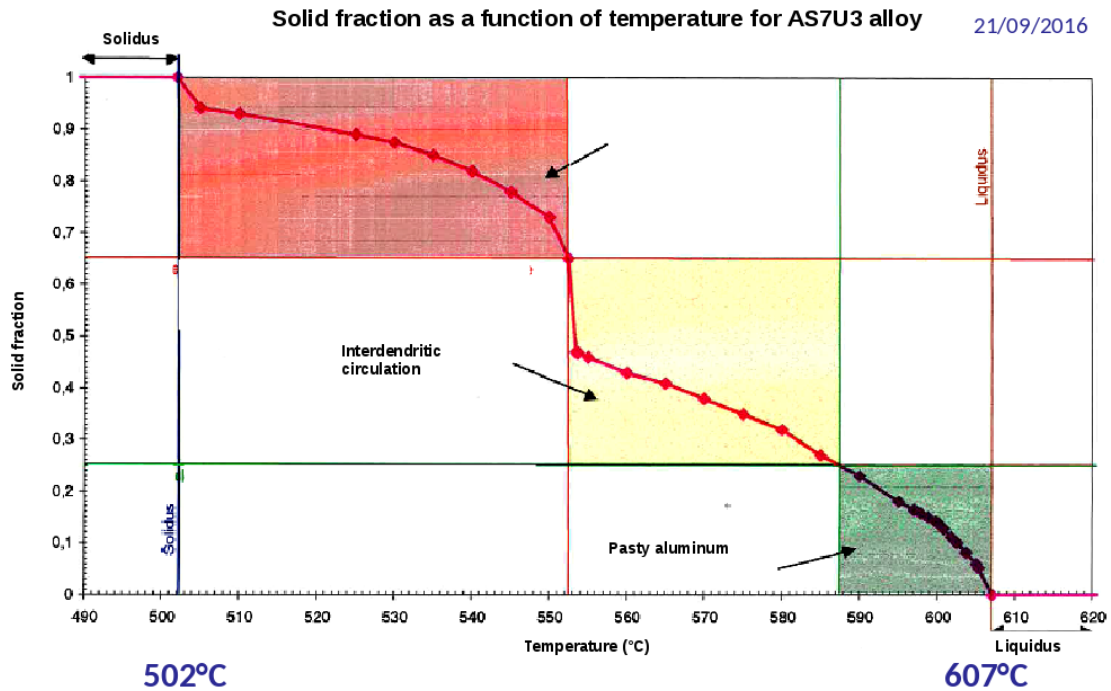


Figure 5.3: Aluminum alloy *AS7U3* selected for the technological specimen [Mon16]

more representative of the industrial core design but too thin for a thermocouple to be placed on it, so there is no temperature measurement for this specimen.

“Dog bone” specimen design. For simplicity reasons, it was decided to start with the design available at Montupet. The specimen is called “dog bone” and classically used for bending tests (Figure 5.4) as shown previously in paragraph 3.2.2. Figure 5.5 shows the specimen placed inside the mold. As mentioned before, the metallic mold is suitable for specimens with cylindrical spans, while the “dog bone” spans are rectangular. The specimen needs additional modifications to be fixed in the mold and to avoid rotations that would generate errors in displacement measurement.

We performed many temperature and displacement measurements on this design and it mainly served to improve the experimental protocol. This will be detailed in the following paragraphs.

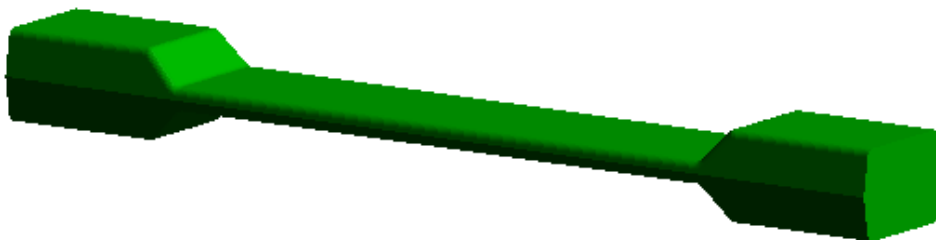


Figure 5.4: View of the “dog bone” specimen

”CDG” specimen design. The design team in Montupet *R&D* developed a new specimen inspired from the industrial cores which present a deformation during casting in



Figure 5.5: View of the “dog bone” specimen placed inside the “clarinet” mold

production environment. The characteristics of this new specimen should allow the production by laboratory machines, but above all to allow a direct measurement of the displacement. The first solution proposed, called “the wave” (Figure 5.6) is inspired from water-jacket sand cores. The main idea was to dispose of an extension where the displacement sensor can be put in direct contact. Unfortunately the design was too complex to be produced with the laboratory coring machine. In fact, the simulations of the mixture shooting during coremaking revealed that the corebox filling pressure was not sufficient. It was therefore required to adopt a thinner and simpler form.

A new 5 mm thickness “CDG” core design was then defined. For cost-saving reasons, the corebox shown in Figure 5.7 is a made out of a polyurethane polymer block already available at Montupet. Because of this choice we first had to face difficulties to extract the cores. Due to their thinness, and since they stick to the corebox, they break in the critical junctions (see Figure 5.7). After many attempts, a satisfactory geometry was found, enlarging the cavities by 0.5 mm. Even in these conditions, handling remains difficult, core extraction is a sensitive operation and damage may be created if not enough care is taken.

5.1.4 Measurement techniques

The displacement measurement is made by means of a laser sensor type “Sick optex” shown in Figure 5.8. It enables to measure displacements in a range from 0 to 150 mm. The protocol used for the measurements will be detailed in the next section.

The temperature measurement on sand core is complex due to its small thickness. Holes should be drilled in the specimen in order to fix the thermocouples with a high-temperature adhesive. The type-K thermocouples used at Montupet have a diameter of 2 mm. This operation is carried out at room temperature before casting. Special care

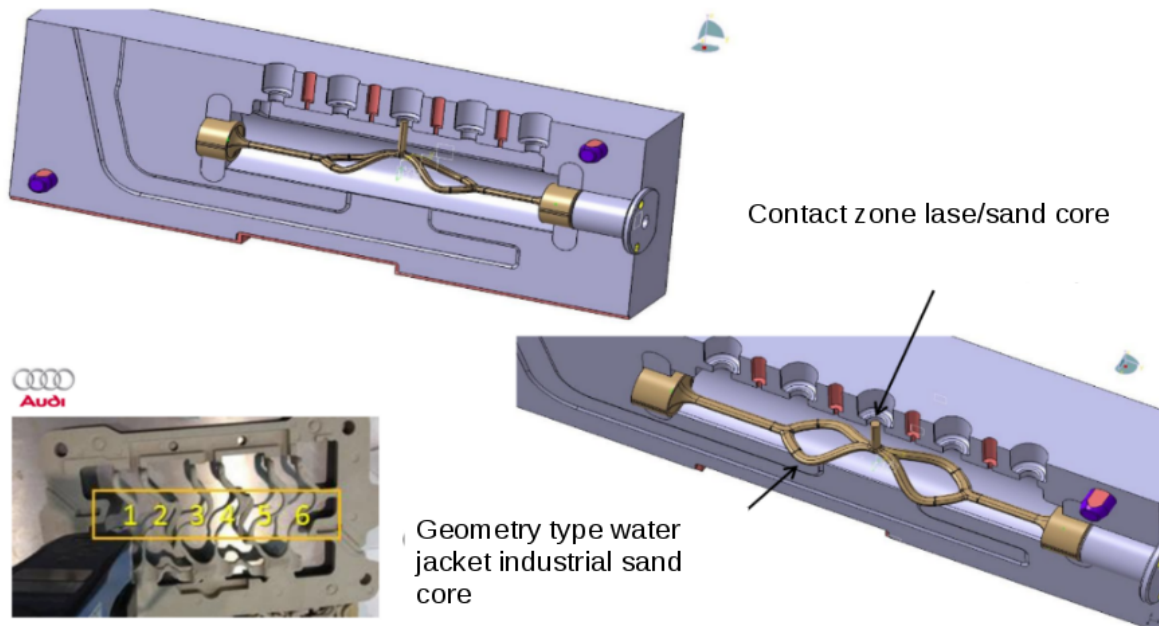


Figure 5.6: An intermediate design for the technological specimen: “the wave”

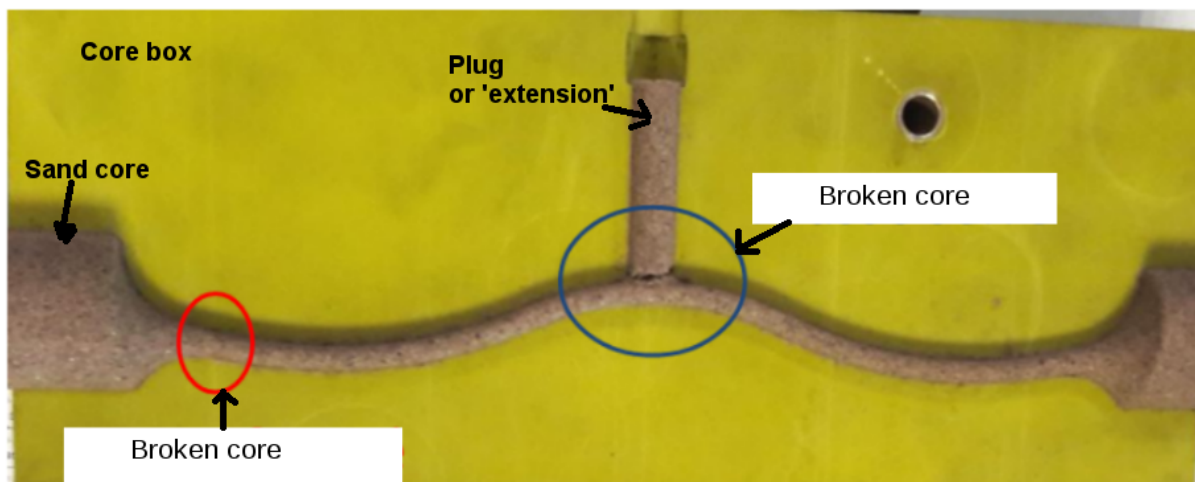


Figure 5.7: Technological specimen “CDG”

must be taken during the operation to avoid breaking the specimen, or to create a crack that would lead to rupture during casting. In fact, since drilling weakens the specimen, the displacement and temperature measurements were performed in separate tests.

5.2 Instrumentation protocol

The workplan was defined as follows:

- Set a protocol for the temperature and displacement measurement during casting;
- Define the steps for the instrumentation (specimen insertion, measurements, timing for pouring, mold opening and closing..);

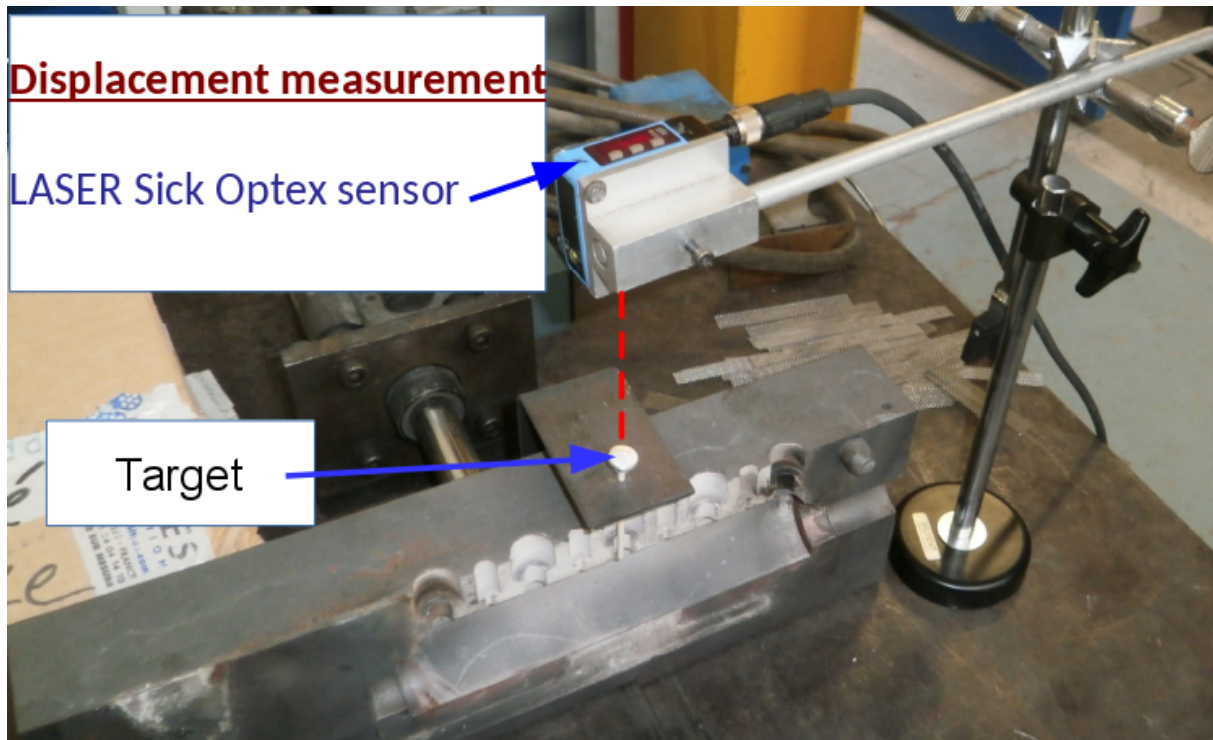


Figure 5.8: Laser sensor used for displacement measurement

In this paragraph, a description of the instrumentation steps and the measurement protocol are detailed.

5.2.1 Specimen preparation

“Dog bone” specimen

1. **Specimen instrumentation with thermocouples.** As shown in Figure 5.9, thermocouples 1 and 5 are placed at the specimen edges which are 20 mm thick, and thermocouples 2, 3 and 4 are introduced at a distance of 20 mm where thickness is 5 mm.

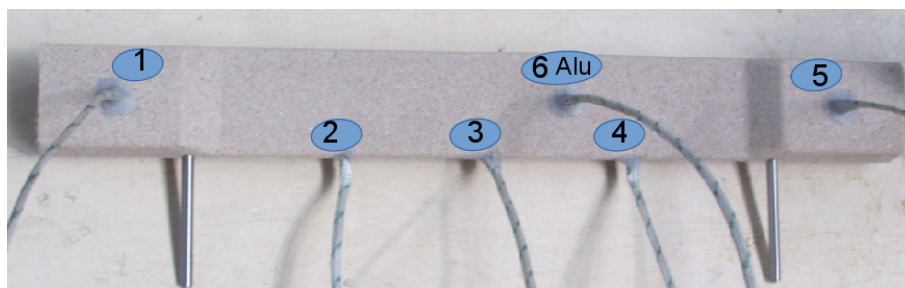


Figure 5.9: “Dog bone” specimen instrumented with thermocouples

2. **Specimen instrumentation for displacement measurement.**

The core displacement is measured at the top center. For this purpose, a ceramic rod was introduced through the mold and put in direct contact with the core just before casting (Figure 5.10). The laser sensor is then used to measure the rod displacement at the top. When measuring the displacement, only the thermocouples 1

and 5, in the massive parts, are kept in order to check the temperature. The tested specimens will then be analyzed by tomography.

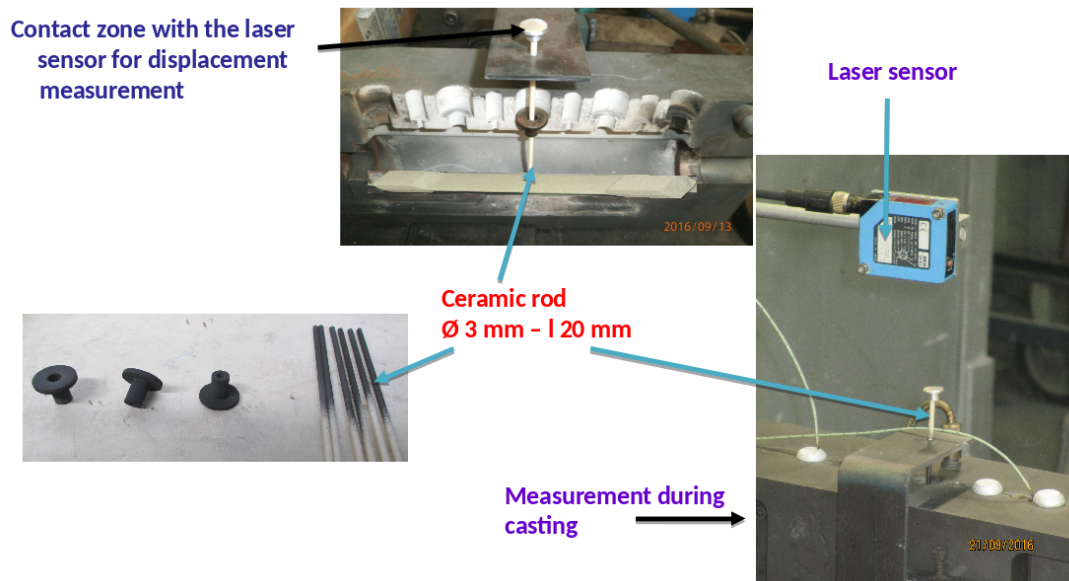


Figure 5.10: “Dog bone” specimen instrumented with a ceramic rod for displacement measurement

”CDG” specimen

The “CDG” specimen has cylindrical spans which are suitable for the “clarinet” metallic mold. Therefore there is no need for rods to fix the specimen in the mold. The core edges are then embedded between the mold screeds.

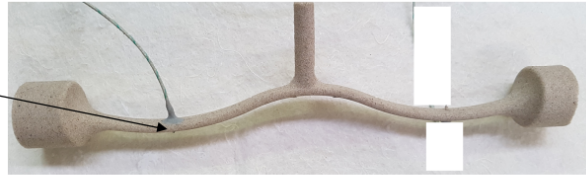
- 1. Specimen instrumentation with thermocouples.** The “CDG” specimen is very thin and brittle. It was not possible to place any thermocouples inside the sand core and to perform a temperature measurement directly on the specimen. The metal temperature was measured at different locations, in order to follow metal solidification and check the computations made with the Magma software. Due to the big amount of aluminum in the mold, there is a risk of early solidification in some places. As summarized in Figure 5.11, a thermocouple denoted “TH metal bottom in core” passes through the sand core specimen to measure the aluminum temperature at the contact surface with the core, while three other thermocouples were inserted at different positions in the metal across the cast width.
- 2. Specimen instrumentation for displacement measurement.** For the displacement measurement, the laser beam is focused on the sand core plug (Figure 5.12), so that the deformation of the sand core is directly measured.

5.2.2 Instrumentation stages

Mold heating. The metallic mold is set up with a thermocouple (Figure 5.13). It is heated before casting up to an average value of 370 °C.

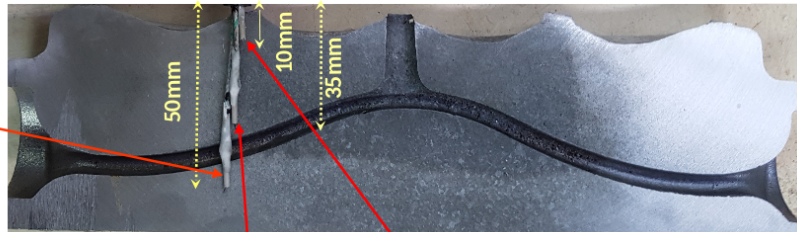
Core "CDG"

TH metal bottom in
core



Cavity of core "CDG"

TH metal bottom in cast



TH metal up in cast

TH metal feeder in cast

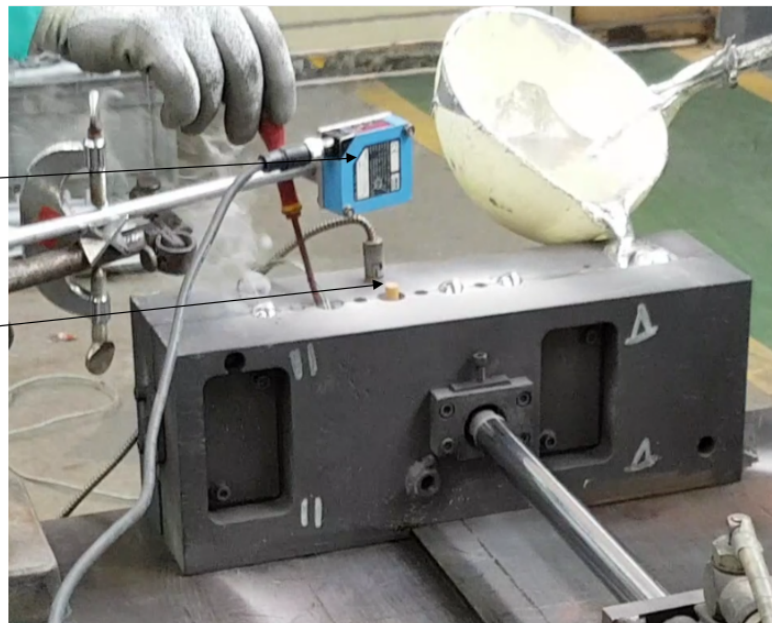
29/09/2017

Figure 5.11: Instrumentation of technological specimen "CDG" with thermocouples

Deformation measurement

Laser sensor

Target
measurement
spot on "CDG"
core plug



29/09/2017

Figure 5.12: Technological specimen "CDG" instrumented with a laser sensor

Core insertion and mold closure Once the mold temperature has reached the target value of 370 °C, the sand core is inserted and fixed. The resulting configurations for temperature and displacement measurements are shown respectively in Figures 5.14a and 5.14b for the "dog bone" specimen. The "CDG" specimen placement inside the mold is given in Figure 5.15 . This step is very delicate. The mold temperature is extremely high and the operator must manipulate the core carefully and place it very rapidly in order to maintain the temperature level (Figure 5.16).

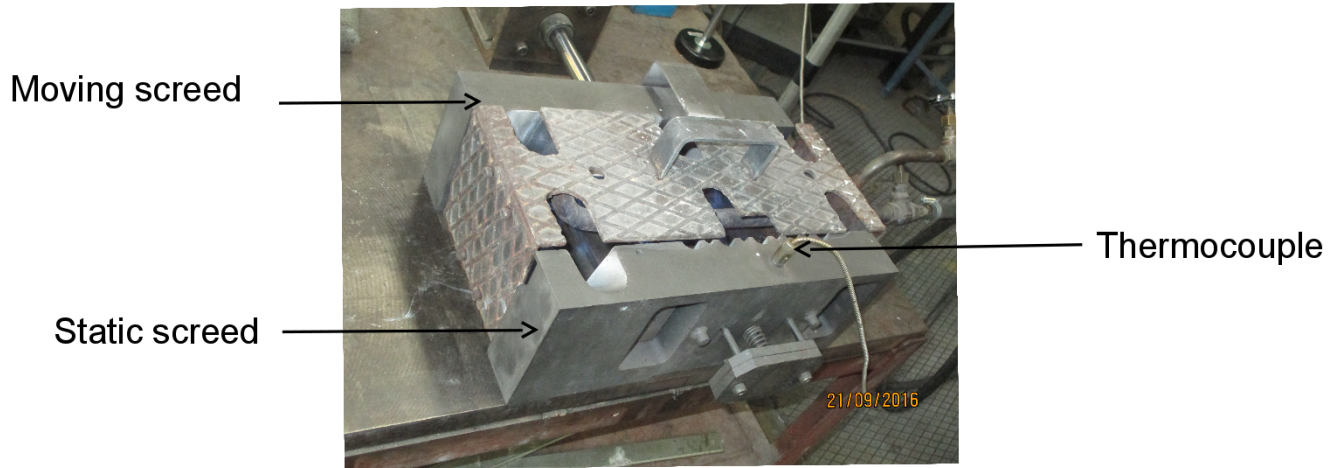


Figure 5.13: Mold heating before casting

Setting up and adjusting the laser sensor. This step is only made for the case of displacement measurements.

- **”Dog bone” specimen.** The ceramic rod is introduced through the metallic rod until it reaches the specimen. In fact, we have here no means to check if the rod is actually in contact with the core and is perfectly perpendicular. Any related error may distort the measurement results. The laser sensor is then set up and adjusted as in Figure 5.17. This step usually takes about 30 s.
- **”CDG” specimen.** The laser is placed in a way that the beam points directly on the “CDG” core plug as shown in Figure 5.18.

Aluminum casting. The aluminum is melted and held at 700 °C then poured in the metallic mold. The filling operation is manual using a ladle instrumented with a thermocouple as shown in Figure 5.19, so that it is almost impossible to ensure an even flow rate. The operation takes between 7 and 10 s.

Aluminum solidification and demolding. Once the mold is filled, the solidification takes place between 600 and 500 °C as shown in Figures 5.20a and 5.20b for the two configurations (respectively displacement and temperature measurements). Once the core temperature stabilizes at around 380 °C, the cast is demolded.

5.3 Instrumentation results

5.3.1 ”Dog bone” design

Table 5.1 provides a summary of the tests performed. Phases A and B consist in measuring respectively the core temperature and displacement during casting. Due to the experimental difficulties, specifically regarding the specimen fixation inside the hot mold, many specimens broke down during the insertion of the metallic rods. Nevertheless, at least three successful trials (with correct output recording) were obtained for each phase.



(a)



(b)

Figure 5.14: Insertion of a sand core inside the mold for the case of (a) temperature instrumentation and (b) displacement instrumentation

5.3.1.1 Phase A: temperature measurement

This study includes two campaigns. In the first testing configuration, the results were not reproducible, but we show the results anyway to point out the difficulty of this kind of test. A second campaign was then launched with new thermocouples and a change in the

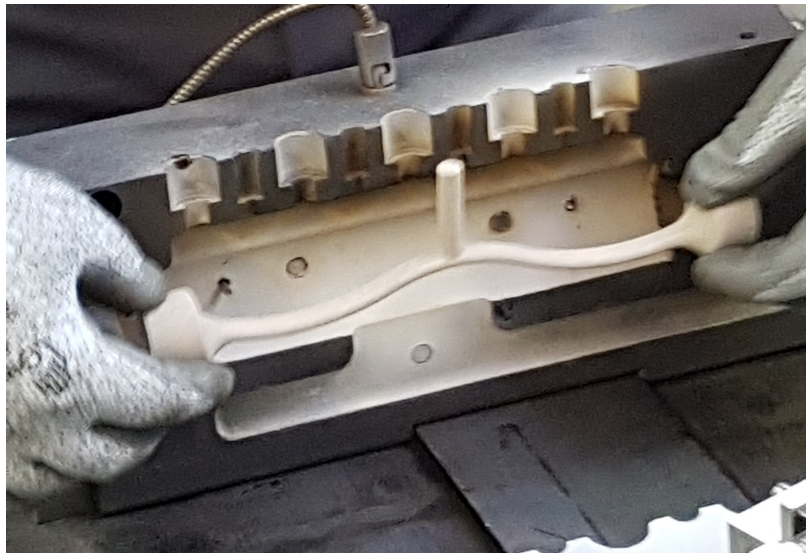


Figure 5.15: "CDG" sand core placement inside the mold



Figure 5.16: Mold closing after core insertion

experimental protocol.

- **Campaign 1.** A typical result of a temperature instrumentation is given in Figure 5.21. Here thermocouples 1 to 5 are embedded in the sand core and thermocouple 6 crosses the specimen to measure the aluminum temperature at the bottom contact surface. The temperature recording goes from the moment the specimen is placed inside the mold to the demolding.

As indicated in Figure 5.21, the casting operation starts when the metal temperature measured in the ladle is about 700 °C. The filling stage lasts from 7 to 9s. The aluminum temperature measured using thermocouples 6 inside the mold at the



Figure 5.17: Ceramic rod insertion and laser sensor set up

Deformation measurement

Laser sensor

Target measurement spot on "CDG" core plug



29/09/2017

Figure 5.18: Technological specimen "CDG" instrumented with a laser sensor during casting

bottom surface with the sand core is $620\text{ }^{\circ}\text{C}$ at the beginning of casting operation and continues to decrease during solidification.

In the sand core, the temperature is around $100\text{ }^{\circ}\text{C}$ in the central area (thermocouples 2, 3 and 4) before casting, while it is $50\text{ }^{\circ}\text{C}$ at the massive edges (thermocouples 1 and 5). During casting, the core temperature increases rapidly and is higher in the center compared to the massive parts. Unfortunately, an important gap was observed when comparing the temperature evolution in all the measurement points.



Figure 5.19: Aluminum casting operation

We performed three tests to validate the reproducibility. Figure 5.22 presents the temperature evolution in each case. A large scatter is observed at each measurement point (see thermocouple 5 for instance).

This dispersion is probably due to the (too big) diameter of the thermocouples which is 2 mm, so that their use is limited to the instrumentation of industrial cores. Also, it seems important to control the duration of the core insertion in order to have the same schedule in all the tests.

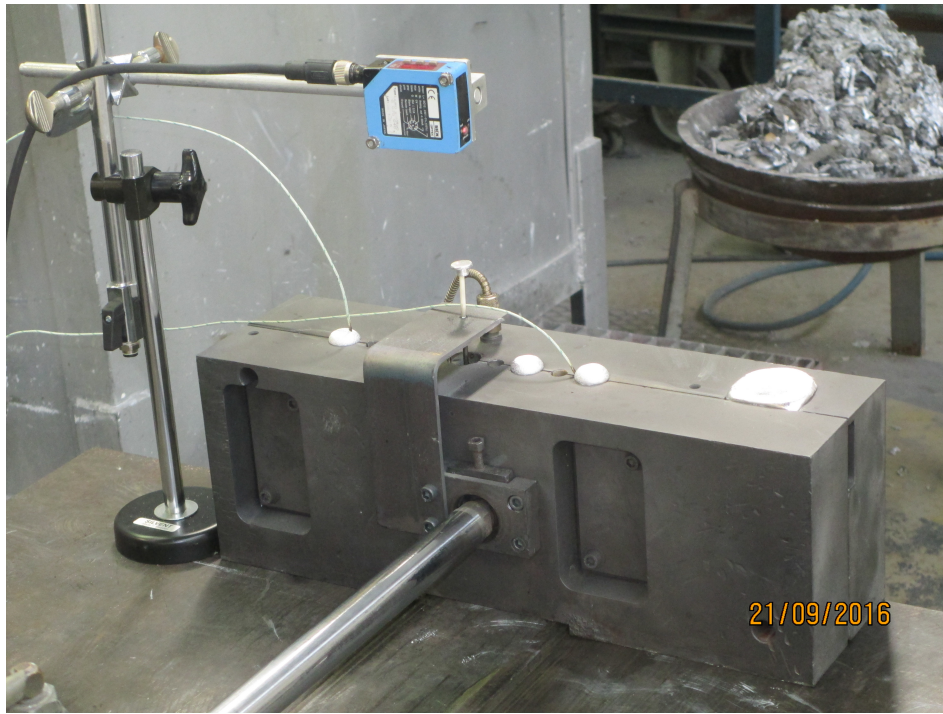
- **Campaign 2.** A new set of tests were performed using thermocouples with a diameter of 1 mm. Special attention was paid to control the duration of the successive stages.

The temperature evolution during casting is presented in Figure 5.23 for two different tests. Unlike the first attempt it can be seen that the temperature curves are superimposed during filling operation (there was a two-minute interruption in the recording of thermocouple 2).

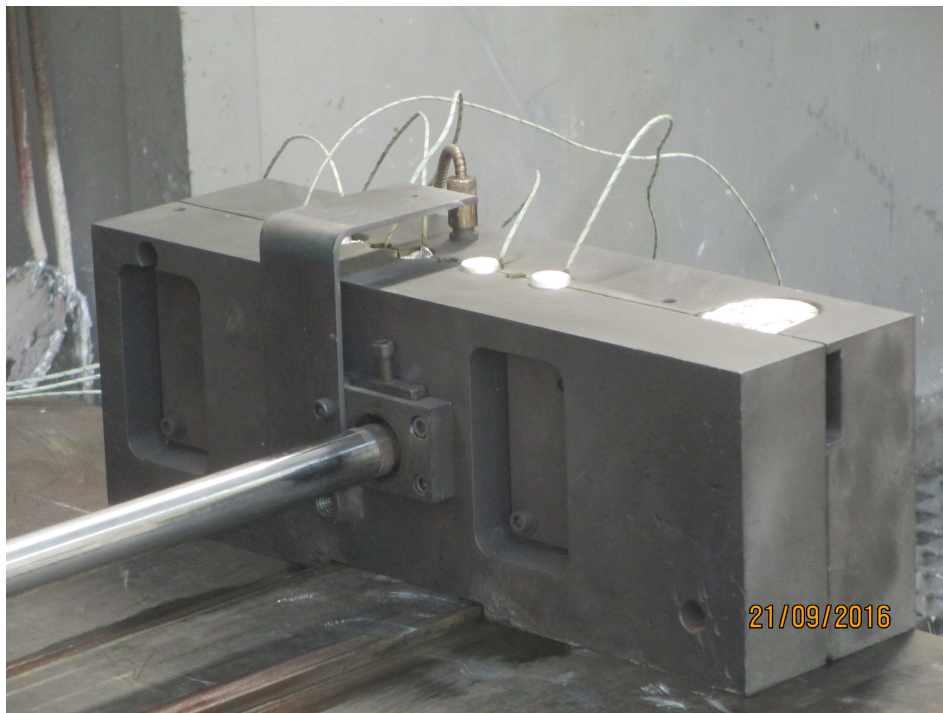
Now if we compare the temperature evolution between the first and second instrumentation in Figure 5.24, we can see that the core temperature is lower in the second instrumentation since the new, thin thermocouples are well embedded inside the sand core.

5.3.1.2 Phase B: Displacement measurement

Figure 5.25 shows an example of the evolution of the core displacement at the center together with the temperature evolution at the core massive edges (only thermocouples



(a)



(b)

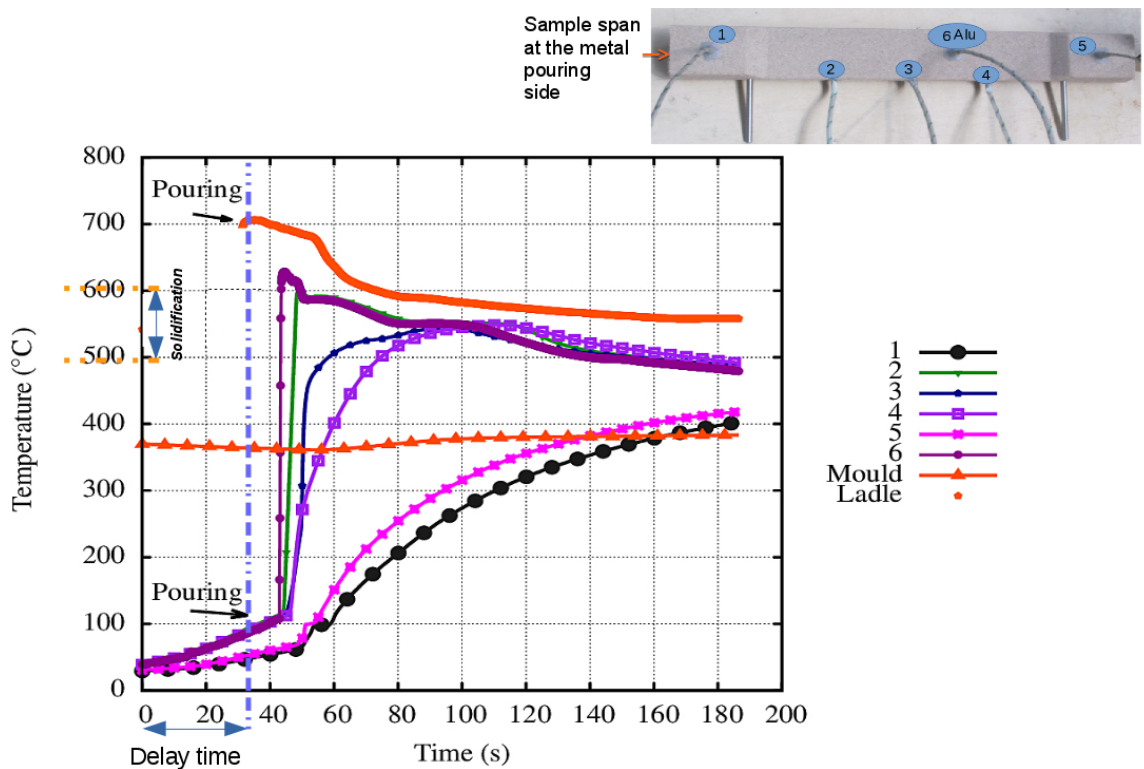
Figure 5.20: Solidification with (a) displacement instrumentation and (b) temperature instrumentation

1 and 5 are used). An evolution upwards of 1 mm, in the metal arrival direction, can be observed only during filling operation. It stabilizes afterwards during solidification.

The results of three tests are presented in Figure 5.26. A variation of the displacement is observed during the filling operation, followed by a stabilization. There is some scatter regarding the steady state, as the asymptotic values vary between 1 and 1.5 mm.

Phase	Instrumentation	Sensors	Aim of the instrumentation	N° trials
A	Temperature	5 thermocouples inside the core + 1 for the aluminum	Measure the core inner temperature and the aluminum temperature at the bottom contact surface	3
B	Temperature + displacement	LASER sensor + 2 thermocouples (at the core massive edges)	Measure the core displacement and compare the core temperature at the edges with phase A	3

Table 5.1: List of the trials made with the “dog bone” specimen



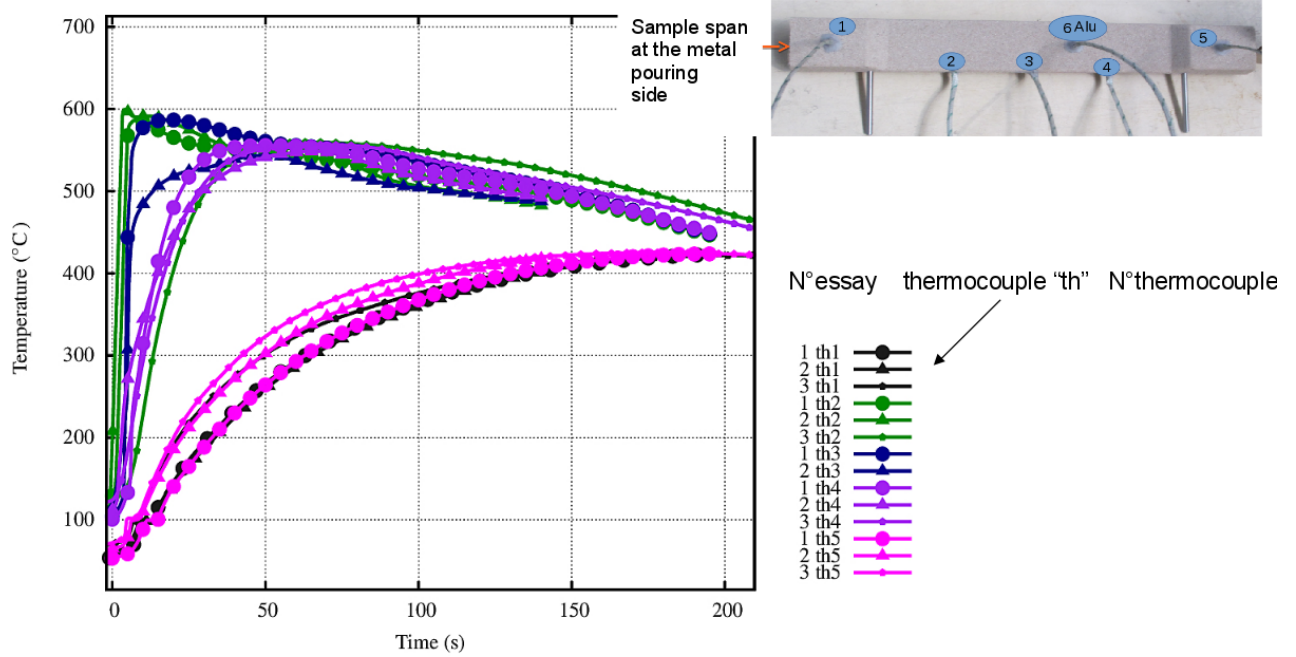
21/09/2016

Figure 5.21: Temperature measurement during casting of a sand core

The third casted part showing a displacement of 1 mm during casting was analyzed after cooling. It was cut at its cross section (see Figure 5.27). The result is in contradiction with the measured value during casting. Indeed, there is a deformation of the core but it is downwards, and the final value is 1.83 mm. It appears to be in the opposite direction with respect to the metal flux.

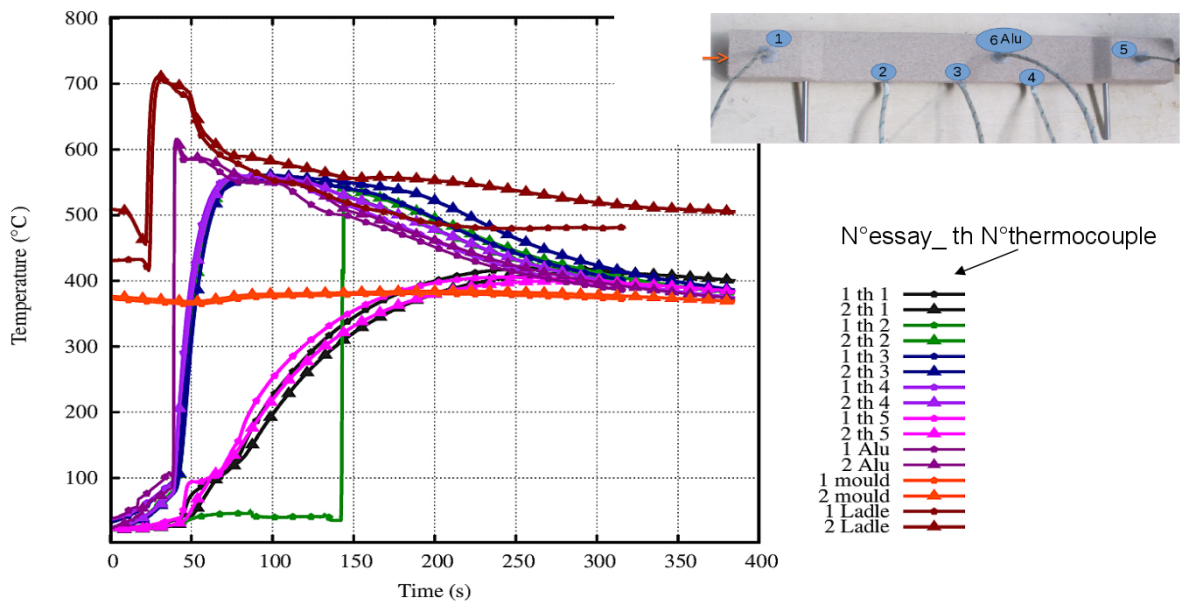
Several hypotheses can be made to explain this point:

- Effect of the measurement tool. The ceramic rod is too light and might be moving with the liquid aluminum;
- Effect of the filling rate. Being manual, it changes from one test to the next;
- The specimen fixation to one side of the mold with the metallic rods may not be



21/09/2016

Figure 5.22: Comparison of the temperature evolution for three different casting operations



25/10/2016

Figure 5.23: Temperature evolution during casting using the second protocol

optimal. The specimen may rotate under the metallo-static pressure;

- Initial state of the sand core at the beginning of casting operation. In fact, as explained earlier, the core fixation inside the mold and the setup of the measurement tool are very delicate. The duration of this stage differs from one specimen to the other and can last up to 40s. One can see in Figure 5.26 that the core temperature in the first test is higher than the other ones because the core spent more time in the mold before being casted.

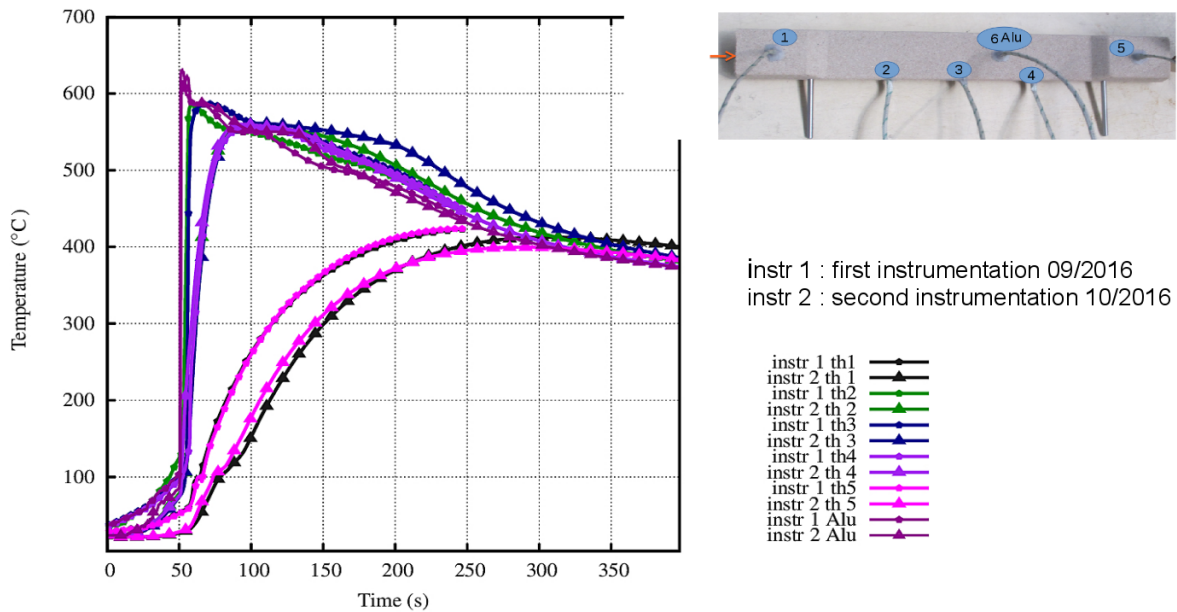


Figure 5.24: Comparison of the temperature evolution between the first and second instrumentation

Tomography analysis

As the results of the experimental measurements of the displacement and the final shape of the casted part gave opposite results, additional investigations are required to make a final assessment regarding the developed protocol. A tomography analysis was then carried out. For this purpose, a part was casted using a “reference” sand core without any instrumentations (neither thermocouples nor ceramic rod). Then, two tomography analyses were performed and compared: this cast without instrumentations and another cast instrumented with a ceramic rod.

- **Tomography analysis of the reference cast without any instrumentations.** Figure 5.28 shows a 2D scan of the specimen. We can see that there is no displacement observed in the core. It is perfectly horizontal. The sand core was also not well centered in the mold as revealed in Figure 5.29. This is probably due to the manual fixation of the specimen inside the core using the metallic rods. The operation is extremely difficult since the mold is too hot and there is not enough time to check if it is well centered, since in case the mold cools down the test has to be interrupted to reheat up to 370 °C.
- **Tomography analysis on a cast instrumented with a ceramic rod during casting.** When measuring the displacement, a metallic rod was put into contact with the sand core at the upper surface, the tomography analysis shows the marks of the metallic rod in Figure 5.30. It reveals that the rod is neither perpendicular to the core nor centered. It is then moving during casting. Moreover, no displacement is observed on the sand core. The deformation observed on the cooled part cross section analysis is then probably due to the specimen rotation and fixation errors.

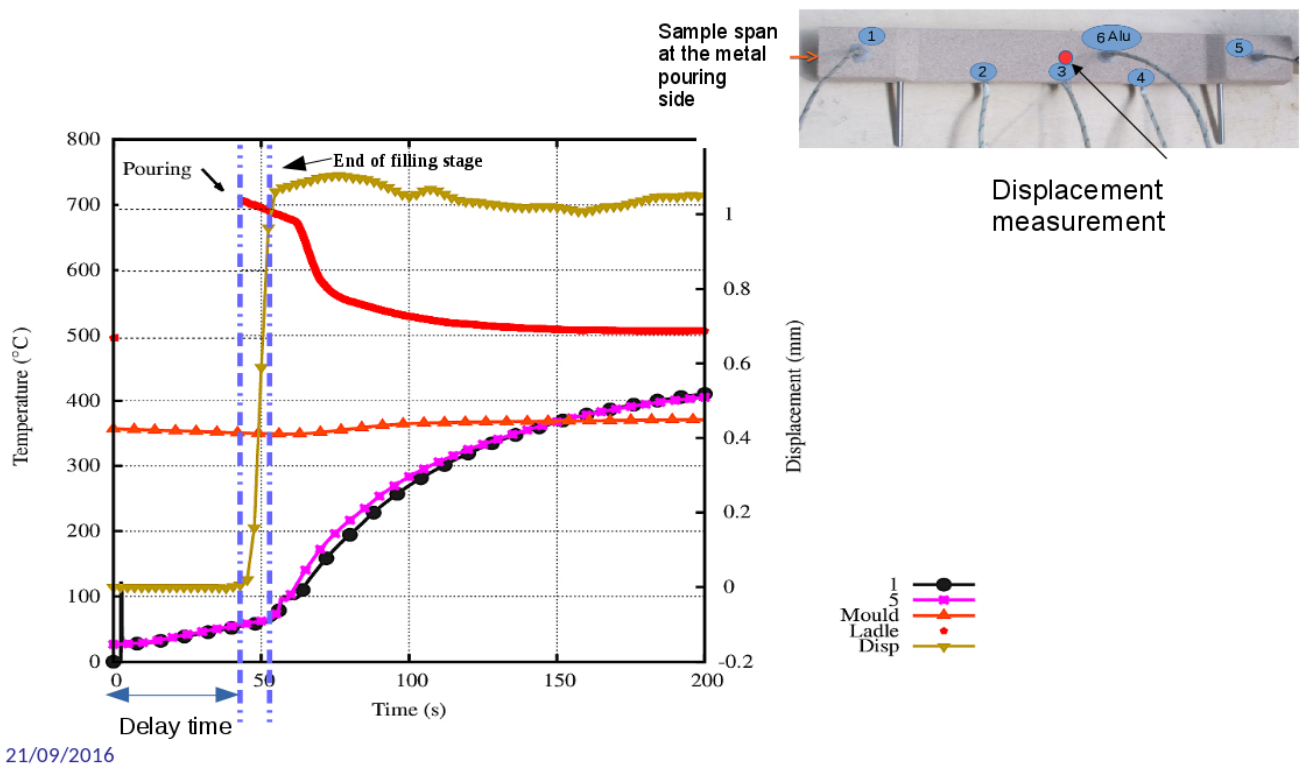


Figure 5.25: Measurement of the displacement and temperature evolution inside the technological specimen

5.3.1.3 Conclusion

At this stage, the efficiency of the experimental protocol is still unclear and several improvements should be done:

- The stage of the core insertion and measurement tools must be optimized;
- The manual filling operation must be optimized to obtain a regular flow rate;
- The design used does not present significant deformation during casting. A thinner design representative of the industrial cores is to be used.

The use of thin thermocouples enabled to measure correctly the core inner temperature. The core temperature was found to be homogeneous at the center. The casting simulation using Magma software revealed that the higher temperature areas lies in the upper and lower central contact surface with the sand core.

The results were not consistent regarding the core deformation measurement. The experiments seemed to show a displacement variation. The examination of the cooled cast cross section showed a deformation in the opposite direction, while the tomography analysis revealed that there is no deformation. We concluded that the measurement setup is not efficient and the experimental protocol is not valid. What we are measuring is mainly artifacts due to the specimen fixation.

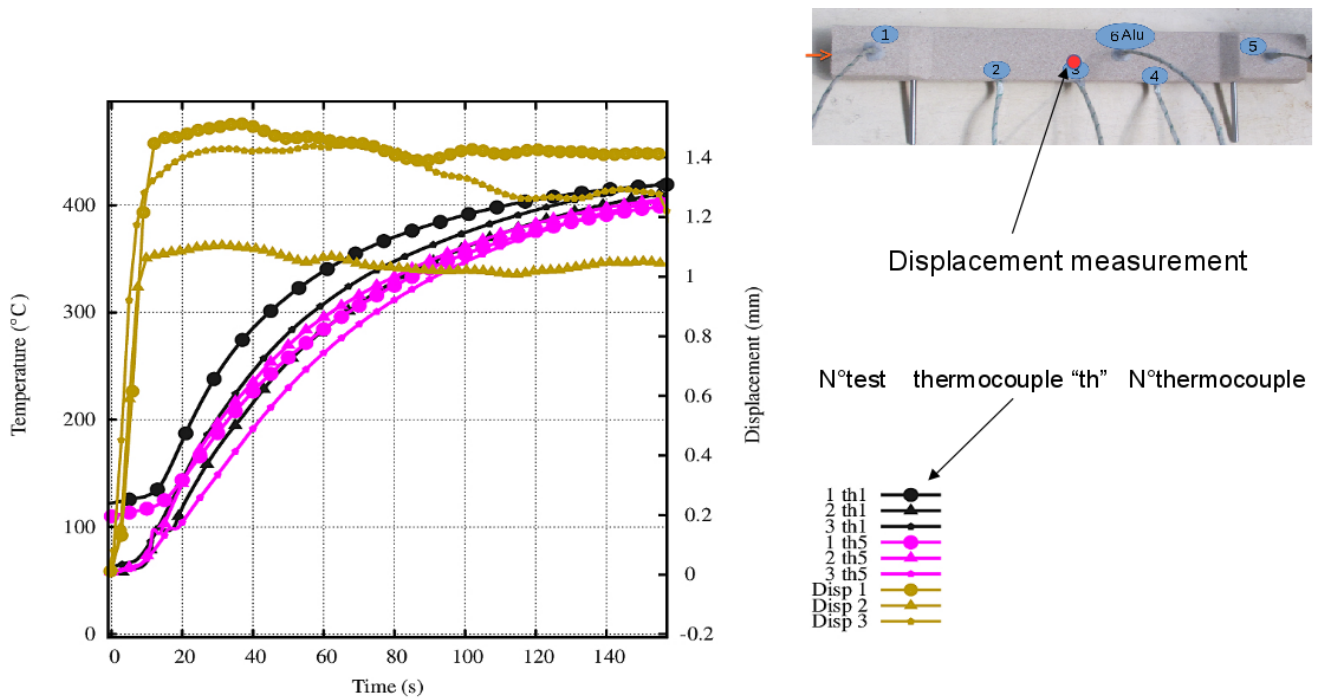


Figure 5.26: Results of the technological part instrumentation with thermocouples and displacement measurement

5.3.2 "CDG" design

The main difference with the "dog bone" design is that the displacement is measured directly on the sand core plug.

The new core was too thin to fix any thermocouples. The core temperature evolution was then not measured. The metal temperature was measured at the contact surface with the core denoted "TH metal bottom in core" shown in Figure 5.31, while three other thermocouples were inserted at different positions in the metal in order to control the risk of early solidification due to the large quantity of aluminum. These results are also necessary for the casting simulation.

The results of the temperature measurement is given in Figure 5.32. There is a small gap of the metal between the different locations of approximately 15 °C and between the feeder and the top of the sand core. So there is no risk of early solidification which may inhibit the core deformation. However, the metal temperature measured at the core bottom contact surface with a thermocouple placed through the sand core denoted "TH metal bottom in core" differs from the measure made with the thermocouple placed directly in the cast denoted "TH metal bottom in cast". The difference is considered to come from a shift in the placement of the thermocouple inside the sand core.

The laser beam is focused on the sand core plug directly. Ten tests were performed but only two were valid. In the rest of the experiments, the core plug broke and was ejected from the mold. In Figure 5.33 we present the evolution of the displacement in these two tests. There is an offset with respect to the beginning of the filling stage. Before filling, there is a variation of 0.7 mm which is probably an artifact due to the thermal radiation. During filling, there is a upwards displacement of 7 mm approximately in both tests. At

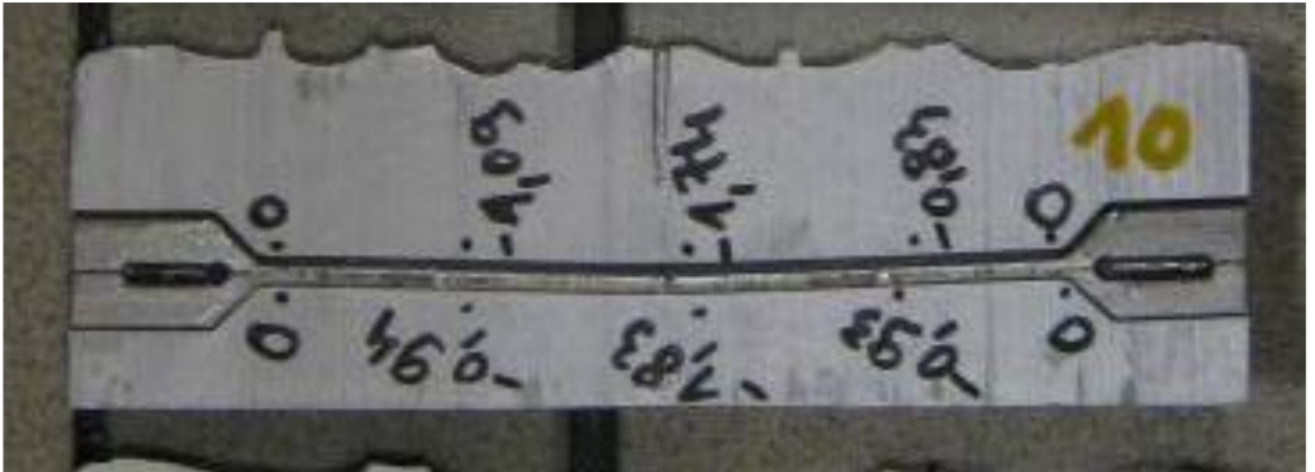
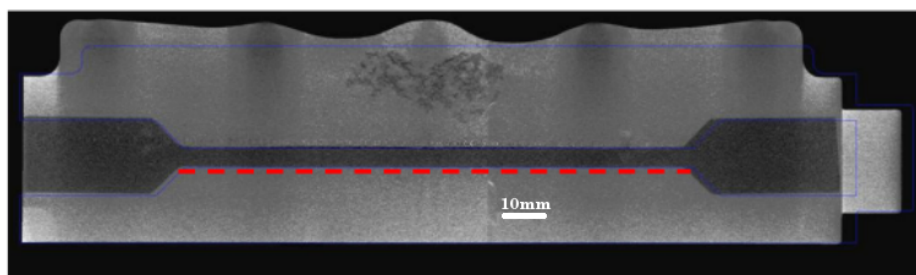
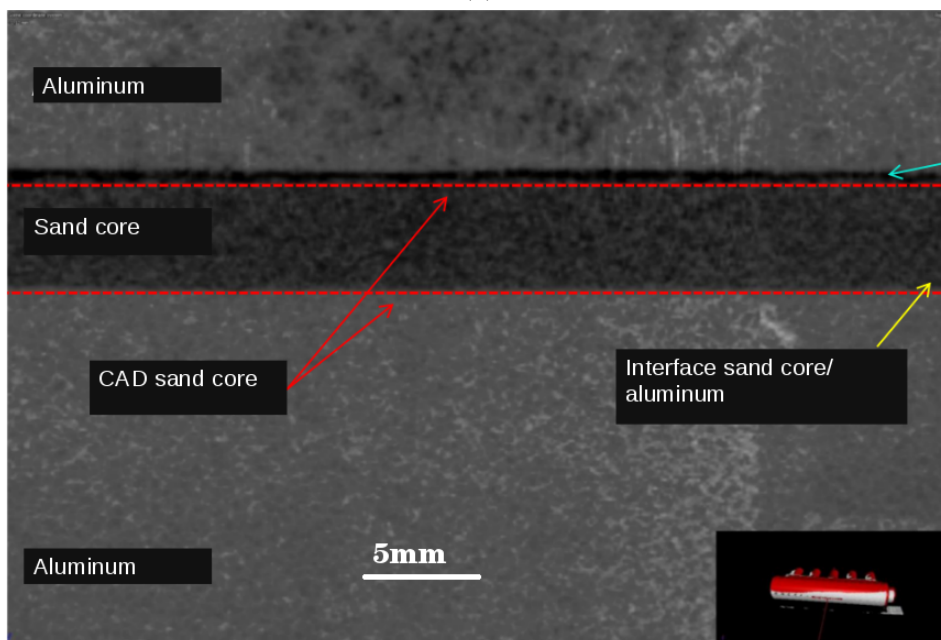


Figure 5.27: Cross section of the cast



(a)



(b)

Figure 5.28: Tomography analysis of a “dog bone” core in (a) and zoom on the central area in (b)

the end of the filling operation, the metal temperature is 600 °C and solidification starts. The deformation process stops.

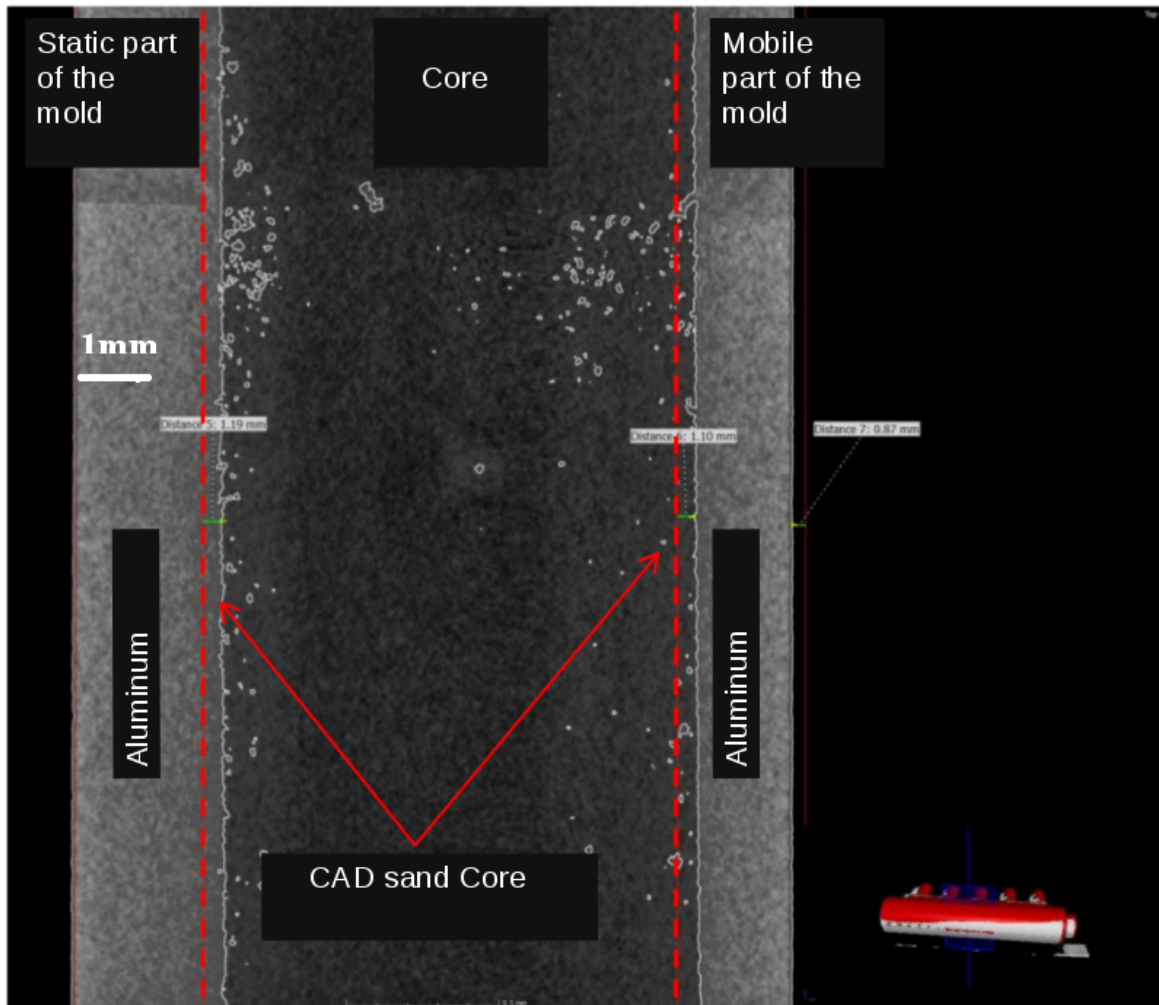


Figure 5.29: Tomography analysis of cast part showing an off centre core

A specimen was analyzed using tomography in order to validate the measured displacement. There is an upwards displacement as shown in Figure 5.34. The maximum of the deflection is located at the center where the laser beam is focused. However, the maximum value is 4.8 mm while the laser provides 7 mm. Furthermore, the specimen seems to be broken at the edges. It is difficult to say if this happened during cast ejection or during casting operation, causing a measurement error.

Several additional tests were performed to measure the displacement. This was done in order to characterize the scatter. The results of six tests are presented in Figure 5.35. In each case, the time needed for the filling operation varies between 7.5 and 9 s. There is a good similarity in the curves shape. However, the responses obtained with the different measures go from 4 to 8 mm at the end of the filling stage. An average final value of 6 mm is considered.

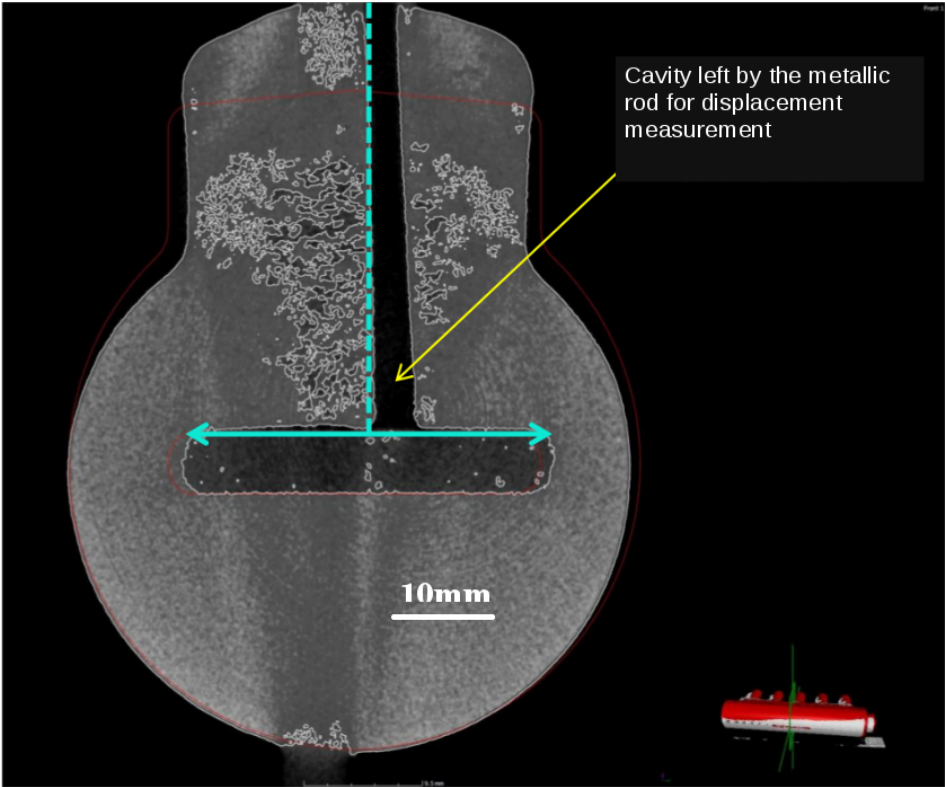
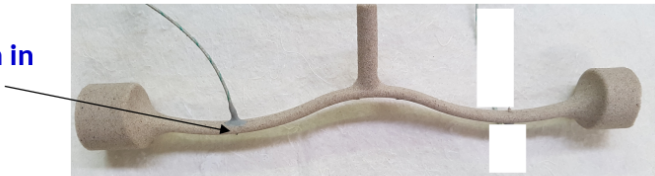


Figure 5.30: Tomography analysis of the “dog bone” core showing the marks of the metallic rod

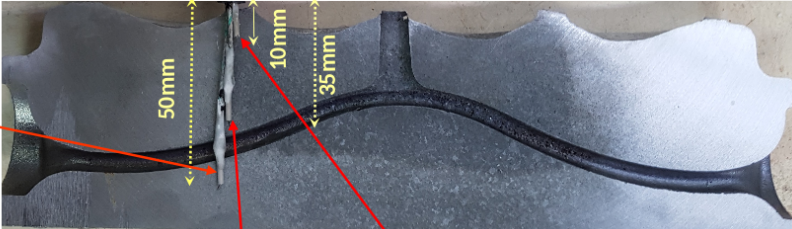
Core “CDG”

TH metal bottom in core



Cavity of core “CDG”

TH metal bottom in cast



TH metal up in cast

TH metal feeder in cast

29/09/2017

Figure 5.31: Instrumentation of the “CDG” specimen with thermocouples

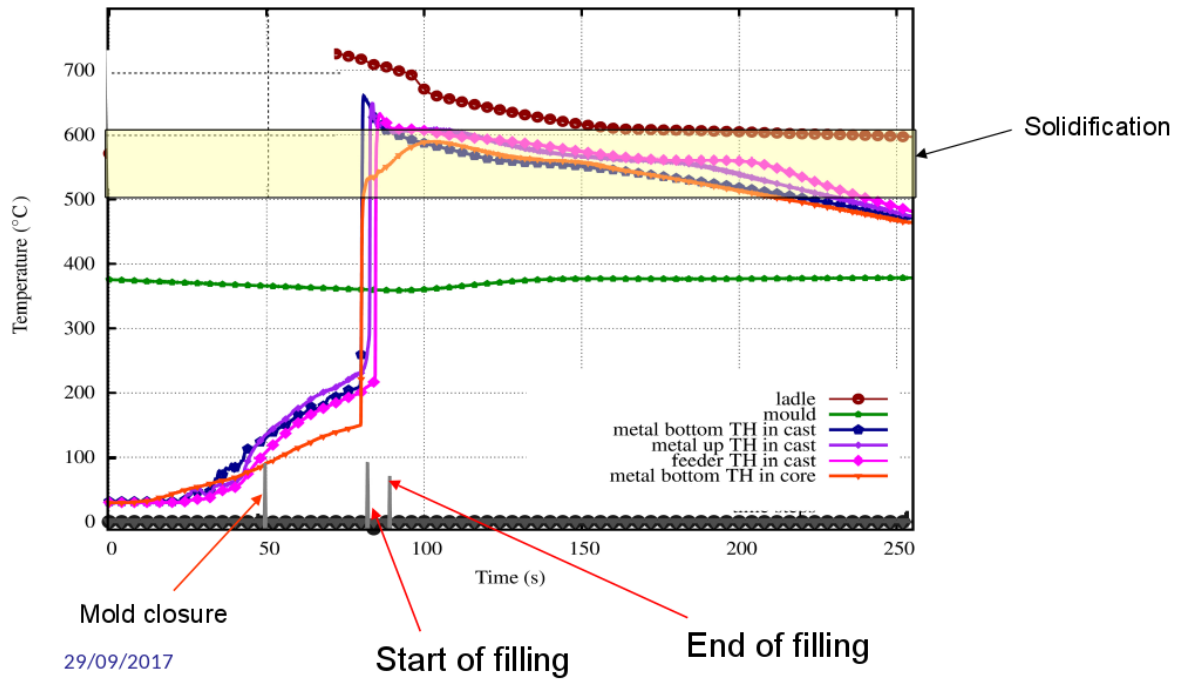


Figure 5.32: Temperature evolution in the “CDG” specimen

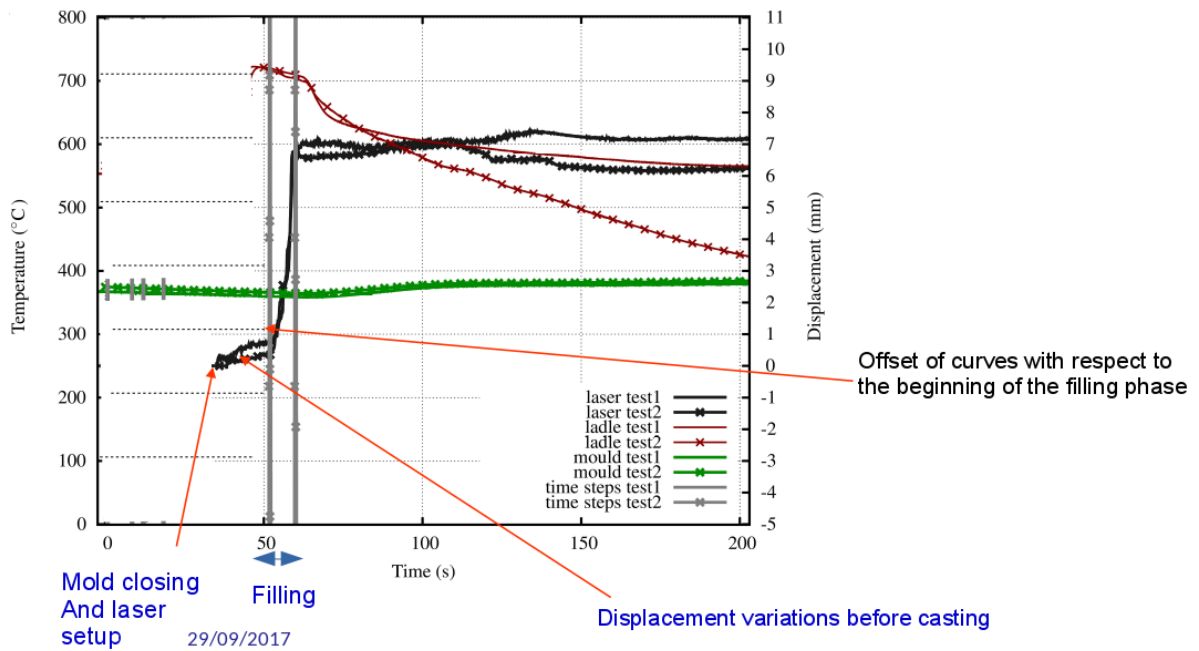


Figure 5.33: Evolution of the displacement for the “CDG” specimen during casting.

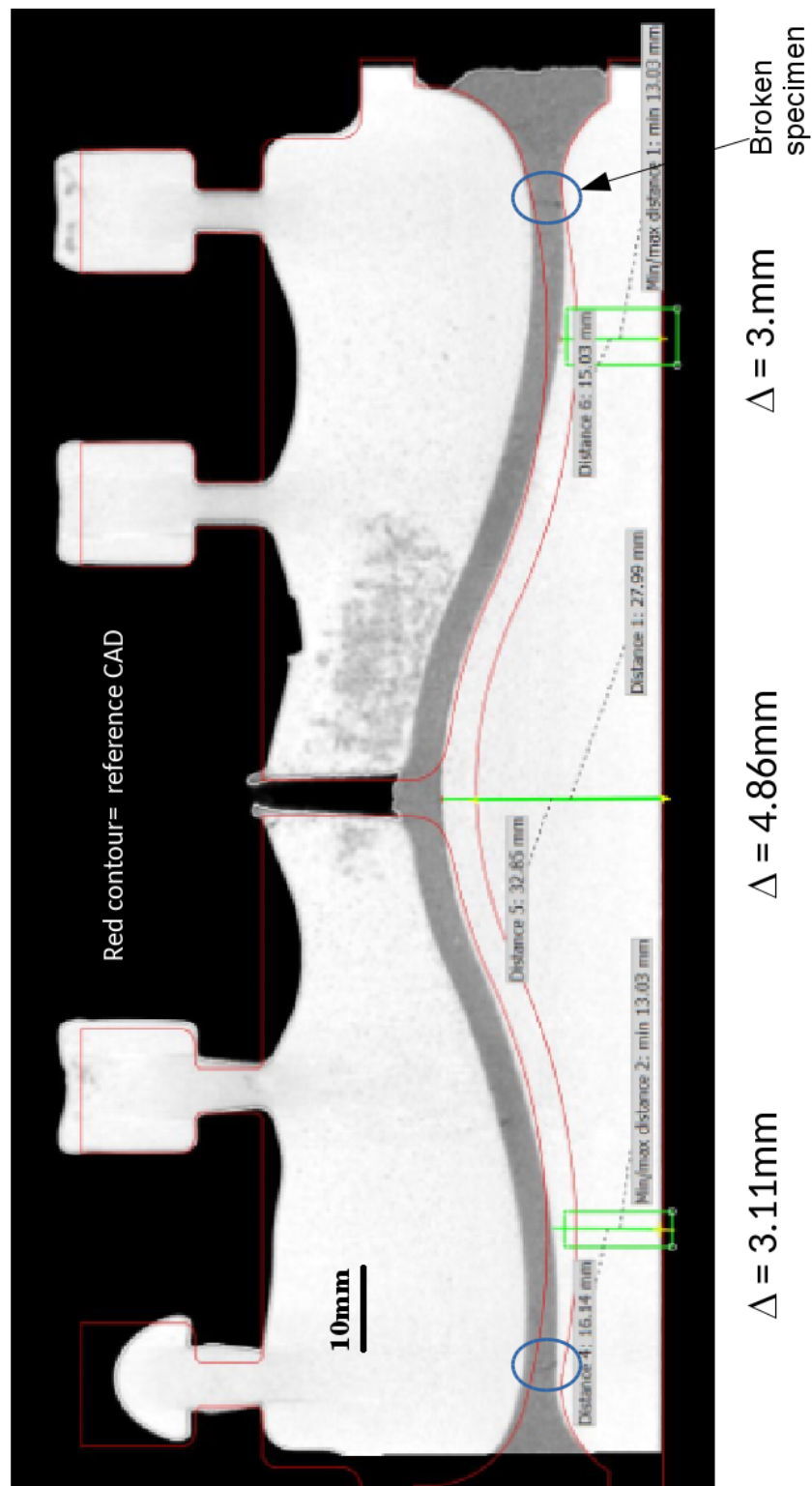


Figure 5.34: Tomography analysis of “CDG” core used for displacement measurement.

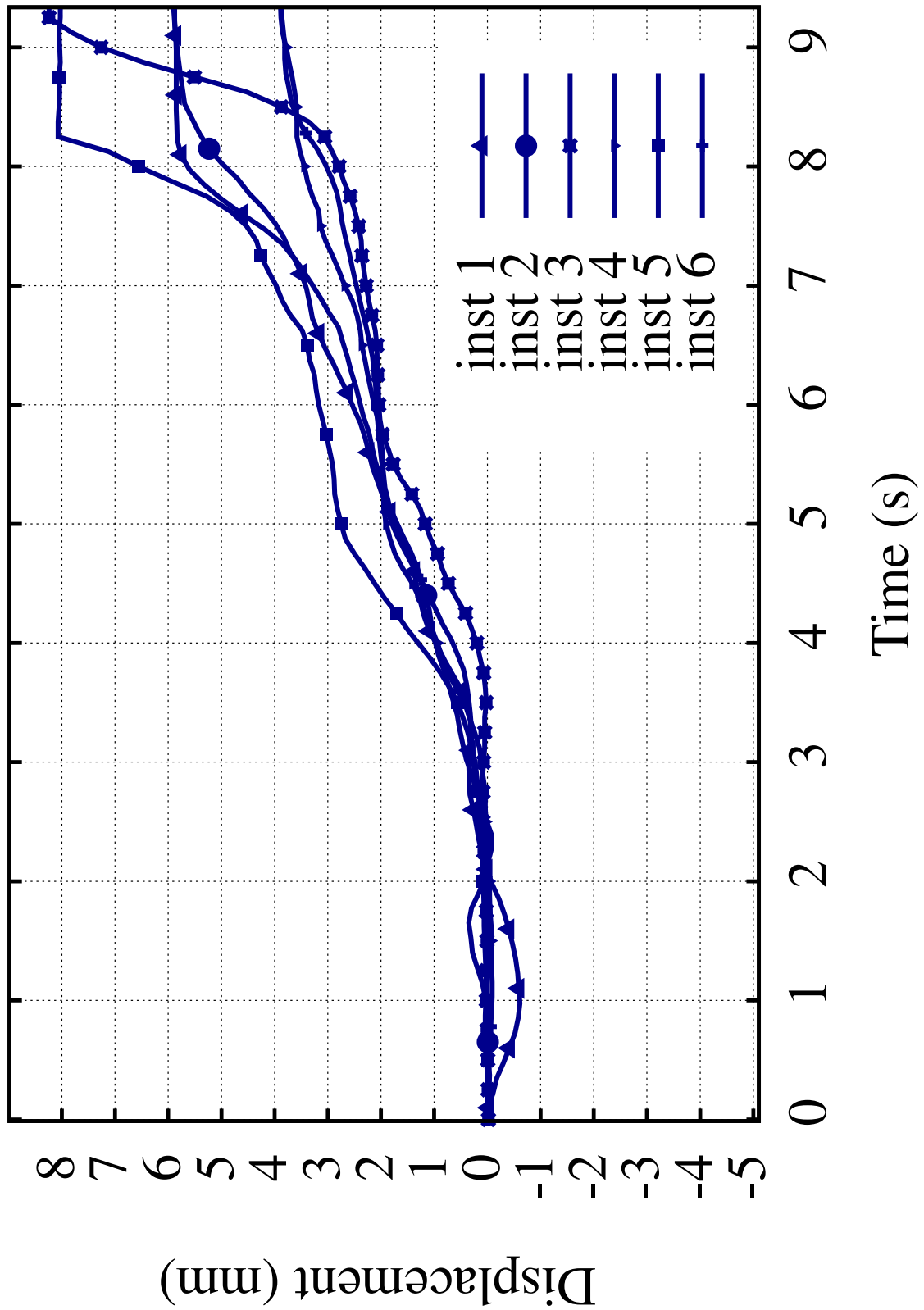


Figure 5.35: Displacement measurement during “CDG” sand core casting.

Conclusion. In this section, we developed different designs and testing protocols for the deformation and temperature measurements. The experimental protocol still needs several improvements, mainly the filling operation which is manual and the timing of the different steps.

The experimental measurements of the “dog bone” design were not consistent with the post analysis made on the cast using tomography. In fact, the 2D scans revealed that the sand core did not present any deformation. The measures were skewed by different factors that produce artifacts (specimen fixation, ceramic rod movement...). On the other hand the temperature measurement was consistent with the thin thermocouples. From the results, the sand core was found to reach high temperatures with high heating rates which are dependent on the specimen thickness.

The “CDG” design was created to obtain a deformation of this specimen and to be able to directly measure the displacement during casting. However, the handling of the specimens was extremely difficult. Many specimen broke down during casting. The displacement measurements are still not reproducible (difference in the initial specimen state, manual filling process...), but the overall evolutions are comparable.

5.4 Numerical validation of the model on “CDG” design

In our study, we are working on the simulation of the sand core deformation during casting. The measured displacement during casting of the technological specimen revealed that there is an evolution of the deformation only during filling operation. It takes place with temperature increase and the applied metallo-static pressure. The final objective is to obtain a reliable numerical tool that can be industrially used for the modeling of the foundry process.

5.4.1 Mesh of the specimen

The “CDG” specimen is used for the validation of our approach. The work consists in modeling the behavior of the technological specimen during the filling operation. The computed displacement evolution is to be compared to the experimental values (presented previously in Figure 5.35).

The technological specimen was meshed using linear C3D4 tetrahedral volumetric elements as presented in Figure 5.36. It includes 65425 elements.

5.4.2 Numerical simulation

Initial boundary conditions. The initial boundary conditions correspond to the sand core state just before the filling operation. They are summarized in Figure 5.37:

- The specimen is fixed at its massive edges between the mold screeds;
- At the core plug which passes through the hot mold aperture (there is a small gap of about 0.5 mm) and the contact areas between the mold and the core (fixed edges), there is heat exchange between the sand core and the metallic steel mold. The core temperature reaches 360 °C. Elsewhere, the sand core initial temperature is approximately equal to room temperature.

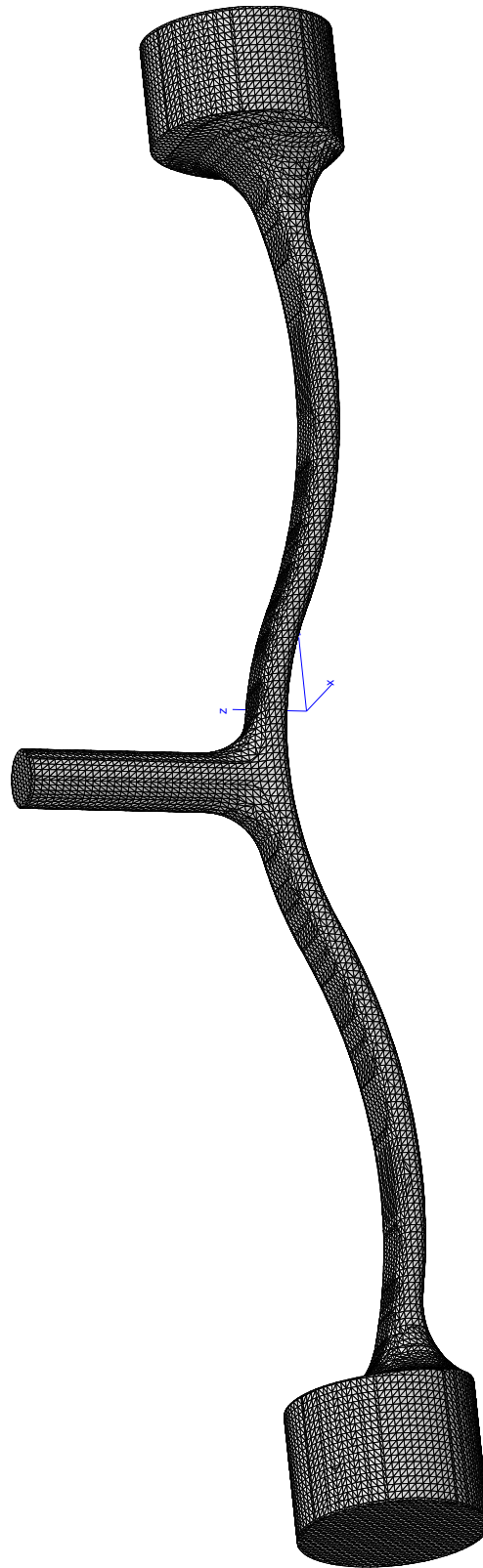


Figure 5.36: Geometry and mesh of the “CDG” sand core.

Aluminium filling simulation. The aluminum filling operation is simulated by Montupet using the Magma software . The considered filling stage duration is equal to 7.5 s.

¹<https://www.magma-soft.de/en/>

An equivalent pressure of 7.2 mb is considered. The heat exchange coefficient between the aluminum and the sand core is a constant equal to 200 (W/m².K). The other used thermophysical properties for the computations available in Magma software were detailed in paragraph 1.1 and reminded in Figure 5.38 and Table 5.2. The temperature field is then extracted in the sand core at each node and time step.

Table 5.2: Standard core database in MAGMA

Parameter	Value
Young modulus	1500 MPa
Yield stress	15 MPa
Poisson ratio	0.3
Thermal expansion coefficient	10 ⁻⁶ °C ⁻¹
Tensile strength	3 MPa
Hardening coefficient (non linear)	10
Permeability	50 cm ³ /min

Sand core thermoelastic behavior modeling. The numerical simulation of the sand core during casting was made using Zset finite elements software. As a first step, the material behavior is assumed to be elastic. This phase is needed to check the global response of the structure. The calculation involving the thermomechanical model, which is the final goal of our work, is not included in the manuscript due to time constraint. Its analysis will be in the perspectives of the thesis. For the moment, we proceeded in two stages: a thermoelastic analysis and then the same analysis with the effect of the pressure due to aluminum:

1. **Thermoelastic analysis.** The temperature fields obtained from the Magma casting simulation are used as input in our computation. The evolution of the Young modulus and expansion coefficient as a function of temperature are also set as inputs (these data were detailed in paragraph 3.7.1).
2. **Thermoelastic analysis considering aluminum pressure.** The same thermal analysis is made while considering the equivalent applied pressure by the aluminum as a function of the position of the sand core in the mold denoted z . It is defined by: $P = \rho * g * H(z)$, where ρ is the liquid aluminum density, g is the acceleration due to gravity and $H(z)$ is the so-called “metal drop height”. This pressure is defined on the core surface exposed to the metal inside the mold (presented in blue in Figure 5.37).

5.4.3 Results and discussion

The computation of the displacement is compared to the experimental results of the “CDG” instrumentation. For this, the displacement values in the simulations will be extracted at the top center surface of the “CDG” technological specimen (presented in Figure 5.39) since this is the point where the displacement is measured.

The results of the numerical analyses are reported in Figure 5.40. It can be observed that the computed displacement curve is in good agreement with experiment. There is first a small increase in the displacement, followed by a decrease and again a strong increase up to a final value of 6 mm. The final computed displacement field is shown in Figure 5.41. The decrease corresponds to the contraction of the sand core due to thermal degradation. The fact that the thermoelastic behavior gives good results demonstrates that the effect of thermal expansion is predominant in the decomposition of the total strain. It is satisfactory from an industrial point of view to observe that a good quality prediction can be made with a simple elastic calculation. On the other hand, the pressure distribution is not uniform along the sand core. The application of the full model using the constitutive equations proposed in our study and the computed pressure field is still of great interest.

5.5 Summary

This chapter presents the instrumentation of two technological specimens and the computations performed so far. The objective is to measure the temperature and displacement of the sand core during casting. By applying a loading close to industrial conditions, the aim is to reveal effects that do not appear on laboratory specimens.

In the first section, a testing protocol was developed with a “dog bone” specimen. The values of the displacement measured during the test were not consistent with subsequent observations by tomography, while the temperature measurements with thin thermocouples were satisfactory, and in good agreement with the results of the casting simulations using Magma software.

A second design was created denoted “CDG” which is thinner and more complex in order to obtain a significant deformation. It presents a plug which enables to directly measure the core displacement during casting. The design extraction and handling were quite complex. It was a challenge to correctly insert the specimen inside the mold without creating a crack. The obtained displacement values presented some scatter. However the overall curves aspects were found to be similar. This specimen design was selected for the numerical analysis. The new developed protocol is an original contribution to the technological field.

At the same time, the experimental instrumentation protocol still needs to be improved mainly regarding the cores. In fact, they are very thin and they stick to the corebox. Extracting the cores already weakens them. The manual filling operation needs to be automated to ensure a constant flow rate.

In the second section, the computations carried out on the “CDG” specimen using Zset software were detailed. A thermoelastic behavior was considered. The sand core thermoelastic properties were introduced as a function of temperature. The temperature map was extracted at each node from the Magma simulation. An analysis including the effect of the applied metal pressure was performed as well. The results of the displacement computation were in good agreement with the experiments. This revealed that the thermal part has a predominant effect. However a full analysis accounting for the real thermomechanical behavior of the sand core needs to be performed.

5.6 Résumé en français

Ce chapitre présente le design, l'instrumentation d'éprouvette technologiques et les calculs effectués jusqu'à présent. L'objectif de l'instrumentation est de mesurer la température et le déplacement du noyau de sable lors de la coulée. Cela peut révéler des mécanismes et des aspects complémentaires à ceux étudiés lors des tests sur les éprouvettes de laboratoire.

Dans la première section, un protocole de test a été développé en utilisant une éprouvette en «os de chien». Les valeurs de déplacement mesurées pendant l'essai se sont avérées incohérentes avec les observations ultérieures par tomographie, alors que les mesures de température avec des thermocouples minces sont satisfaisantes, et en accord avec les résultats des simulations de moulage utilisant le logiciel Magma. Un deuxième design a été créé, noté «CDG», qui est plus mince et plus complexe afin d'obtenir une déformation significative. Il présente une extension qui permet de mesurer directement le déplacement du noyau lors de la coulée. L'extraction et la manipulation de l'éprouvette sont assez complexes. Il est difficile d'insérer correctement l'échantillon dans le moule sans créer de fissure. Les valeurs de déplacement obtenues présentent de la dispersion. Cependant, les courbes globales ont été jugées comparables. C'est ce design qui a été retenu pour effectuer la modélisation numérique. Le nouveau protocole développé est une contribution originale dans le domaine technologique. En même temps, le protocole d'instrumentation expérimentale doit encore être amélioré, principalement en ce qui concerne la fabrication des noyaux utilisés. En fait, ils sont tellement minces et collent à la boîte à noyaux, si bien que le simple fait d'extraire les noyaux les affaiblit déjà. L'opération de remplissage manuel doit être automatisée pour assurer un flux constant.

Dans la deuxième section, les calculs effectués sur l'échantillon " CDG " à l'aide du logiciel Zset ont été détaillés. Un comportement thermoélastique a été utilisé, avec des propriétés du noyau de sable dépendant de la température. La carte de température a été extraite à chaque nœud du maillage de la simulation Magma. Une analyse comprenant l'effet de la pression appliquée sur le métal a également été effectuée. Les résultats du calcul du déplacement sont en bon accord avec les expériences. Ceci révèle que la partie thermique a un effet prédominant. Cependant, une analyse complète tenant compte du comportement thermomécanique réel du noyau de sable doit encore être effectuée.

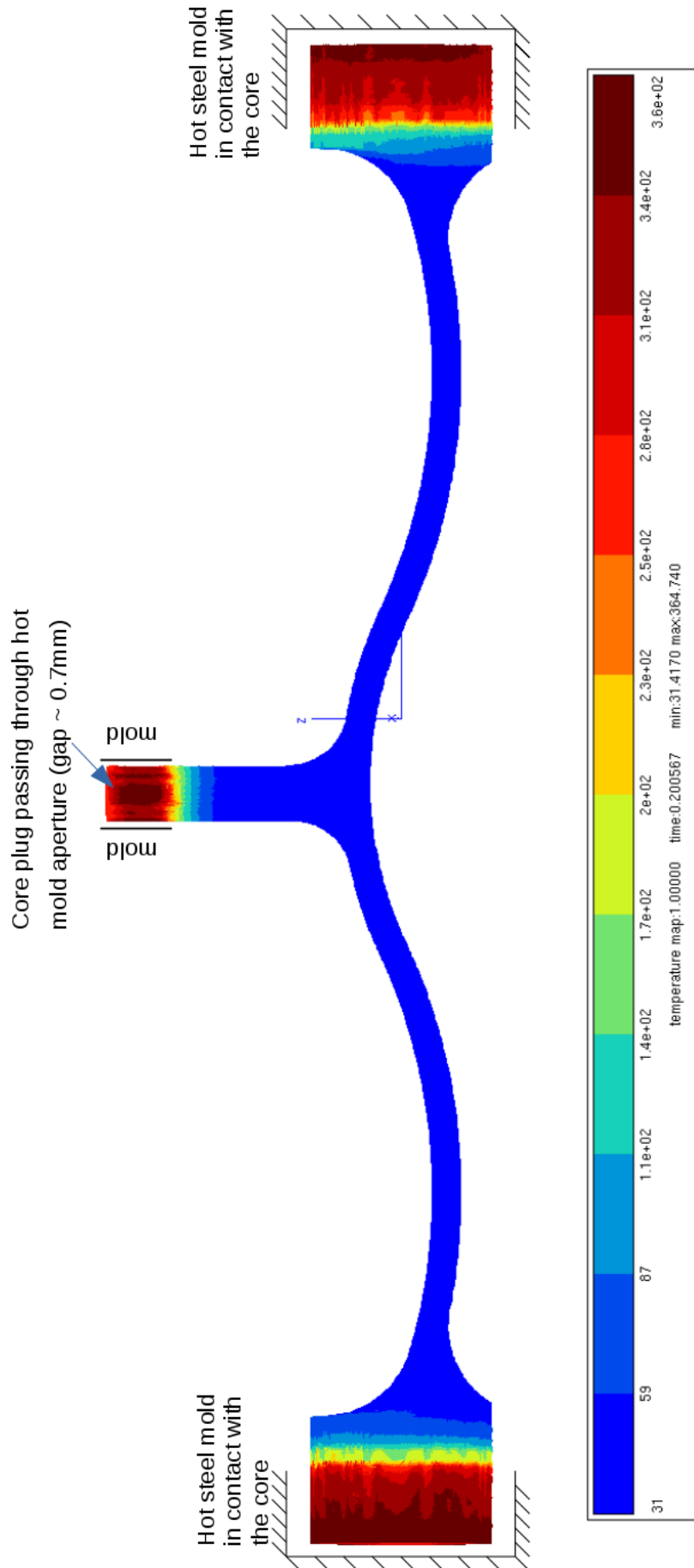


Figure 5.37: Initial temperature and boundary conditions in “CDG” technological specimen.

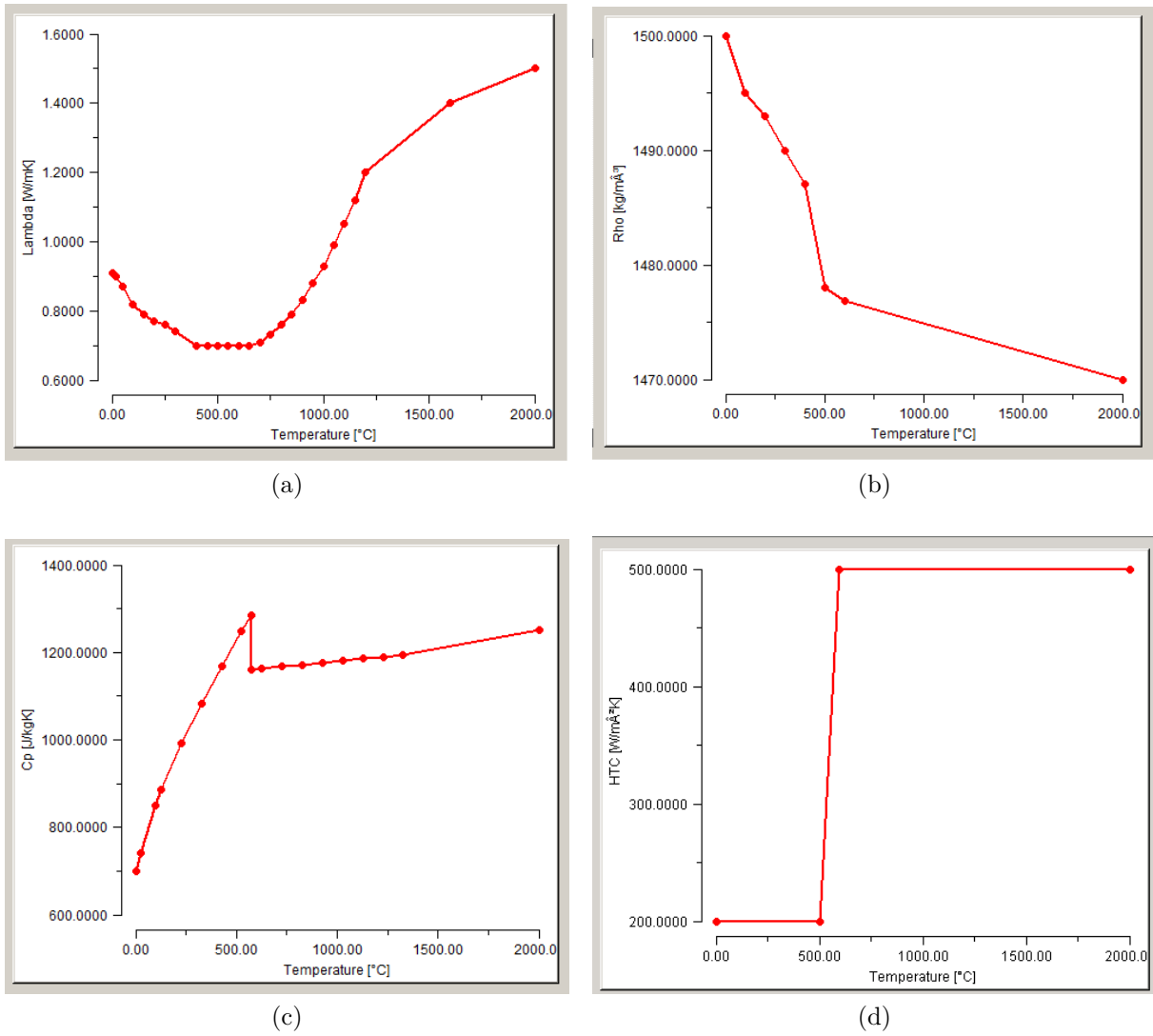


Figure 5.38: Evolution with temperature of (a) thermal conductivity (b) density (c) specific heat and (d) heat exchange coefficient with aluminum ¹.

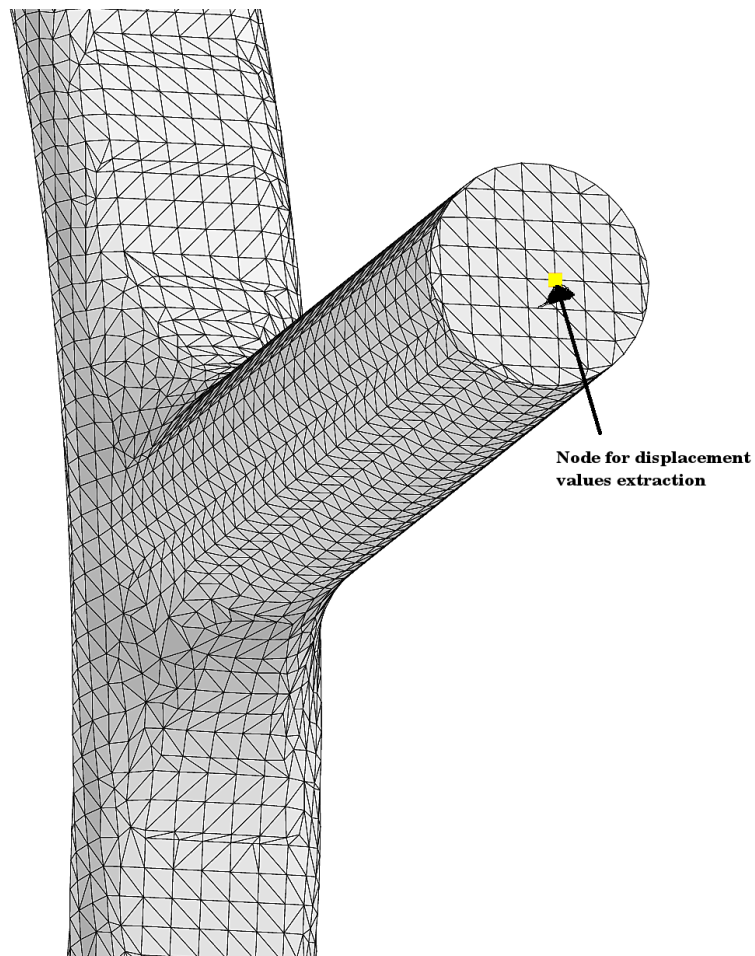


Figure 5.39: Location of the point used on “CDG” sand core specimen for the validation of the displacement.

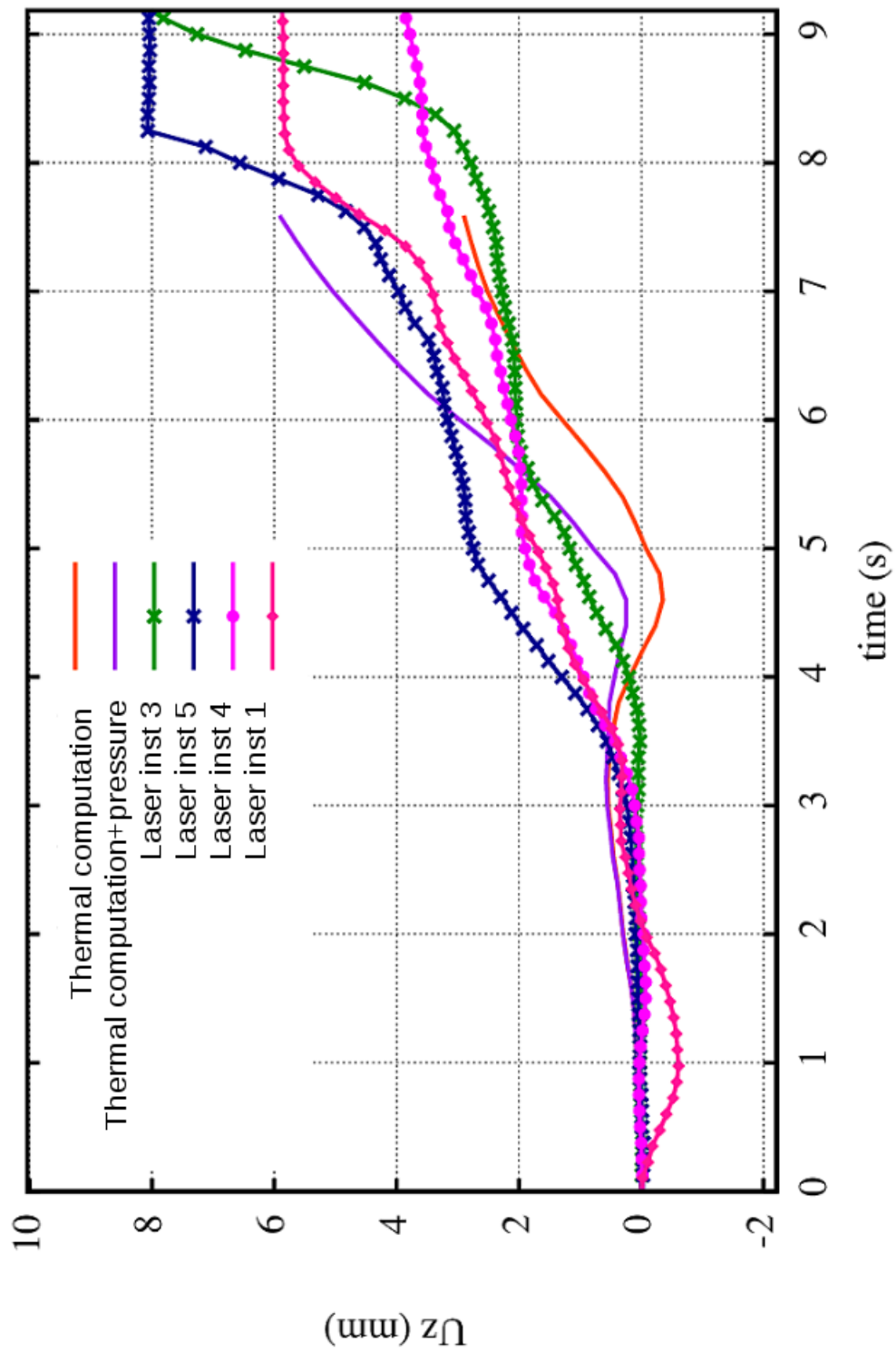


Figure 5.40: Computation of the “CDG” sand core deformation during casting.

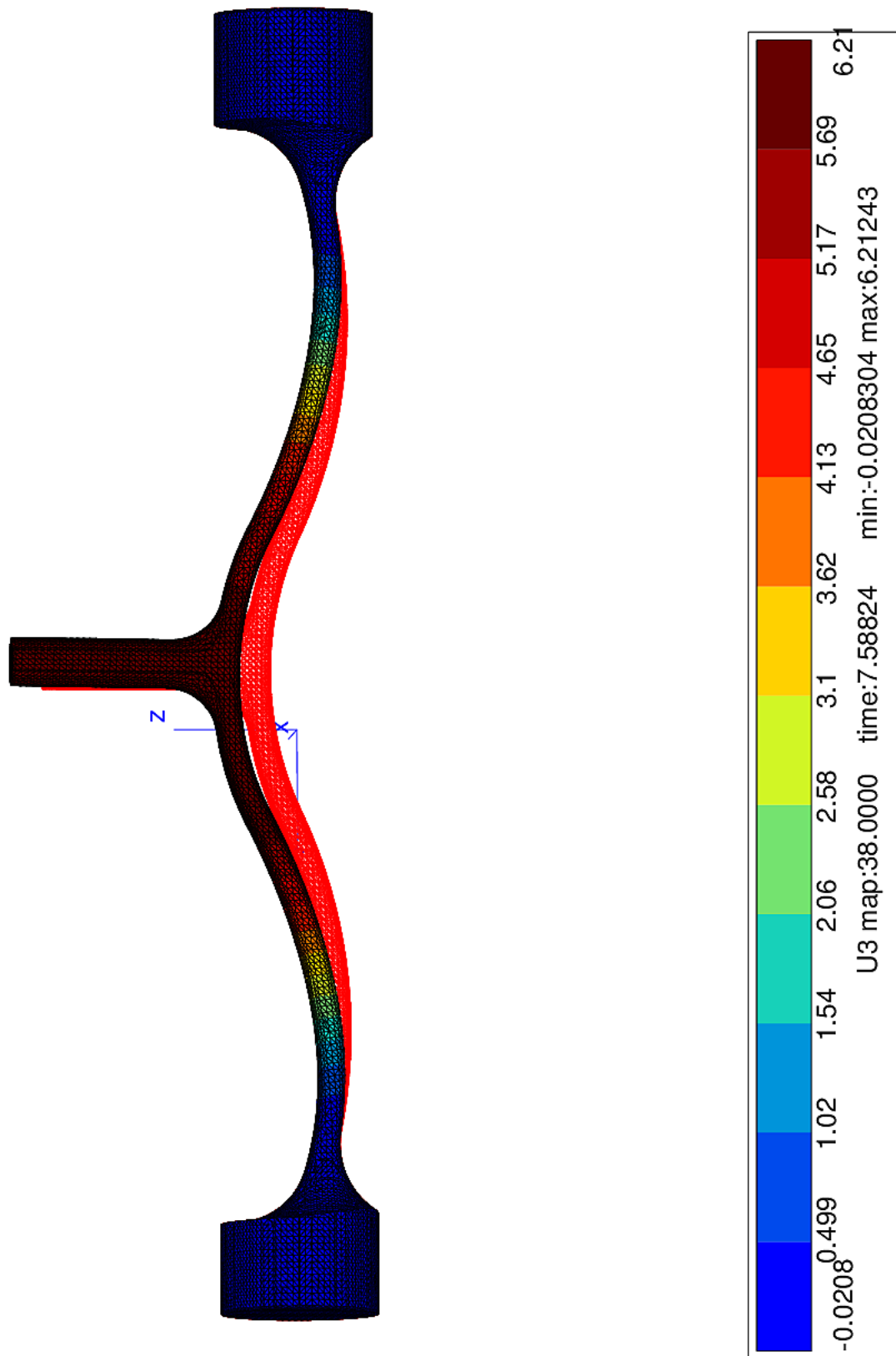


Figure 5.41: Comparison of the final computed deformation of “CDG” sand core and initial core geometry.

Chapter 6

Conclusion and perspectives

Contents

6.1	Conclusion	172
6.2	Perspectives	173

6.1 Conclusion

This study is a part of a program aiming at the optimization of the manufacturing process of the aluminum cylinder heads. In particular we are dealing with the industrial issue related to the deformation of foundry sand cores during casting which causes defects in the final part. The problem becomes crucial, as sand core designs introduce thinner and thinner walls, so the risk of deformation is increasing. But for the time being commercial softwares contain rather poor databases and the sand core is considered as non deformable in the classical calculations.

The main objective was then to propose a new approach for both experimental characterization and numerical modeling. As summarized below, three main tasks have been completed:

1. A large program of thermomechanical and thermophysical tests was carried out with different loading configurations on both the sand core and bonding resin. The main deformation mechanisms were identified.
2. A phenomenological model of sand core behavior was developed and implemented in the finite elements software Zset. The model parameters were identified.
3. A technological specimen design was created for the model validation. An experimental protocol was set up to measure displacement and temperature on sand cores. The final numerical validation on the technological specimen was not fully accomplished due to time constraints.

Experimental study. The strategy followed was to decouple the study on sand core and bonding resin then in a second step to identify the deformation mechanisms of the mixture. Four-point bending creep tests were mainly used on the sand core. The deformation of the sand core was found to be directly controlled by the behavior of the binding resin: once the thermal degradation process is activated, irreversible transformations driven by the decomposition kinetics take place, inducing irreversible deformation in the sand core. The viscoplastic character of resin behavior was also highlighted by specific mechanical tests.

Sand core behavior is sensitive to hydrostatic stress. In absence of triaxial tests, an original procedure was used to characterize the asymmetric mechanical response in tension/compression in the 20–300 °C temperature range. As for the resin, it is not possible to characterize its mechanical behavior above 200 °C, while the tests on technological specimens revealed that the core deformation takes place essentially during the first filling seconds when the temperature reaches 350/400 °C in the sand core. As a consequence, it was decided to build macroscopic constitutive equations for the sand core. Their formulation is directly supported by the knowledge of the local mechanisms and our findings about deformation governing phenomena.

Numerical model. An original model of sand core behavior has been developed and implemented. The fact of using a macroscopic phenomenological approach makes it appropriate for use in an industrial context on full size components. The thermal degradation process, the evolution of the thermoelastic and the inelastic parts with temperature are taken into account. The inelastic strain part results from two contributions, the first

coming from resin thermal decomposition, the second from classical viscoplasticity. The model is valid over a wide temperature range, thanks to the fact that its parameters depend on temperature. The model parameters were identified and the bending tests were simulated. There is a good agreement between the simulations and the tests. Unfortunately, it was not possible to carry out triaxial tests, so the good relevance of the model to this type of load case remains unknown. However, the fact that the model is physically based may give reason for optimism about this open challenge.

Instrumentation and validation on the technological specimen. An original technological specimen was created in the framework of the study. The tests were carried out at the industrial plant. The instrumentation protocol was set up to measure directly the sand core displacement and the temperature during casting. We have faced major difficulties due to the dimensions of the specimen and the presence of very thin walls, which make it too weak to be handled manually. The specimen preparation (extraction from the box, insertion inside the core, the time spent inside the mold before casting) was critical and may induce defects in the material prior to casting. The filling operation was also manual and a source of scatter in the results. It is clear that the test procedure can be further improved in order to obtain more reproducible results.

Finite element computations were performed considering a thermoelastic behavior (evolution of the thermoelastic properties with temperature and the effect of thermal degradation). The temperature field comes from a simulation of the filling process by means of the Magma software. The effect of the metallo-static pressure was negligible. The results revealed that the thermal part is probably predominant in the deformation process. After this first step, it remains interesting to improve the displacement measurement and to perform a numerical simulation with the full constitutive model in order to refine the understanding of the process.

6.2 Perspectives

Many topics are of prime interest for future studies:

1. **Experimental work.** It is necessary to perform multi-axial mechanical tests on sand cores to better calibrate the implemented model for a better precision and representation of the material behavior and to carry out tests at temperatures above 300 °C. In this respect, resin binder tests raise specific problems.
2. **Numerical model.** In the present study, the constitutive equations are purely phenomenological. Improvements might be made to better calibrate the model with additional tests.
3. **Validation.** The improvement of the displacement measurement and of the filling operations during casting is needed to secure the information coming from the tests on technological specimens. This would allow a complete numerical simulation to be carried out, including the interactions between the cast and the core and the full model developed in our study. This would open up the way for systematic use at the industrial design stage.

References

- [Ala07] W. Alan and S. John. Combined deformation-and temperature-induced scission in a rubber cylinder in torsion. *International Journal of Non-Linear Mechanics* 42.2 (2007), pp. 330–335.
- [Ala08] W. Alan and S. John. Influence of thermally induced scission and crosslinking on the post-scission inflation of circular elastomeric membranes. *International Journal of Engineering Science* 46.8 (2008), pp. 758–774.
- [Aro86] M. Aronhime, X Peng, J. Gillham, and R. Small. Effect of time-temperature path of cure on the water absorption of high Tg epoxy resins. *Journal of applied polymer science* 32.2 (1986), pp. 3589–3626.
- [Arr12] M. Arroyo, M. Ciantia, R. Castellanza, A. Gens, and R. Nova. Simulation of cement-improved clay structures with a bonded elasto-plastic model: A practical approach. *Computers and Geotechnics* 45 (2012), pp. 140–150.
- [AS96] R. Ami Saada, G. Bonnet, and D. Bouvard. Thermomechanical behavior of casting sands: experiments and elastoplastic modeling. *Int. J. of Plasticity* 12 (1996), pp. 273–294.
- [Azz95] F. Azzouz. Modélisation du comportement thermo-hydro-mécanique d'un sable de fonderie. PhD thesis. Univ. Paris VI, 1995.
- [Bar04] B. Barlas. Etude du comportement et de l'endommagement en fatigue d'alliages d'aluminium de fonderie. PhD thesis. École Nationale Supérieure des Mines de Paris, 2004.
- [Bar17] H. Bargaoui, F. Azzouz, D. Thibault, and G Cailletaud. Thermomechanical behavior of resin bonded foundry sand cores during casting. *Journal of Materials Processing Technology* 246 (2017), pp. 30–41.
- [Ber81] H. Berndt. Molding sands and technology of the shell molding process. *VDG-Taschenbuch* 9 (1981).
- [Bes09] J. Besson, G. Cailletaud, J.-L. Chaboche, and S. Forest. *Nonlinear Mechanics of Materials*. Springer, 2009.
- [Bil03] N. Billon. Effet de couplage thermomécanique dans la caractérisation du comportement de polymères solides. *Mécanique & industries* 4.4 (2003), pp. 357–364.
- [Boe85] D Boenisch. The Coldbox-Plus Process—Higher Core Quality With Reduced Binder Consumption. *Giesserei* 72.15 (1985), pp. 435–444.
- [Bri08] H. Brinson and L. Brinson. *Polymer engineering science and viscoelasticity: an introduction*. 2008.

- [Bri15] H. Brinson and L. Brinson. *Polymer Engineering Science and Viscoelasticity: An Introduction*. Springer, 2015.
- [Bri16] H. Brinson and L. Brinson. *Polymer engineering science and viscoelasticity*. Springer, 2016.
- [Bri91] L. Brinson and W. Knauss. Thermorheologically complex behavior of multi-phase viscoelastic materials. *Journal of the Mechanics and Physics of Solids* 39.7 (1991), pp. 859–880.
- [Cam00] F. Camborde, C. Mariotti, and F. Donzé. Numerical study of rock and concrete behaviour by discrete element modelling. *Computers and geotechnics* 27.4 (2000), pp. 225–247.
- [Cam15] J. Campbell. *Complete casting handbook: metal casting processes, metallurgy, techniques and design*. Butterworth-Heinemann, 2015.
- [Car95] P. Carey and M. Lott. Sand binder systems. Furan no-bake. *Foundry Manage. Technol.(USA)* 123.7 (1995), pp. 26–30.
- [Cay10] I. Caylak and R. Mahnken. Thermomechanical characterisation of cold box sand including optical measurements. *International Journal of Cast Metals Research* 23.3 (2010), pp. 176–184.
- [Cha09] D. Chattopadhyay and D. Webster. Thermal stability and flame retardancy of polyurethanes. *Progress in Polymer Science* 34.10 (2009), pp. 1068–1133.
- [Che82] W. Chen and A. Saleeb. Uniaxial behavior and modeling in plasticity. *West Lafayette: Purdue University* (1982).
- [Cri89] J. Criado, J Malek, and A Ortega. Applicability of the master plots in kinetic analysis of non-isothermal data. *Thermochimica Acta* 147.2 (1989), pp. 377–385.
- [Cun71] P. Cundall. A computer model for simulating progressive, large-scale movement in blocky rock system. *Proceedings of the International Symposium on Rock Mechanics, 1971*. 1971.
- [Cun79] P. Cundall and O. Strack. A discrete numerical model for granular assemblies. *geotechnique* 29.1 (1979), pp. 47–65.
- [Dar95] F. Darve, P. Hicher, and J. Reynouard. *Les géomatériaux*. Hermès, 1995.
- [Dor08] H. DorMohammadi and A. Khoei. A three-invariant cap model with isotropic–kinematic hardening rule and associated plasticity for granular materials. *International Journal of Solids and Structures* 45.2 (2008), pp. 631 – 656.
- [Dru52] D. Drucker and W. Prager. Soil mechanics and plastic analysis or limit design. *Quarterly of applied mathematics* 10.2 (1952), pp. 157–165.
- [Efs11] K. Efstathiou. Synthesis and characterization of a Polyurethane Prepolymer for the development of a novel Acrylate-based polymer foam. *Budapest University of Technology and Economics (BME)* (2011), pp. 1–57.
- [Eri12] A. Eringen. *Microcontinuum field theories: I. Foundations and solids*. Springer Science & Business Media, 2012.

- [Fay08] B. Fayolle, E. Richaud, X. Colin, and J. Verdu. Review: degradation-induced embrittlement in semi-crystalline polymers having their amorphous phase in rubbery state. *Journal of Materials Science* 43.22 (2008), pp. 6999–7012.
- [Fly66] J. Flynn and L. A. Wall. General treatment of the thermogravimetry of polymers. *J Res Nat Bur Stand* 70.6 (1966), pp. 487–523.
- [Fra08] E. Frangin. Adaptation de la méthode des éléments discrets à l'échelle de l'ouvrage en béton armé: une approche couplée éléments discrets/éléments finis. PhD thesis. Université Joseph-Fourier-Grenoble I, 2008.
- [Gar13] T. García, S. Jhaveri, A. Sáenz-Valadez, A. Velasco-Téllez, E. Cedillo-Saucedo, and J. Talamantes-Silva. *Method and composition of binder for manufacturing sand molds and/or cores for foundries*. US Patent 8,567,481. 2013.
- [Gar86] J. Gardikes. *Phenolic resin-polyisocyanate binder systems*. US Patent 4,590,229. 1986.
- [Gar88] A. Gardziella. Foundry auxiliaries based on reactive resins. *Becker/Braun (eds) Kunststoffhandbuch* 10 (1988), pp. 958–960.
- [Gib08] S. Gibbs. Illuminating Core Gas-Chemically bonded cores can lead to gas defects, but you can stop them. *Modern Casting* 98.10 (2008), p. 34.
- [Gie09] S. Giese, S. Roorda, and M. Patterson. Thermal analysis of phenolic urethane binder and correlated properties. *Transactions of the American Foundry Society, Vol. 102* 102 (2009), pp. 1–12.
- [Gon11] R. Gonzalez, R. Colas, A. Velasco, and S. Valtierra. Characteristics of phenolic-urethane cold box sand cores for aluminum casting. *International Journal of Metalcasting* 5 (2011), pp. 41–48.
- [Gra93] M. Grayson and C. Fry. On the use of a kinetic map to compare the thermal stability of polymeric materials undergoing weight loss. *McDonnell-Douglas, unpublished research* (1993).
- [Gui01] I. Guillot, B. Barlas, G. Cailletaud, M. Clavel, and D. Massinon. Thermomechanical fatigue and aging of cast aluminum alloy : a link between numerical modeling and microstructural approach. *Journées de printemps de la SF2M*. Paris, 2001.
- [Gur77] A. Gurson. Continuum theory of ductile rupture by void nucleation and growth: Part I— Yield criteria and flow rules for porous ductile media. *J. of Engng. Mat. Technol.* 44 (1977), pp. 2–15.
- [Hau01] J. Haudin and B. Monasse. “Plasticity of Polymers”. *Handbook of Materials Behavior Models*. Elsevier, 2001, pp. 255–264.
- [Hen04] S. Hentz, L. Daudeville, and F. Donzé. Identification and validation of a discrete element model for concrete. *Journal of engineering mechanics* 130.6 (2004), pp. 709–719.
- [Hip94] R. Hipp, D. Harmon, and P. McClellan. Accelerated Aging and Methodology Development for Polymeric Composite Material Systems. *McDonnell Douglas Co. preprint, St. Louis, MO* (1994).
- [Hol15] M. Holtzer, M. Górný, and R. Daňko. Microstructure and Properties of Ductile Iron and Compacted Graphite Iron Castings: The Effects of Mold Sand/Metal Interface Phenomena. Springer, 2015.

- [Hwa92] K. Hwang and T. Tsou. Thermal debinding of powder injection molded parts: Observations and mechanisms. *Metallurgical transactions A* 23.10 (1992), pp. 2775–2782.
- [Ide12] F. Iden. *Structures of Cold-Box binder systems and the possibility of influencing them*. Tech. rep. Huettenes-Albertus, 2012.
- [Ino13] Y. Inoue, Y. Motoyama, H. Takahashi, K. Shinji, and M. Yoshida. Effect of sand mold models on the simulated mold restraint force and the contraction of the casting during cooling in green sand molds. *J. of Materials Processing Technology* 213 (2013), pp. 1157–1165.
- [Joh05] A. John, S. Alan, and S. Alan. Chemorheological response of elastomers at elevated temperatures: Experiments and simulations. *Journal of the Mechanics and Physics of Solids* 53.12 (2005), pp. 2758–2793.
- [Joh10] M. Johlitz, D. Scharding, S. Diebels, J. Retka, and A. Lion. Modelling of thermo-viscoelastic material behaviour of polyurethane close to the glass transition temperature. *ZAMM - Journal of Applied Mathematics and Mechanics / Zeitschrift für Angewandte Mathematik und Mechanik* 90.5 (2010), pp. 387–398.
- [Joh13] M. Johlitz and A. Lion. Chemo-thermomechanical ageing of elastomers based on multiphase continuum mechanics. *Continuum Mechanics and Thermodynamics* 25.5 (2013), pp. 605–624.
- [Jom14] G. Jomaa. Etude des dégagements gazeux survenant pendant la coulée de pièces d’Aluminium. PhD thesis. ENSMP, 2014.
- [Jom15] G. Jomaa, P. Goblet, C. Coquelet, and V. Morlot. Kinetic modeling of polyurethane pyrolysis using non-isothermal thermogravimetric analysis. *Thermochimica Acta* 612 (2015), pp. 10–18.
- [Kar07] D. Karunakar and G. Datta. Controlling green sand mould properties using artificial neural networks and genetic algorithms — A comparison. *Applied Clay Science* 37 (2007), pp. 58–66.
- [Kon86] E. Kong. “Physical aging in epoxy matrices and composites”. *Epoxy Resins and Composites IV*. Springer, 1986, pp. 125–171.
- [Kov12] L. Kovačević, P. Terek, D. Kakaš, and A. Miletić. A correlation to describe interfacial heat transfer coefficient during solidification of Al–Si alloy casting. *J. of Materials Processing Technology* 212 (2012), pp. 1856–1861.
- [Lad13] G. Ladégourdi, M. Dörschel, U. Wichmann, A. Anbari, and D. Strunk. *Cold-box binding agent systems and mixtures for use as additives for such binding agent systems*. US Patent App. 13/763,150. 2013.
- [Lai85] R. A. Laitar and E. Gomez. *Polyurethane binder compositions*. US Patent 4,546,124. 1985.
- [Lie12] C. Liebl, M. Johlitz, B. Yagimli, and A. Lion. Simulation of curing-induced viscoplastic deformation: a new approach considering chemo-thermomechanical coupling. *Archive of Applied Mechanics* 82.8 (2012), pp. 1133–1144.

-
- [Mah11] R. Mahnken and I. Caylak. “Optical Measurements for a Cold-Box Sand and Aspects of Direct and Inverse Problems for Micropolar Elasto-Plasticity”. *Advances in Extended and Multifield Theories for Continua*. Ed. by B. Markert. Vol. 59. Lecture Notes in Applied and Computational Mechanics. Springer Berlin Heidelberg, 2011, pp. 175–196.
- [Man92] F. Manguin. Modélisation et optimisation de la dégradation thermique de liants utilisés en injection de céramiques. PhD thesis. 1992.
- [Mar06] L. Martin. Intégration du métier de la fonderie dans les processus de conception: méthodologies et outils associés. PhD thesis. Paris, ENSAM, 2006.
- [Mar12] R. Martinez. Modélisation multiéchelles du vieillissement des alliages d’aluminium – Multiscale modeling of the ageing of cast aluminium alloys. PhD thesis. Paris XII–Créteil University, 2012.
- [Mar81] R. Martin, W. Dunnivant, G. Sturtz, and H. Langer. *Urethane binder compositions for no-bake and cold box foundry application utilizing isocyanato-urethane polymers*. US Patent 4,293,480. 1981.
- [Met01] D. Metzger, J. New, and J. Dantzig. A sand surface element for efficient modeling of residual stress in castings. *Appl. Math. Modelling* 25 (2001), pp. 825–842.
- [Mon08] Montupet. *Noyautage*. Internal report. 2008.
- [Mon09] C. Monroe, C. Beckermann, and J. Klinkhammer. Simulation of Deformation and Hot Tear Formation using a visco-plastic Model with Damage. *Modeling of Casting, Welding, and Advanced Solidification Processes-XII*, eds. *SL Cockcroft and DM Maijer*, TMS, Warrendale, PA (2009), pp. 313–320.
- [Mon13] Montupet. *Sand core deformation during casting*. Internal report. 2013.
- [Mon14] Montupet. *Formation noyautage*. Internal report. 2014.
- [Mon15] Montupet. *Sand core instrumentation*. Internal report. 2015.
- [Mon16] Montupet. *Technological specimen instrumentation*. Internal report. 2016.
- [Mot12] Y. Motoyama, H. Takahashi, Y. Inoue, K. Shinji, and M. Yoshida. Development of a device for dynamical measurement of the load on casting and the contraction of the casting in a sand mold during cooling. *J. of Materials Processing Technology* 212 (2012), pp. 1399–1405.
- [Mot13a] Y. Motoyama, Y. Inoue, G. Saito, and M. Yoshida. A verification of the thermal stress analysis, including the furan sandmold, used to predict the thermal stress in castings. *J. of Materials Processing Technology* 213 (2013), pp. 2270–2277.
- [Mot13b] Y. Motoyama, H. Takahashi, Y. Inoue, K. Shinji, and M. Yoshida. Dynamic measurements of the load on castings and the contraction of castings during cooling in sand molds. *J. of Materials Processing Technology* 213 (2013), pp. 238–244.
- [Nav15] B. Navarro, M. Arrieta, A. Mujica-Garcia, V. Sessini, D. Lopez, J. Kenny, and L. Peponi. Thermal Degradation Effects on Polyurethanes and Their Nanocomposites. *Reactions and Mechanisms in Thermal Analysis of Advanced Materials*. John Wiley & Sons, Inc., 2015, pp. 165–189.

- [Nic99] B. Nicouveau. Etude expérimentale et numérique du vieillissement d'un alliage d'aluminium. Application aux culasses automobiles. PhD thesis. École Nationale Supérieure des Mines de Paris, 1999.
- [Núñ00] L. Núñez, F. Fraga, M. Nunez, and M. Villanueva. Thermogravimetric study of the decomposition process of the system BADGE (n= 0)/1, 2 DCH. *Polymer* 41.12 (2000), pp. 4635–4641.
- [Oza65] T. Ozawa. A new method of analyzing thermogravimetric data. *Bulletin of the chemical society of Japan* 38.11 (1965), pp. 1881–1886.
- [Pab05] W. Pabst. Micropolar materials. *Ceramics- Silikaty* 49.3 (2005), pp. 170–180.
- [Pan14] X. Pan, Y. Yang, G. Yang, D. Yin, and Y. Zhou. Design and Simulation Optimization of Casting Process for Aluminum Alloy Engine Cylinder Head. *Appl. Mechanics and Materials* 494–495 (2014), pp. 593–597.
- [Par11] C. Paris. Étude et modélisation de la polymérisation dynamique de composites à matrice thermodurcissable. PhD thesis. INPT, 2011.
- [Pas02] J. Pascault, H. Sautereau, J. Verdu, and R. Williams. Thermosetting polymers. Vol. 64. CRC Press, 2002.
- [Ped92] C. Pederson. The effect of temperature on transverse cracking in high performance composites. PhD thesis. University of Delaware, 1992.
- [Pil10] L. Pilato. Phenolic resins: a century of progress. Springer, 2010.
- [Pri14] C. Priebe and D. Koch. *Binder system based on polyurethane for producing cores and casting molds using cyclic formals, molding material mixture, and method*. US Patent App. 13/813,062. 2014.
- [Rah93] K. Rahmoeller. Mold binder decomposition: prime source of cast iron gas defects. *Modern casting* 83.10 (1993), pp. 36–39.
- [Rin08] V. Rinaldi and J. Santamarina. Cemented soils: small strain stiffness. *Deformational Characteristics of Geomaterials* 1 (2008), pp. 267–273.
- [Rio16] S. Rios, M. Ciantia, N. Gonzalez, M. Arroyo, and A. Viana da Fonseca. Simplifying calibration of bonded elasto-plastic models. *Computers and Geotechnics* 73 (2016), pp. 100–108.
- [Rob71] S. Robert. Practice of the shell molding process. *Giesserei, Düsseldorf* (1971).
- [Rod14] F. Rodriguez, C. Cohen, C. Ober, and L. Archer. Principles of polymer systems. CRC Press, 2014.
- [Ros58] K. Roscoe, A. Schofield, and C. Wroth. On the yielding of soils. *Geotechnique* 8.1 (1958), pp. 22–53.
- [Ros68] K. Roscoe and J. Burland. On the generalized stress-strain behaviour of wet clay. *Engineering Plasticity* (1968), pp. 535–609.
- [Sai12] S. Saikaew and S. Wiengwiset. Optimization of molding sand composition for quality improvement of iron castings. *Applied Clay Science* 67–68 (2012), pp. 26–31.
- [Sal06] R. Salapete, B. Barlas, E. Nicouveau, D. Massinon, G. Cailletaud, and A. Pineau. Modelling of Fatigue Damage in Aluminum Cylinder Heads. Jan. 2006, pp. 837–838.

-
- [Sam12] G. Samuels and C. Beckermann. Measurement of gas evolution from PUNB bonded sand as a function of temperature. *International Journal of Metalcasting* 6.2 (2012), pp. 23–40.
- [Sam85] M. Samonds, K. Morgan, and R. Lewis. Finite element modelling of solidification in sand castings employing an implicit-explicit algorithm. *Appl. Math. Modelling* 9 (1985), pp. 170–174.
- [Sch14] C. Schuch, D. Vicentim, L. Sereda, and S. Silva. *Foundry binder systems*. US Patent App. 14/001,241. 2014.
- [Sha03a] J. Shao, Q. Zhu, and K Su. Modeling of creep in rock materials in terms of material degradation. *Computers and Geotechnics* 30.7 (2003), pp. 549 –555.
- [Sha03b] S. Sharma and M. Fahey. Degradation of stiffness of cemented calcareous soil in cyclic triaxial tests. *Journal of Geotechnical and Geoenvironmental engineering* 129.7 (2003), pp. 619–629.
- [Sha06] J. Shao, Y. Jia, D. Kondo, and A. Chiarelli. A coupled elastoplastic damage model for semi-brittle materials and extension to unsaturated conditions. *Mechanics of Materials* 38.3 (2006), pp. 218 –232.
- [Sta06] M. Stancliffe. Phenolic Urethane Cold-box Binders—A Study of Global Properties, Variables, Causes and Effects. *Casting the Future, World Foundry Congress, 67; 118/1-118/10; Casting the Future, World Foundry*. Institute of Cast Metals Engineers (ICME), West Bromwich; 2006.
- [Sta09a] A. Starobin, C. Hirt, and D. Goettsch. A Model for Binder Gas Generation and Transport in Sand Cores and Molds. *Modeling of Casting, Welding and Advanced Solidification Processes-XII* (2009), pp. 345–352.
- [Sta09b] A. Starobin and C. Hirt. FLOW-3D Core Gas Model: Binder Gas Generation and Transport in Sand Cores and Molds. *Santa Fe, New Mexico, USA: Flow Science Inc* (2009).
- [Sta11] A. Starobin, D. Goettsch, M. Walker, and D. Burch. GAS PRESSURE IN ALUMINUM BLOCK WATER JACKET CORES. *International Journal of Metalcasting* 5.3 (2011), pp. 57–64.
- [Sta16] B. J. Stauder, H. Kerber, and P. Schumacher. Foundry sand core property assessment by 3-point bending test evaluation. *Journal of Materials Processing Technology* 237 (2016), pp. 188 –196.
- [Sto10] R. Stotzel, K. Eising, and K. Smarzoch. *Coating compounds for casting moulds and cores that prevent reaction gas defects*. US Patent App. 12/598,348. 2010.
- [Str77] L. Struik. Physical aging in amorphous polymers and other materials (1977).
- [Sul12] S. Sulaiman and A. Hamouda. Modeling of the thermal history of the sand casting process. *J. of Materials Processing Technology* 22 (2012), pp. 1884–1890.
- [Sul90] J. Sullivan. Creep and physical aging of composites. *Composites Science and Technology* 39.3 (1990), pp. 207–232.
- [Sun12] S. Sun, B. Yuan, and M. Liu. Effects of moulding sands and wall thickness on microstructure and mechanical properties of Sr-modified A356 aluminum casting alloy. *Trans. Nonferrous Met. Soc. China* 22 (2012), pp. 1884–1890.
-

- [Tan81] M. Tant and G. Wilkes. An overview of the nonequilibrium behavior of polymer glasses. *Polymer Engineering & Science* 21.14 (1981), pp. 874–895.
- [Thi01] E. Thian, N. Loh, K. Khor, and S. Tor. Effects of debinding parameters on powder injection molded Ti-6Al-4V/HA composite parts. *Advanced Powder Technology* 12.3 (2001), pp. 361–370.
- [Thi07] J. Thiel, M. Ziegler, P. Dziekonski, and S. Joyce. Investigation into the Technical Limitations of Silica Sand Due to Thermal Expansion. *Transactions of the American Foundry Society, Vol. 115* 115 (2007), pp. 383–400.
- [Thi08] J. Thiel. High Temperature Physical Properties of Chemically Bonded Sands Provide Insight into Core Distortion. *National Technical and Operating Conference* 91 (2008).
- [Tho10] J. Thole and C. Beckermann. Measurement of elastic modulus of PUNB bonded sand as a function of temperature. *International Journal of Metalcasting* Fall 10 (2010), pp. 7–18.
- [Tho99] D. Thompson, L. Markoski, and J. Moore. Rapid synthesis of hyperbranched aromatic polyetherimides. *Macromolecules* 32.15 (1999), pp. 4764–4768.
- [Tob60] A. Tobolsky. Properties and structure of polymers. Wiley, New York, 1960.
- [Tri99] D. Trinowski, G. Ladegourdie, and K. Löchte. New coldbox binder system for improved productivity. *Transactions of the American Foundry Society* 107 (1999), pp. 51–57.
- [Tro14] G. Trovati, E. A. Sanches, S. M. de Souza, A. L. dos Santos, S. C. Neto, Y. P. Mascarenhas, and G. O. Chierice. Rigid and semi rigid polyurethane resins: A structural investigation using DMA, SAXS and Le Bail method. *Journal of Molecular Structure* 1075 (2014), pp. 589–593.
- [Tve84] V. Tvergaard and A. Needleman. Analysis of cup–cone fracture in a round tensile bar. *Acta Metall.* 32 (1984), pp. 157–169.
- [Tve90] V. Tvergaard. Material failure by void growth to coalescence. *Advances in Appl. Mech.* 27 (1990), pp. 83–151.
- [Vau03] J. Vaunat and A. Gens. Bond degradation and irreversible strains in soft argillaceous rock. *Proceedings of the 12th panamerican conference on soil mechanics and geotechnical engineering.* 2003.
- [VH10] B. Van Hemelryck, P. Vacelet, J. Roze, J. Muller, and D. Koch. *Use of amine blends for foundry shaped cores and casting metals.* US Patent App. 12/523,089. 2010.
- [War93] I. Ward and D. Hadley. An introduction to the mechanical properties of solid polymers. John Wiley & Sons, Inc., 1993.
- [War94] T. E. Warner. *Method of curing hot box sand cores.* US Patent 5,365,995. 1994.
- [Won10] T. Wongsiriamnuay and N. Tippayawong. Non-isothermal pyrolysis characteristics of giant sensitive plants using thermogravimetric analysis. *Bioresour technology* 101.14 (2010), pp. 5638–5644.
- [Yu98] H. Yu. CASM: A unified state parameter model for clay and sand. *International Journal for Numerical and Analytical Methods in Geomechanics* 22.8 (1998), pp. 621–653.

Appendix

Appendix of chapter 1

A: Resin binder components

Information produit | Systèmes de liants

AVECURE 331 Partie I

Procédé « boîtes froides »

Système spécialement développé pour la coulée d'aluminium et plus particulièrement pour les coulées dans des moules métalliques permanents (coquilles)

Dégagement de fumée réduit

Time (s)	Standard (Smoke)	AV 331/AV 631 (Smoke)
0	0.0	0.0
100	0.0	0.0
200	0.35	0.1
250	0.4	0.15
300	0.35	0.1
400	0.0	0.0
500	0.0	0.0
600	0.0	0.0

Désignation chimique

- Résine d'éther de benzyle en solvant

Valeurs analytiques

- Masse volumique [20 °C] : env. 1,07 g/cm³
- Viscosité [25 °C] : env. 160 mPa.s
- Mélange de sable : 100 T. Sable siliceux, AFS 55
0,5 % AV 331
0,5 % AV 631
- Solidité au prélèvement [N/cm²] : ≥ 170
- Solidité finale [N/cm²] : ≥ 350
[20 °C, 50 % hum. relative]

Durée et conditions de conservation du produit

- 6 mois (température de stockage entre 10 et 30 °C)
- La durée de stockage diminue à température supérieure
- Eu égard à la viscosité, ne pas stocker en dessous de 10 °C

Manipulation de l'AVECURE 331 Partie I

Ne pas mélanger AVECURE Partie II et Partie I. Les matériaux réagissent par un fort développement de chaleur. Protéger contre les flammes nues. Les vapeurs de solvants peuvent avoir un effet irritant sur les muqueuses. Éviter l'inhalation des vapeurs. En cas de contact avec la peau, laver abondamment à l'eau et au savon ; le cas échéant, laver également avec du « Lutrol ». En cas de contact avec les yeux, rincer abondamment à l'eau. Consulter un ophtalmologue.

Étiquetage : cf. fiche de données de sécurité

La responsabilité en matière de conseil et d'information sur le produit est limitée aux obligations d'information contractuelles annexes, sauf stipulation contraire expresse.

Propriétés techniques et avantages écologiques :

- Résistance mécanique élevée en sortie de boîte.
- Longue durée de vie du sable, malgré la grande réactivité du système
- Réduction des fumées et des condensats
- Dégagement de gaz réduit
- Réduction du collage

Composants de système Partie II appropriés :

- AVECURE 631

Agent de démoulage recommandé :

- ECOPART™ 756

Agent de nettoyage recommandé :

- ZIP CLEAN™ 1000

Product Management
Boîte froide

cold-box@ask-chemicals.com

ASKCHEMICALS
We advance your casting

Dernière mise à jour : octobre 2014

ASK Chemicals GmbH | Reisholzstr. 16-18 | 40721 Hilden | Tél. : +49 (0)211 71103-0 | www.ask-chemicals.com

Figure A.1: Polyol part datasheet

Information produit | Systèmes de liants

AVECURE 631 Partie II

Procédé « boîtes froides »

Système spécialement développé pour la coulée d'aluminium et plus particulièrement pour les coulées dans des moules métalliques permanents (coquilles)

Propriétés du système

AVECURE 631 est le composant polyisocyanate destiné au procédé « boîtes froides ». Les propriétés optimales peuvent être obtenues grâce à la mise en œuvre à l'aide de l'un des composants de système Partie I appropriés.

Désignation chimique

Polyisocyanate dans des solvants non aromatiques

Valeurs analytiques

- Masse volumique [20 °C] : env. 1,12 g/cm³
- Viscosité [25 °C] : env. 20 mPa.s

Capacité et conditions de stockage du produit

- 6 mois (température de stockage entre 10 et 30 °C).
- La durée de stockage diminue à température supérieure
- Eu égard à la viscosité, ne pas stocker en dessous de 10°C


Manipulation de l'AVECURE 631 Partie II

Ne pas mélanger AVECURE - Partie I et Partie II. Les matériaux réagissent par un fort dégagement de chaleur. Protéger contre les flammes nues. Les vapeurs de solvants peuvent avoir un effet irritant sur les muqueuses. Éviter l'inhalation des vapeurs. En cas de contact avec la peau, laver abondamment à l'eau et au savon . En cas de contact avec les yeux, rincer abondamment à l'eau. Consulter un ophtalmologue.

Étiquetage : cf. fiche de données de sécurité

La responsabilité en matière de conseil et d'information sur le produit est limitée aux obligations d'information contractuelles annexes, sauf stipulation contraire expresse.

Gestion de produit
Boîte froide
 cold-box@ask-chemicals.com



ASKCHEMICALS
We advance your casting

Dernière mise à jour : octobre 2014

Figure A.2: Polyisocyanate datasheet

Appendix of chapter 4

B: mesh sensitivity study

Table A.1: Comparison of the results of the simulation of four-point bending tests during heating at 2 °C/min up to 200 °C

mesh	number of elements	CPU time (min)
1: C2D4	420	150
2: C2D8	2500	110
3: C2D8	1080	47
4: C2D8	420	26

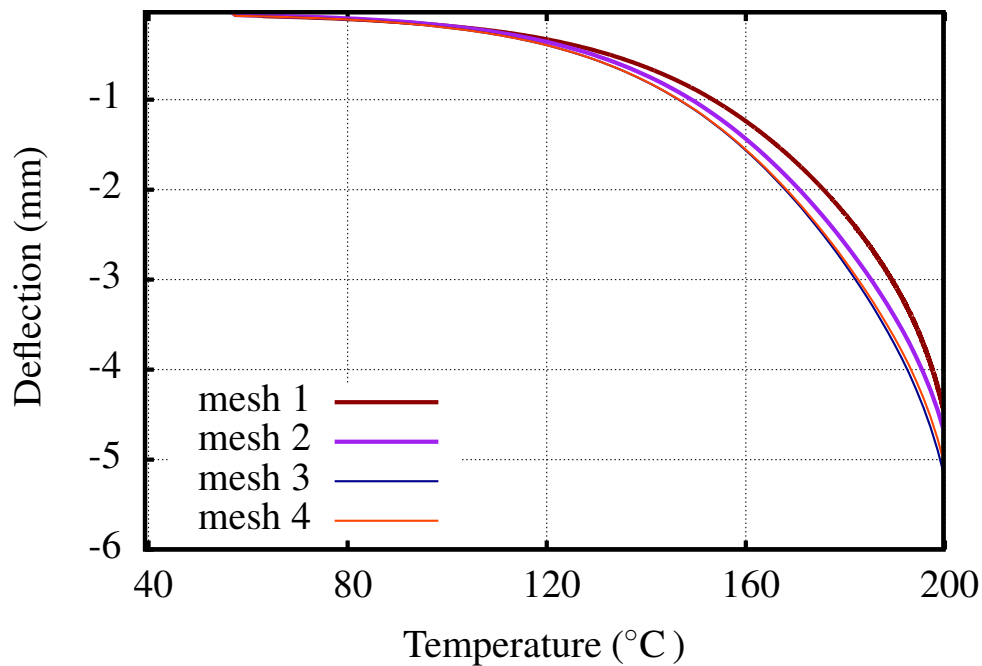


Figure A.1: Deflection evolution using four types of meshes

RÉSUMÉ

Les cavités intérieures des culasses d'aluminium sont réalisées à l'aide de noyaux de sable, qui sont constitués d'un mélange de silice et d'une résine Polyuréthane. Ils sont placés dans le moule métallique juste avant la coulée. Durant celle-ci, ils subissent la pression métallo-statique et sont soumis à des températures élevées. Sous ces conditions extrêmes, avec l'apparition de parois de plus en plus fines et de formes plus complexes, les noyaux peuvent présenter des déformations qui induisent des défauts dimensionnels sur les pièces finales. Pour contrôler la déformation des noyaux, il faut d'abord disposer d'une caractérisation robuste de leurs propriétés thermiques et mécaniques, qui puisse être utilisée dans des calculs de structures simulant le flux du métal liquide, la solidification, les champs thermiques. Cette approche n'est pas encore pratiquée de façon complète dans l'industrie. Une revue de la littérature confirme que cette connaissance n'est que très parcellaire pour le moment. Le travail a donc d'abord été concentré sur la caractérisation expérimentale du comportement thermomécanique et des propriétés thermophysiques des noyaux de fonderie et du liant résine. Ensuite, un modèle de comportement capable de prendre en compte la viscosité du matériau, son endommagement, et surtout son évolution en fonction du temps et de la température en raison de la dégradation thermique du liant résine a été développé. Une éprouvette technologique a finalement été conçue et un protocole expérimental a été mis en place pour mesurer la déformation d'un noyau durant la coulée et de valider numériquement le modèle de comportement sous des chargements thermiques et mécaniques complexes.

MOTS CLÉS

Noyau de fonderie, liant résine, coulée, simulation par éléments finis, modèle de comportement thermomécanique, déformation

ABSTRACT

The inner cavities of aluminum cylinder heads are made using sand cores, which are made of silica sand and of a polyurethane resin binder. The cores are placed in the metallic mold just before casting. During this stage, the cores are submitted to the metallo-static pressure and high temperatures. Under these extreme loading conditions, with the development of thinner and thinner walls with complex designs, the cores exhibit significant deformation causing dimensional defects in the final cast. To control the deformation of the sand core, it is necessary to possess a robust characterization of their thermal and mechanical properties, that could be introduced in structural computations simulating the flow of the liquid metal, the solidification and the thermal fields. This approach is still not fully in use in the industry. A review of the literature confirms that this knowledge is incomplete for the moment. The work was therefore concentrated on the experimental characterization of the thermomechanical behavior and the thermophysical properties of the foundry cores and Polyurethane resin binder. Then, a behavior model capable of taking into account the viscosity of the material, damage development, and especially its evolution as a function of time and temperature because of the thermal degradation of the binder resin was developed. A technological specimen was finally designed and an experimental protocol has been established to measure the deformation of a core during casting and numerically validate the constitutive equations under complex thermal and mechanical loadings.

KEYWORDS

Foundry sand core, resin binder, casting, finite elements simulation, thermomechanical behavior model, deformation